# ODESSA ASTRONOMICAL PUBLICATIONS

Volume 18 (2005)

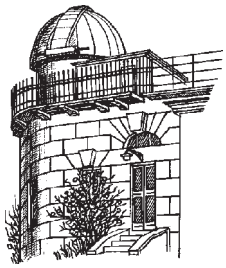

Odessa
«AstroPrint»

# FOREWORD

This issue of the Odessa Astronomical publications (volume 18) is devoted in part to the International conference "Variable stars – 2005" that was held in Odessa in August 2005. Some contributions that were presented on that conference can be found in this volume of OAP. In addition,

The Editorial board is not responsible for the English of contributions submitted by their authors and printed in the original form.

## заменить!!!

Together with Odessa national University the following organizations took part in the conference preparation: Euro-Asian Astronomical Society (Moscow), Ukrainian Astronomical Association (Kiev), Odessa Astronomical Society, Department of astronomy, Department of theoretic physics and Research Institute "Astronomical Observatory" of I.I. Mechnikov Odessa national University. The SOC was headed by Prof. G. S. Bisnovaty-Kogan, while the Memorial and Local organizing committees – by rector of Odessa University – Prof. V. A. Smyntyna.

The scientific program of the conference included seven main sections and two affiliated sections: 1. Memorial Meeting. 2. Cosmology and Gravitation. 3. Large-Scale Structure of the Universe. 4. Gravitational Lenses in the Universe. 5. Neutron Stars and Black Holes. 6. Nucleosynthesis in Stars, Starbursts and Interstellar Medium. 7. High Energy Astrophysics. Among affiliated sections there were: 1. Small Bodies of the Solar System. 2. Astronomy in Odessa. The Memorial part of the conference was devoted to the Gamov's life, his scientific, pedagogical and popularization activity.

About 200 scientists from 18 countries of the America, Asia and Europe participated in the conference. More that 100 scientific talks were delivered there (20 of them were the plenary talks). The total number of the poster presentations was about 30. In the conference resolution it was noted that the Gamov conferences are very productive. The present conference was the third one (the first Gamov conference was held in 1994, and the second one – in 1999). It was decided to establish a good tradition for the future to organize the Gamov's conferences every three years at the regular base. We hope to see participants of the next conference in 2009.

According to the SOC decision the publication of the Gamov's conference proceeding was divided into two parts. The first part consists of the invited talks and reviews. They are published by Cambridge Press as a separate issue (Eds. Prof. G. S. Bisnovaty-Kogan and S.A. Silich). The rest of the contributions are presented here, in this Volume 17 of "Odessa Astronomical Publications".

V. G. Karetnikov

# CONTENTS

# STABILITY OF PULSATIONAL AMPLITUDE FOR CEPHEIDS OF PERIOD = $6\pm1^d$

M.A. Abdel-Sabour
National Research Institute of Astronomy and Geophysics
Helwan, Cairo, Egypt *Sabour2000@hotmail.com*

ABSTRACT. Fourier decomposition of light curves used to obtain rigorous estimates of the pulsational amplitudes. A limit sample of Cepheids of period = $6\pm1^d$ ,was chosen to demonstrate the capabilities of this technique. The pulsational amplitude shows significant increase and decrease for some stars.

**Key words**: Cepheids, Evolution

## 1. Introduction

The study of Cepheids and pulsating stars in general has a very important field in astronomy, also regular pulsation of Cepheids variables makes these stars to be ideal targets for studying subtle secular phenomena due to stellar evolution. A goodbye to Polaris as a Cepheids was announced (Fernie et al. 1993) predicting that Polaris will stop pulsating in 1995. About a hundred years ago it was spotted having a pulsational amplitude of dv 0.12 magnitude, which by now has declined to 0.01 magnitude. Kamper and Fernie (1998) discussed a serious error in their earlier paper, which predicted decline in amplitude of Polaris in 1995. They corrected this error and no longer predict cessation of pulsation in 1995. Not so longer ago Fernie (1990) suggested that another Cepheid Y Oph, shows that the amplitude of this Cepheid varies periodically on a time scale of about 1400 days (Burki et. al. 1986). Platis and Mandushev (1993), studied the stability of the pulsational amplitude for a sample of three s-Cepheids, SU Cas, SZ Tau and V1726 Cyg, using the Fourier decomposition of light curves. The pulsational amplitude shows no decisive change as a function of time in any of three Cepheids. Sandage and Tammann (1971), have argued that for a restricted period range $0.4 < \log p < 0.86$ Cepheids have their largest amplitudes at the blue (hot) edge of the instability strip. Yakimova et al. (1975), have examined more extensive but less accurate photographic data and concluded that irrespective of period range, amplitude is largest on the red edge of instability strip. In the opposite direction Butler (1976), found no strong evidence for any amplitude mapping. Evans et al. (2002), studied the amplitude of Polaris, they found that, the evidence from amplitude, period change and Fourier diagnostic all agree with overtone pulsation for Polaris. Polaris has an increasing period, which can be interpreted in evolutionary terms as the stars moving toward cooler temperatures. This is this original reason why the decrease in amplitude was thought to series from evolution out of the instability strip. But they found that Polaris is near the blue edge of the strip, which means that the period change as an evolutionary affect would mean that Polaris is moving into the instability strip (i.e. Polaris should increasing in pulsational amplitude). A number of studies, (e.g. Szabados, 1977) have been devoted to the Cepheid period stability; however, with a few exceptions stated above, the pulsational amplitude was scrutinized for possible trends and secular evolution. Turner and et al.(2005) studed the pulsation amplitude of Polaris underwent a marked change. Prior to 1963 the V amplitude was in excess of about 0.1 mag, possibly decreasing at a rate of 0.019 mag century. Following the hiatus of 1963-1966, the pulsation amplitude underwent a sharp decline and now appears to be erratic on a cycle-to-cycle basis, always smaller than 0.05 mag. Here we present an analysis of the pulsational amplitude stability, utilizing the Fourier fits of light curves parameters for Cepheids of period between $6\pm1^d$, which have a long history of observations. This was carried out by analysis of their light curves obtained over a long period (depending on the observational record available) to investigate if the light curves obtained for each star are stable or showing temporal variations in light curve parameters.

## 2. Data and Technique of Reduction

In collecting our data, we bear in mind that the data should cover the minimum and maximum parts of the light curves to enable reliable amplitude estimation using the Fourier decomposition technique, which has a widely use in light curve analysis of pulsating stars (Simon 1988). This technique can provide quantative parameters to define the shape of light curves and it is for this reason a powerful tool classification purpose. It's worthy to mentioned that we applied our investi-

Table 1: Mathematical results of the liner fit for the total Fourier amplitude in visual mag.

| Name | A | $B \times 10^{-7}$ | $\log dP/dt$ | Expected $\delta V$ |
|---|---|---|---|---|
| AP Sgr | -4.16±3.71 | 10.85±0.15 | -0.70 | increase |
| AX Cir | 0.89±0.81 | -2.21±0.003 | -0.44 | increase |
| BG Vel | 1.09±0.52 | -3.58±2.137 | -0.26 | increase |
| CV Mon | 0.08±2.27 | 0.99±9.290 | -0.74 | increase |
| FM Aql | 0.71±0.82 | 4.25±3.360 | -1.14 | increase |
| S Tra | 0.84±1.16 | -2.02±4.75 | -0.61 | increase |
| ST Vel | 1.77±2.37 | -6.07±9.60 | -0.61 | increase |
| U Aql | -5.37±1.95 | 23.46±7.97 | -0.81 | increase |
| U Sgr | 2.12±0.98 | -7.29±4.01 | -0.47 | increase |
| V419 Cen | 1.18±1.33 | -4.17±5.46 | -0.43 | increase |
| V Cen | 3.32±3.08 | -10.2±10.26 | -0.34 | increase |
| RS Cas | -0.30±0.72 | 2.68±2.95 | -1.23 | increase |
| T Cru | -1.61±0.93 | 7.48±3.76 | 0.76 | increase |
| V386 Cyg | -3.17±0.84 | 14.26±3.96 | -1.08 | increase |
| V378 Cen | -0.22±0.15 | 1.67±1.44 | -0.22 | increase |
| X Lac | -2.67±1.64 | 10.18±6.7 | 0.10 | increase |
| V733 Aql | -2.33±3.16 | 10.034±10.29 | -1.00 | increase |
| Y Sgr | 3.89±2.26 | -10.45±6.22 | -0.89 | increase |
| AP Pup | 3.76±1.67 | -10.41±0.68 | -0.64 | decrease |
| AY Sgr | 2.70±3.85 | -9.46±0.157 | -2.49 | decrease |
| CR Ser | -2.76±9.13 | 10.26±30.73 | -0.54 | decrease |
| AT Pup | 1.85±1.41 | -5.84±0.057 | -0.99 | decrease |
| R Cru | 1.63±1.6 | -5.22±6.58 | -1.09 | decrease |
| BP Cir | 3.15±1.47 | -10.22±6.003 | 0.05 | decrease |
| V737 Cen | -8.34±4.32 | 30.48±10.76 | 0.40 | decrease |
| VW Cas | -0.66±1.77 | 3.99±7.24 | -1.93 | decrease |
| GH Car | 0.79±0.60 | -2.6±2.46 | -0.53 | decrease |
| V1162 Aql | 8.13±4.37 | -30.22±10.78 | 0.33 | decrease |
| WW Pup | -1.14±8.13 | 6.44±3.32 | -0.26 | decrease |
| XX Vel | 2.21±2.51 | -7.42±10.02 | -1.28 | decrease |
| XX Sgr | -7.17±1.81 | 30.09±7.39 | -0.66 | decrease |

gation on V band only. we did not use B, I or U bands, since the infrared technique is relatively new and the investigated stars had no long term observations in this band, also the U band was not used due to the faintness of the studied stars in that band, While B band is very important in our study, because the amplitude is greater in B band than in V band, but unfortunately we haven't sufficient observations in that band. Following Antonello et al. (1990), we applied the Fourier decomposition technique to the light curves in V-bandpass. It is based upon Fourier decomposition of the light curves by series:

$$V(t) = V_o + \sum A_z \cos[2\pi f_z(t - T_o) + \Phi_z] \quad (1)$$

Where $A_z$ is a semi-amplitude of light variation, $\Phi$ is the phase shift, $T_o$ and $f$ are the adopted epoch of light maximum and frequancy. The program package Mufran (Kollath, 1990), which is a user friendly software for period analysis was used to determine the numerical parameters describing the light curves of the studied stars

## 3. Result and Conclution

The final results of the total Fouries harmonic amplitude of all studied stars in visual and photographic bands are represented in Table 1 The mathematical form of the long term behavior for the light curves of the studied stars were calculated in visual and photographic bands. The results can be summarized into two categiries: First: Included those stars that show significant secular increase in total harmonic Fourier amplitude. This result, were confirmed by Turner and et al. (2006), where they studied the rate of period change for the same sample of stars and found that the evolution of these stars is toward the cool side in the instability strip of H-R diagram, i.e the crossing numbers of the stars in the instability strip are first and third crossing Second: Some stars show significant secular decrease in total harmonic Fourier amplitude. From Turner at al. (2006) this result can be confirmed, where the evolutionary trend of these stars is toward

the hot side of the H-R diagram, i.e the crossing number of the stars in the instability strip are second and forth crossing. There are miss-understand in results of two stars, AP Pup and AY Sgr, which show significant secular decrease in their total harmonic Fourier amplitude, while from Turner et al. (2005) studied their O-C diagrams and found that their period increase (positive change) and their crossing number is odd, which means that the amplitude must change in increasing manner, but unfortunately we found that the trend of amplitude variation is in decreasing manner. Our interpretation for this result is that, the available observations for these stars may not be sufficient to give complete information about the behavior of amplitude stability with time. Last column of table 1, shows the results of the behavior of each star (increase or decrease).

**References**

Burki G., Schmidt E., Arellano Ferro A., Fernie J., Sasselov D., Simon N., Percy J., Szabados L.: 1986, *A&A*, **168**, 139.

Butler C.J.: 1976, *Mem R. Astro. Soc.*, **24**, 299.

Evans Nancy, Sassalove D., Ian Short: 2002, *Astrophys. J.*, **567**, 1121-1130.

Fernie J.D., Kamper K.W., Seager S.: 1993, *APJ*, **416**, 820.

Kamper K.W., Fernie J.D.: 1998, *AJ*, **116**, 936.

Kollath Z.: 1990, Occasional Technical Notes, Konkoly Observatory, No.1.

Platais I., Mandushev G.: 1993, *JAVSO*, **22**, 100.

Sandage A., Tammann G. : 1971, *Ap.J.*, **167**, 293.

Simon Norman R.: 1988, pmls. Conf. 27.

Szabados L.: 1977, Mitt. Sternw. Ung. Akad. Wiss., Budapest, No. 70.

Turner D., Abdel-Sabour M.A., Berdnikov L.: 2006, has been accepted for publication in the March 2006 issue of PASP.

Turner D.G., Savoy J., Derrah J., Abdel-Sabour A.M., Berdnikov L.: 2005, *PASP*, **117**, 207.

Yakimova M., Nikolov N., Ivanov G.: 1975, Var. star and stellar evolu. //eds. Sherwood and Plaut, 201.

# THE METHOD FOR FAST DETERMINATION OF GEOSTATIONARY EARTH SATELLITE ORBIT FROM ANGULAR COORDINATES MEASUREMENTS

O.A. Bazyey[1,2] , E.S. Sibiryakova[2], and A.V. Shulga[2]

[1] Department of Astronomy, Odessa State University
T.G.Shevchenko Park, Odessa 65014 Ukraine, *creator@sky.od.ua*
[2] Nikolayev Astronomical Observatory
Observatorna 1, 54030 Mykolaiv, Ukraine *dir@mao.nikolaev.ua*

ABSTRACT. Classical Laplas method for determination of Keplerian orbital elements is described. The values obtained are improved by the method of differential corrections. The software has been provided and realizes such an algorithm to calculate orbital elements for high artificial Earth satellites. The approach suggested is used in processing artificial Earth satellites observations at Nikolayev Astronomical Observatory (NAO). Examples are given of orbit calculations for some geostationary satellites.

**Key words**: Satellites: optical observations, satellite orbits.

## Introduction

Regular optical observations of geostationary artificial Earth satellites (GEO) have been carried out at Nikolaev Astronomical Observatory since 2002. The observations are made with two telescopes by using a "combined method" which was suggested by Nikolayev astronomers in 2000 Kovalchuk at al.(2000): with a multichannel telescope (MKT) (D=120 mm, F=2040 mm) and a speedy automatic complex (SAC) (D=300 mm, F=1500 mm). When using MKT telescopes the active telecommunication GEO are observed as a continious row within 2 or 5 howrs, when observing with SAC passive GEO (cosmic debris) are seen as short series only 20 minutes long in every two hours. We have already obtained and stored considerable bulk of observations. In order to estimate the accuracy of satellite observation, the knowledge of trajectory motion is needed. As is known, for the calculation of a satellite orbit it is necessary to take into account a lot of perturbing forces – the Earth's nonsphericity, the Moon's, the Sun's gravity, as well as atmospere resistance, the light pressure and so on. However, if it is necessary to obtain osculatory keplerian orbital elements for the epoch of observation, wilhout taking interest in a prolonged prediction of the satellite motion, this problem can be solved comparatively in a non-complicated way. Created and tested at the obtained NAO observations GEO algorithm for calculating osculatory elements has shown a good stability and convergence in calculating process. On the basis of the suggested software it is possible to rapidly and efficiently evaluate the error of observations due to comparing the individual observation with the satellite position on the osculating orbit.

## 1. The structure of calculations

In calculating, the system the Earth-satellite is examined within the frames of the problem with 2 bodies and is considered isolated. A twoaxial ellipsoid of rotation is taken for the Earth's form. At some moments of time ti the angular observations in the 2rd equatorial system $\alpha_i, \delta_i, i = 1, 2, ..., N$ are obtained from the Earth's surface.

The geocentric observer's position at the moment $t_i$, a radius-vector of the observing site $\vec{R}_i$ can be found if the geographical latitude of observing site $\varphi$ and local sidereal time $s_i$ are known Abalakin at al. (1971), Aksenov (1977):

$$R_{xi} = -G_1 \, cos\varphi \, coss_i,$$

$$R_{yi} = -G_1 \, cos\varphi \, sins_i,$$

$$R_{zi} = -G_2 \, sin\varphi,$$

where

$$G_1 = \frac{1}{\sqrt{1 - (2f - f^2 \sin^2 \varphi)}} + h,$$

$$G_2 = \frac{(1-f)^2}{\sqrt{1-(2f-f^2\sin^2\varphi)}} + h,$$

f – the Earth's polar compression,

h – altitude of the observing site above the sea level.

The process of orbit determination is divided into two stages: initial orbit determination – an approximate construction of a wholly unknown orbit initiallv and improvement of the orbit.

### *1.1. An initial orbit determination*

An initial orbit determination is carried out by using Laplas method Escobal (1965). Theoretically, for the initial orbit determination only three observations of the satellite positions are needed. This method is based upon the investigation of differential equation of celestial body motion

$$\frac{d^2\vec{r}}{dt^2} = -k_E^2 M_E \frac{\vec{r}}{r^3},$$

where

$\vec{r}$ is a geocentric satellite radius-vector, $k_E = 0.07436574 \frac{r.e.^{3/2}}{min\, m.e.^{1/2}}$ is a geocentric gravitational constant, $M_E$ – the Earth's mass.

Passing in these differential equations to the modified time we obtain

$$\frac{d^2\vec{r}}{dt^2} = \ddot{\vec{r}} = -\frac{\vec{r}}{r^3},$$

where

$$\tau \equiv k_E(t-t_0),$$

$t_0$ is the time referred to the beginning of the year, t is nowdays.

The unit vector $\vec{L}_i$ directed along the vector of inclined distance $\rho_i\vec{L}_i = \vec{\rho}_i$ of the satellite:

$$\vec{L}_i = \begin{pmatrix} L_x \\ L_y \\ L_z \end{pmatrix} = \begin{pmatrix} cos\delta_i\, cos\alpha_i \\ cos\delta_i\, sin\alpha_i \\ sin\delta_i \end{pmatrix}_i, i = 1,2,3.$$

Differentiating the previous equation twice we substitute the second derivative $\ddot{\vec{r}}$ and taking into account $\vec{r} = \rho\vec{L} - \vec{R}$, we obtain

$$\ddot{\rho}\,\vec{L} + 2\,\dot{\vec{L}}\dot{\rho} + \rho\Big(\ddot{\vec{L}} + \frac{\vec{L}}{r^3}\Big) = \ddot{\vec{R}} + \frac{\vec{R}}{r^3}.$$

The vector $\vec{L}$ is known from observations, the radius-vector $\vec{R}$ has been found earlier; the derivatives $\dot{\vec{L}},\ddot{\vec{L}},\dot{\vec{R}},\ddot{\vec{R}}$ can be determined numerically by using the Lagrangian polynomial for three nodes.

For the second observation we have

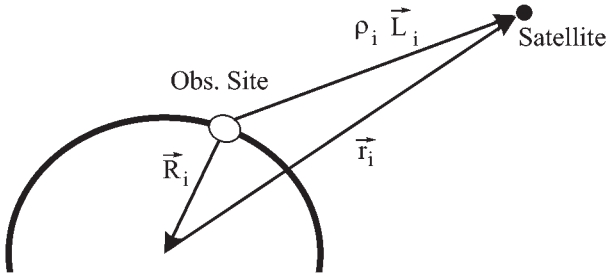


Figure 1: Basic vectors of the model

$$\dot{\vec{L}}_2 = \frac{\tau_3}{\tau_1(\tau_1-\tau_3)}\vec{L}_1 - \frac{\tau_1+\tau_3}{\tau_1\tau_3}\vec{L}_2 - \frac{\tau_1}{\tau_3(\tau_3-\tau_1)}\vec{L}_3,$$

$$\ddot{\vec{L}}_2 = \frac{2}{\tau_1(\tau_1-\tau_3)}\vec{L}_1 + \frac{2}{\tau_1\tau_3}\vec{L}_2 + \frac{2}{\tau_3(\tau_3-\tau_1)}\vec{L}_3,$$

$$\dot{\vec{R}}_2 = \frac{\tau_3}{\tau_1(\tau_1-\tau_3)}\vec{R}_1 - \frac{\tau_1+\tau_3}{\tau_1\tau_3}\vec{R}_2 - \frac{\tau_1}{\tau_3(\tau_3-\tau_1)}\vec{R}_3,$$

$$\ddot{\vec{R}}_2 = \frac{2}{\tau_1(\tau_1-\tau_3)}\vec{R}_1 + \frac{2}{\tau_1\tau_3}\vec{R}_2 + \frac{2}{\tau_3(\tau_3-\tau_1)}\vec{R}_3,$$

where $\tau_1 = k_E(t_1 - t_2)$, $\tau_3 = k_E(t_3 - t_2)$.

Taking into account that $r_2$ is known, we write the system in three scalar equations

$$\ddot{\rho}_2\, L_{2x} + 2\,\dot{L}_{2x}\dot{\rho}_2 + \rho_2\Big(\ddot{L}_{2x} + \frac{L_{2x}}{r_2^3}\Big) = \ddot{R}_{2x} + \frac{R_{2x}}{r_2^3},$$

$$\ddot{\rho}_2\, L_{2y} + 2\,\dot{L}_{2y}\dot{\rho}_2 + \rho_2\Big(\ddot{L}_{2y} + \frac{L_{2y}}{r_2^3}\Big) = \ddot{R}_{2y} + \frac{R_{2y}}{r_2^3},$$

$$\ddot{\rho}_2\, L_{2z} + 2\,\dot{L}_{2z}\dot{\rho}_2 + \rho_2\Big(\ddot{L}_{2z} + \frac{L_{2z}}{r_2^3}\Big) = \ddot{R}_{2z} + \frac{R_{2z}}{r_2^3},$$

The determinant of this system is easily brought into the form

$$D_\Delta = 2\begin{vmatrix} L_{2x} & \dot{L}_{2x} & \ddot{L}_{2x} \\ L_{2y} & \dot{L}_{2y} & \ddot{L}_{2y} \\ L_{2z} & \dot{L}_{2z} & \ddot{L}_{2z} \end{vmatrix}.$$

By the Kramer rule, considering $D_\Delta \neq 0$,

$$\rho_2 = 2\frac{\begin{vmatrix} L_{2x} & \dot{L}_{2x} & \ddot{R}_{2x} \\ L_{2y} & \dot{L}_{2y} & \ddot{R}_{2y} \\ L_{2z} & \dot{L}_{2z} & \ddot{R}_{2z} \end{vmatrix}}{D_\Delta} + 2\frac{\begin{vmatrix} L_{2x} & \dot{L}_{2x} & R_{2x} \\ L_{2y} & \dot{L}_{2y} & R_{2y} \\ L_{2z} & \dot{L}_{2z} & R_{2z} \end{vmatrix}}{r_2^3 D_\Delta},$$

and similarly

$$\dot{\rho}_2 = \frac{\begin{vmatrix} L_{2x} & \ddot{R}_{2x} & \ddot{L}_{2x} \\ L_{2y} & \ddot{R}_{2y} & \ddot{L}_{2y} \\ L_{2z} & \ddot{R}_{2z} & \ddot{L}_{2z} \end{vmatrix}}{D_\Delta} + \frac{\begin{vmatrix} L_{2x} & R_{2x} & \ddot{L}_{2x} \\ L_{2y} & R_{2y} & \ddot{L}_{2y} \\ L_{2z} & R_{2z} & \ddot{L}_{2z} \end{vmatrix}}{r_2^3 D_\Delta}.$$

Introducing notations

$$D_a = \begin{vmatrix} L_{2x} & \dot{L}_{2x} & \ddot{R}_{2x} \\ L_{2y} & \dot{L}_{2y} & \ddot{R}_{2y} \\ L_{2z} & \dot{L}_{2z} & \ddot{R}_{2z} \end{vmatrix}, \; D_b = \begin{vmatrix} L_{2x} & \dot{L}_{2x} & R_{2x} \\ L_{2y} & \dot{L}_{2y} & R_{2y} \\ L_{2z} & \dot{L}_{2z} & R_{2z} \end{vmatrix},$$

$$D_c = \begin{vmatrix} L_{2x} & \ddot{R}_{2x} & \ddot{L}_{2x} \\ L_{2y} & \ddot{R}_{2y} & \ddot{L}_{2y} \\ L_{2z} & \ddot{R}_{2z} & \ddot{L}_{2z} \end{vmatrix}, \; D_d = \begin{vmatrix} L_{2x} & R_{2x} & \ddot{L}_{2x} \\ L_{2y} & R_{2y} & \ddot{L}_{2y} \\ L_{2z} & R_{2z} & \ddot{L}_{2z} \end{vmatrix},$$

we have

$$\rho_2 = 2\frac{D_a}{D_\Delta} + \frac{2}{r_2^3}\frac{D_b}{D_\Delta},$$

$$\dot{\rho}_2 = \frac{D_c}{D_\Delta} + \frac{2}{r_2^3}\frac{D_d}{D_\Delta},$$

where all the determinants $D, D_a, D_b, D_c, D_d$ are known. If we introduce the equation symbols

$$A = 2\tfrac{D_a}{D_\Delta},\; B = 2\tfrac{D_b}{D_\Delta},\; C = \tfrac{D_c}{D_\Delta},\; D = \tfrac{D_d}{D_\Delta},$$

and add here an evident geometric bond (theorem of cosines)

$$r_2^2 = \rho_2^2 - 2\rho_2 \vec{L}_2 \vec{R}_2 + R_2^2,$$

taking into account that the scalar product of two known vectors in the coordinate form is

$$-2\vec{L}_2\vec{R}_2 = -2(L_{2x}R_{2x} + L_{2y}R_{2y} + L_{2z}R_{2z}) \equiv C_S$$

then the problem is reduced to solving the system of three nonlinear equations with three unknowns:

$$\rho_2 = A + \tfrac{B}{r_2^3},\; \dot{\rho}_2 = C + \tfrac{D}{r_2^3},\; r_2^2 = \rho_2^2 + C_S\,\rho_2 + R_2^2.$$

Solving it by numerical methods we can find all the unknown scalars $\rho_2, \dot{\rho}_2, r_2$. After this we find vectors as well

$$\vec{r}_2 = \rho_2\vec{L}_2 + \vec{R}_2,\; \dot{\vec{r}}_2 = \dot{\rho}_2\,\vec{L}_2 + \rho_2\,\dot{\vec{L}}_2 + \dot{\vec{R}}_2,$$

from which it is easy to pass over to Keplerian orbital elements of the satellite.

*1.2. Orbital elements improvement*

At the next stage of calculations the improvement of orbital elements obtained by differential correction takes place Escobal (1965).

Let for the given satellite the measurements of angular coordinates be carried out which we conventionally designate by letter $A_0$. Using the first obtained approximation of orbital elements for the corresponding moments we calculate angular coordinate values. Let $A_c$ denote the results obtained. If the orbital elements have been determined correct, the residual $\Delta = A_0 - A_c$ must be equal to zero. However, commonly this residual does not turn into zero. This testifies to the inaccuracy of initial orbit determination, to the errors of observing site position determination, to the presence of perturbations influencing the satellite when it moves from the p osition towards the epoch to any other position.

Let us we residuals $\Delta_i$ obtained which represent the differences between observational results and calculated positions for the moments of observation $t_i$.

Thus, the vector of state

$$\left[\vec{r}_2, \dot{\vec{r}}_2\right]_{t=t_2} = \left[x_2, y_2, z_2, \dot{x}_2, \dot{y}_2, \dot{z}_2,\right]_{t=t_2}$$

is determined in the first approximation. Suppose further, that the satellite's positions and velocities are precomputed for two moments of time

$$\left[x_i, y_i, z_i, \dot{x}_i, \dot{y}_i, \dot{z}_i,\right]_{t=t_i}, i = 1, 3.$$

Then for all the moments of time $t_i$ $(i = 1, 2, 3)$ we can find topocentric satellite's coordinates $\alpha_{tc}, \delta_{tc}$ – these are calculated values of measured magnitudes. Moreover, there are measured values of topocentric coordinates corresponding to moments $t_i$, so

$$\Delta\alpha_i = (\alpha_{t0})_i - (\alpha_{tc})_i,$$

$$\Delta\delta_i = (\delta_{t0})_i - (\delta_{tc})_i$$

represent 6 residuals. These residuals show the degree of perturbations affecting the orbit and the magnitude of the above inaccuracies.

As the measured angles are functions of a state vector at some arbitrary epoch, they can be presented in the form of functions.

$$\alpha_t = \alpha_t\Big(x_2, y_2, z_2, \dot{x}_2, \dot{y}_2, \dot{z}_2\Big),$$

$$\delta_t = \delta_t\Big(x_2, y_2, z_2, \dot{x}_2, \dot{y}_2, \dot{z}_2\Big).$$

Substituting differentials of these functions for finite increments:

calculated. Because of errors in observations, inaccuracies of observational site coordinates and deviation of the satellite motion from the Keplerian orbit the discrepancies between the observed and estimated $(O-C)$ positions increase faster and faster in the course of time. Much better agreement with a number of observation is attained if a series points for the orbit determination is located at the beginning, in the middle and at the end of the series. However, it is evident that the orbit determination from three points will inevitably result in observational information losses.

*1.3 The orbit improvement by using all the observations*

The described method of differential corrections or differential orbit correlation has been extended for N-observations. In this case we don't obtain 6 but 2N conventional equation of the form

$\Delta\alpha_i = \frac{\partial\alpha_i}{\partial x_k}\Delta x_k + \frac{\partial\alpha_i}{\partial y_k}\Delta y_k + \frac{\partial\alpha_i}{\partial z_k}\Delta z_k + \frac{\partial\alpha_i}{\partial \dot{x}_k}\Delta\ \dot{x}_k + \frac{\partial\alpha_i}{\partial y_k}\Delta\ \dot{y}_k + \frac{\partial\alpha_i}{\partial z_k}\Delta\ \dot{z}_k,$

$\Delta\delta_i = \frac{\partial\delta_i}{\partial x_k}\Delta x_k + \frac{\partial\delta_i}{\partial y_k}\Delta y_k + \frac{\partial\delta_i}{\partial z_k}\Delta z_k + \frac{\partial\delta_i}{\partial \dot{x}_k}\Delta\ \dot{x}_k + \frac{\partial\delta_i}{\partial \dot{y}_k}\Delta\ \dot{y}_k + \frac{\partial\delta_i}{\partial \dot{z}_k}\Delta\ \dot{z}_k,\ i = 1, 2, ..., N.$

with six unknown corrections to the vector of state at the moment $t_k$ - $\Delta x_k, \Delta y_k, \Delta z_k, \Delta\ \dot{x}_k, \Delta\ \dot{y}_k, \Delta\ \dot{z}_k$.

This system is solved by the least square method, as a result we have 6 normal equations of the form

$\lambda_j = a_j\Delta x_k + b_j\Delta y_k + c_j\Delta z_k + d_j\Delta\ \dot{x}_k + e_j\Delta\ \dot{y}_k + f_j\Delta\ \dot{z}_k$, where j=1,2,...6.

Or in the matrix form

$$\begin{bmatrix}\lambda_1\\ \lambda_2\\ \lambda_3\\ \lambda_4\\ \lambda_5\\ \lambda_6\end{bmatrix} = M_N \begin{bmatrix}\Delta x_N\\ \Delta y_N\\ \Delta z_N\\ \Delta\ \dot{x}_N\\ \Delta\ \dot{y}_N\\ \Delta\ \dot{z}_N\end{bmatrix}, \text{ where}$$

$$M_N = \begin{bmatrix} a_1 & b_1 & c_1 & d_1 & e_1 & f_1\\ a_2 & b_2 & c_2 & d_2 & e_2 & f_2\\ a_3 & b_3 & c_3 & d_3 & e_3 & f_1\\ a_4 & b_4 & c_4 & d_4 & e_4 & f_4\\ a_5 & b_5 & c_5 & d_5 & e_5 & f_5\\ a_6 & b_6 & c_6 & d_6 & e_6 & f_6\end{bmatrix}.$$

The further decision course is not different from the method described above for three observations.

## 2. The obtained result

The described method of orbital elements determination was algorithmized and the software was created on its basis.The following examples illustrate the processing of GEO observations carried out at Scientific Reseach Institute NAO.

The use of this software enables to solve various problems starting from finding out the malfunction moments of the observational apparatus complex to high-accurate determination for telecommunication GEO orbits observed in long uniform series and "cosmic refuse".

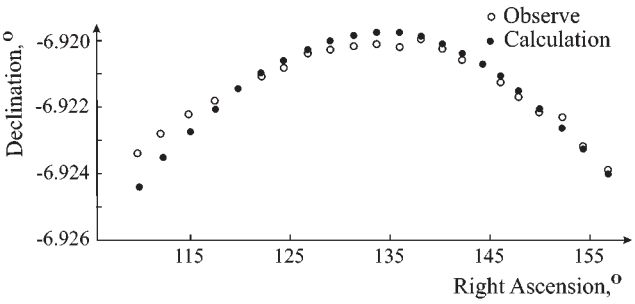


Figure 2: The positions of satellite 25515 on the 17th-18th, January, 2003.

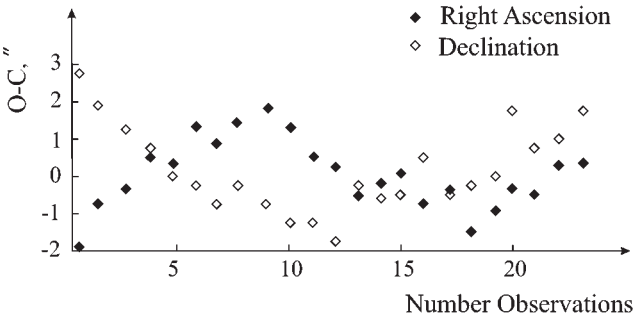


Figure 3: Residuals $O-C$ of satellite 25515 within 17-18th, January, 2003.

The absolute values $O-C$ proved to be rather significant (Fig.3). Observational data analysis shows that in the middle of observations after point 13 a malfunction in the apparatus part has taken place. Therefore, the first and the second part of the evening should be processed independently. The values of residuals $O-C$ do not exceed $1'' - 1.5''$.

The procedure suggested was tested on a short series of observations for passive geostationars (cosmic refuse) and it showed a good convergence (Fig.4,5).

In case within an observational period the perturbed accelerations can be neglected (for the high satellites it is justified) and the observational site is known with

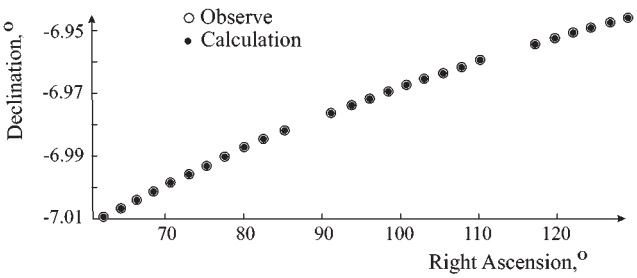


Figure 4: The positions of satellite 27441 during the 7-8th of November 2003

orbit determination is located at the beginning, in the middle and at the end of the series. However, it is evident that the orbit determination from three points will inevitably result in observational information losses.

*1.3. The orbit improvement by using all the observations*

The described method of differential corrections or differential orbit correlation has been extended for N-observations. In this case we don't obtain 6 but 2N conventional equation of the form

$$\Delta\alpha_i = \frac{\partial\alpha_i}{\partial x_k}\Delta x_k + \frac{\partial\alpha_i}{\partial y_k}\Delta y_k + \frac{\partial\alpha_i}{\partial z_k}\Delta z_k + \frac{\partial\alpha_i}{\partial x_k}\Delta\ \dot{x}_k + \frac{\partial\alpha_i}{\partial y_k}\Delta\ \dot{y}_k + \frac{\partial\alpha_i}{\partial z_k}\Delta\ \dot{z}_k,$$

$$\Delta\delta_i = \frac{\partial\delta_i}{\partial x_k}\Delta x_k + \frac{\partial\delta_i}{\partial y_k}\Delta y_k + \frac{\partial\delta_i}{\partial z_k}\Delta z_k + \frac{\partial\delta_i}{\partial\dot{x}_k}\Delta\ \dot{x}_k + \frac{\partial\delta_i}{\partial y_k}\Delta\ \dot{y}_k + \frac{\partial\delta_i}{\partial z_k}\Delta\ \dot{z}_k,\ i = 1, 2, ..., N.$$

with six unknown corrections to the vector of state at the moment $t_k$ – $\Delta x_k, \Delta y_k, \Delta z_k, \Delta\ \dot{x}_k, \Delta\ \dot{y}_k, \Delta\ \dot{z}_k$.

This system is solved by the least square method, as a result we have 6 normal equations of the form

$$\lambda_j = a_j\Delta x_k + b_j\Delta y_k + c_j\Delta z_k + d_j\Delta\ \dot{x}_k + e_j\Delta\ \dot{y}_k + f_j\Delta\ \dot{z}_k,$$ where j=1,2,...6.

Or in the matrix form

$$\begin{bmatrix} \lambda_1 \\ \lambda_2 \\ \lambda_3 \\ \lambda_4 \\ \lambda_5 \\ \lambda_6 \end{bmatrix} = M_N \begin{bmatrix} \Delta x_N \\ \Delta y_N \\ \Delta z_N \\ \Delta\ \dot{x}_N \\ \Delta\ \dot{y}_N \\ \Delta\ \dot{z}_N \end{bmatrix},$$

where

$$M_N = \begin{bmatrix} a_1 & b_1 & c_1 & d_1 & e_1 & f_1 \\ a_2 & b_2 & c_2 & d_2 & e_2 & f_2 \\ a_3 & b_3 & c_3 & d_3 & e_3 & f_1 \\ a_4 & b_4 & c_4 & d_4 & e_4 & f_4 \\ a_5 & b_5 & c_5 & d_5 & e_5 & f_5 \\ a_6 & b_6 & c_6 & d_6 & e_6 & f_6 \end{bmatrix}.$$

The further decision course is not different from the method described above for three observations.

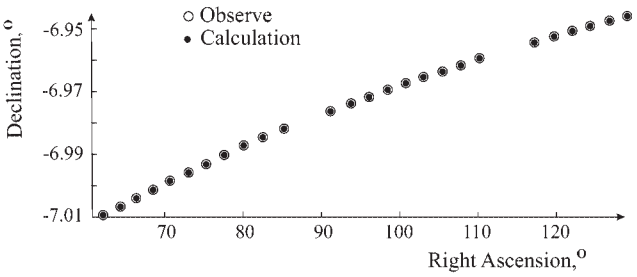


Figure 4: The positions of satellite 27441 during the 7-8th of November 2003.

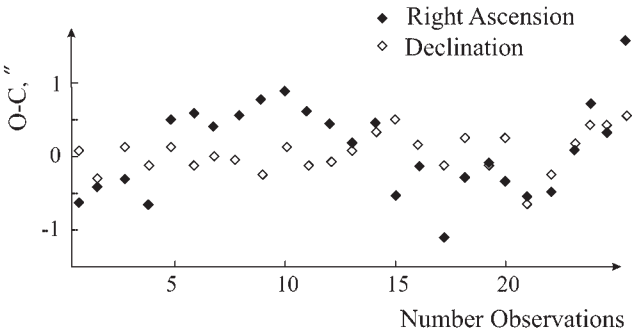


Figure 5: Residuals $O - C$ of satellite 27441 within 7-8th of November 2003.

## 2. The obtained result

The described method of orbital elements determination was algorithmized and the software was created on its basis.The following examples illustrate the processing of GEO observations carried out at Scientific Reseach Institute NAO.

The use of this software enables to solve various problems starting from finding out the malfunction moments of the observational apparatus complex to high-accurate determination for telecommunication GEO orbits observed in long uniform series and "cosmic refuse".

The absolute values $O-C$ proved to be rather significant (Fig. 3). Observational data analysis shows that in the middle of observations after point 13 a malfunction in the apparatus part has taken place. Therefore, the first and the second part of the evening should be processed independently. The values of residuals $O-C$ do not exceed $1'' - 1.5''$.

The procedure suggested was tested on a short series of observations for passive geostationars (cosmic refuse) and it showed a good convergence (Fig. 4, 5).

In case within an observational period the perturbed accelerations can be neglected (for the high satellites it is justified) and the observational site is known with a sufficient accuracy (the error does not exceed several metres), then the value of residuals $O - C$ can serve as an accuracy criterion for observations. On this basis the software enables to evaluate the accuracy of the

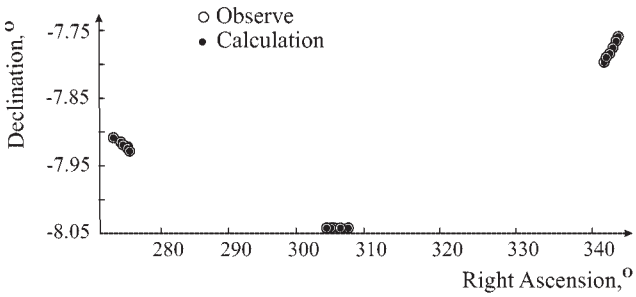


Figure 6: The positions of satellite 95035 within 21st-22nd of July 2004.

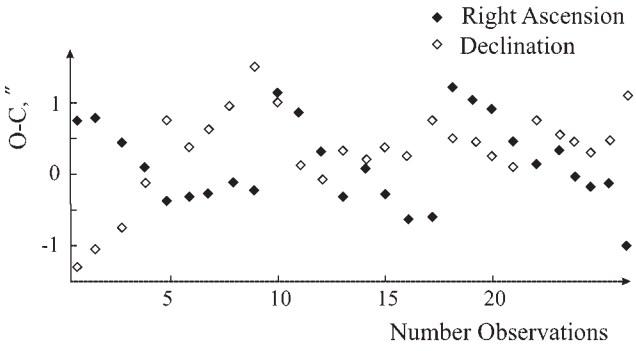


Figure 7: Residuals $O - C$ of satellite 95035 during 21st and 22nd of July 2004.

calculated orbital elements.

For this purpose, in the numerical model each observed coordinate pair is incremented within the limits of O to $O - C$. The value of increment satisfies a uniform distribution. Based upon modified observed coordinates the modified orbital elements are calculated. This process is repeated 150 times, thereafter from the obtained data files of modified orbital elements, their average values and root-mean-square deviations are computed. The value of a root-mean-square orbital element deviation from the mean value of data files specifies the accuracy of this element determination derived from angular observations.

An example of a good continious series of observations can be given. It was the evening of the 7-8th of November, 2003, satellite 27441 was observed. The root-mean-square deviations of orbital elements are as follows:

$p = 42160 \pm 0.6$ km,
$e = 0.00026 \pm 0.00002$,
$M_0 = 224 \pm 4^o$,
$i = 0.05021 \pm 0.00004^o$,
$\omega = 179.9 \pm 0.8^o$,
$\Omega = 84.02 \pm 0.05^o$.

The example of a good series of observations is the evening on the 21st-22nd July, 2004, satellite 95035. The root-mean-square deviations of orbital elements are as follows:

$p = 38307.1 \pm 1.3$ km,
$e = 0.001497 \pm 0.000005$,
$M_0 = 310 \pm 3^o$,
$i = 0.96779 \pm 0.00005^o$,
$\omega = 350.6 \pm 0.7^o$,
$\Omega = 32.01 \pm 0.002^o$.

## Summary

On the Laplas method basis with further improving the method of differential corrections, the software has been created which permits to carry out the primary processing of terrestrial optical observations of geostationary satellites. Though the process of calculations is of an iteration character, it converges rather fast, and in practice it has shown good stability. As a result, both the quality of observations and the expected accuracy of the satellite's orbital elements can be estimated. The possibilities of modern computer facilities enable to perform all the computations within several seconds. The procedure described has been tested and is successfully used at Scientific Reseach Institute "Nikolayev Astronomical observatory".

## References

Abalakin V.K., Aksenov E.P., Grebennikov E.A., Rjabov Y.A.: 1971, The reference manual on the celestial mechanics and astrodynamics, Nauka.

Aksenov E.P.: 1977, The theory of motion Earth artificial satellites, Nauka.

Escobal P.: 1965, Methods of orbit determination, New York-London-Sydney.

Kovalchuk A., Shulga A., Martynov M. in: *Combined CCD observational method of GSS //"Extension and connection of reference frames using ground based technique"*, Nikolaev, 2001, p.199-205.

# INTEGRATION OF DIFFERENTIAL EQUATION FOR CELESTIAL BODIES' MOTION BY THE RUNGE-KUTT METHOD IN THE THIRD ORDER

O. A. Bazyey, I. V. Kara
Department of Astronomy, Odessa National University
T.G.Shevchenko Park, Odessa 65014 Ukraine,
*creator@sky.od.ua*, *LionKIV@mail.ru*

ABSTRACT. Equations of celestial bodies' motion in coordinates are solved by numerical Runge-Kutt method. The coefficients of Runge-Kutt method in the 10th order are obtained. The solutions are compared by methods of different order, for this purpose Runge-Kutt methods of the 4th, 5th and 10th orders have been realized in programs.

**Key words**: numerical integration; numerical simulation; methods of integration.

The Runge-Kutt method (hereafter R-K) is the highest order for the developed explicit R-K methods for solving differential equations. This 17-staged method was constructed by Hairer (1978). The method provides accuracy not worse than $10^{-15}$. As is seen from the general scheme of R-K methods, it is necessary to know $a_{ij}$, $b_i$, $c_i$ coefficients to construct an integration algorithm. In the general case these can be obtained from system solutions of linear equations with matrices of Wandermond type and free parameters. Hairer was thee first to obtain the above systems of linear equations. The analytical solution of these equation systems has been performed by us. At first coefficients ci and bi are determined from independent formulae with free parameters. Then nonzero coefficients $a_{ij}$ are calculated. All in all the calculation of 119 coefficients $a_{ij}$, $b_i$, $c_i$ for the R-K method of the 10th with the accuracy of 16 significant figures.

Table 1: The coefficients $c$ and $b$

| c | b |
|---|---|
| 0.00000000000000000 | 0.03333333333333333 |
| 0.50000000000000000 | -0.03333333333333333 |
| 0.52650910328800298 | -0.12000000000000000 |
| 0.78976365493200447 | 0.00000000000000000 |
| 0.39392357321878806 | 0.00000000000000000 |
| 0.76665400000000000 | -0.13000000000000000 |
| 0.28976365493200447 | -0.18000000000000000 |
| 0.10847769751115627 | 0.00000000000000000 |
| 0.35738424175967745 | 0.27742918851774318 |
| 0.88252766196473235 | 0.18923747814892349 |
| 0.64261575824032255 | 0.27742918851774318 |
| 0.11747233803526765 | 0.18923747814892349 |
| 0.76665400000000000 | 0.13000000000000000 |
| 0.28976365493200447 | 0.18000000000000000 |
| 0.52650910328800298 | 0.12000000000000000 |
| 0.50000000000000000 | 0.03333333333333333 |
| 1.00000000000000000 | 0.03333333333333333 |

Table 2: The coefficients $a_{ij}$

| | a |
|---|---|
| $a_{2,1}$ | 0.500000000000000000 |
| $a_{3,1}$ | 0.249297267442865990 |
| $a_{3,2}$ | 0.277211835845136990 |
| $a_{4,1}$ | 0.197440913733001120 |
| $a_{4,3}$ | 0.592322741199003350 |
| $a_{5,1}$ | 0.197320549901158990 |
| $a_{5,3}$ | 0.295083336687500560 |
| $a_{5,4}$ | -0.098480313369871490 |
| $a_{6,1}$ | 0.131313418369284120 |
| $a_{6,4}$ | 0.110154448085213840 |
| $a_{6,5}$ | 0.525186133545502040 |
| $a_{7,1}$ | 0.134200343335776690 |
| $a_{7,4}$ | 0.696089003913604790 |
| $a_{7,5}$ | 0.250497724903820550 |
| $a_{7,6}$ | -0.791023417221197550 |
| $a_{8,1}$ | 0.072218277827166180 |
| $a_{8,5}$ | -0.058336331150054700 |
| $a_{8,6}$ | 0.003047557905261750 |
| $a_{8,7}$ | 0.091548192928783030 |
| $a_{9,1}$ | 0.031255012451346830 |
| $a_{9,6}$ | 0.000109123767407210 |
| $a_{9,7}$ | 0.156725749578665400 |
| $a_{9,8}$ | 0.169294355962258020 |

| | a |
|---|---|
| $a_{10,1}$ | 0.011906555199089780 |
| $a_{10,6}$ | 0.283437053152611850 |
| $a_{10,7}$ | -0.416312681148122000 |
| $a_{10,8}$ | 0.264646513240441260 |
| $a_{10,9}$ | 0.738850221520711440 |
| $a_{11,1}$ | 0.023406547057290240 |
| $a_{11,6}$ | 0.094493110802080540 |
| $a_{11,7}$ | -0.272872353991762250 |
| $a_{11,8}$ | 0.224022150430302150 |
| $a_{11,9}$ | 0.604381676387011710 |
| $a_{11,10}$ | -0.030815372444599860 |
| $a_{12,1}$ | 0.045443773723211270 |
| $a_{12,6}$ | -0.001187993701161070 |
| $a_{12,7}$ | 0.012035612762074010 |
| $a_{12,8}$ | 0.075126916373159330 |
| $a_{12,9}$ | -0.018220889985728930 |
| $a_{12,10}$ | -0.000257153155717400 |
| $a_{12,11}$ | 0.004532072019430440 |
| $a_{13,1}$ | 0.178401191494440070 |
| $a_{13,4}$ | 0.110154448085213840 |
| $a_{13,5}$ | 0.525186133545502040 |
| $a_{13,6}$ | -0.489148527185302110 |
| $a_{13,7}$ | 0.932444760083765200 |
| $a_{13,8}$ | -0.774475454248542890 |
| $a_{13,9}$ | -1.054903091927034580 |
| $a_{13,10}$ | 0.131046704391395180 |
| $a_{13,11}$ | 0.587049782903478850 |
| $a_{13,12}$ | 0.620898052857084390 |
| $a_{14,1}$ | 0.130220809295963570 |
| $a_{14,4}$ | 0.696089003913604790 |
| $a_{14,5}$ | 0.250497724903820550 |
| $a_{14,6}$ | -0.758949296998121780 |
| $a_{14,7}$ | -0.171517080561449580 |
| $a_{14,8}$ | -0.370217728103958150 |
| $a_{14,9}$ | 0.124980912719016210 |
| $a_{14,10}$ | 0.003353109831913580 |
| $a_{14,11}$ | -0.006632530935512160 |
| $a_{14,12}$ | 0.429116584466715440 |
| $a_{14,13}$ | -0.037177853599988010 |
| $a_{15,1}$ | 0.249297267442865990 |
| $a_{15,2}$ | 0.277211835845136990 |
| $a_{15,6}$ | -0.145940581850349860 |
| $a_{15,7}$ | -0.799015888201494970 |
| $a_{15,13}$ | 0.145940581850349860 |
| $a_{15,14}$ | 0.799015888201494970 |
| $a_{16,1}$ | 0.500000000000000000 |
| $a_{16,3}$ | -0.807097065368871710 |
| $a_{16,15}$ | 0.807097065368871710 |
| $a_{17,1}$ | 0.057320857210991220 |
| $a_{17,2}$ | -0.500000000000000000 |
| $a_{17,3}$ | -0.897470162794317560 |
| $a_{17,6}$ | -1.039909940192961010 |
| $a_{17,7}$ | -0.407356461949683440 |
| $a_{17,8}$ | -0.182830381505614480 |
| $a_{17,9}$ | -0.333659682493437140 |
| $a_{17,10}$ | 0.395648533418683930 |

| | a |
|---|---|
| $a_{17,11}$ | 0.695056982748296490 |
| $a_{17,12}$ | 0.271487312143254720 |
| $a_{17,13}$ | 0.585423714778675740 |
| $a_{17,14}$ | 0.958819065841793960 |
| $a_{17,15}$ | 0.897470162794317560 |
| $a_{17,16}$ | 0.500000000000000000 |

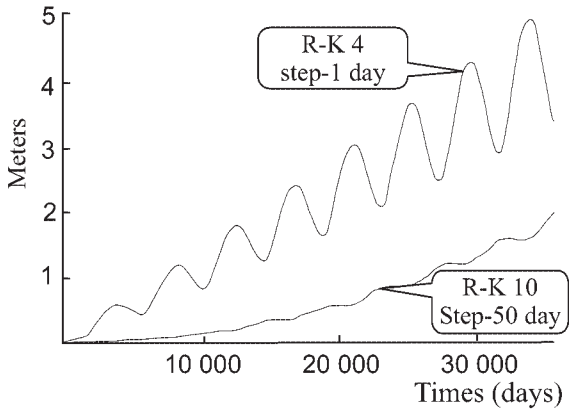


Figure 1: Accumultion of errors in integrating the motion: system of the Sun-Jupiter.

To illustrate the accuracy if R-K method of the 10th order (Kara, 2006), we have compared his solution with the accurate analytical one, and with a numerical solution by R-K method of the 4th order of a problem with 2 bodies in a pointwise approximation of the Sun-Jupiter and the Sun-Mercury system. The distance growth between analytical and numerical orbits is given in Fig.1 and Fig.2.

In case of the problem with N bodies there is not any analytical solution. Therefore the accuracy is estimated by Richardson method. The idea consists in our comparing simultaneosly two orbits in the node: orbits

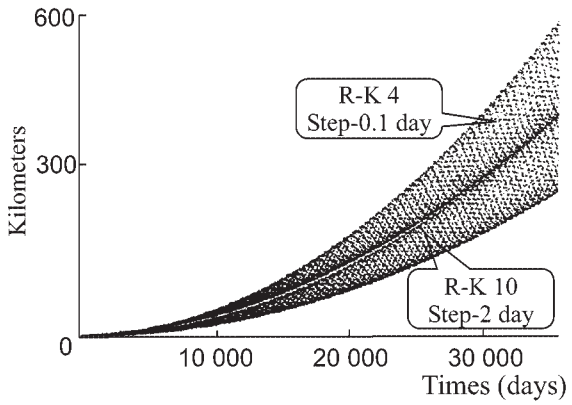


Figure 2: Accumultion of errors in integrating the motion: system of the Sun-Mercury.

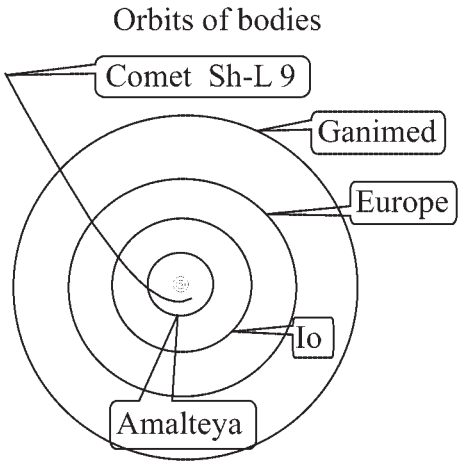


Figure 3: The orbit of Shoemaker - Levy 9 comet in joviocentric coordinate system (07.07.1990).

obtained with the whole and half-whole step of integration. The curve obtained like this is characterized by the growth of local itegration error. The comparison of error curves obtained by using the analytical method and a curve obtained by Richardson method demonstrates the growth of curves to be similar. The accuracy estimation by Richardson method can be obtained for the system with an arbitrary number of bodies. We have obtained the curves of integration error accumulation for the system the Sun - the Jupiter - the Saturn. These curves are similar to those in Fig.1 and Fig.2.

We can illustrate the use of R-K method of the 10th order for modeling motion in the solar system, as an example, consider the motion of comet Shoemacer-Levy 9. This well-known comet was captured by Jupiter in july 1992, and in july 1994 it collided with the planet. To determine initial conditions we took advantage of orbital element for the comet borrowing them from the paper by G. Sitarsky.

Two problems were set. The first problem by 29th of January the initial parameters for major planets of the solar system well have been obtained and equation of motions integrated. The second problem. Using the initial conditions obtained it is necessary to integrate the motion system approximately 200 years back for investigations the comet orbit evolution.

To solve the first problem the coordinates and velocities of major planets for 29th of January 1990 were borrowed from Astronomical Year - book 1990. In calculations the mass planets were used from the theory of DE405/LE405. The motion equations were integrated up to the moment of the 8th of July 1992. As a result of integration it was found that the moment of the first approximation was on the 7th of July 1992 at 18:36 of Universal Time, minimum distance between the comet and Jupiter amounted to 11000km (Fig.3).

This date differs from that shown in the paper by G. Sitarsky in 3.5 hours. Further integration within the frame of point model is impossible. At small reciprocal distances the tidal forces and perturbations arising because of nonsphericity of mass distribution in Jupiter are getting essential. Besides, we have not taken into account Jupiter's satellites influence.

To solve the second problem we took advantage of the same initial conditions. As a result of integration we have got a set of trajectories indicating the comet orbit evolution in the past. The comet orbit has not practically changed for the last 50 years of its existence.

As is seen from calculations, the comet orbit was more distant from the Sun before close approach Jupiter in January 1945. As a result of calculation the orbits lying between Jupiter and Saturn have been obtained. The outcome of this work is calculation of coefficients for the algorithm by R-K method 10 as accurate as 16 signs. This method can be successfully used for integration of celestial bodies motion in coordinates.

**References**

Hairer E.: 1978, A Runge-Kutta method of order 10, *J. Inst. Maths. Applics*, **21**, 47-59.

http://adsbit.harvard.edu G. Sitarski Motion of Comet D/Shoemaker-Levy 9 before the Breakup.

Kara I.V.: 2006, *Physics of space. Transactionses of 35-th International student's scientific conference.* The Ural State University, p. 221.

# THE MODELING OF THE CHROMOSPHERE OF THE R CrB STAR

E. Baranovsky[1], A. Rosenbush[2]

[1] SRI Crimean Astrophysical Observatory, Ukraine, Crimea, Nauchny, *edward@crao.crimea.ua*

[2] Main astronomical observatory NANU, Kyiv, Ukraine, *mijush@mao.kiev.ua*

ABSTRACT. An attempt is made to model some spectral properties of the stars with the R Coronae Borealis variability.

**Key words**: Stars: variable; stars: individual: R CrB.

The variability of R Coronae Borealis stars is usually explained as a consequence of the circumstellar carbon-rich dust formation. Absorption lines are replaced by emission lines when star is obscured by the dust cloud (see review by Clayton 1996, Rosenbush 1996) or by the dust envelope (Rosenbush 2000). The absorption by the dust decreases the photospheric radiation, but the extended chromosphere remains visible and it produces the emission lines.

We calculated the profiles of chromospheric lines in time of the obscuration and compared them to the profiles observed at minima. As a starting model chromosphere we used the model of Eps Gem star which is similar to R CrB by the $T_{eff}$ and gravity. As a model photosphere we took Asplund model (Asplund et al. 2000 and private communication). We used non-LTE program with a plane-parallel layers approach when calculating the source function but took into account the curvature of layers when calculating the emerging intensity. After trying many models we came to the conclusion that the model chromosphere in hydrostatic equilibrium is not suitable for the explanation of the observed emission of chromospheric lines. The extension and the mass of hydrostatic models are not big enough and the line emissions are too small. For the explanation of the observed emission the mass of chromosphere must be two orders higher as compared to that of hydrostatic models. The density of the chromosphere must be rather low, so that the extension of chromosphere would be 2-3 radii of the star. With such models we have received good agreement between observed and calculated profiles of $H_{alpha}$ and H and K Ca II lines both for undisturbed state of the star and for the minima of different depth. But we could not get the agreement for the D lines of Na I. The calculated

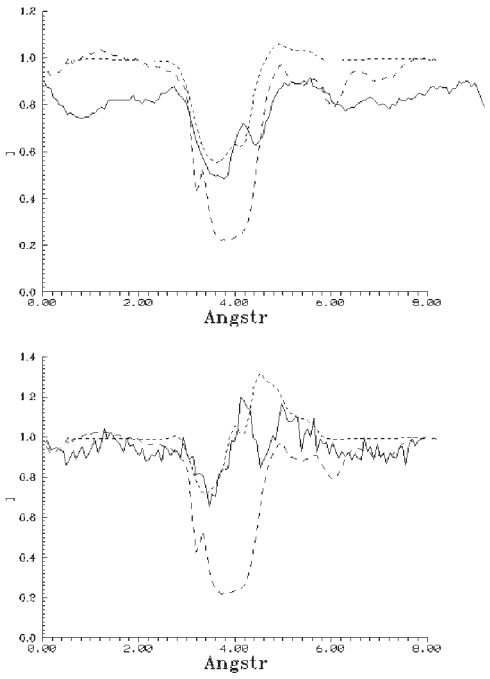


Figure 1: Calculated (short dashed) and observed (solid) profiles of D 2 Na I in minima with $2.4^m$ and $3.5^m$ weakening; long dashed- undisturbed profile.

profiles of D lines are much too narrow as compared to the observed ones for maximum and show very low emission for minimum.

We could get the agreement of the D line profiles only with the assumption that there exist around the star the cold envelope of Na I atoms. In the undisturbed state the envelope produces the additional absorption in the D lines. In the minimum the envelope, illuminated by the star radiation produces also the emission in the D lines induced by the resonance scattering in the D lines. The optical thickness of the envelope in the D 2 line is about 2-2.5. Nearly all radiation of the star in the D lines is absorbed in the envelope and after scattering goes away from star. In the minimum the

dust cloud screens the star but the envelope remains visible. The emission from the envelope is calculated by the same non-LTE program as by the emission from chromosphere, only in this case the primary source is determined by the scatter of star radiation on the Na I atoms.

The existence of Na I atoms beyond the chromosphere of the star is connected with mass loss of this star. Na I atoms are just a constituent of the material that flowed from the star and cooled to temperature below 1000 K.

We obtained the best agreement for D lines profiles with the envelope having the radial velocity 30-35 km/sec directed away from the star. In the final model the density is equal to $1.2^8$ in upper chromosphere and $1.0^{10}$ in low chromosphere, the turbulent velocity varies from 6 km/sec to 1.2 km/sec, the temperature from 7000 K to 5000 K. The extension of the chromosphere is about 3 star radii.

The comparison between the calculated and observed profiles of D 2 line for minimum is shown on fig.1.

**References**

Clayton G.C.: 1996, *Publ. Astron. Soc. Pacif*, **108**, 225.

Rosenbush A.E.: 1996, *Astrophysics*, **39**, 78.

Rosenbush A.E.: 2000, *Astrophysics*, **43**, 435.

Asplund M. et al.: 2000, *A&A*, **353**, 287.

# HISTOGRAMS OF PERIODS DISTRIBUTION AND MODE IDENTIFICATIONS OF RRc LYR STARS

Vladimir P. Bezdenezhnyi
Department of Astronomy, Odessa National University
T.G.Shevchenko Park Odessa 65014 Ukraine
*astro@paco.odessa.ua*

ABSTRACT. On the base of GCVS (General Catalogue of Variable Stars) sampling (381 stars with the known periods) has been carried out the analysis of periods of RRc Lyr stars. It has been given an interpretation of the histogram of periods distribution of these stars. All the peaks in the histogram were identified as radial overtones and their harmonics. It was proposed a new classification of these variable stars according to their mode identifications. The comparisons with the distributions of periods of $\delta$ Sct and other pulsating stars are carried out.

**Key words:** Stars: $\delta$ Scuti, RR Lyrae, RV Tau, classical Cepheids, bimodal Cepheids, $\beta$ Cep stars, histogram of periods distribution, mode identifications

RR Lyrae stars have been studied for over a century now, and play an important role in astrophysics. They served as standard candles to fix the cosmological distance scale, these stars were considered to be prototypes of radially pulsating stars. They are radially pulsating giant A-F stars having amplitudes from 0.2 to 2 mag in V, belong to the galactic halo (Population II); often found in globular clusters. These pulsating variables have periods of 0.2-1.2 days. Some of these stars exhibit the Blazhko Effect - periodic variations in period and lightcurve.

Depending on their light curves and pulsation characteristics RR Lyrae stars are divided into different subclasses (Bailey classification). Three subtypes are recognized: RRab - the RRab stars, with high-amplitude non-sinusoidal light curves, pulsate in the fundamental radial mode. They have periods from 0.3 to 1.2 days, and amplitudes from 0.5 to 2 mag in V. RRc - RR Lyrae variables with nearly symmetric, sometimes sinusoidal, light curves, periods from 0.2 to 0.5 days, and smaller amplitudes not greater than 0.8 mag in V. They pulsate in the radial first overtone. RRd or RR(B) - bimodal (or double - mode) RR Lyrae variables showing two simultaneously operating pulsation modes (fundamental F and the first overtone 1H). RRe - Variables of the RR Lyrae type, which are the second overtone radial pulsators, are discussed recently.

In present work we analyzed GCVS IV sample of periods of RRc Lyr stars (381 variables with the known periods) for searching for the regularities in their periods distribution and identifications of peaks of their periods. Three histograms have been constructed for three different intervals of periods with three steps dP: 0.02, 0.01 and 0.005 days for control. The first histogram of periods distribution (for dP=0.02 days) shows two broad peaks at periods $P_0$=0.33 and $P_1$=0.29 days. The ratio of these periods is equal to 0.88. The theoretical ratio for periods $P_g$ and $P_{1H}$ is 0.(8). Overtone $P_g$ was introduced by author (Bezdenezhnyi, 1994a,b) earlier. For this rough step of period fragmentation we have small precision of period determination. Therefore, two more histograms of period distribution (for dP=0.01 and 0.005 days) were constructed. The latter one is present in Figure 1.

In the network of workable by author (see Bezdenezhnyi, 1994a,b; 1997a,b,c,d,e; 2001a,b,; 2004) harmonic analysis we cannot present all the peaks of periods in one consistent sequence. We can see three harmonic sequencies respective to three splite primary (fundamental) periods: $P_\alpha$ =0.1081, $P_\beta$=0.1126 and $P_\gamma$=0.1042 days. At that $P_\beta$ coincide with radial fundamental period of the Sun oscillation. Periods $P_\alpha$ and $P_\beta$ and their sequences are found in $\beta$ Cep stars too (Bezdenezhnyi, 2001a). We can transform periods into respective frequencies (which are additive): 9.25, 8.88 and 9.60 $\frac{c}{d}$. Mean difference between central and side frequencies is 0.36 $\frac{c}{d}$ that gives spliting period of 2.8 days or 11.1 days, taking into account that we have periods four-multiple to fundamental ones. Thus, we have three groups of periods, inside of which multiple relations take place. In periods distridutios are present the following periods of $\alpha$-sequence: $4P_s$=0.230, $4P_{2H}$=0.258, $4P_g$=0.288, $4P_{1H}$=0.328, $4P_e$=0.345, $4P_r$=0.388, $4P_f$=0.428, $8P_s$=0.462 days. The solar or $\beta$- sequence is present with periods: $2P_f$=0.222, $4P_s$=0.238, $4P_{2H}$=0.270, $4P_g$=0.298, $4P_{1H}$=0.338, $4P_e$=0.358, $4P_r$=0.398, $4P_f$=0.451, $8P_s$=0.475, $8P_{2H}$= 0.532, $8P_g$=0.598, $9P_{2H}$=0.608 days. These two sequencies are present rather enough.

Two more remaining periods of 0.308 and 0.368 days belong to the third sequence. The ratio of these periods is equal to 0.834, that is nearly to the ratio $\frac{5}{6}$=0.833. For the ratio of periods $P_f$ and $P_{2H}$ is $\frac{5}{3}$, than $\frac{5}{6}$ is the ratio $P_f$ to $2P_{2H}$. The ratio of period of 0.308 days to the fundamental one (0.1042 days) of $\gamma$-sequence is 2.96 - nearly to integer 3.We take period of 0.308 days for $4P_{1H}$ of this sequence, than period of 0.368 days may be identified with $4P_r$ of $\gamma$-sequence. This period evidently is observed in RS Boo (P=0.377 days). RW Dra has period of 0.443 days that is multiple with fundamental one (0.1126 days) of $\beta$-sequence. Their ratio is 3.934, that is nearly to integer 4. Period of 0.522 days for Y Leo Minor gives ratio 5.01 to $P_f$=0.1042 days - the fundamental period of $\gamma$-sequence. Period of 0.567 days of RR Lyr is multiple to the fundamental period of $\beta$-sequence. This ratio is 5.04 - nearly coinside with integer 5.

Thus, individual values of periods of RRc Lyr stars confirm their commensurability with these three primary periods of above sequencies. One of this periods (0.1126 days) coincide with fundamental radial period of the Sun oscillation. But, apparently, this period is not the main one. It appears (as well as the period of 0.1042 days) because of splitting of period of 0.1081 days thanks to the influence of disturbing period of 11.1 days. Histograms of periods distribution of radial pulsating stars of different types: (RR Lyr, RV Tau, $\beta$ Cep, $\delta$ Sct, classical and bimodal Cepheids and other ones, and even for pulsars (Bezdenezhnyi, 1994a,b; 1997a,b,c,d,e; 2001a,b; 2004, 2005a,b) only reflect this commensurability. At that, for different types of radial pulsating stars the ratios of their periods to one of above three fundamental periods change in rather large ranges, reflecting big differences in their periods. At that point of view a lot of periods may be identify with radial ones without attracting non-radial oscillations. Our Sun is a variable star with radial oscillations of small amplitude, it follows the same law. The ratio of its period to the fundamental one is just equal 1! For different $RR_c$ Lyr stars these ratios are equal from 2 to 5, for $\beta$ Cep stars - from 0.25 to 6, for $\delta$ Sct stars - from 0.1 to 2, for RV Tau stars they are in the range 260-3330 (Bezdenezhnyi, 2005a in this volume). For bimodal Cepheids (using periods data from Berdnikov (1993)) ratios are in range 13-37. So for bimodal Cepheids individual ratios are equal 18.999 for $P_0$ of TU Cas and 19.002 for $P_1$ of VX Pup! Our analysis (Bezdenezhnyi, 1997a) has given more detailed subdivision of bimodal Cepheids, pulsating in the frequencies $f_{1H}$ and $f_s$, into two subgroups. The average ratios of periods P1/P0 for two samples are equal to 0.703 and 0.711. This follows also from Berdnikov's data (1993) for 13 bimodal Cepheids.

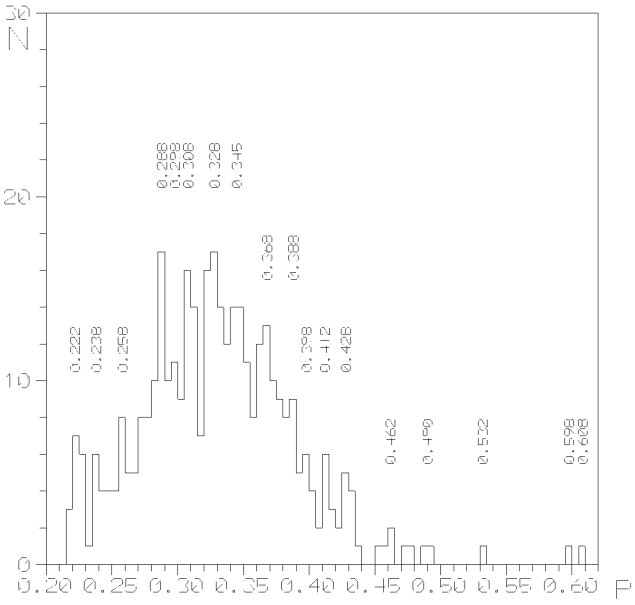


Figure 1: The distribution of RRc Lyr stars' periods based on the data of the sampling according to GCVS (dP=0.005 d).

**References**

Berdnikov L.N.: 1993, *Pis'ma A. Zh.*, **19**, no. 7, 619.

Bezdenezhnyi V.P.: 1994a, *Odessa Astron. Publ.*, **7**, 55.

Bezdenezhnyi V.P.: 1994b, *Odessa Astron. Publ.*, **7**, 57.

Bezdenezhnyi V.P.: 1997a, *Odessa Astron. Publ.*, **10**, 89.

Bezdenezhnyi V.P.: 1997b, *Odessa Astron. Publ.*, **10**, 92.

Bezdenezhnyi V.P.: 1997c, *Odessa Astron. Publ.*, **10**, 93.

Bezdenezhnyi V.P.: 1997d, *Odessa Astron. Publ.*, **10**, 95.

Bezdenezhnyi V.P.: 1997e, *Odessa Astron. Publ.*, **10**, 96.

Bezdenezhnyi V.P.: 2001a, *Odessa Astron. Publ.*, **14**, 118.

Bezdenezhnyi V.P.: 2001b, *Odessa Astron. Publ.*, **14**, 122.

Bezdenezhnyi V.P.: 2004, *Odessa Astron. Publ.*, **17**, 8.

Bezdenezhnyi V.P.: 2005a, *Odessa Astron. Publ.*, **18**, in this volume.

Bezdenezhnyi V.P.: 2004b, *Odessa Astron. Publ.*, **18**, this article.

Kholopov P.N. (ed.): 1985a, 1985b, 1987, General Catalogue of Variable Stars (Volumes 1-3, abbr. GCVS), Nauka, Moscow.

# ON THE PERIODS OF RV TAU STARS

Vladimir P. Bezdenezhnyi
Department of Astronomy, Odessa National University
T.G.Shevchenko Park Odessa 65014 Ukraine
*astro@paco.odessa.ua*

ABSTRACT. On the base of GCVS (General Catalogue of Variable Stars) sampling has been carried out the analysis of periods of RV Tau stars (87 RV Tau stars with the known periods). We have given an interpretation of the histogram of periods distribution of these stars on the base of mode composition. All the peaks were identified as a fundamental period, its first, second and other overtones and their harmonics. It was proposed a new classification of these variable stars according to their mode identifications.

**Key words:** Stars: $\delta$ Scuti, RR Lyrae, RV Tau, classical Cepheids, bimodal Cepheids, $\beta$ Cep stars, histogram of periods distribution, mode identifications

On the base of the sampling (87 RV Tau stars with the known periods) taken from the fourth edition of the General Catalogue of Variable Stars (volumes 1-3, hereafter GCVS) we have constructed two histograms of periods distribution of these variable stars. They are given in Tables 1 and 2 and shown in Figures 1 and 2.

The intervals of periods in these two histograms are 5 and 2 days respectively. As we can see (Tab.1 and Fig.1), the main peak of periods distribution (with the amplitude N=11 stars) is at the mean period about 78 days. But more detailed histogram (see Fig. 2) shows two peaks at 75 and 80 days with the equal amplitudes. The ratio of these periods is equal 0.9375 - this rate coincides with one for a fundamental period $P_f$ to double period $P_s$, the latter has found by us in frequency analysis of bimodal Cepheids and RR Lyrae - type stars (Bezdenezhnyi, 1997a, 1997b). So we have: $P_f$=75 days and $2P_s$=80 days.

The following significant peak is at the mean period about 62.5 days with the amplitude N=8 stars (see Fig. 1). It furcates in two peaks (see Fig. 2): at 61 and

Table 1: The histogram of RV Tau stars' periods distribution (dP=5 days)

| ΔP | N | ΔP | N | ΔP | N |
|---|---|---|---|---|---|
| 25 - 30 | 1 | 105 - 110 | 1 | 190 - 195 | 0 |
| 30 - 35 | 1 | 110 - 115 | 2 | 195 - 200 | 1 |
| 35 - 40 | 1 | 115 - 120 | 2 | 200 - 205 | 1 |
| 40 - 45 | 2 | 120 - 125 | 1 | 205 - 210 | 0 |
| 45 - 50 | 2 | 125 - 130 | 1 | 210 - 215 | 2 |
| 50 - 55 | 3 | 130 - 135 | 1 | 215 - 260 | 0 |
| 55 - 60 | 4 | 135 - 140 | 5 | 260 - 265 | 1 |
| 60 - 65 | 8 | 140 - 145 | 2 | 265 - 275 | 0 |
| 65 - 70 | 7 | 145 - 150 | 1 | 275 - 280 | 1 |
| 70 - 75 | 1 | 150 - 155 | 1 | 280 - 285 | 0 |
| 75 - 80 | 11 | 155 - 160 | 1 | 285 - 290 | 2 |
| 80 - 85 | 5 | 160 - 165 | 1 | 290 - 355 | 0 |
| 85 - 90 | 4 | 165 - 170 | 1 | 355 - 360 | 1 |
| 90 - 95 | 2 | 170 - 175 | 0 | 375 - 380 | 1 |
| 95 - 100 | 0 | 175 - 180 | 1 | | |
| 100 - 105 | 4 | 180 - 185 | 0 | | |

Table 2: The histogram of RV Tau stars' periods distribution (dP=2 days)

| ΔP | N | ΔP | N | ΔP | N |
|---|---|---|---|---|---|
| 28 - 30 | 1 | 74 - 76 | 5 | 120 - 122 | 1 |
| 30 - 32 | 0 | 76 - 78 | 1 | 126 - 128 | 1 |
| 32 - 34 | 1 | 78 - 80 | 5 | 130 - 132 | 1 |
| 34 - 36 | 0 | 80 - 82 | 4 | 134 - 136 | 4 |
| 36 - 38 | 0 | 82 - 84 | 1 | 136 - 138 | 1 |
| 38 - 40 | 1 | 84 - 86 | 1 | 142 - 144 | 2 |
| 40 - 42 | 2 | 86 - 88 | 2 | 146 - 148 | 1 |
| 42 - 44 | 0 | 88 - 90 | 1 | 150 - 152 | 1 |
| 44 - 46 | 0 | 90 - 92 | 1 | 156 - 158 | 1 |
| 46 - 48 | 1 | 92 - 92 | 1 | 162 - 164 | 1 |
| 48 - 50 | 1 | 94 - 96 | 0 | 168 - 170 | 1 |
| 50 - 52 | 2 | 96 - 98 | 0 | 174 - 176 | 1 |
| 52 - 54 | 0 | 98 - 100 | 0 | 194 - 196 | 1 |
| 54 - 56 | 3 | 100 - 102 | 1 | 200 - 202 | 1 |
| 56 - 58 | 0 | 102 - 104 | 2 | 210 - 212 | 1 |
| 58 - 60 | 2 | 104 - 106 | 0 | 212 - 214 | 1 |
| 60 - 62 | 5 | 106 - 108 | 0 | 260 - 262 | 1 |
| 62 - 64 | 2 | 108 - 110 | 1 | 278 - 280 | 1 |
| 64 - 66 | 4 | 110 - 112 | 1 | 284 - 286 | 1 |
| 66 - 68 | 2 | 112 - 114 | 1 | 286 - 288 | 1 |
| 68 - 70 | 2 | 114 - 116 | 0 | 352 - 354 | 1 |
| 70 - 72 | 1 | 116 - 118 | 1 | 374 - 376 | 1 |
| 72 - 74 | 0 | 118 - 120 | 1 | | |

65 days. These ones are nearby to the periods $P_e$=60 days and $P_r$=66.7 days identified from multiple ratios with the fundamental period. The periods $P_e$ and $P_r$ were introduced by the author earlier (Bezdenezhnyi, 1994a, 1994b) for RR Lyrae-type and $\delta$ Scuti stars. To the left of these periods we find out the step with the mean period 57.5 days coincident to the theoretical first overtone $P_{1H}$=56.2 days.

The following step with the main period 52.5 days (to the left) in the histogram (see Fig. 1) coincident to the period $P_g$=2/3 $P_f$=50 days, that was introduced by us in above works (Bezdenezhnyi, 1994a, 1994b). We have the peak at period 51 days in the Fig. 2. And on to the left we have the step with the mean period about 45 days. It coincident to the second overtone period $P_{2H}$=0.6$P_f$=45 days. Then one can see (Fig. 2) the peak (with amplitude N=2) at period of 40 days equal to $P_s$=40 days and two periods with small amplitudes (N=1): at period of 33 days next to one $P_r/2$=33.3 days and at period of 29 days close to $P_e/2$=30 days.

Now let us identify the periods bigger than the main peak one (to the right). In the both pictures (Fig. 1 and 2) are seen distinct peaks at period of 102 days. It can be identified as double period $P_g$: $2P_g$=100 days. To the left of this one we can see the step (Fig.1) and the peak (Fig.2) coincident to period of the second overtone $2P_{2H}$=90 days. Then (to the right) follows three double periods: $2P_{1H}$=112 days, $2P_e$=120 days and a higher peak at 135 days coincident to $2P_r$=133.3 days. The mean of seven periods in the region of $2P_r$ is equal 133.8 days, that is close to the theoretical meaning 133.3 days. We can notice that the small peaks (N=1) at the multiple periods are present too: 2Pf=150 days, 4Ps=160 days, $4P_{2H}$=180 days, 4Pg=200 days, 4Pr=266.6 days and $8P_{2H}$=360 days.

Though the sampling of RV Tau stars with the known periods in GCVS is not large, we could identify the primary peaks in the histogram of periods distribution. The ratios of periods show that periods are commensurable (often - multiple ones), as in the case of other types pulsating stars. The histogram of RV Tau stars' periods distribution is similar to ones of $\delta$ Scuti, $\beta$ Cep, RR Lyr stars, classical and bimodal Cepheids, and even of pulsars (Bezdenezhnyi, 1994b, 1997a,b,c,d,e, 2001a,b, 2004, 2005a,b). Individual values and mean peaks of periods of RV Tau stars confirm their commensurability with three splite primary periods: $P_\alpha$=0.1081, $P_\beta$=0.1126 and $P_\gamma$=0.1042 days. One of this periods (0.1126 days) coincide with radial fundamental period of the Sun oscillation (Bezdenezhnyi, 2005b, in this volume). The ratios of these commensurabilities are in rather large ranges (260 - 3330), reflecting big differences in periods of RV Tau stars. At that point of view a lot of periods may be identify with radial ones without attracting non-radial oscillations.

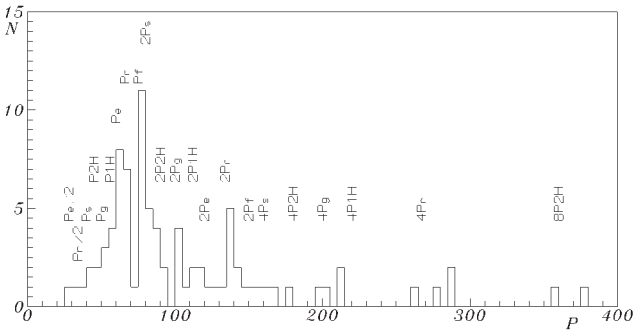


Figure 1: The periods distribution of RV Tau stars (dP=5 days)

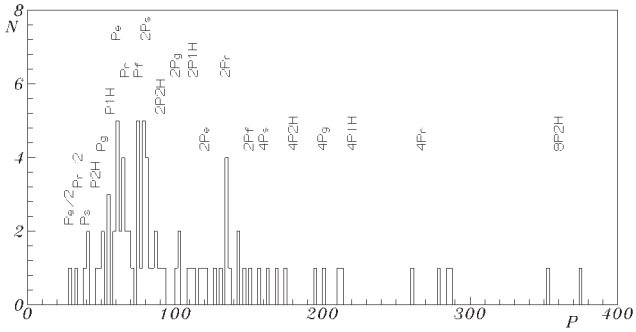


Figure 2: The periods distribution of RV Tau stars (dP=2 days)

**References**

Bezdenezhnyi V.P.: 1994a, *Odessa Astron. Publ.*, **7**, 55.

Bezdenezhnyi V.P.: 1994b, *Odessa Astron. Publ.*, **7**, 57.

Bezdenezhnyi V.P.: 1997a, *Odessa Astron. Publ.*, **10**, 89.

Bezdenezhnyi V.P.: 1997b, *Odessa Astron. Publ.*, **10**, 92.

Bezdenezhnyi V.P.: 1997c, *Odessa Astron. Publ.*, **10**, 93.

Bezdenezhnyi V.P.: 1997d, *Odessa Astron. Publ.*, **10**, 95.

Bezdenezhnyi V.P.: 1997e, *Odessa Astron. Publ.*, **10**, 96.

Bezdenezhnyi V.P.: 2001a, *Odessa Astron. Publ.*, **14**, 118.

Bezdenezhnyi V.P.: 2001b, *Odessa Astron. Publ.*, **14**, 122.

Bezdenezhnyi V.P.: 2004, *Odessa Astron. Publ.*, **17**, 8.

Bezdenezhnyi V.P.: 2005a,b *Odessa Astron. Publ.*, **18**, this article and another in this volume.

Kholopov P.N. (ed.): 1985a, 1985b, 1987, General Catalogue of Variable Stars (Volumes 1-3, abbr. GCVS), Nauka, Moscow.

# NEW CATALOG OF DISTANCES AND LIGHT CURVE PARAMETERS OF CLASSICAL CEPHEIDS

L.N. Berdnikov

Sternberg Astronomical Institute, 13 Universitetskij prosp.,
Moscow 119992, Russia, *berdnik@sai.msu.ru*

ABSTRACT. A new version of the catalogue of distances and light-curve parameters for galactic classical Cepheids is presented. The catalogue lists amplitudes, magnitudes at maximum light, and intensity means for 515 stars in $UBVRI$ filters of the Johnson system and $(RI)_{\rm C}$ filters of the Cron-Cousins system. The distances are based on our multicolour set of PL relations and on our Cepheid-based solution for interstellar extinction law parameters and are referred to an LMC distance modulus of 18.25.

**Key words**: Stars: Cepheids: light curves; Stars: Cepheids: distances

## 1. Introduction

In 1981 we started our long-term program of regular photoelectric photometry of Galactic classical Cepheids. By now we have already obtained a total of more than 70 000 measurements in the $UBV(RI)_{\rm C}$ system for almost 600 objects both in the Northern and Southern sky. Most of our observations have been published by Berdnikov (1986, 1987, 1992a-g, 1993), Berdnikov and Turner (1995a,b, 1998a,b, 2000a,b, 2001a,b, 2004a,b,c), Berdnikov and Vozyakova (1995) and Berdnikov et al. (1998). All our observations are available in the INTERNET at:

http://www.sai.msu.su/groups/cluster/CEP/PHE/cepheids-16-03-2006.zip

Earlier (Berdnikov et al. 2000) we used our observations, in combination with those published by other authors, to determine distances and light-curve parameters for Galactic classical Cepheids with available photoelectric photometry in the $BVRI$ filters of the Johnson system and $(RI)_{\rm C}$ filters of the Cron-Cousins system. The resulting catalogue contained homogeneous data for 455 stars and proved to be a very useful tool for the study of the distribution and kinematics of Cepheids in the Milky Way (Kervella et al. 2001, Alessi et al. 2003, Sitnik 2003, Tammann et al. 2003, Ngeow and Kanbur 2004, Sakai et al. 2004, Sandage et al. 2004, Bono et al. 2005, Sabbadin et al 2005, Soszynski et al. 2005). Since the publication of this catalogue we have collected extensive photoelectric data which, combined with published photometry, allows us to increase the number of stars with reliable light curves by ∼15 per cent. This made it necessary to prepare a new version of our catalogue, which we present in this paper.

## 2. Light-curve parameters

In our previous work (Berdnikov et al. 2000) we derived the Cepheid light-curve parameters for photometric passbands BVRI of the Johnson system and for the $(RI)_{\rm C}$ filters of the Cron-Cousins system. In this version of the catalogue we derived light-curve parameters for U passband as well.

To derive light-curve parameters in the $UBVRI(RI)_{\rm C}$ filters we first selected for each Cepheid and filter the observations that most accurately outlined the shape of the light curve. In most of cases these were either our own observations or those of Gieren (1981), Dean et al. (1977), Coulson and Caldwell (1985), Moffet and Barnes (1984), and Pont et al. (1997) whose photometric systems are virtually identical to our own. We then fitted the light curve, either on the entire [0, 1] phase interval or on its subintervals, by a Fourier series (with 3 to 45 terms), a spline, or a second-to-tenth-order polynomial and joined the resulting fragments to obtain the so-called master light curve. We then used the linear least squares technique to reduce all other observations to the photometric system of the master curve (a detailed description of the algorithm can be found in Berdnikov 1992f) with subsequent refinement of the initial master curve based on all available observations. We used the final master curve to determine the principal parameters of the light-curves: magnitude at maximum light, amplitude, and intensity-mean magnitude.

Reduction of ∼ 130 000 photoelectric observations in our Cepheid data bank (Berdnikov 1995) yielded reliable and accurate light curves for 647 Cepheids including 515 classical ones.

### 3. Distances

We inferred the distances to Cepheids using the light-curve parameters derived as described above and the following procedure suggested by Berdnikov et al. (1996b):

(1) We use the period-colour relation by Dean et al. (1977) to determine the intrinsic colour, $(< B > - < V >)_0$, and the colour excess:

$$E_{\rm B-V} = (< B > - < V >) - (< B > - < V >)_0.$$

In the absence of accurate $< B >$ magnitude we first determine the intrinsic colour

$$(< V > - < m_\lambda >)_0 = < M_V > - < M_\lambda >,$$

using PL relations for $< M_V >$ and $< M_\lambda >$ from Berdnikov et al. (1996b). We then calculate the corresponding colour excess $E_{V-m_\lambda}$ and convert it into $E_{B-V}$ using interstellar extinction law parameters from Berdnikov et al. (1996a,b).

(2) If the mean magnitude, $< K >$, is not available directly from observations (Berdnikov et al. 1996a), it is derived from formula (5) or an appropriate formula from Table 7 in Berdnikov et al. (1996b) based on known $< V >$ and $< m_\lambda >$. Here $m_\lambda$ can be any of the $B$, $R$, $I$, $R_{\rm C}$, or $I_{\rm C}$ filters. The galactocentric distance of the star, which is required to allow for the abundance gradient in the disk, is calculated from the preliminary heliocentric distance inferred from $< B >$, $< V >$, and log P. To this end, we adopt $R_0 = 7.1$ kpc, where $R_0$ is the distance of the Sun from the Galactic centre. Note that we derived the formulas used to infer $< K >$ from, say, $< B >$, $< V >$, log P, and $R_{\rm g} - R_0$ without adopting any specific value for the abundance gradient in the galactic disk. Each of these formulas simply establishes a relation between two observed colours (e.g., $< V > - < K >$ and $< B > - < V >$), the period, P, and the difference of galactocentric distances of the star ($R_{\rm g}$) and the Sun ($R_0$). The coefficients at $R_{\rm g} - R_0$, if combined with some relation connecting abundance differences into colours, can be used to estimate the abundance gradient.

(3) $< K >$ is then corrected for interstellar extinction:

$$< K >_0 = < K > -0.274 \cdot E_{B-V}.$$

(4) The absolute magnitude of a star is then determined from the following formula:

$$< M_K > = \ -5.462 - 3.517 \cdot (\log P - 1).$$

(5) The true distance modulus is then calculated as:

$$DM_0 \ = < K >_0 - < M_K > .$$

(6) And, finally, the distance $r_{\rm hel}$ (in kpc) is given by:

$$r = 10^{0.2 \cdot (DM_0 - 10)}.$$

The distances thus derived are on a short distance scale consistent with an LMC distance modulus of 18.25 (Berdnikov et al. 1996b).

#### 3.1 The catalogue

The resulting light-curve parameters and distances of 515 Galactic classical Cepheids are summarised in the table. The first column of the table gives the name of the Cepheid; the second column, its variability type according to GCVS (Kholopov et al. 1985-1987). The third column gives the fundamental period $P_0$, which is equal to the observed variability period for most of the Cepheids (DCEP or CEP type in GCVS). We assumed that small-amplitude Cepheids (DCEPS type in GCVS) are first-overtone pulsators and therefore calculated their fundamental periods by dividing the GCVS value by a factor of $0.716-0.027 \cdot \log$ P as found by Alcock et al. (1995) and slightly modified by Feast and Catchpole (1997). Note that we give $P_0$ only up to the third digit after the decimal point because this precision is sufficient for distance determination. More accurate period values can be found in the GCVS.

The fourth column gives the heliocentric distance. The fifth column indicates how the intensity-mean $< K >$ magnitude was derived. $K$ means that it is known directly from observations; $V$, $Rc$, $Ic$, and $I$, that it was inferred from observed $< B >$ and $< V >$, $< V >$ and $< R_{\rm C} >$, $< V >$ and $< I_{\rm C} >$, $< V >$ and $< I >$, respectively. The subsequent columns give light-curve parameters – amplitude, magnitude at maximum light, intensity-mean magnitude, and quality of a light curve (one to nine) – for each of the filters $U$, $B$, $V$, $R_{\rm C}$, $R$, $I_{\rm C}$ and $I$.

The catalog itself is available on request. The complete paper is to be published elsewhere.

### 4. Conclusion

Our analysis of all available photoelectric photometry of Galactic Cepheids in filters $U$, $B$, $V$, $R$, and $I$ of Johnson's broad-band system and filters $R_{\rm C}$ and $I_{\rm C}$ of the Cron-Cousins system yielded reliable and accurate light curves (at least in two filters) for 515 classical Cepheids. For these stars we derived accurate light-curve parameters (amplitudes, magnitudes at maximum light, and intensity means) and distances. The

resulting catalogue will be used to analyse the properties and space distribution of Cepheids and to investigate the structure and kinematics of the Galactic disk. The data can also be used to test theories of stellar pulsation and late stages of stellar evolution.

*Acknowledgements.* The author gratefully acknowledges partial support for this work by research funding awarded through the Russian Foundation of Basic Research.

**References**

Alcock C., Allisman R.A., Axelrod T.S., et al.: 1995, *AJ,* **109**, 1653.
Alessi B. S., Moitinho A., Dias W. S.: 2003, *Astron. and Astrophys.*, **410**, 565.
Berdnikov L.N.: 1986, *Peremennye Zvezdy,* **22**, 369.
Berdnikov L.N.: 1987, *Peremennye Zvezdy,* **22**, 530.
Berdnikov L.N.: 1992a, *Astron. and Astrophys. Trans.,* **2**, 1.
Berdnikov L.N.: 1992b, *Astron. and Astrophys. Trans.,* **2**, 31.
Berdnikov L.N.: 1992c, *Astron. and Astrophys. Trans.,* **2**, 43.
Berdnikov L.N.: 1992d, *Astron. and Astrophys. Trans.,* **2**, 107.
Berdnikov L.N.: 1992e, *Astron. and Astrophys. Trans.,* **2**, 157.
Berdnikov L.N.: 1992f, *Pis'ma Astron. Zh.,* **18**, 519.
Berdnikov L.N.: 1993, *Pis'ma Astron. Zh.,* **19**, 210.
Berdnikov L.N.: 1995, *ASP Conf. Ser.,* **83**, 349.
Berdnikov L.N., Dambis A.K., Vozyakova O.V.: 2000, *Astron. and Astrophys. Suppl. Ser.,* **143**, 211
Berdnikov L.N., Turner D.G.: 1995a, *Pis'ma Astron. Zh.,* **21**, 603.
Berdnikov L.N., Turner D.G.: 1995b, *Pis'ma Astron. Zh.,* **21**, 803.
Berdnikov L.N., Turner D.G.: 1998a, *Astron. and Astrophys. Trans.,* **16**, 205.
Berdnikov L.N., Turner D.G.: 1998b, *Astron. and Astrophys. Trans.,* **16**, 291.
Berdnikov L.N., Turner D.G.: 2000a, *Astron. and Astrophys. Trans.,* **18**, 657.
Berdnikov L.N., Turner D.G.: 2000b, *Astron. and Astrophys. Trans.,* **18**, 679.
Berdnikov L.N., Turner D.G.: 2001a, *Astron. and Astrophys. Trans.,* **19**, 689.
Berdnikov L.N., Turner D.G.: 2001b, *Astrophys. J. Suppl. Ser.*, **137**, 209.
Berdnikov L.N., Turner D.G.: 2004a, *Astron. and Astrophys. Trans.,* **23**, 253.
Berdnikov L.N., Turner D.G.: 2004b, *Astron. and Astrophys. Trans.,* **23**, 395.
Berdnikov L.N., Turner D.G.: 2004c, *Astron. and Astrophys. Trans.,* **23**, 599.
Berdnikov L.N., Vozyakova O.V.: 1995, *Pis'ma Astron. Zh.,* **21**, 348.
Berdnikov L.N., Vozyakova O.V., Dambis A.K.: 1996a, *Pis'ma Astron. Zh.,* **22**, 372.
Berdnikov L.N., Vozyakova O.V., Dambis A.K.: 1996b, *Pis'ma Astron. Zh.,* **22**, 936.
Berdnikov L.N., Vozyakova O.V., Ignatova V.V.: 1998, *Astron. and Astrophys. Trans.,* **17**, 87.
Bono G., Marconi M., Cassisi S., et al.,: 2005, *Astrophys. J.*, **621**, 966.
Coulson I.M., Caldwell J.A.R.: 1985, *SAAO Circ.,* **9**, 5.
Dean J.F., Cousins A.W.J., Bywater R.A., et al.: 1977, *Mem. Roy. Astron. Soc.,* **183**, 69.
Dean J.F., Warren P.R., Cousins A.W.J.: 1978, *Mon. Not. Roy. Astron. Soc.,* **183**, 569.
Feast M.W., Catchpole R.M.: 1997, *Mon. Not. Roy. Astron. Soc.,* **286**, L1.
Gieren W.: 1981, *Astrophys. J. Suppl. Ser.,* **47**, 315.
Kervella P., Coudi du Foresto V., Perrin G., et al.: 2001, *Astron. and Astrophys.*, **367**, 876.
Kholopov P.N., Samus' N.N., Frolov M.S., et al.: 1985-1987, The General Catalogue of Variable Stars, Vols. I -III, Nauka, Moscow.
Moffett T.J., Barnes T.G.: 1984, *Astrophys. J. Supl. Ser.,* **55**, 389.
Ngeow, C., Kanbur S.M.: 2004, *Mon. Not. Roy. Astron. Soc.*, **349**, 1130.
Pont F., Queloz D., Bratschi P., et al.: 1997, *Astron. and Astrophys.,* **318**, 416.
Sabbadin F., Benetti S., Cappellaro E., et al.: 2005, *Astron. and Astrophys.*, **436**, 549.
Sakai S., Ferrarese L., Kennicutt R. C. Jr., et al.: 2004, *Astrophys. J.*, **608**, 42.
Sandage A., Tammann G. A., Reindl B.: 2004, *Astron. and Astrophys.*, **424**, 43.
Sitnik T. G.: 2003, *Aston. Lett.*, **29**, 311.
Soszynski I., Gieren W., Pietrzynski G.: 2005, *Publ. Astron. Soc. Pacif.*, **117**, 823.
Tammann G. A., Sandage A., Reindl B.: 2003, *Astron. and Astrophys.*, **404**, 423.

# GROUPINGS OF POPULATION I OBJECTS IN THE GALAXY

L. N. Berdnikov[1], Yu. N. Efremov[1], E. V. Glushkova[1], D. G. Turner[2]

[1] Sternberg Astronomical Institute, 13 Universitetskij prosp., Moscow 119992, Russia, *berdnik@sai.msu.ru, efremov@sai.msu.ru, elena@sai.msu.ru*

[2] Department of Astronomy and Physics, Saint Mary's University Halifax, Nova Scotia B3H 3C3, Canada, *turner@ap.smu.ca*

ABSTRACT. The distribution of Cepheids in the Galaxy is studied using a new catalogue of Cepheid distances in conjunction with the method of hierarchical clustering. The resulting delineation of Cepheid complexes is compared with those for other Population I objects: open clusters and OB-associations. Parameters derived for complexes of Cepheids are very similar to those for open clusters and OB-associations: the typical dimension of first level groups is ∼0.2 kpc, while the size of complexes is ∼0.9 kpc. Mostly the complexes of different objects are spatially coincident, but not always.

**Key words**: Stars: Cepheids; open clusters; OB-associations; stars: complexes

## 1. Introduction

The distribution of Cepheids (Berdnikov 1987a) and Cepheid groupings (Berdnikov & Efremov 1989) in the Galaxy were studied previously using an earlier version of a Catalogue of distances for Galactic Cepheids (Berdnikov 1987b), containing data for 363 objects. We have since collected extensive new photoelectric data (available on-line at http://www.sai.msu.su/groups/cluster/CEP/PHE/cepheids-16-03-2006.zip) that, in combination with published photometry, increases the number of stars with reliable distances by ∼42% (Berdnikov 2006). Additional refinements were to the distances of open clusters observed photoelectrically (Glushkova, in preparation). As a result, it is possible to conduct a new study of groupings of Cepheids in our Galaxy and to compare Cepheid complexes with complexes of open clusters and OB-associations (Melnik & Efremov 1995), whose distances are on the same scale as those for Cepheids and open clusters.

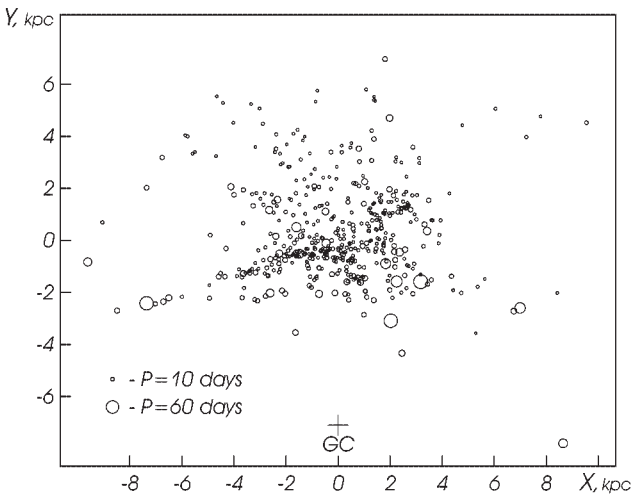


Figure 1: Distribution of Cepheids in the Galaxy.

## 2. The Distribution of Cepheid Complexes

The resulting distribution of 515 Cepheids in the Galactic plane, shown in Fig. 1, was analyzed by the method of hierarchical clustering described in the previous analysis of Cepheid spatial distributions (Berdnikov & Efremov 1989). Clustering results are depicted for two maximal distances, $D_{max}$, between Cepheid subgroups united in the same complex: 600 pc (Fig. 2) and 800 pc (Fig.3).

The resulting distribution of Cepheid clusterings in the Galactic plane is about the same in both cases, apart from a bit different separation between the Car-Sgr arm and the Local arm. It is important to note that within ∼2 kpc of the Sun the density of Cepheids (and open clusters) seems higher because of the reduced effects of observational selection.

Figs. 2a and 3a both illustrate the chain of Cepheid complexes lying along the Car-Sgr arm separated in distance by about 1 kpc. First level groups have roughly the same size, about 200 pc (Figs. 2b and

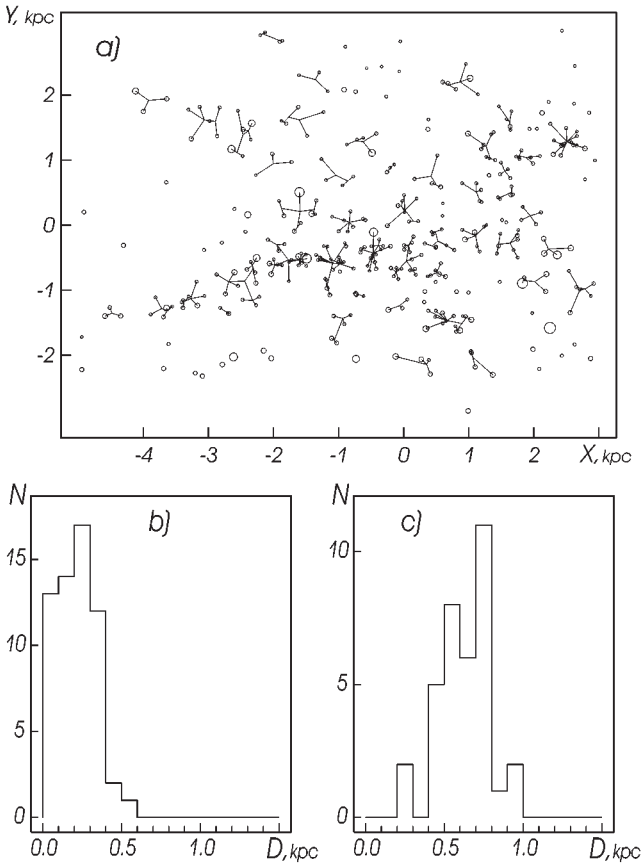


Figure 2: Results for $D_{max} = 600$ pc. a) Complexes of Cepheids in the galactic plane. b) Distribution in size of first level groupings. c) Distribution in size of Cepheid complexes.

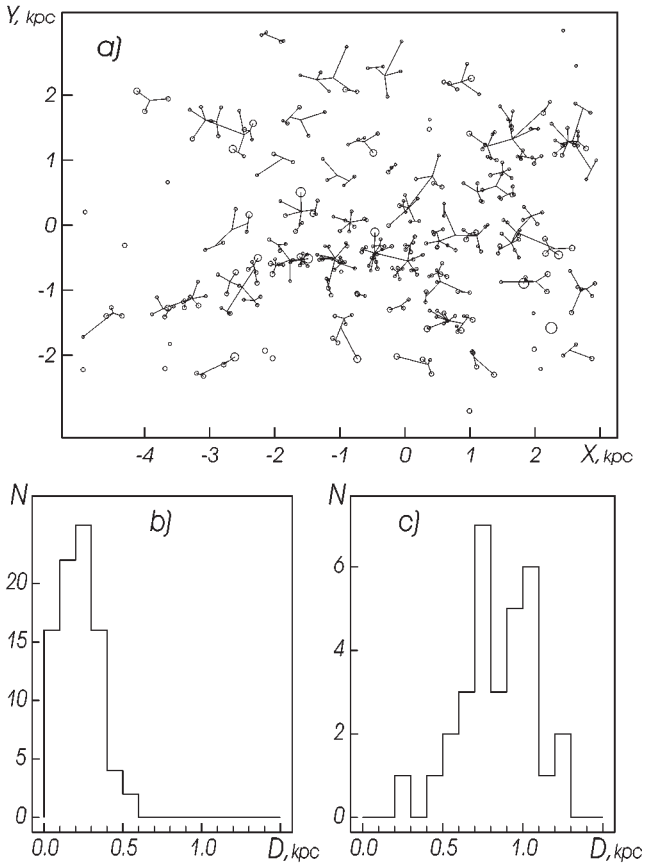


Figure 3: The same as Fig. 2 for $D_{max} = 800$ pc.

3b), whereas the average size of the entire complexes are ∼640 pc for $D_{max} = 600$ pc and ∼900 pc for $D_{max} = 800$ pc (Figs. 2c and 3c).

### 3. Comparing the Distributions of Cepheids, Open Clusters, and OB-associations

Concentrations of open clusters and field stars mostly coincide, but notable differences sometimes occur. Examples of such disparities are recognized in the Milky Way galaxy, and more dramatically, in the LMC (Efremov 1989, p.204; Efremov 2002). In Fig. 4 complexes of Cepheids are depicted along with the location of open cluster complexes. Three clumps of clusters located well outside Cepheid complexes are found at $(X = 0.2, Y = 1, 4)$, $(X = -0.3, Y = -1.1)$ and $(X = -2.0, Y = -1.0)$.

The distribution of young Cepheids, those with periods longer than 10 days, is shown in Fig. 5. The delineation of the Car-Sgr arm is evident from long-period Cepheids, while the existence of another inner arm (Cru-Scu) is strongly suspected. The Car-Sgr arm is also seen distinctly in the distribution of OB-associations (Fig. 6a), using data from the catalogue by Melnik & Efremov (1995). The size of first level groups is again ∼0.200 pc (Fig. 6b), while that of complexes is ∼1.0 kpc (Fig. 6c). We note the similarity of these dimensions to those obtained for Cepheids, which are on average ten times older than OB-stars.

OB-associations are located mostly along the inner part of the Car-Sgr arm relative to Cepheids (compare Fig. 3a and Fig. 6a). They form four complexes along the Car-Sgr arm that may be united into two super-complexes (similar to ones outlined by Efremov, 1995, fig. 4), between which lies a complex of older objects at $(X = -1.0, Y = -1.0)$, as first noted by Avedisova (1989). The essential difference in age between adjacent complexes located along a spiral arm is also observed in other galaxies, such as M31 and M51; it is also seen in many color images of galaxies where pink complexes, bright in $H_\alpha$, are adjacent to blue ones. The connection of the phenomenon to theories for the formation of gas/star complexes along a spiral arm should be studied.

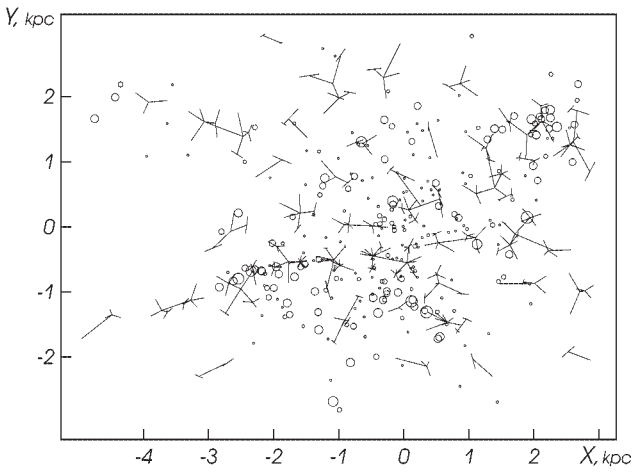


Figure 4: Complexes of Cepheids and open clusters (circles) in the Galactic plane.

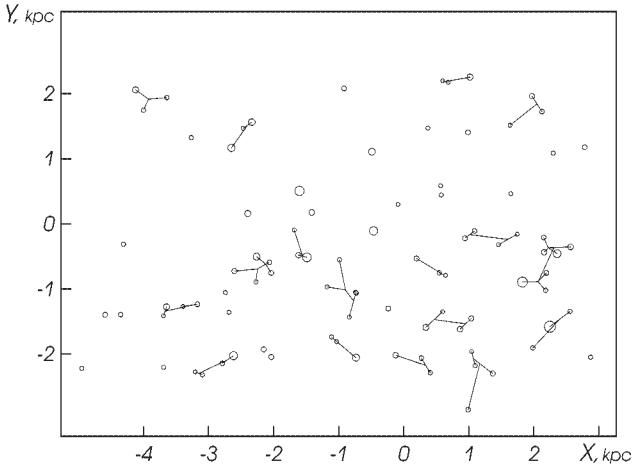


Figure 5: Distribution of Cepheids with periods longer than 10 days in the Galactic plane.

## 4. Conclusion

The parameters found for complexes of Cepheids, open clusters, and OB-associations are very similar. The size of the first level groups is always ∼0.2 kpc, while the average size of the associated complexes is between ∼0.6 kpc and ∼1.0 kpc. The different types of complexes are mostly spatially coincident, but not always.

So far our conclusions are based upon a small number of complexes. It is necessary to initiate further searches for Cepheids and open clusters in order to increase the statistical confidence level of the results.

A complete study is to be published elsewhere. The catalogues of distances to Cepheids and open clusters are available upon request.

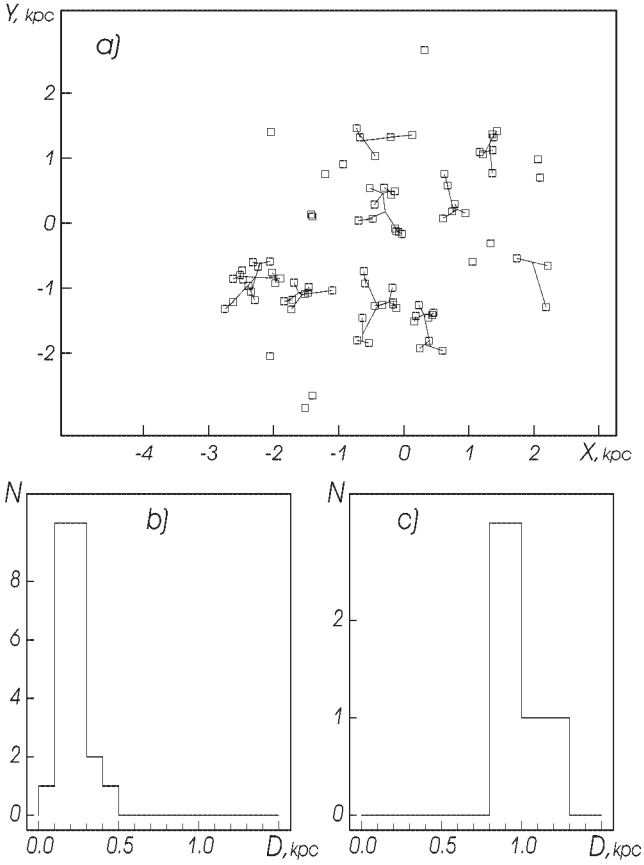


Figure 6: The same as Fig. 2 for OB-associations and $D_{max} = 800$ pc.

*Acknowledgements.* The authors gratefully acknowledge partial support for this work by research funding awarded through the Russian Foundation of Basic Research and through the Natural Sciences and Engineering Research Council of Canada.

## References

Avedisova V.S., 1989, *Astrofisica*, **30**, 83.
Berdnikov L.N.: 1987a, *Pis'ma Astron. Zh.*, **13**, 110.
Berdnikov L.N.: 1987b, *Peremennye Zvezdy*, **22**, 505.
Berdnikov L.N.: 2006, *Odessa Astron. Publ.*, **16**, ???.
Berdnikov L.N., Efremov Yu.N.: 1989, *Astron. Zh.*, **66**, 537.
Efremov Yu. N.: 1983, *Sov. Astron. Lett.*, **9**, 51.
Efremov Yu.N.: 1989, Star formation sites in galaxies (in Russian). Moscow, 1989.
Efremov Yu.N.: 1995, *Astron. J.*, **110**, 2757.
Efremov Yu.N.: 1998, *Astron. and Astrophys. Trans.*, **15**, 3.
Efremov Yu.N.: 2002, *Astron. Rep.*, **46**, 791.
Glushkova E.V. in: Melnik A.M., Efremov Yu.N.: 1995, *Astron. Lett*, **21**, 10.

# PERIOD CHANGES IN CEPHEIDS BELONGING TO OPEN CLUSTERS AND ASSOCIATIONS

L.N. Berdnikov[1], E.V. Glushkova[1], D.G. Turner[2]

[1] Sternberg Astronomical Institute
13 Universitetskij prosp., Moscow 119992, Russia, *berdnik@sai.msu.ru, elena@sai.msu.ru*
[2] Deparatament of Astronomy and Physics, Saint Mary's University
Halifax, Nova Scotia B3H 3C3, Canada, *turner@ap.smu.ca*

ABSTRACT. Cepheids belonging to open clusters and associations exhibit identical characteristics to field Cepheids in terms of their period changes.

**Key words**: Stars: Cepheids; Open Clusters.

## 1. Introduction

The distances to open clusters are presently established with considerable precision through main-sequence fitting. Cepheids belonging to open clusters therefore have accurately established luminosities, making them ideal calibrators for the period-luminosity relation. Yet it is also important to establish that cluster Cepheids do not differ fundamentally from field Cepheids in their properties. A prominent and very important characteristic observed in Cepheids is the systematic manner in which they undergo changes in their periods of pulsation. Here we compare the behavior of such changes in 170 field Cepheids with those exhibited by the 40 cluster Cepheids listed by Turner and Burke (2002).

## 2. Method of Analysis and Observational Data

To study period changes in Cepheids we applied the generally used analytical technique of O–C diagrams in conjunction with our version of the well-known Hertzsprung method (Berdnikov, 1992). We calculated O–C data from published photoelectric, photographic, and visual observations collected in our Cepheid database, as well as from magnitudes for some stars estimated from patrol plates of their fields contained in both the Harvard College Observatory and Sternberg Astronomical Institute Photographic Plate Collections. Moreover, we used the photometric data obtained in frames of ASAS and ROTSE projects.

## 3. Results

We investigated the O–C diagrams for 40 cluster Cepheids (T Ant, U Car, VY Car, GH Car, GT Car, SU Cas, BD Cas, CF Cas, CG Cas, DL Cas, V Cen, $\delta$ Cep, TV CMa, R Cru, T Cru, X Cyg, SU Cyg, V1726 Cyg, $\zeta$ Gem, T Mon, CV Mon, S Nor, QZ Nor, TW Nor, V340 Nor, UY Per, RS Pup, AQ Pup, KQ Sco, RU Sct, EV Sct, V367 Sct, GY Sge, U Sgr, WZ Sgr, BB Sgr, SZ Tau, $\alpha$ UMi, RZ Vel, SW Vel, CS Vel, S Vul, and SV Vul), 30 of which exhibit systematic parabolic trends indicative of period increases (21 stars) and period decreases (9 stars). Figures 1-4 display results for VY Car, S Vul, CG Cas and CF Cas, where the O–C data are dominated by cubic or parabolic trends expected for stellar evolution.

In the cluster sample 10 Cepheids exhibit frequent, abrupt, period changes that result in cyclical waves in their O–C diagrams. For 9 of them the amplitude of such oscillations in the O–C residuals exceeds 10% of their period lengths.

In Table 1 we compare the results with the statistics obtained for 170 field Cepheids studied previously. The two groups are essentially identical in terms of the proportions of objects in each category of period change.

The complete paper is to be published in PASP.

*Acknowledgements.* The authors gratefully acknowledge partial support for this work by research funding awarded through the Russian Foundation of Basic Research and through the Natural Sciences and Engineering Research Council of Canada.

### References

Berdnikov L.N.: 1992, *Sov. Astron. Lett.,* **18**, 207.
Turner D.G. and Burke J.F.: 2002, *Astron. J.,* **124**, 2931.

Table 1: Comparison of Period Changes in Cluster Cepheids and Field Cepheids

| Group | No. of Stars | Increasing Periods | Decreasing Periods | No Systematic Trends | Abrupt Period Changes $\geq 0.1P$ |
|---|---|---|---|---|---|
| Field Cepheids | 170 | 86 (51%) | 33 (19%) | 51 (30%) | 37 (22%) |
| Cluster Cepheids | 40 | 21 (53%) | 9 (23%) | 10 (25%) | 9 (23%) |

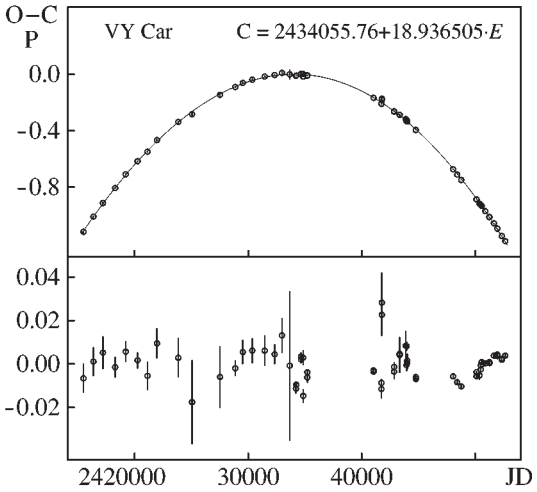


Figure 1: O–C data, calculated evolutionary trend, and residuals from a cubic fit (below) for VY Car.

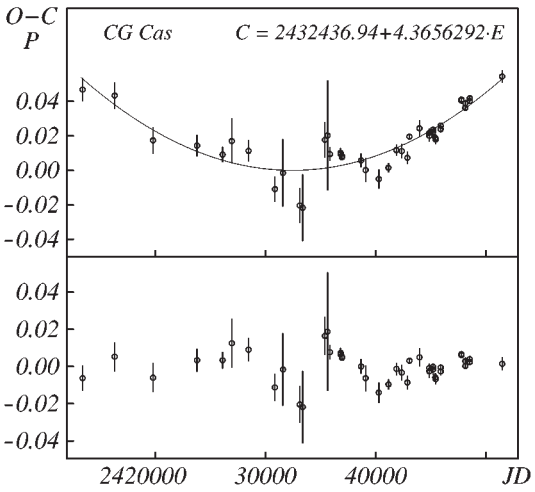


Figure 3: O–C data, calculated evolutionary trend, and residuals from a parabolic fit (below) for CG Cas.

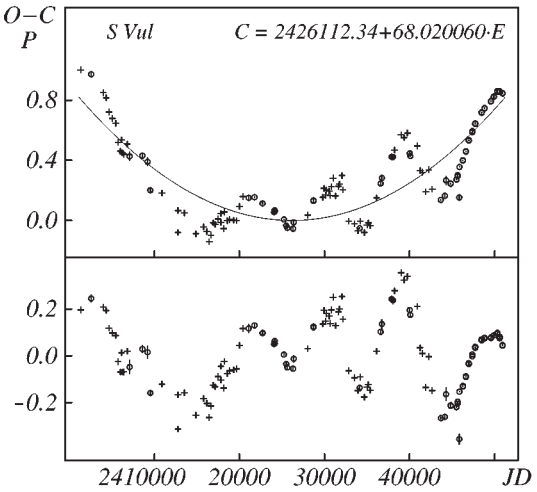


Figure 2: O–C data, calculated evolutionary trend, and residuals from a parabolic fit (below) for S Vul.

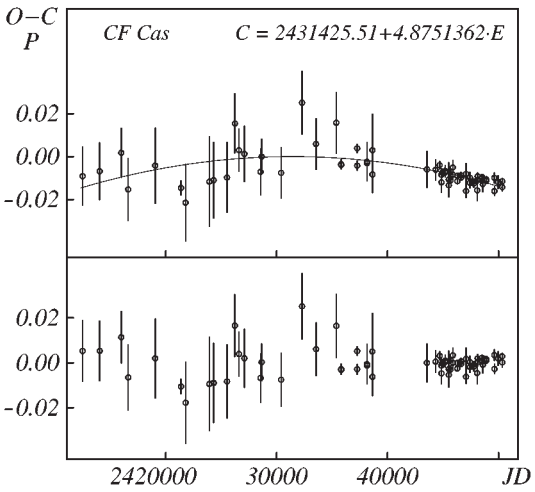


Figure 4: O–C data, calculated evolutionary trend, and residuals from a parabolic fit (below) for CF Cas.

# ПЗС-ФОТОМЕТРИЯ ЗВЕЗД ТИПА RV TAU

В.И. Бурнашев, Б.А. Бурнашева

Крымская Астрфизическая Обсерватория
98409, Украина, Крым, п. Научный, *bella@crao.crimea.ua*

ABSTRACT. On the figure 1 there are the result of the wavelet-analysis of the common data of the visual and photograpic photometry of the variables. Besides of the nearly cyclic variations of the duration of the primary *RV Tau*-type cycle, there are also chaotic variations of the cycle too.

**Key words**: *CCD – photometry, RV Tau stars, AC Her, V Vul, R Sge, DF Cyg.*

Переменные типа *RV Tau* представляют собой немногочисленный класс маломассивных ($M \simeq 1M_o$) пульсирующих $F - K$-сверхгигантов ($M_v = -3 \div -5$). На диаграмме Герцшпрунга–Рессела они находятся между полосой нестабильности классических цефеид и виргинид и последовательностью полуправильных и долгопериодических переменных. Эволюционное происхождение этих звезд неясно. Возможно, что стадия звезд типа *RV Tau* следует за стадией асимптотической ветви гигантов, когда вследствие неустойчивости горения гелия в слоевом источнике звезда уходит в голубую сторону, описывая петли на диаграмме Герцшпрунга-Рессела. Большая часть звезд типа *RV Tau* превращается в планетарные туманности, другие, возможно, эволюционируют медленнее, так что их оболочки диссипируют, прежде чем будут фотоионизованы излучением ядра. (Джура, 1986; Цесевич, 1970; Фокин, 1984). Первым на звезды типа *RV Tau*, как прародителей планетарных туманностей, указал Шкловский (1957).

Несмотря на то, что первая звезда этого типа была открыта почти 200 лет назад, сведения о звездах типа *RV Tau* все еще скудны. Довольно длинные периоды и относительная слабость являются препятствием для наблюдений. Объяснение неустойчивости блеска этих звезд, возможно, связано с переходным характером. Устойчивые колебания сменяются через бифуркацию удвоения периода неустойчивыми хаотическими, представляемыми в фазовой плоскости странным аттрактором. Возможно, что звезды *RV* представляют собой набор звезд на поздней стадии эволюции, испытывающих переход от периодических радиальных цефеидоподобных колебаний к хаотическим. Разнообразие фотометрического поведения их связано с разной степенью развития этого переходного процесса.

В Крымской обсерватории выполнена ПЗС-фотометрия нескольких звезд типа *RV* в системе *BVRI* Джонсона. Установлена фотометрическая последовательность звезд сравнения в ближайшей окрестности каждой переменной. Проведен периодограммный и вейвлет-анализ полученных нами и опубликованных другими авторами данных, а также проанализированы диаграммы $O - C$, как определенные нами, так и взятые из литературы.

Анализ наблюдений *AC* подтвердил среднее значение основного цикла переменности $P = 75.^d424$ на протяжении почти 104 лет. При этом изменения блеска, вызванные двойственностью, не превышают ошибок измерений. Изменения длительности основного цикла исследованы по совокупности значений $O-C$. Характерное время его изменений составляет $\Pi = 9491^d$.

На основании квазиодновременных измерений лучевой скорости и блеска модифицированным методом Весселинка оценен средний радиус звезды $R = 22 \pm 8$ солнечных радиусов.

Наблюдения *V* подтвердили среднее значение основного цикла переменности $P = 76.^d2593$ на протяжении почти 100 лет. Периодичность изменения длительности основного цикла исследована по совокупности значений $O - C$. Характерное время его изменений составляет $\Pi = 12728^d$. Анализ результатов наблюдений позволил установить наличие сложного изменения блеска, обусловленного как последовательным удвоением основного периода, так и возникновением дополнительных нечетных гармоник, свидетельствующих о том, что звезда находится в переходном режиме от периодических колебаний к хаотическим. Из анализа диаграмм $O - C$ для главного и вторичного минимума установлено их сложное поведение со временем, возможно, объясняющее некоторые особенности фотометрического поведения переменной. Кроме полуправильных изменений длительности основного периода в пределах от $74^d$ до $79^d$, заметны и более длительные изменения, характерное время которых составляет несколько тысяч дней.

Среднее значение основного цикла переменности

для *R Sge* составляет $P = 70.^d757$. Периодичность изменения длительности основного цикла исследована по совокупности значений $O - C$. Характерное время его изменений с 1881 года около П = 6.8 тыс. дней. Подтвердилось наличие вторичного цикла переменности, открытого Цесевичем(1953). Его уточненное значение составляет 1120 дней. Наличие дополнительных гармоник, повидимому, свидетельствует о том, что звезда находится в переходном режиме от периодических колебаний к хаотическим.

На основе всех имеющихся фотометрических данных были построены графики изменения блеска в течение почти полутора веков. Из этих графиков виден сложный характер колебаний яркости звезды, показывающей иногда цефеидоподобные изменения с половинным, 35-дневным периодом, сменяющиеся полуправильными, почти хаотическими колебаниями. Иногда вообще трудно увидеть какие-либо изменения, звезда практически постоянна. На основании графиков O-C сделан вывод о наличии двух близких колебаний, $70.^d757$ и $70.^d393$ дней. Моменты минимумов этих колебаний как бы "мигрируют"в течение принятого периода, соответствующего наибольшему пику на периодограмме. Обращает на себя внимание и следующее обстоятельство: "стабилизация"или перестройка длины периода произошла около *JD* 2408000, затем через 56 тыс. дней, около *JD* 2432000, также происходили некоторые события, связанные с изменением периода. В связи с этим возможно ожидать, что подобные изменения могут случиться в недалеком будущем, в 2010-2014 гг.

ПЗС-фотометрия звезды *DF Cyg*, принадлежащей к более редкому типу переменности *RV b*, показывающему как короткопериодические, так и долговременные колебания, выполнена в 2002 г. Из анализа этих наблюдений вместе с литературными данными на протяжении почти 114 лет с 1890 по 2004 гг.получено среднее значение длительного цикла переменности $P = 776.^d595$. Средняя величина переменности блеска от $10.^m0$ до $13.^m0$.

Основной особенностью короткопериодических 50-дневных колебаний является то, что амплитуда этих колебаний больше в максимуме долговременного цикла (и составляет в среднем $0.^m5$) и существенно меньше в минимуме цикла (около $0.^m3$). Длительность короткого периода была оценена с помощью периодограммы, построенной для разности блеска между наблюденными значениями $m_{vis}$ и интерполированными для средней кривой $m_{vis}(P = 776.^d595)$.

Сводные кривые для значения короткого периода, равного $49.^d839$, типичны для переменных типа *RV Tau*, но имеют и некоторые характерные для данной звезды особенности: почти одинаковую высоту обоих максимумов и слабо различающуюся глубину минимумов, при этом вторичный мини-

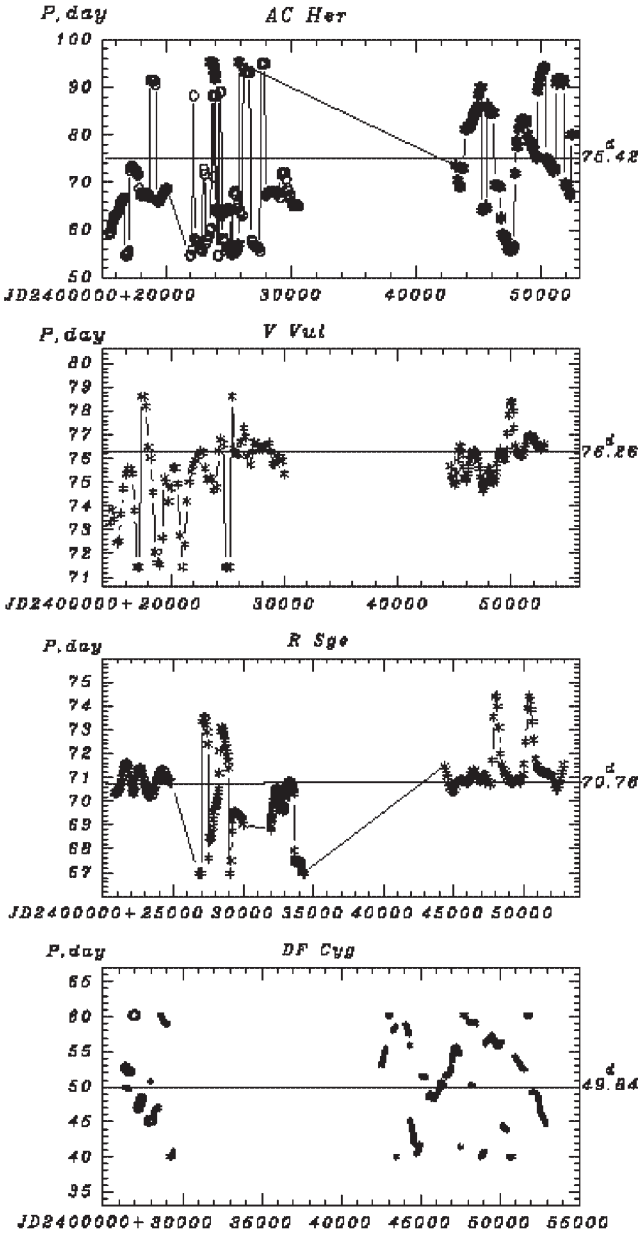


Рис. 1: Результат вейвлет-анализа фотометрических наблюдений RV-Tau звезд. Горизонтальными прямыми отмечены средние значения периодов изменения блеска для каждой переменной.

мум прослеживается довольно слабо. В минимуме 776-дневных колебаний блеска кривые более или менее симметричны и практически имеют вид удвоенной цефеидоподобной кривой. Периодограммы, полученные для двух независимых рядов, фотографического и визуального, повторяются даже в деталях. При этом видно, что наибольший пик соответствует периоду первой гармоники, $24.^d92$.

Из диаграммы $O-C$ следует, что в колебаниях длительности основного 50-дневного периода, возможно, прослеживается тенденция к его увеличению. Возможно, что такое изменение происходит скачкообразным образом: около $JD$ 2427500 период изменился от $P = 49.^d70$ до $P = 49.^d8398$ и после $JD$ 2451500 он продолжает возрастать.

Характерной особенностью для исследовавшихся звезд является то, что на более или менее плавные изменения основного периода колебаний с характерным временем порядка десятков лет накладываются хаотические "выбросы", которые, возможно, представляют изменения длительности основного цикла переменности. То есть, иногда происходит как бы "переключение"близких мод колебаний, которое носит, судя по рисунку, довольно хаотический характер.

Авторы глубоко благодарны наблюдателям и составителям базы данных AAVSO (Вааген, 2004), использованных в данном исследовании.

**Литература**

Вааген (Waagen E.O.): 2004, *Observations from the AAVSO International Database. Private communication.*

Джура (Jura M.): 1986, *Astrophys. J.*, **309**, 732.

Фокин А.Б.: 1984, *Научн. информ. Астрон. совета АН СССР*, **57**, 17.

Цесевич В.П.: 1970, *Звезды типа RV Тельца в: Переменные звезды*, 280.

Цесевич В.П.: 1953, *Переменные звезды*, **9**, No. 3, 215.

Шкловский И.С.: 1957, *Астрон. ж.*, **33**, 315.

# SPECTROPOLARIMETRY OF $\beta Cephei$ TYPE STAR $\gamma Pegasi$

V.V. Butkovskaya

Crimean Astrophysical Observatory, Nauchny, Crimea 98409 Ukraine,
*varya@crao.crimea.ua*

ABSTRACT. Results of an intensive spectropolarimetric study of the small-amplitude purely radial pulsating $\beta$ Cephei-type star $\gamma$ Pegasi are presented. It was shown that residual intensity, full width at half maximum and equivalent width of the He I 6678 line vary during 0.15-day pulsation period and reach its maximal value when the temperature of the star is highest. The line parameter variations due to pulsation were explained as a temperature effect. Although no strong signatures appear in the individual longitudinal magnetic field measurements, its probable coherent variation with the well-known 0.15-day pulsation period is an indication of the presence of a weak magnetic field in $\gamma$ Pegasi. The values of $\gamma$-velocity and $2K$-amplitude of the pulsation velocity curves are presented as well as the results of its variations due to the 6.83-day orbital period.

**Key words**: stars: atmospheres, early-type; oscillations; stars: binary: spectroscopic; stars: individual: $\gamma$ Pegasi; magnetic field

## 1. Introduction

The $\beta$ Cephei-type star $\gamma$ Pegasi (HR 39, B2 IV) has one of the smallest amplitude variations in radial velocity $2K = 7\ km\ sec^{-1}$ (McNamara, 1953), light $\Delta m_v = 0.017$ (Sareyan et al., 1975) and short pulsation period $P \sim 0.15$ day. The star is believed to pulsate in a low-order, purely radial mode. De Jager et al. (1982) show that $\gamma$ Pegasi has a virtually zero rotational velocity component i.e. the star is seem rotation pole-on.

Small-amplitude pulsating stars have not often been an object of intensive high-resolution study for variation of spectral line parameters due to pulsations. In this paper the results of high-accuracy study of variation of the He I 6678 line parameters due to the radial pulsation of $\gamma$ Pegasi are presented. Photosphere displacement curves were calculated for different pulsation cycles. The difference between amplitudes of the individual curves was analysed.

Results of a number of attempts to detect magnetic field on this star (Babcock, 1958; Rudy and Kemp, 1978; Landstreet, 1982, Butkovskaya and Plachinda, 2004) left this problem unsolved. However, magnetic field with polar strength of several hundred gauss were detected on four early B-type pulsating stars: $\beta$ Cep (Donati et al., 2001), $\zeta$ Cas, $\omega$ Ori and V 2052 Oph (Neiner et al., 2003a,b,c). It was shown (Butkovskaya et al., 2006) if rotation axis of $\gamma$ Pegasi and line of sight are almost coincide, and the star hosts a dipole magnetic field then dipole axis would be situated near rotation equator plane and longitudinal component can be equal to some dozens. Using our high-accuracy measurements of the magnetic field of $\gamma$ Pegasi the variation of its longitudinal component due to pulsation cycle was studied here.

Harmanec et al. (1979) have determined the 6.83-day period of variation of the $\gamma$-axis of the pulsation velocity curves and concluded that the star is a spectroscopic binary. Ducatel et al. (1981) clearly detected day-to-day variation of the $\gamma$-velocity, but they assumed that the $\gamma$-axis probably varies due to the stellar oscillations. Today Butkovskaya et al. (2006) after careful analysis of possible origins of the 6.83-day periodic variation of the $\gamma$-velocity have concluded that the variation occurs owing to orbital motion of the star. Results of the measurements of the $\gamma$-velocity and $2K$-amplitude of the pulsation velocity curves are presented as well as the results of its variations due to the orbital period.

## 2. Observations

An intensive study of $\gamma$ Pegasi has been performed in the line He I 6678.149Å during 23 nights from 1997 to 2005, and 405 high-accuracy spectra were obtained using coude spectrograph of the 2.6-m Shajn telescope at the Crimean Astrophysical Observatory. Signal-to-noise ratios of a single spectrum were typically 350-600 with resolving power of spectra approximately $2.2 \times 10^4$.

## 3. Discussion and conclusions

### *3.1. Pulsation*

The phases of the basic pulsation period have been computed from the ephemeris $JDh = 2451060.461 \pm$

0.15175039 (Butkovskaya and Plachinda, 2004).

In Figure 1a,c,d,e radial velocity (RV) as well as core residual intensity (RI), full width at half maximum (FWHM), equivalent width (EW) of the line He I 6678 as a function of the pulsation period phase are presented. The mean pulsation cycle values of both radial velocity and all three spectral line parameters were subtracted.

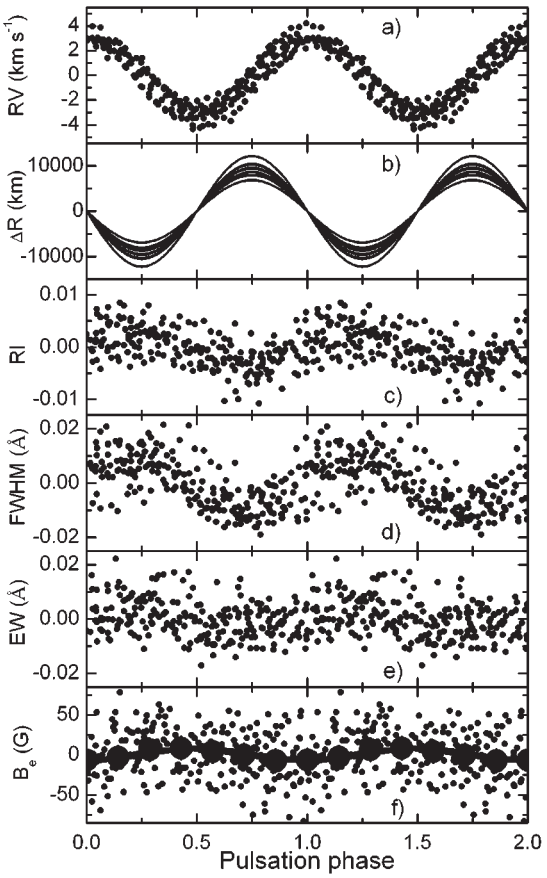


Figure 1: Pulsation

The RI, FWHM and EW of the helium line rich its maximal values in maximum compression phase when the temperature of the star is highest. The line parameter variations due to pulsation would be explained as a temperature effect.

The photosphere displacement curves calculated in standard manner (see Mathias et al., 1991, Appendix B) are presented in Figure 1b. The amplitude of photosphere displacement differs from one pulsation cycles to another. The star is an open thermodynamic system, and the discrepancy between the individual curves occurs because these values are determined in a highly non-linear fashion by the physical conditions in and above the He ionization zones in the star, so that small variations in the structure of the outer layers of these stars could easily lead to significant changes in pulsation properties (Christy, 1966). $\gamma$ Pegasi is a spectroscopic binary and the instability in the ionization zone can be owing to tidally effect of the secondary component.

In the Figure 1f longitudinal magnetic field against pulsation phases is presented (small filled circles) as well as the same data binned into 7 bins (large filled circles). The least-square sinusoidal fitting is shown by solid line As it has been estimated by Butkovskaya et al. (2006) that owing to frizzing of magnetic field into plasma the longitudinal magnetic field variation due to the radial pulsation of $\gamma$ Pegasi would be less than 1 G. But in the Figure 1f the longitudinal magnetic field shows periodic variation with amplitude of about 7 G, moreover, the reverse of its polarity exists. Therefore, in the case of $\gamma$ Pegasi the variation of the magnetic field due to the radial pulsations of the star could not be explained only in the frame of the pulsation motion of stellar atmosphere. Additional data, which will require further precise observations are needed in order to confirm these results.

### *3.2. Binarity*

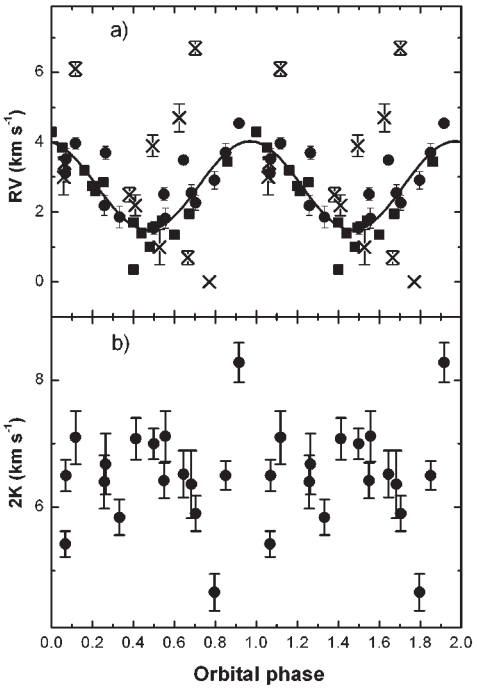


Figure 2: Orbital motion

McNamara (1955) pointed out a possibility that $\gamma$-axis of the 0.15-day velocity curve of $\gamma$ Pegasi varies. Harmanec at al. (1979) have determined the 6.83-day

period for the variations of the $\gamma$-axis and concluded that the star is a spectroscopic binary. Later, Ducatel et al. (1981) also clearly detected day-to-day variation of $\gamma$-axis, but they supposed that the variation can be associated with stellar oscillation. Recently Butkovskaya et al. (2006) after careful analysis of possible origin of the 6.83-day periodic variation of the $\gamma$-axis concluded that the star is a spectroscopic binary as it was claimed by Harmanec et al. (1979). In the Figure 2a,b $\gamma$-velocities and $2K$-amplitude of the pulsation velocity curves folded with the orbital period phase are presented. In the Figure 2a filled circles represent our $\gamma$-velocity data, filled squares are data taken from Figure 1 in paper of Harmanec et al. (1979), and crosses are data of Ducatel et al. (1981). The $\gamma$-velocity and $2K$-amplitude values are given in Table 1 (columns 2 and 3). Here the column labeled JDh indicate the Heliocentric Julian Date.

Table 1: $\gamma$-velocity and $2K$-amplitude

| *JDh* | $\gamma$ $(km\ s^{-1})$ | $2K$ $(km\ s^{-1})$ |
|---|---|---|
| 2451060.481 | 2.27 ± 0.22 | 5.90 ± 0.28 |
| 2451061.480 | 3.71 ± 0.26 | 6.50 ± 0.23 |
| 2451088.430 | 2.91 ± 0.25 | 4.66 ± 0.29 |
| 2451171.218 | 4.54 ± 0.13 | 8.28 ± 0.31 |
| 2451172.251 | 3.11 ± 0.27 | 5.42 ± 0.20 |
| 2451488.272 | 1.86 ± 0.32 | 5.84 ± 0.28 |
| 2452217.366 | 3.52 ± 0.30 | 6.50 ± 0.25 |
| 2453280.317 | 2.55 ± 0.23 | 6.36 ± 0.53 |
| 2453283.283 | 3.97 ± 0.17 | 7.10 ± 0.42 |
| 2453284.284 | 3.70 ± 0.19 | 6.68 ± 0.48 |
| 2453598.455 | 2.19 ± 0.29 | 6.40 ± 0.42 |
| 2453600.448 | 2.52 ± 0.18 | 6.42 ± 0.28 |
| 2453627.426 | 1.54 ± 0.18 | 7.00 ± 0.24 |
| 2453628.421 | 3.49 ± 0.08 | 6.52 ± 0.37 |
| 2453688.308 | 6.49 ± 0.24 | 7.08 ± 0.33 |
| 2453689.294 | 1.82 ± 0.29 | 7.12 ± 0.40 |

*Acknowledgements.* The author is thankful to Sergei Plachinda for helpful discussion.

## References

Babcock H.W.: 1958, *Astrophys. J. Suppl. Ser.*, **3**, 141.
Butkovskaya V.V. & Plachinda S.I.: 2004, *JQSRT*, **88**, 17.
Cristy R.F.: 1966, *Astrophys. J.*, **144**, 108.
De Jager C. et al.: 1982, *Astrophysic and Space Science*, **83**, 411.
Donati J.-F. et al.: 2001, *MNRAS*, **326**, 1265.
Ducatel D. et al.: 1981, *Astron. Astrophys. Suppl. Ser.*, **43**, 359.
Harmanec P. et al.: 1979, *IBVS*, **1590**, 1.
Landstreet J.D.: 1982, *Astrophys. J.*, **258**, 639.
Mathias, P. et al.: 1991, *Astron. Astrophys.*, **252**, 245.
McNamara D.H.: 1955, *Astrophys. J.*, **122**, 95.
Neiner C. et al.: 2003a, *Astron. Astrophys.*, **406**, 1019.
Neiner C. et al.: 2003b, *Astron. Astrophys.*, **409**, 275.
Neiner C. et al.: 2003c, *Astron. Astrophys.*, **411**, 565.
Rudy R.J. & Kemp J.C.: 1978, *MNRAS*, **183**, 595.
Sareyan J.-P. et al.: 1975, *Astron Astrophys.*, **44**, 215.

# NEW PERIOD OF THE LONGITUDINAL MAGNETIC FIELD VARIABILITY IN Ap STAR $\gamma$ EQU

V.D. Bychkov[1,3], L.V. Bychkova[1], J. Madej[2]

[1] Special Astrophysical Observatory of the Russian Academy of Sciences, Nizhnij Arkhyz, 369167 Russia, *lbych@sao.ru*
[2] Warsaw University Observatory, Al. Ujazdowskie 4, 00-478 Warsaw, Poland, *jm@astrouw.edu.pl*
[3] Stavropol State University, ul. Pushkina 1, 355009 Russia, *vbych@sao.ru*

ABSTRACT. We present an analysis of the secular variability of the longitudinal magnetic field $B_e$ in the roAp star $\gamma$ Equ (HD 201601). Measurements of the stellar magnetic field $B_e$ were mostly compiled from the literature. We appended our new 33 $B_e$ observations which were obtained at the Special Astrophysical Observatory. All the available data cover the time period of 58 years, and include both phases of the maximum and minimum $B_e$. We determined that the period of long-term magnetic variations in $\gamma$ Equ equals to $91.1 \pm 3.6$ years. **Key words**: Stars: magnetic field; stars: individual: Gam Equ.

## 1. Introduction

The Ap star $\gamma$ Equ (HD 201601, BS 8097) is one of the brightest objects of this class, with the apparent luminosity $V = 4.66$ mag. Magnetic field of $\gamma$ Equ was studied from over 50 years, starting from October 1946 (Babcock 1958). Longitudinal magnetic field $B_e$ of this star does not exhibit periodic variations in time scales of usual stellar rotation, $0.5 - 30$ days. Such a variability of $B_e$ field was observed in most of Ap stars. The above effect is commonly interpreted as the result of stellar rotation (oblique dipole model).

The first measurements by Babcock (1958) showed, that the value of the longitudinal magnetic field $B_e$ of $\gamma$ Equ was positive in 1946–52, and approached +900 G. From that time on the value of $B_e$ slowly decreased and even changed sign in 1970/71. One could interpret magnetic behavior of $\gamma$ Equ either as secular variations, or variations caused by extremely slow rotation.

Behavior of the $B_e$ field in $\gamma$ Equ was investigated by many authors in the second half of the twenty*th* century. The previously determined period of secular magnetic variations, $P_{sec} = 27027^d = 74.0$ years (cf. the extensive catalog by Bychkov et al. 2005a). This research and the analysis of a new, longer time series of $B_e$ data is a major revision of the above magnetic period of $\gamma$ Equ.

We appended here our unpublished magnetic $B_e$ measurements (33 points), which were obtained during the recent 7 years. All the new magnetic observations showed, that slow decrease of the $B_e$ field in $\gamma$ Equ apparently reached the minimum value in 1996–2002 and actually started to increase.

## 2. Observations and data processing

We have performed spectropolarimetric observations of Zeeman line splitting for $\gamma$ Equ in the Coude focus of the 1-m optical telescope (Special Astrophysical Observatory, Russian Academy of Sciences).

## 3. Magnetic period of $\gamma$ Equ

The $\gamma$ Equ exhibited slow and systematic decrease of the longitudinal magnetic field $B_e$ starting from 1946, when the global magnetic field of this star was discovered (Babcock 1958). We have compiled the full set of 298 existing $B_e$ measurements, which consists of the $B_e$ data published in the literature and our observations obtained during recent 7 years (33 $B_e$ points). New magnetic observations, which were obtained at SAO in 1997–2004, include the phase when the effective magnetic field $B_e$ in $\gamma$ Equ apparently reached its minimum value over the recordedv 58 years of observations. This fact is of extraordinary importance, because it allows one for a fairly accurate determination of the magnetic period and the amplitude of $B_e$ variations in $\gamma$ Equ.

1946–2004 (58 years), see Fig1 (Bychkov et al. 2005c). Assuming that the run of the observed longitudinal field $B_e$ with time $T$ can be approximated by a sine wave

$$B_e(t) = B_0 + B_1 \sin\left[\frac{2\pi(t - T_0)}{P} - \frac{\pi}{2}\right], \qquad (1)$$

we determined all four parameters and their errors simultaneously, using the least squares method.

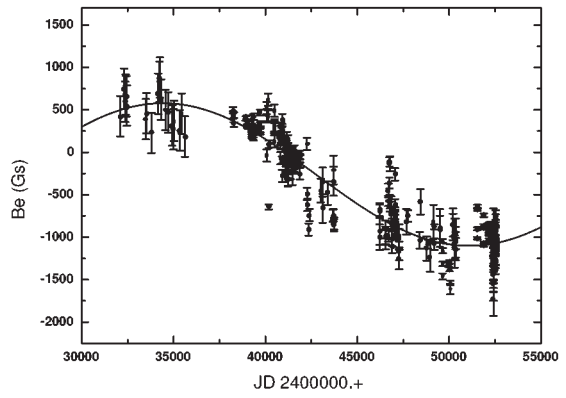


Figure 1: Longitudinal magnetic field $B_e$ for $\gamma$ Equ in years 1946–2004.

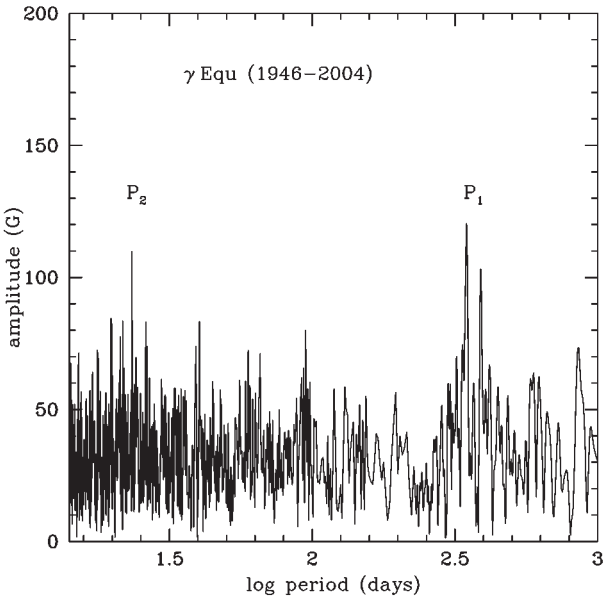


Figure 2: Amplitude spectrum of the $B_e$ time series for $\gamma$ Equ, years 1946–2004.

## 4. Search for additional periods in $\gamma$ Equ

All the available data cover the time period of 58 years (1946-2004) and include both phases of the maximum and minimum $B_e$. Significant scatter of the observed points in the long-term run of $B_e(t)$ in Fig. 1 suggests the search for short-term periodicities. We applied the strategy of prewhitening to the set of available $B_e$ measurements, and removed the principal sine-wave variations from the data. Prewhitened data were then analysed with the method developed by Kurtz (1985), and with his Fortran code (Kurtz 2004). We have identified two additional periods of statistically low significance, see Fig.2:

$P_1 = 348.07$ days, amplitude = 122 G
$P_2 = 23.44$ days, amplitude = 110 G

Both peaks in the amplitude spectrum in Fig.2 exhibit low signal to noise ratio, with noise level at ca. 80 G. The period $P_1$ is close to 1 year. Since most of the existing $B_e$ observations for $\gamma$ Equ were performed in months August-October, then the peak $P_1$ in the amplitude spectrum represents a false period which most likely reflects the average 1-year repetition time in the acquisition of the existing magnetic measurements.

## 5. Summary

Assuming that the secular variability of the $B_e$ field is a periodic feature, we determined parameters of the magnetic field curve in $\gamma$ Equ and give the value of its period, $P = 91.1 \pm 3.6$ years, with the zero phase (maximum of $B_e$) at $T_0 =$ JD $2417794.9 \pm 62.7$. Sine-wave fit to the $B_e$ phase curve yields $B_e(\max) = +578$ G and $B_e(\min) = -1102$ G.

Spectral analysis of the 58-year long $B_e$ time series essentially do not show the existence of shorter periods, down to trial periods of $\approx 1$ day. More specifically, there are no real shorter periods in the run of the longitudinal magnetic field $B_e$ with amplitudes exceeding the noise level of 80 G.

There exists a possibility that $\gamma$ Equ exhibits periodic variability of its magnetic field $B_e$ in time scale of the order 10 minutes (Bychkov at al. 2005b). Such a variability can be due to nonradial pulsations of this star.

*Acknowledgements.* We thank Don Kurtz for providing his Fortran software used here to compute the amplitude spectrum of $\gamma$ Equ. We acknowledge support from the Polish Committee for Scientific Research grant No. 1 P03D 001 26.

## References

Babcock H.W.: 1958, *Ap.J.S.* **3**, 141.
Bychkov V.D., Bychkova L.V., Madej J.: 2003, *A.&A.* **407**, 631.
Bychkov V.D., Bychkova L.V., Madej J.: 2005a, *A.&A.* **430**, 1143.
Bychkov V.D., Bychkova L.V., Madej J.: 2005b, *Acta Astronomica*, **55**, 141.
Bychkov V.D., Bychkova L.V., Madej J., Sarkisyan A.N.: 2005c, *Bull. GAISh*, **LXXVIII**, 76.
Bychkov V.D., Romanenko V.P., Bychkova L.V.: 1998, *Bull.SAO*, **45**, 110.
Bychkov V.D., Romanenko V.P., Bychkova L.V.: 2000, it Bull.SAO, **49**, 147.
Kurtz D.W.: 1985, *M.N.R.A.S.*, **213**, 773.
Kurtz D.W.: 2004, *personal communication.*

# MAGNETIC FIELD VARIABILITY OF STARS

V.D. Bychkov[1,3], L.V. Bychkova[1], J. Madej[2]

[1] Special Astrophysical Observatory of the Russian Academy of Sciences, Nizhnij Arkhyz, 369167 Russia, *lbych@sao.ru*
[2] Warsaw University Observatory, Al. Ujazdowskie 4, 00-478 Warsaw, Poland, *jm@astrouw.edu.pl*
[3] Stavropol State University, ul. Pushkina 1, 355009 Russia, *vbych@sao.ru*

ABSTRACT. We present in this paper a description for various types of the apparent variations of stellar magnetic fields, which we actually recognise.

**Key words**: Stars: magnetic field; stars: fundamental parameter

## 1. Introduction

Recently we investigated magnetic behavior of 139 stars, including 134 Ap stars and 5 solar-type stars (Bychkov et al. 2005a). Results of this research allowd us to recognize 7 classes of stars which exhibit specific types of the apparent magnetic field variations.

Ap stars usually exhibit strong global magnetic fields. Occurence of global magnetic field of a given strength in subclasses of Ap stars of various chemical peculiarities was studied e.g. by Bychkov et al. (2003).

In the following sections we discuss variability of the so-called effective magnetic field $B_e$, which is the most easily observable quantity derived from the real magnetic field of a star. The actual value of $B_e$ is usually determined from the Zeeman splitting of hydrogen or metal spectral lines.

## 2. Types of the stellar magnetic variability

**Type I. Simple harmonic.** Variability of the effective magnetic field $B_e$ in most of Ap-stars investigated up to now ($\approx 87\%$) exhibits form of a simple sine wave. Half-amplitudes of the sine wave typically are in the range from few tens to few thousands G, see Fig. 1 (Bychkov et al. 2005a). Period of the above magnetic variations equals to the rotational period of a given star. Such a variability is fully described in frame of the Stibbs-Preston oblique rotator model.

**Type II. Double wave variations.** Behavior of the effective magnetic field $B_e(t)$ as a function of time $t$ is not as simple as the sine wave. In such a case the shape of $B_e$ is best described by a sine wave with overlying second harmonic term, the latter with the amplitude typically $10 - 20\%$ of the main harmonic.

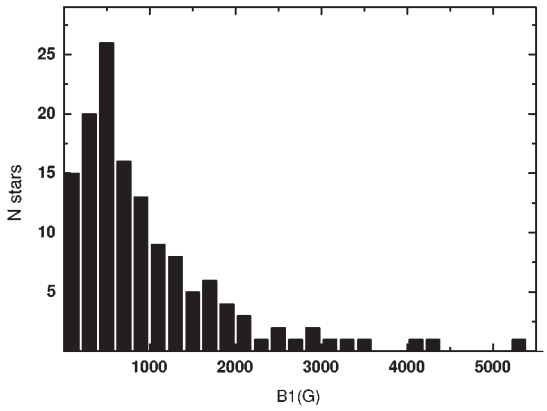


Figure 1: Number distribution of the half-amplitude $B_e$ variability.

The number of stars with double wave $B_e(t)$ is $\approx 13\%$ of the total number of known stars which have measurable global magnetic fields. Well known magnetic stars which exhibit double wave variations of $B_e$ is HD 32633, named Renson's star (Renson 1984), see Fig. 2.

Such the form of the curve $B_e(t)$ is generated by a rotating quadrupole.

**Type III. Complex variations.** There exist stars where $B_e(t)$ cannot be given by simple formulae. Example of such a star is HD 37776 (Thompson & Landstreet 1985), see Fig. 3. The number of stars with complex $B_e(t)$ is less than 1% of the total number.

**Type IV. Long period variations.** Research on magnetic fields of stars has started over 50 years ago. During that time period researchers accumulated long time series of magnetic measurements for a number of stars. Such series allow one to study of the long-period (secular) variability of the global magnetic field. The

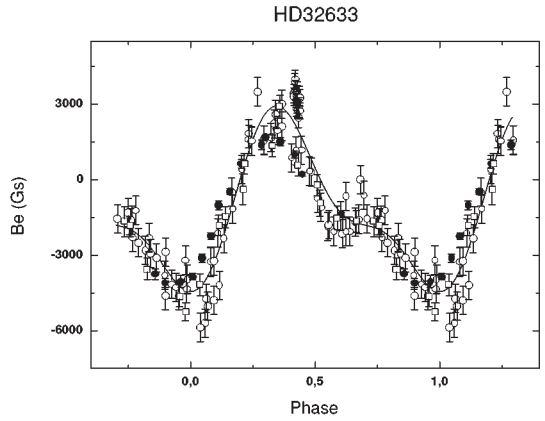


Figure 2: Magnetic phase curve $B_e$ for HD 32633 (Renson 1984).

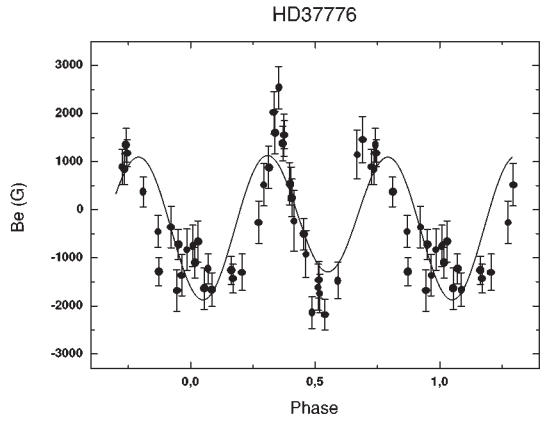


Figure 3: Magnetic phase curve $B_e$ for HD 37776 (Landstreet & Thompson 1985).

occurence of such a variability in stars is low, and do not exceed 3 %.

The outstanding example is the Ap star HD 201601 ($\gamma$ Equ) (Bychkov et al. 2006).

**Type V. Irregular magnetic variations.** The only known star with irregular magnetic variations is 52 Her. This star usually displays typical sine wave $B_e(t)$ with the average intensity +500 G. However, in the time interval JD 2442400 – 2444200 the average intensity of the effective magnetic field decreased to −3500 G, and later the value of $\langle B_e \rangle$ in slowly increased to +500 G.

Actually there is no convincing explanation for such a behavior of 52 Her.

**Type VI. Rapid variations.** There exist a group of rapidly oscillating Ap-stars, with display also rapid variations of the global effective magnetic field $B_e$ (Leone & Kurtz 2003; Bychkov et al. 2005b). Rapid variations proceed with periods 3 – 12 min. and are caused by non-radial pulsations of the star and its magnetic field.

**Type VII. Late-type stars with global magnetic fields.** The use of new technologies for the measurements of stellar magnetic fields has lead to the discovery of weak magnetic fields in late-type stars. Strong local magnetic fields in surface layers of late-type stars were known from a long time. However, weak global fields recently were found in a number of stars, see Plachinda & Tarasova (2000), Neiner et al. (2003). The amplitude of periodic variations of $B_e$ in late-type stars does not exceed few tens of G.

## 3. Summary

In this paper we presented general description of stellar magnetic variability of all types which were recognised up to date. The principal aim of such a description is the search of an answer for the principal question: **what is the origin and evolution of global magnetic fields in stars ?**

*Acknowledgements.* We acknowledge support from the Polish Committee for Scientific Research grant No. 1 P03D 001 26.

## References

Bychkov V.D., Bychkova L.V., Madej J.: 2003, *A.&A.* **407**, 631.

Bychkov V.D., Bychkova L.V., Madej J.: 2005a, *A.&A.* **430**, 1143.

Bychkov V.D., Bychkova L.V., Madej J.: 2005b, *Acta Astronomica*, **55**, 141.

Bychkov V.D., Bychkova L.V., Madej J.: 2006, *MNRAS*, **365**, 585.

Bychkov V.D., El'kin V.G., Shtol' V.G.: 1992, *Stellar Magnetism, International Conference Proceedings*, Russia, Nauka, 211.

Leone F. and Kurtz D.: 2003, *A&A*, **407**, L67.

Neiner C., Geers V.C., Henrichs H.F., Floquet M., Hubert A.M., Preuss O., Wiersema K.: 2003, *A&A*, **406**, 1019.

Placinda S.I., Tarasova T.N.: 2000, *Ap.J.*, **533**, 1016.

Renson P.: 1984, *A&A*, **139**, 131.

Thompson I.B., Landstreet J.D.: 1985, *Ap.J.*, **289**, L9.

# roAp STARS AS OBJECTS FOR ASTEROSEISMOLOGY

T.N. Dorokhova, N.I. Dorokhov
Astronomical Observatory of Odessa National University
Marazlievskaya, 1v 65014 Odessa, Ukraine,
*astro@paco.odessa.ua*

ABSTRACT. To date the rapidly oscillating Ap (roAp) stars are one of the best-studied objects of the Main Sequence. There are reviewed the recent results for HD 99563 and $\gamma$ Equ as examples of stars with stable and unstable oscillations. HD 99563 for its turn compared with the well-studied HR 3831. There are shown how the data obtained in multi-longitudinal photometric campaigns using small apertures' telescopes and the data of time-resolved spectroscopy from large telescopes, even the VLT (Very Large Telescope), supplement each other promoting the high specification of the atmospheric and fundamental stellar parameters, of the magnetic fields' geometries and evolutionary state. There are described the difficulties and recent results of roAp stars' searching in the northern hemisphere and, particularly, the data from the Mt. Dushak-Erekdag survey of Odessa Astronomical Observatory.

**Key words:** Stars: Chemically peculiar - stars: Oscillations - stars: Variables - stars: individual: $\gamma$ Equ, HD 99563, HR 3831.

## 1. Introduction

This rare type of pulsating peculiar A stars was discovered by Donald Waine Kurtz in 1978 in the South-African Observatory. The history of its discovery and investigations (Kurtz,1990, Kurtz& Martinez, 2000) is one of the best samples of a "good study" of small, but extremely important for astroseismology group of stars.

The roAp stars lie within the $\delta$ Scuti instability strip and exhibit high-overtone non-radial p-mode pulsations in contrast to low-overtone modes which characterize typical variables of the strip. Such a way, the roAp stars have considerably smaller periods, for today are known from 5.65 to 21.0 min and ampitudes of an order of mmag. Most of the stars are multiperiodical, and that is the main concern of asteroseismology. Another important thing these chemically peculiar cool A and early F stars evolutionary are close to the Sun at the Main Sequence.

The features of this group of Ap stars:

- belong to the mostly cool ($T_{eff} \sim 7400°K$) SrCrEu group of the chemically peculiar A-F IV-V stars;
- are slow rotators, vsini $\leq$ 100 km/sec;
- have strong magnetic fields with variation from some days to decades;
- magnetic fields cause that abundance anomalies are accumulated in spots on the stellar surface.

The last attribute appears in the modulation of the mean apparent brightness of the star with the rotation period. Stibbs (1950) produced the oblique rotator model suggesting that the axis of dipol magnetic field is not aligned with the stellar rotation axis. Kurtz (1982) developed this model for oscillating Ap stars, so called the oblique pulsator model (OPM) with the assumption that the pulsation axis coincides with the magnetic axis of the star. The OPM suggests that for a rotating star dipole (l= 1) pulsation modes will be split into equally spaced triplets, quadrupole (l= 2) modes will be split to equally spaced quintuplets, and the frequency differencies are exactly the rotation frequency.

Further Dziembowski & Goode (1985) expanded the OPM for the presence of magnetic field which affects the pulsations that observationally bring the additional multiplet components surrounding the first-order frequency configuration. Developing of these models and the possibility checking the models with high accuracy (see Kurtz, 1992) shows roAp stars as ideal laboratories for application of the theory of asteroseismology. Such a way, the seaches for and comprehensive investigations of these stars consider a specially actual matter.

## 2. Searching for roAp stars in the Northern hemisphere observatories

Up to date the list of roAp stars comprises 34 objects, and about 80 % of the stars were discovered in South-African Observatory (see Kurtz, 1990; Martinez et al., 1991; Martinez & Kurtz, 1994a, 1994b). Probably, that is one of the reasons of a mysterious disproportion in the number of known roAp stars in the two hemispheres of the sky. Until 1998 only two roAp stars with positive declination were discovered although several surveys were aimed for searches of especially northern roAp stars (Mattews & Wehlau 1985,

Heller & Kramer 1988, Nelson & Kreidl 1993).

Afterwards some new substantial projects were initiated:

- Handler & Paunzen (1999) in a frame of the Vienna survey examined for rapid oscillations 17 objects, with twin 0.75 m APT in Arizona, and 0.9 m and 2.1 m telescopes at McDonald Observatory, discovered 1 northern roAp star (HD122970) and 3 $\delta$ Scuti variables.
- The Naini Tal, Indo-SA (South-african) survey has been initiated by using the 1-m telescope at Naini Tal Observatory (Ashoka et al. 2000) There were investigated more than 150 candidates, discovered 1 northern roAp star (HD12098), two Ap stars were suspected for the rapid oscillations and 3 $\delta$ Scuti variables (see Joshi, 2005, Girish, 2005).
- The UBC-OAN Survey (Canada & México) monitored about 50 cool A-Fp stars with a single-channel photoelectric photometer and a Johnson B filter, attached to 84-cm and 1.5-m telescopes at the Observatorio Astronomico Nacional (OAN) in Mexico.

After all efforts the list of roAp stars with positive declination run up to 4.

Actually, the detection of roAp stars in the Northern hemisphere seems a stubborn problem. The reason, possibly, is that the Northern hemisphere's atmospheric transparency is distorted by an influence of so-called "a human factor", it is much more polluted with products of a human vital activity, than an atmosphere of Southern hemisphere.

## 3. Latter results on field stars from the Mt. Dushak-Erekdag Survey

We continued the observations for Mt. Dushak-Erekdag Survey which was initiated in 1993. The search scheme and the first results have been presented with details in Dorokhova (1997).

Table 1 lists for all observed field stars HD numbers, visual magnitudes, spectral types from HD Catalogue and spectral types from Catalogue of Am and Ap stars (Renson, 1991), observational interval in hour (for HD 217401 for 2 nights, BD 8087 for 4 nights), mean deviation $\sigma$ for high-frequency region in mmag. The bottom part of the table under the line presents the observations of 2001-2003 years.

Since we could use only the short fragments of observational time we have developed the methods of clearing data which were obtained under a non-ideal atmospheric transparency. A low-frequency atmospheric and instrument trends of the data were removed with using Butterworth's filters of the different degrees and cutoff frequencies (Dorokhova & Dorokhov, 2005).

A rectangle filters were applied to comparison stars' data for smoothing. The programs PERIOD (Breger 1990), FOUR (Andronov 1994) and Period98 (Sperl 1998) were used for the frequency analysis.

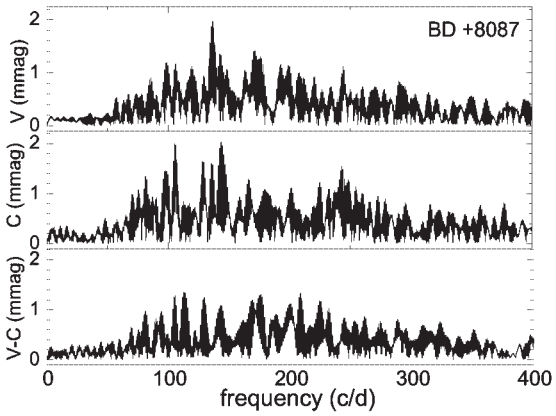


Figure 1: Fourier spectra of BD +8087 (upper), comparison star (middle) and differences var-comp (bottom).

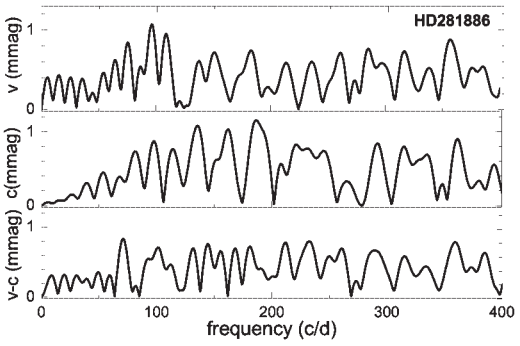


Figure 2: Fourier spectra of HD281886 (upper), comparison star (middle) and differences var-comp (bottom).

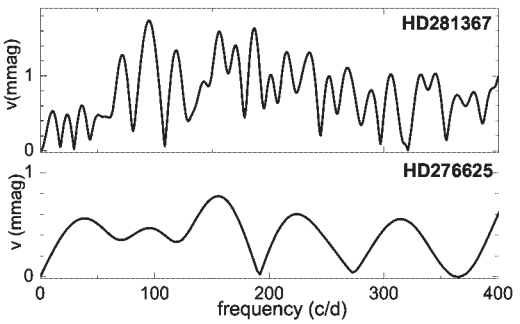


Figure 3: Fourier spectra of HD281367 and HD276625.

Table 1: List of field Ap stars tested for the rapid oscillations.

| Star | $m_v$ | Sp | Sp (Rn) | $\Delta$ T | $\sigma$ |
|---|---|---|---|---|---|
| HD15257 | 5.4 | F0 | | 6.0 | 0.9 |
| HD17317 | 8.3 | A5p | | 1.1 | 6.5 |
| HD99563 | 8.2 | F0 | F0 Sr | 2.0 | 1.6 |
| HD115606 | 8.3 | A2 | A2 Sr | 4.0 | 1.1 |
| HD217401 | 8.0 | A2p | A2 Sr | 7.2 | 1.2 |
| HD276625 | 10.0 | A7 | A7 CrEu | 1.5 | 1.0 |
| HD281367 | 10.0 | A7 | A8 SrEu | 2.2 | 1.6 |
| HD281886 | 8.9 | F0p | F0 Sr | 2.5 | 1.0 |
| BD+8087 | 9.6 | Ap | F0 SrEu | 15.5 | 2.8 |

We concentrated our efforts on researches of the northernmost star BD+8087 (Fig.1). In a single non-ideal photometric night of 2001 the target revealed oscillations with period about 11 min and amplitude of 7 mmag. In the data of 2003 once more the peak at 136 c/d was detected, however, the comparison star data showed the peak at 142 c/d. Nevertheless, rather large standard deviations of about 3 mmag indicate the possible rapid variability.

HD281886 was observed simultaneously with the comparison star in the channel 2. The Fourier spectra at the Fig.2 show the absence of rapid variability within the detection limits of 0.8 mmag. HD281367 and HD276625 (Fig.3) are less investigated, and we suggest to continue testing them for rapid oscillations.

## 4. NGC752

The attempts testing cluster stars for the presence of rapid oscillations were undertaken earlier (e.g. Matthews et al. 1988), however, so far none roAp stars were revealed in cluster.

NGC 752 provides an ideal test of a variety of evolutionary phenomena and it seems a very suitable due to plenty of early F type stars. This intermediate-age, estimations from 1.7 $\pm$ 0.1 Gyr to 1.9 $\pm$ 0.2 Gyr, open cluster for which full suite of comprehensive investigations has been performed (see, for example, Daniel et al. 1994). There were also some efforts hunting for variable stars, especially, for variable blue strugglers in the cluster (Milone &Latham 1994).

However, a test for the presense of roAp stars in this cluster was never carried out, possibly, considering its metal-poor nature although estimates of Fe/H are rather different: -0.09 (Hobbs & Thorburn 1992), -0.15 (Daniel et al.1994). -0.27 (Dinescu et al. 1995).

The list of stars tested for the rapid oscillations in NGC 752 presented in Table 2: in the columns 1, 2, 3, 4 the numbers of investigated stars are indicated according to lists of K - Kazanasmas et al. (1981), H - Heinemann (1926), R - Rebeirot (1970) and BD catalogue; the columns 5 and 6 show photographic magnitudes and spectral type.

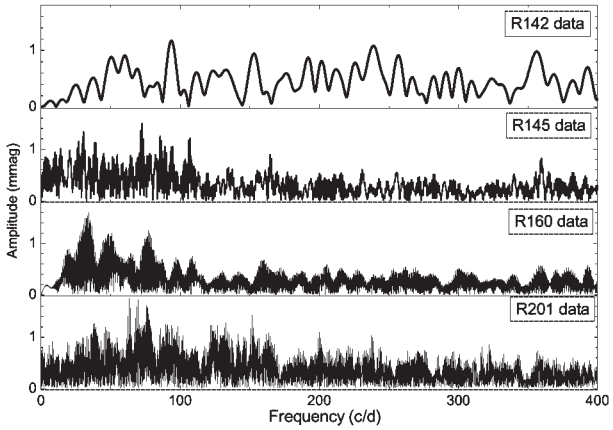


Figure 4: Fourier spectra of NGC 752 objects, the numbers in the right corners according to Rebeirot (1970).

Table 2: List of stars tested for the rapid oscillations in NGC 752.

| No K | No H | No R | BD | mg | Sp |
|---|---|---|---|---|---|
| 47 | 171 | 142 | +36 363 | 10.6 | F2V |
| 56 | 193 | 145 | +36 365 | 10.4 | F0III |
| 59 | 205 | 160 | +37 431 | 10.5 | F2III |
| 81 | 263 | 201 | | 11.1 | F3 |

According Niedzielski & Muciek (1988) and Renson (1989) all selected stars are peculiar, however, its Strömgren indices from Catalogue by Hauck & Mermilliod (1990) do not fall within the margins indicated for roAp stars by Martinez, Kurtz & Kauffmann (1991).

The results of these observations:
- R142 is a constant within limits of 1 mmag;
- R143 frequency spectrum have showed some very low amplitudes and not stable from night to night peaks, apparently, being attributed to atmospheric transparency;
- in the data of R160 possible the presence of pulsations of 34 and 77 c/d but very low amplitudes and not stable from night to night;
- the frequency spectrum of R201 shows some peaks in the 60-75 c/d with amplitudes of 2 mmag, which are unstable from night to night and, apparently, caused by variations of atmospheric transparency.

We regret that this work was unfinished from political obstacles and hope that we continue the search of roAp stars in clusters with modern CCD techniques.

### 5. HD 99563 and HR 3831

A rapid variability of HD 99563 (XY Crt) was discoverd within the framework of Mt. Dushak-Erekdag Survey (Dorokhova, 1997). A year latter the periodic oscillations were confirmed by Handler & Paunzen (1999).

In 1998 Handler et al. (2002) carried out the multisite campaign for the star. 125 hours of the high speed photometry have been obtained using seven telescopes at four different longitudes' observatories. Handler et al. (2005) also acquired mean light observations for the star over four seasons. Here we explicate the recent campign results as an example of an advanced study of roAp stars.

HD 99563 classified as F0 in HD catalogue and F0 Sr in the Ap and Am stars Catalogue by Renson (1991), its Strömgren indices (H$\beta$ = 2.830, $\delta m_1$ = 0.000 and $\delta c_1$ = -0.109) fall into a margin marked by Martinez, Kurtz and Kauffmann (1991). The star belongs to a binary system ADS 8167, B component is in a distance 1.7 arcsec and lighter on $\Delta$ V= $1.^m2$. This involves the correction of photometric amplitudes which should be increased by 30%. Handler et al. (2002) revealed 8 frequencies in the preliminary analysis which were equally separated in two group around 1.557 mHz and 3.115 mHz. Then Handler et al. (2005) ascertain position of the physical pair HD 99563 in the HR Diagram applying a complete set of the data from HIPPARCOS, Tycho-2, high resolved spectroscopy and fundamental photometry. On this base there were obtained the fundamental parameters of the components in the first approximation. From the analysis of the splitting in the frequency spectrum and mean light data they determined the rotation period of HD 99563A with accuracy of $\pm$6 sec.

Assuming that HD 99563A pulsates with a single pulsation mode 1.557653 mHz and some first harmonics of it Handler et al. (2005) consider an equally spaced frequency triplet appears due to the rotation of the star. The additional components from quintuplet appear due to the distorting effect of magnetic field of the star. Then for HD 99563A the distortion of the pulsation modes has been modeled and the all parameters of the star were obtained and corrected. This complete set of the accurate parameters for both stars of HD 99563 binary we collected in the Table 4. With these model parameters Handler et al. (2005) perfectly reproduced the observed pulsational amplitudes and phases over the stellar rotation cycle. The fig.6 from Handler et al. (2005) is very similar to the inverse problem solutions which were obtained a decade before by Kurtz, Kanaan, Martinez (1993) for another roAp star HR 3831.

HR 3831 (HD 83368) is one of the best-studied roAp star, even so called prototype (see Kochukhov, 2004), and it is also a wide binary. In HR 3831 the separation between the components is 3.29 arcsec and difference in brightness is $\Delta$V= 2.84.

Now after the work of Hundler et al. (2005) it is possible comparing HD 99563 and HR 3831 fundamental data (see the Table 3). The data in table 3 are mainly extracted from Hundler et al. (2005) for HD 99563 and from Kurtz, Kanaan, Martinez (1993) for HR 3831. The measurements of the mean magnetic field of HD 99563 are taken from Hubrig et al. (2004).

Both objects are remarkably similar but HD 99563 is more massive and, accordingly, more evolved system. If for HR 3831 there were carried out some multisite campaigns for consecutive years whereas HD 99563 is recently started for investigations.

Elkin, Kurtz & Mathys (2005) discovered from the series of 110 time-resolved spectra of HD 99563 the most extreme example of pulsational radial velocity variations with semi-amplitudes of up 5 kms$^{-1}$ for some EuII and TmII lines. Such high amplitudes could yield the information on the structure of the Ap star's atmosphere with the best possible signal to noise. This factor and the favourable geometry of the star which allows seeing both pulsation poles during the small rotation period gives an opportunity to obtain the Doppler imaging (DI) of its surface.

In the recent work by Kochukhov (2004) the precise velocity map was recovered for HR 3831 with the DI techniques and it permits testing the theoretical speculations with the high accuracy. Kochukhov (2004) discovered that pulsations of the star are strongly confined to the magnetic field axis, that specifies the dominant role of a magnetic field in forming of pulsations' geometry completely according to predictions of Saio & Gautschy (2004) calculations.

These two stars are examples of typical roAp stars for which the stable pulsations during decades or, at least, years are proper. However, there exist a few of roAp stars which have very unstable frequencies and amplitudes of pulsations, for example, the well-known $\gamma$ Equ.

### 6. $\gamma$ Equ

$\gamma$ Equ (HD 201601, V=$4^m.71$, F0p) - one of the brightest and, accordingly, the most investigated roAp stars. Babcock (1958) has discovered the Zeeman effect splitting lines in the star's spectrum with testified to a significant magnetic field. Intensity of a field slowly changed from 500 Gs in 1950s, passing through zero in early 1970s [74], and achieving -1000 Gs in 1988 (Mathys, 1991). Bonsack & Pilachowski (1974) have assumed, that the magnetic field of a star varies with the period 72 years.

Table 3: Fundamental data and parameters for components of HD 99563 and HR 3831 systems.

| Parameter | HD 99563A | HR 3831A |
|---|---|---|
| Spectral type | F0p Sr | A7p V SrCrEu |
| Frequency | 1.557653 mHz (P= 10.7 min) | 1.4280128 mHz (P = 11.7 min) |
| Johnson's indices | V = 8.72, B-V = 0.20 | V = 6.168, B-V = 0.25 |
| Rotation period | 2.91179 d | 2.851982 d |
| Absolute magnitude $M_v$ | 1.9 | 2.0 |
| $T_{eff}$ | $\sim 8000°K$ | $\sim 8000°K$ |
| $vsini$ | $28.5 \pm 1.1 kms^{-1}$ | $33 \pm 3 kms^{-1}$ |
| Radius | $\sim$2.38 $R_\odot$ | $\sim$1.9 $R_\odot$ |
| Mass | $\sim$2.03 $M_\odot$ | $\sim$ 2 $M_\odot$ |
| Rotational inclination $i$ | 43.6 $\pm$2.1° | 70° |
| Magnetic obliquity $\beta$ | 86.4$\pm$0.3° | 70° |
| Magnetic field | -688 Gs< $B_{eff}$ <+ 580 Gs | -720 Gs< $B_{eff}$ <+ 780 Gs |
| Age | 620 Myr | 1000 Myr |
| | HD 99563B | HR 3831B |
| Spectral type | A7V | G2V |
| Johnson's indices | V = 9.91, B-V=0.285 | V=9.09, B-V=0.64 |
| Absolute magnitude | $M_v$ 3.1 | $M_{bol}$ 5.0 |
| $T_{eff}$ | $\sim 7400°$ K | $\sim 5800°K$ |
| Radius | $\sim$ 1.1 $R_\odot$ | $\sim$ 0.9 $R_\odot$ |
| Mass | $\sim$1.58 $M_\odot$ | $\sim$1 $M_\odot$ |

Leroy et al. (1993) by using polarimetric measurements determined the period of change of the star's magnetic field as 77$\pm$10 years, and assumed, that it coincides with the rotation period. Such a way, $\gamma$ Equ is an example of an almost non-rotating star that makes it the best candidate for applying of simplified models.

Pulsations of $\gamma$ Equ with the frequency 1.339 mHz (the period of 12.5 min) and the amplitude which is not exceeded of 0.8 mmag, were discovered by Kurtz (1983). He has paid attention to modulation of the amplitude.

Then during a decade there was discussion on the pulsation activity of the star (see for example, Weiss & Shneider, 1989).

The culmination of photometric testing of $\gamma$ Equ pulsations was the multisite campaign of 1992 (Martinez et al., 1996). There were revealed unambiguously 4 pulsation frequencies of magneto-acoustic modes (see table 4).

Table 4: The results of the frequency analysis of $\gamma$ Equ data (from Martinez et al., 1996)

| f | $\mu$Hz | c/d | Period (min) | $\Delta$f ($\mu$Hz) |
|---|---|---|---|---|
| 1 | 1339 | 115.7 | 12.35 | |
| 2 | 1366 | 117.9 | 12.18 | 27 |
| 3 | 1397 | 120.7 | 11.93 | 31 |
| 4 | 1427 | 123.3 | 11.68 | 30 |

Here we dwell upon the problem of the short time scale pulsation instability of the star which was only slighly touched in Martinez et al. (1996). We involve also the photometry obtained at the Mt. Dushak-Erekdag Observatory before and after the campaign.

Fig.4 showed as far as the frequency spectrum of the star proves to be unsteady. If in JD 2448893 predominates the frequency 117.13 /d of a pretty amplitude A=0.64 mmag, then to JD 2448897 it transformed to the frequency 125.6 /d with amplitude at the noise level, A=0.29 mmag. Then the amplitudes gradually increased, however, the frequencies varied from night to night:

JD 2448898: f=117.7 /d, A=0.38 mmag;

JD 2448899: f=121.1/d, A=0.5 mmag;

JD 2448900: f=124.8 /d, A=0.53 mmag.

Fig.5 showed the enlarged part of the frequency spectrum within the interesting region. It is seen how the prominent peak at f=199.9 c/d tranformed to the peak at f=122 c/d. So far it is unknown the reason of such instability.

These solutions and questions were put with using small telescopes and simple photometric techniques. Recent investigations of $\gamma$ Equ were made with analysis of high-resolution time-resolved spectral data from large telescopes, and even from VLT (Very Large Telescope). The spectroscopic study of the oscillations is very advanced due to narrow and sharp lines and, actually, the star is one of the most investigated with radial velocity measurements.

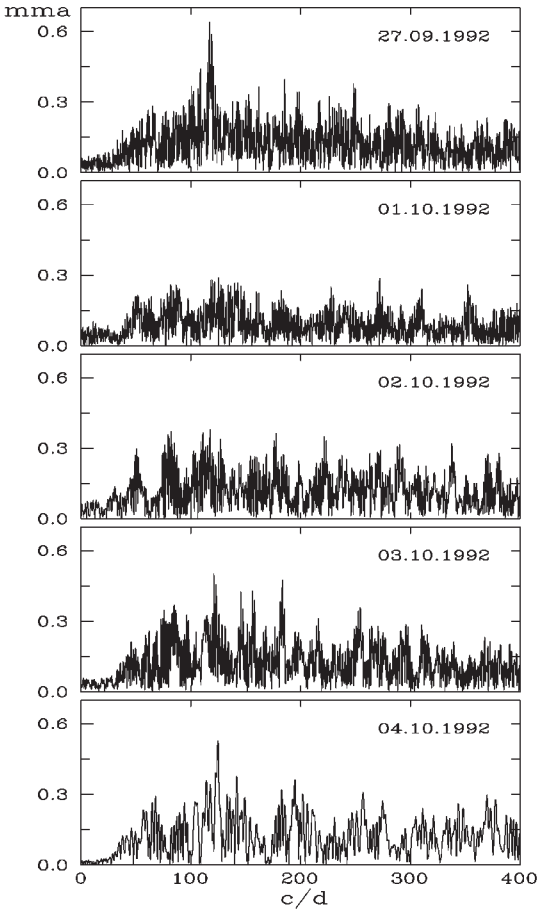


Figure 5: Fourier spectra of $\gamma$ Equ for united series of data from 0.8 m telescope of the Mt. Dushak-Erekdag Observatory and 1.1 m telescope of the Lowell Observatory for the consequent nigts.

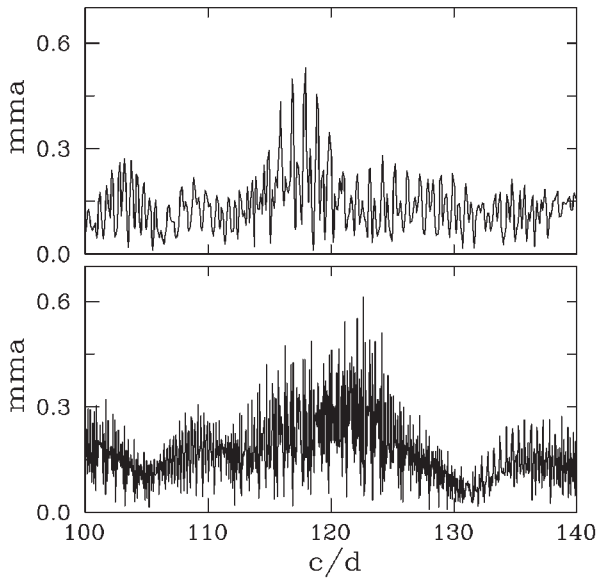


Figure 6: Fourier spectra of Strömgren $v$ photometry of $\gamma$ Equ: upper panel shows the data from JD 2448897 to JD 2448900, the most prominent peak is at the frequency 117.9 c/d; bottom panel shows the same data with adding the observations of JD 2448893 and JD 2448957, the maximal peak is at the frequency 122 c/d.

The first attempt was made by Libbrecht(1988) on observations in Fe I (6495 Å) at the Mt. Palomar 5m telescope. He reported about the detection of radial velocity variations of $\gamma$ Equ with an amplitude of 42 m/s at two frequencies at 1366 $\mu$Hz and 1427$\mu$Hz.

Kanaan & Hatzes (1998) have considered RV variations of individual lines and showed that pulsations change visibly from one spectral line to another, however, they did not detected systematic trends or dependencies of these variations.

Further, Malanushenko, Savanov, Ryabchikova (1998) detected that the highest amplitudes of RV (radial velocity) variations are associated with the lines of NdIII and PrIII. Kochukhov &Ryabchikova (2001) analysed time-resolved line profile variations of REE (rare-earth elements, specially, PrIII and Nd III) and obtained a detailed picture of the vertical stratification of chemical elements and showed the possibility extracting the main characteristics of the pulsational modes taking into account the interaction between inhomogeneous vertical and horizontal distributions of chemical elements.

Leone& Kurtz (2003) discovered the magnetic field variations with the photometric 12.1-minute pulsation period. The origin of this phenomenon is still unclear but, possibly, it could clarify on the reasons of the intrinsic instability of $\gamma$ Equ pulsations. But so far the question of exiting of magnetic variations is controversial. Kochukhov, Ryabchikova & Piskunov (2004) in the analysis of 210 high-resolution time-resolved spectropolarimetric observations find no evidence for variation of the mean longitudinal magnetic field over the pulsation period.

Returning to the $\gamma$ Equ pulsations, it should be noticed their similarity to solar-like oscillations, e.g., in $\alpha$ Cen A & B (see Kjeldsen et al., 2005). Their mode lifetimes are about 2 d, similar to those in the Sun. Apparently, such type of pulsations is stochastically exited by turbulent motions in the uppermost part of the star's convective zone (see, for example, Samadi & Goupil, 2001).

## 7. Discussion

Asteroseismology as a whole and, specially of roAp stars, is evidently becoming a powerful diagnostic of stellar parameters.

By comparing the precise and thorough frequency spectrum to the modern pulsation theories, it is be-

came a reality to specify the rotation periods, temperatures, luminosities, radii, masses of roAp stars, geometries of their magnetic fields, the vertical and gorizontal stratification of the elements in their atmospheres, the evolutionary scenarios.

Hubrig et al. (2000) detected the existence of significant kinematical differences between roAp and noAp stars, suggesting that roAp stars are older and less luminous than their non-pulsating counterparts. However, the authors noticed also that, statistically speaking, noAp stars truly represent a group where pulsations have very small amplitudes. This opinion corroborates by the theoretical point of view that pulsations are ubiquitous property of stars in general (Shibahashi, 2005).

On the other hand, Cunha (2002), developing the recent model (Balmforth et al. 2001) of pulsation mechanism in roAp stars, showed that oscillations with the periods from 15 up to 40 min are possible in Ap stars of a higher luminosity and temperature than in known roAp stars. This prediction was verified by detecting of 21 min oscillations in the radial velocities of the luminous Ap star HD 116114 (Elkin et al., 2005) by using the Ultraviolet-Visual Echelle Spectrograph at the VLT. The recent discoveries have demonstrated that radial velocity approach turn to be considerably more sensitive than traditional photometry. It becomes possible to extend swift the set of roAp stars partly from the numerous noAp stars with improving of an instrumentation and techniques.

However, at present the spectroscopy cannot supply with thorough knowledge of the stellar pulsation spectrum which could afford the multi-site photometric campaigns. Indeed, the mentioned paper by Handler at al. (2005) could give the comprehensive analysis and determine fundamental parameters and status of HD 99563 only uniting the data from the prolonged photometric campaign with the data from the VLT and prevous conclusions of time-resolved spectroscopy.

**Acknowledgments.** The data from NASA ADS, SIMBAD, CADC, and VALD databases were used. We acknowledge the participation of Dr. Mkrtichian in observations of NGC 752. We express thanks to Prof. Don Kurtz and Dr. G. Handler for presenting their papers before publication. The program package SPE by S. Sergeev was used for ininitial reducing of the Mt. Dushak-Erekdag data.

**References:**

Andronov I.L.: 1994, *Odessa Astronomical Publications*, **7**, 49

Ashoka B. N., Seetha, S., Raj E., Chaubey U. S., et al.: 2000, *BASI*, **28**, 251.

Babcock H.W. 1958. *Ap. J. Suppl.*, **3**, 141

Balmforth N. J., Cunha M. S., Dolez N., Gough D. O., Vauclair, S., 2001, *MNRAS* **323**, 362.

Bonsack W., Pilachowski C.:1974, *Ap.J.*, **190**, 327.

Breger M. 1990, *Comm. Asteroseismology*, **20**, 1.

Cunha M. S. 2002, *MNRAS* **333**, 47.

Daniel S., Latham D.W., Mathieu R. D., Twarog B. A. 1994, *PASP*, **106**, 281.

Dinescu, D. I.; Demarque, P., Guenther, D. B.; Pinsonneault, M. H. 1995 *Astron. J.*, **109**, 2090.

Dorokhov N.I., Dorokhova T.N., 1994a, *Odessa Astron. Pub.*, **7**, 167.

Dorokhova T.N., 1997, *Odessa Astron. Pub.*, **10**, 101.

Dorokhova T.N., Dorokhov N.I.: 2005, Comm. Asteroseismology, **146**, 40.

Dziembowski W.A., Goode P. R.: 1985, *Ap.J. Lett.*, **296**, L27.

Elkin V.G., Riley J.D., Cunha M.S., Kurtz D.W.,: 2005, *MNRAS*, **358**, 665.

Elkin V.G., Kurtz D.W., Mathys G.: 2005, *MNRAS*, **364**, 864.

Joshi S.: 2005, *JApA*,**26**, 193.

Girish V.: 2005, *JApA*,**26**, 203.

Handler G., Paunzen E., 1999, *As. Ap. Spl*, **135**, 57.

Handler G., Weiss W. W., Shobbrook R. R., Garrido R., Paunzen E. et al.: 2002, *ASP Conf. Proc.*, ed. C. Sterken and D. Kurtz., **256**, 109.

Handler G., Weiss W. W., Shobbrook R. R., Paunzen E., Hempel A., Anguma S. K., Kalebwe P. C., Kilkenny D., Martinez P., et al.: 2005, *MNRAS*, in press.

Hauck B., Mermilliod M. 1990, *As. Ap. Spl.*, **86**, 107.

Hauck B., Mermilliod M. 1998, *As. Ap. Spl.*, **129**, 431.

Heinemann K. 1926, *Astr. Nachr.*, **227**, 193.

Heller C.H., Kramer K.S. 1988, *PASP*, **100**, 583.

Hobbs, L. M.; Thorburn, J. A.: 1992, *Astron. J.*, **104**, 669.

Hubrig S., Kharchenko N., Mathys G., North P.: 2000, *As. Ap.*, **355**, 1031.

Hubrig, S., Kurtz, D. W., Bagnulo S. et al.: 2004, *As. Ap.*, **415**, 661.

Kanaan A., Hatzes A.P.: 1998, *Astrophis. J*, **503**, 848.

Kazanasmas M.S., Zavershneva L.A., Tomak L.Ph. 1981, *The atlas and catalogue of photoelectric standard magnitudes*, Kiev, Naukova Dumka, 189p.

Kjeldsen H., Bedding T.R., Butler R. et al.: 2005, *Astrophis. J.*, **635**, 1281.

Kochukhov O., Ryabchikova T.: 2001, *As. Ap.*, **374**, 615.

Kochukhov O., Ryabchikova T., Piskunov N.: 2004, *As. Ap.*, **415L**,13.

Kochukhov O.: 2004, *Astrophys. J.*, **615**, L149.

Kurtz D.W.: 1983 *MNRAS* , **202**, 23.

Kurtz D.W.: 1990, *Ann. Rev. Astr. Astroph.*, **28**, 607.

Kurtz D. W.: 1992, *MNRAS*, **259**, 701.

Kurtz D. W., Kanaan A., Martinez P.: 1993, *MNRAS*, **260**, 343.

Kurtz, D. W.; Martinez, P.: 2000, *Balt. Astr.*, **9**, 253.
Leroy J.L., Landi Degl'Innocenti E., Landolfi M.: 1993, *As. Ap.*, **270**, 335.
Leone F. & Kurtz D. W.: 2003, *As. Ap.*, **407L**, 67.
Libbrecht K.G.: 1988, *Ap.J.*, **330**, 55.
Malanushenko V., Savanov I., Ryabchikova T.: 1998, *IBVS*, **4650**.
Martinez P., Kurtz D. W., Kauffmann G. M. 1991, *MNRAS*, **250**, 666.
Martinez, P.; Kurtz, D. W 1994a, *MNRAS*, **271**, 118.
Martinez, P.; Kurtz, D. W. 1994b, *MNRAS*, **271**, 129.
Martinez P., Weiss W.W., Kreidl T.J., Nelson M.J., Roberts G.R., Mkrtichian D.E.,.Dorokhov N.I, Dorokhova T.N., Crake P.E.: 1996, *MNRAS*, **282**, 243.
Mathys G.: 1991, *As. Ap. Suppl.*, **89**, 121.
Matthews J.M., Wehlau W.H. 1985, *PASP*, **97**, 841.
Matthews J., Kreidl T.J., Wehlau W.H. 1988, *PASP*, **100**, 255.
Milone, A. A. E.; Latham, D. W. 1994, *Astron. J.*, **108**, 1828.
Nelson M.J., Kreidl T.J.: 1993, *Astron.J.*, **105**, 1903.
Niedzielski A., Muciek M. 1988, *Acta Astronomica* **38**, 225.
Rebeirot E. 1970, *As. Ap.*, **4**, 404.
Renson P. 1989, *As. Ap.*, **78**, 533.
Renson P. 1991, *Catalogue Genegal des etoiles Ap et Am*, 149 p.
Saio H., Gautschy A.: 2004, *MNRAS*, **350**, 485.
Samadi R., Goupil M.-J.: 2001,*As. Ap.***370**, 136.
Shibahashi H.: 2005, *JApA*, **26**, 139.
Sperl M.: 1998, *Commun. Asteroseismology*, **111**, 1.
Stibbs D.W.: 1950, *MNRAS*, **110**, 395.
Weiss W.W., Shneider H.: 1989, *As. Ap.*,**224**, 101.

# SOME PECULIARITIES OF THE RADIAL GAS DISTRIBUTION IN GALACTIC DISC

M.V. Dzyubenko

Department of Astronomy, Odessa National University
T.G.Shevchenko Park, Odessa 65014 Ukraine

ABSTRACT. This paper reports on the theoretical investigation of evolution of the Galaxy. The spiral arms and radial gas flows can be considered as some kind of indicators of the dynamical processes in the disc. Investigation the surface density of gas. The velocity profiles of radial gas flows were selected in such a way to have an agreement between the model predictions and observational data. The model with the radial gas flows gives the results that appear to be in the better agreement with the observations. The results of the model predictions differ significantly comparing to the case of the standard Galactic evolutionary model.

**Key words**: Galaxy: dinamic: spiral pattern.

## 1. Introduction

At present the very important problem is an investigation of the gas distribution in Galactic disc with an account of the spiral arms. These arms can be considered as some kind of indicators of the dynamical processes in the disc. If one includes into the consideration the radial gas flows then the results of the model predictions could differ significantly comparing to the case of the standard Galactic evolutionary model (see, for example, Lacey & Fall, 1985; Lacey & Fall, 1983). The main criteria of the model reliability is a comparison with some observational data. It is know that spiral arm affect significantly the star formation processes. As a rule, for the angular velocity of the arm rotation is adopted to be 20 km $s^{-1}kpc^{-1}$ (sometimes the value 27 km $s^{-1}kpc^{-1}$ is used), while corotation radius is 9 kpc. There are also two specific regions of the Lindblad resonances in the disc at 2.8 and 12.8 kpc (Andrievsky et al. 2004).

## 2. Main assumptions and basic equations

In order to determine the evolutionary model parameters of the Galactic disc (or its selected part) let us consider one element of the disc surface (1 $pc^2$). For this element we can define the surface gas density. Then the system of equations that describe the evolution of this selected area is the following: $\mu_g$ - are the surface density of gas, $[\mu_g] = \frac{M_\odot}{pc^2}$; $\Psi$ - the star formation rate, $[\Psi] = \frac{M_\odot}{pc^2 Gyr}$; $f(t)$ - infall rate, $[f] = \frac{M_\odot}{pc^2 Gyr}$; $\alpha$ - is an inverse characteristic distance for the infall rate in the disc, $\frac{1}{\alpha} = 4300$ pc; $\tau$ - the characteristic time of infall, $[\tau] = Gyr$; $M_p$ - the present-day mass of the galactic disc, $6 \cdot 10^{10} M_\odot$; $M_\odot$ - mass of sun; $(1-R)\cdot C$ - the part of the matter that is created after the SNe explosions; $C$ - const; $t_p$ - the age of the Galaxy; $t_p = 15$ Gyr; $\frac{z}{y}$ - the gas metallicity normalized to the yield of the primary elements; $R_G$ - the galactocentric radius.

Let us write the following equation for the gas surface density.

$$\{\frac{d\mu_g}{dt} = -(1-R)\Psi + f \tag{1}$$

As it was showed by Andrievsky et al. (2004) some characteristics can be written as follows:

$$\Psi = C\mu_g^k$$

$$f(t) = \frac{\alpha^2 M_p \exp\left(-\alpha R_G - \frac{t}{\tau}\right)}{2\pi\tau\left(1 - \exp\left(-\frac{t_p}{\tau}\right)\right)} \tag{2}$$

The result of the analytical solution (1) is the next equation:

$$\mu_g = [\exp\left(-\frac{t}{\tau}\right) - \exp(-(1-R)Ct)] \cdot \frac{A}{(1-R)C - \frac{1}{\tau}}$$

If we consider the spiral arms, then the function of the star formation rate can be modified:

$$\Psi = C\mu_g^k(1+\Delta)$$

$$\Delta = \varepsilon_1\theta_1\frac{\mid \Omega_D - \Omega_P \mid}{C_s}R_G \tag{3}$$

$\varepsilon_1$ - factor which define an efficiency of the star formation, $\varepsilon_1 = 0.2$; $\theta_1$ - the cut-off factor, $\theta_1 = 0$ for

$R_G < 7$ kpc, $\theta_1 = 1$ for $7 < R_G < 15$ kpc, $\theta_1 = 0$ for $R_G > 15$ kpc; $\Omega_D$ - angular speed of rotation of disc of the Galaxy, $\Omega_D = \Omega_D(R_G)$, $[\Omega_D] =$ km $s^{-1}kpc^{-1}$; $\Omega_P$ - angular speed of the rotation of the spiral pattern, $\Omega_P = 20$ km $s^{-1}kpc^{-1}$; $C_s$ - the speed of the sound in the interstellar environment, $C_s = 20$ km $s^{-1}$

To include in addition into consideration of the radial gas flows we use the following equation:

$$\frac{\partial \mu_g}{\partial t} = -(1-R)\Psi + f - \frac{1}{r}\cdot\frac{\partial}{\partial r}(rV_r\mu_g) \qquad (4)$$

$V_r$ - the speed of the radial gas flows.

The gas in-fall from the Galactic halo can be modified too:

$$f(t, R_G) = \frac{\alpha^2 M_p(t_p)\exp\left(-\alpha R_G - \frac{t}{\tau}\right)}{2\pi\tau\left(1-\exp\left(-\frac{t_p}{\tau}\right)\right)} \qquad (5)$$

The characteristic time of infall:

$$\tau_1 = 6.5$$

$$\tau_2 = 0.075\sqrt{R_G} + 5$$

$$\tau_3 = 0.007\exp\left(\frac{R_G}{2000}\right) + 3.5$$

The velocity of the radial gas motion is approximated using the following equations:

$$V_r[1] = \left(5.6 + \frac{181.94}{R_G} + 0.45R_G - 0.069R_G^2 - 20\right)R_G$$

$$V_r[2] = -0.0081R_G^2 + 0.5315R_G - 3.6591$$

$$V_r[3] = \left(5.6 + \frac{181.94}{R_G} + 0.45R_G - 0.069R_G^2 - 27\right)R_G$$

These velocity profiles were selected in such a way to have an agreement between the model predictions and observational data (Dickey, 1993, Kuijken & Gilmore, 1991). Below we give our model results (Table 1,2,3) on the gas evolution in the disc taking into account the spiral arms and radial gas flows. $\mu_g^*$ - the surface density of gas without spiral pattern. The good model: a. b. respectively

$$k = 1, V_r[2], \tau_i, i = 1, 2, 3$$

$$k = 1, V_r[3], \tau_i, i = 1, 2, 3$$

Inclusion in a researched problem of radial gas flows in a disk results in change of results of modelling.

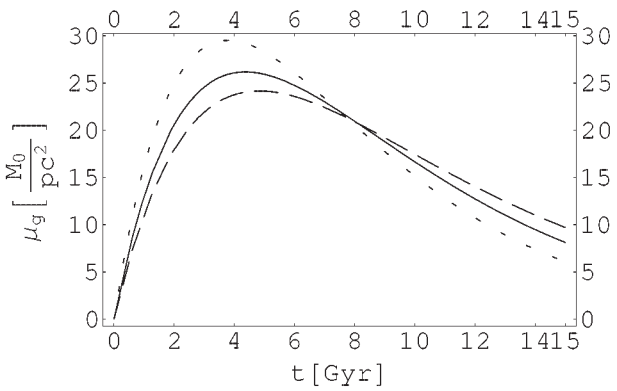


Figure 1: The surfase density of gas, model *a*. (--- $\tau_1$; _ $\tau_2$; ... $\tau_3$)

Table 1: Theoretical values of the surface density of gas at various parameters $k$ and $\tau$ in the solar neighborhood. $t = 15$ Gyr, model $V_r[1]$

| $\tau$ | $k1$ | $\mu_g$ | $\mu_g^*$ | $k2$ | $\mu_g^*$ | $\mu_g$ |
|---|---|---|---|---|---|---|
| $\tau_1$ | 1 | 11.278 | 5.123 | 1.4 | 3.955 | 2.643 |
| $\tau_2$ | 1 | 9.317 | 3.765 | 1.4 | 3.077 | 2.005 |
| $\tau_3$ | 1 | 7.362 | 2.488 | 1.4 | 2.218 | 1.3904 |

Table 2: Same as Table 1, model $V_r[2]$

| $\tau$ | $k1$ | $\mu_g$ | $\mu_g^*$ | $k2$ | $\mu_g^*$ | $\mu_g$ |
|---|---|---|---|---|---|---|
| $\tau_1$ | 1 | 9.705 | 9.457 | 1.4 | 3.808 | 3.760 |
| $\tau_2$ | 1 | 7.853 | 7.624 | 1.4 | 2.948 | 2.909 |
| $\tau_3$ | 1 | 6.076 | 5.881 | 1.4 | 2.127 | 2.01 |

Table 3: Same as Table 1, model $V_r[3]$

| $\tau$ | $k1$ | $\mu_g$ | $\mu_g^*$ | $k2$ | $\mu_g^*$ | $\mu_g$ |
|---|---|---|---|---|---|---|
| $\tau_1$ | 1 | 11.368 | 11.044 | 1.4 | 3.985 | 3.943 |
| $\tau_2$ | 1 | 9.404 | 9.010 | 1.4 | 3.114 | 3.072 |
| $\tau_3$ | 1 | 7.478 | 7.227 | 1.4 | 2.269 | 2.241 |

Table 4: The observational data of $\mu_g$ of Dickey (1993) and Kuijken & Gilmore (1991)

| $\mu_g$ | Dickey | Kuijken & Gilmore |
|---|---|---|
| The bottom limit | 6.25 | 10 |
| Average value | 7.5 | 12.7 |
| The top limit | 8.75 | 15.8 |

### 3. Conclusion

It is showed that:

1. Contribution of the spiral arms to the star formation rate changes the resulting radial gas distribution making it non-monotoneous.

2. The model with the radial gas flows gives the results that appear to be in the better agreement with the observations.

### References

Andrievsky S.M., Luck R.E., Martin P., Lepine J.R.D.: 2004, *A&A*, **413**, 159.

Lacey S., Fall M.: 1983, *Royal Astron. Soc.*, **204**, 791-810.

Lacey S., Fall M.: 1985, *Astrophys. J.*, **290**, 154-170.

Dickey J.M.: 1993, The Minnesota lectures on clusters of galaxies and large-scale structure. ASP Conf. Ser., Ed. Humphreys R.M., San Francisco, 93.

Kuijken & Gilmore: 1991, Mon. Not. *Royal Astron. Soc.*, **250**, 320-356.

# HYDRODYNAMIC MODEL FOR A $\beta$ Cephei VARIABLE BW Vulpeculae

A. Fokin[1], Ph. Mathias [2], E. Chapellier [3], D. Gillet [4] and N. Nardetto [5]

[1] Institute of Astronomy of the Russian Academy of Sciences, 48 Pjatnitskaya Str., Moscow 109017 Russia, *fokin@inasan.ru*

[2] Observatoire de la Côte d'Azur, Dpt. Gemini, UMR 6203, F-06304 Nice Cedex 4, *mathias@obs-nice.fr*

[3] Observatoire de la Côte d'Azur, Dpt. Gemini, UMR 6203, F-06304 Nice Cedex 4, *chapellier@obs-nice.fr*

[4] Observatoire de Haute Provence, CNRS, F-04870, Saint Michel l'Observatoire, France, *gillet@obs-hp.fr*

[5] Observatoire de la Côte d'Azur, Dpt. Gemini, UMR 6203, F-06304 Nice Cedex 4, *nardetto@obs-nice.fr*

ABSTRACT. A hydrodynamical model for the high-amplitude $\beta$ Cephei star BW Vulpeculae is generated, and the spectral line profiles are calculated for different pulsational phases. The pulsational characteristics and line profiles are compared with recent observational data obtained during seven consecutive nights in August 2000. We found a generally good agreement in the basic photometric and spectral parameters. Two strong shock waves appear during one period, and the "stillstand" is due to the gas dynamics between the passages of these shocks. Note that this good agreement suppose a metallicity $Z = 0.03$, while a metallicity $Z = 0.02$ does not lead to the correct amplitudes and shapes of the curves.

**Key words**: Line: profiles, stars: oscillations, stars: variable: general, stars: individuals: BW Vulpeculae

## 1. Introduction

Among the $\beta$ Cephei stars, BW Vulpeculae (HD 199140, B2 III) exhibit the most extreme variability of light, radial velocity and line profiles. With a period of 0.201 days, the peak-to-peak amplitude of the radial velocity variation amounts to more than $2K = 200$ km/s, the total range of the light variation is approximately 0.2 mag in $V$, and, finally, the spectra show well-marked line-doubling. A prominent feature of both the radial velocity curve and the light curve is the presence of a bump. This bump occurs around pulsation phase $\varphi = 0.8$ in the light curve, whereas it occurs at pulsation phase $\varphi = 1.0$ in the radial velocity variation and is usually called "stillstand". On each side of the stillstand, the velocity curve shows discontinuities due to line-doubling phenomena.

The interpretation of these unusual observational phenomena in a $\beta$ Cephei star is not clear yet. Up to now, the only one attempt to model the observations was performed by Moskalik & Buchler (1994). They used a nonlinear pulsation model where the dynamics was governed by the unique outward propagating shock originating at the bottom of the HeII ionization zone. In this view, the consecutive strong compression provokes a sudden jump of the Rosseland-mean opacity which contributes to the formation of an apparent discontinuity in the observed radial velocities. However, this results in a stillstand which is at a value of about -100 km/s in the rest frame of the star, whereas its observed value is around the stellar $\gamma$-velocity at -9.2 km/s (MGFC).

Our main objective was to interpret observations of BW Vulpeculae using an auto-coherent pulsation model which has already been successfully used for different classes of radial pulsators, from RR Lyrae (Fokin & Gillet 1997) to RV Tauri (Fokin 2000) and post-AGB (Jeannin et al. 1997).

## 2. Observations

Spectra were obtained at the Observatoire de Haute-Provence with the 1.52 m telescope using the AURELIE spectrograph during 7 consecutive nights, from August 14 to 21, 2000. The spectral resolution was

around 25 000 along a 120 Å spectral range centered on the SiIII triplet at 4552, 4567 and 4574 Å. This relatively low spectral resolution allowed a very good temporal sampling: with a mean exposure time around 2 min, more than 100 spectra per pulsation period were obtained. The measured signal-to-noise is between 100 and 150. Reductions were performed using the standard IRAF package.

Since we have no simultaneous photometric observations, dates of maximum luminosity were computed following the most recent ephemeris provided by Horvath et al. (1998. Because this ephemeris gives dates concerning light minima, we added 0.1116 d (0.555 P) to retrieve the usual phase convention (Sterken et al. 1987).

### 3. Nonlinear model

The basic stellar parameters for BW Vul are still uncertain. According to different authors, the mass vary from 11 to 14 M⊙, luminosity from $\log L/L_\odot = 4.146$ to 4.431 and $\log T_{eff}$ from 4.33 to 4.386 (Aerts et al. 1998; Lesh & Aizenman 1978; Heynderickx 1992; Moskalik & Buchler 1994). We tried different sets of parameters, and finally have chosen a model close to the second turn-over point on the $11\,M\odot$ evolutionary track of Dziembowski & Pamyatnykh (1993). The parameters of this 150-zone model are: $M = 11\,M\odot$, $\log L = 4.176$, $\log T_{eff} = 4.362$.

Our model was calculated with the radiative Lagrangian code by Fokin (1990). The inner boundary has been fixed to $T = 4.4 \cdot 10^7$ K, corresponding to about 5 % of the photometric radius and the envelope contained 83% of the stellar mass. We used the OPAL92 opacity tables, and studied both $Z = 0.02$ and 0.03 metallicity.

The model with $Z = 0.02$ (the metallicity used by Moskalik & Buchler (1994) reached its fundamental limit cycle with the period of 0.211 days and bolometric and radial velocity amplitudes $\Delta m = 0.15$ mag and $2K = 40$ km/s, respectively. Relative radial amplitude at the surface is $\Delta R/R = 2.5$ %. Its pulsation is sinusoidal and represents a typical $\beta$ Cepheid star having very small amplitude, and has little in common with BW Vul.

The model with $Z = 0.03$, on the contrary, has reached the limit cycle with very large amplitudes, $\Delta m_{\rm bol}$=0.7 mag and $2K = 260$ km/s, with the period $P = 0.217$ days. The relative radial amplitude at the surface is $\Delta R/R = 12$ %. This model is presented in Fig. 1 where one can clearly see the bump of the light curve at phase 0.8, as well as complicate motions in high atmosphere with shock waves. According to Barry et al. (1984), the estimated bolometric magnitude should be about 0.75 mag, which is close to our theoretical value of 0.7 mag.

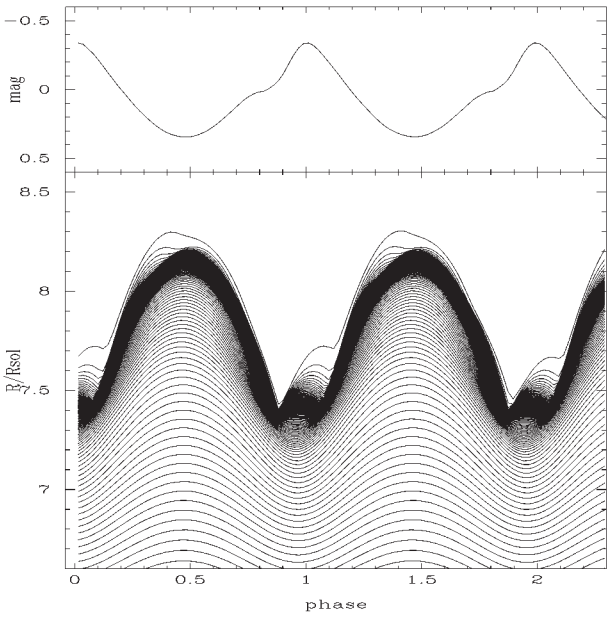


Figure 1: Theoretical bolometric light curve (upper diagram) and displacement of different mass zones (lower panel) for a BW Vul model with $M = 11\,M\odot$, $\log L/L_\odot = 4.176$, $\log T_{eff} = 4.362$ and $Z = 0.03$

The amplitude and the character of pulsation are not sensible to small variations of $L$, $T_{eff}$ and $M$. All these models have the characteristic bump on their light curves and a stillstand on the velocity curves. We found that the bump and the stillstand are the results of a passage of **two strong shocks** formed closely to the region of instability ($T \approx 2.5 \cdot 10^5$ K). The LNA analysis reveals that there is no low-mode resonance in the BW Vul model up to the third overtone, so the Cepheid-like explanation of the bump is not relevant.

### 4. Nature of the two shocks

The two shocks can be followed as maxima of compression rate for the most important compression/shock waves versus the mass zone in Fig. 2. We also indicated the position of the zone $T = 250\,000$ K where the Z-peak $\kappa$-mechanism acts, the photosphere and both boundaries of the He ionization zone. We remark that the outer boundary of the He ionization zone (at about $T = 40\,000$ K) remains strangely flat during the phase of "stillstand" between the two shock waves (Fig. 5).

After $\varphi$=0.1 the atmospheric expansion slows down and after the phase 0.45 turns to contraction with almost constant deceleration, $\approx 13\,{\rm m\,s^{-2}}$, which is about 4 times less than the mean gravity in the model atmosphere. During the contraction phase, the compression of the gas is not homogeneous.

In the same time the luminosity from the inner zones

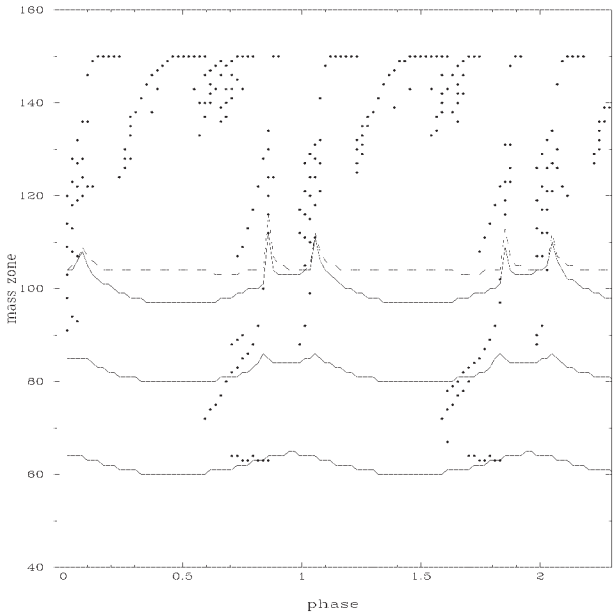


Figure 2: Shock propagation through the mass grid. Points mark the maxima of compression corresponding to the most important compression/shock waves. Solid curve below corresponds to $T = 250\,000$K. Two upper solid curves limit the He ionization region. The dashed curve indicates the photospheric level

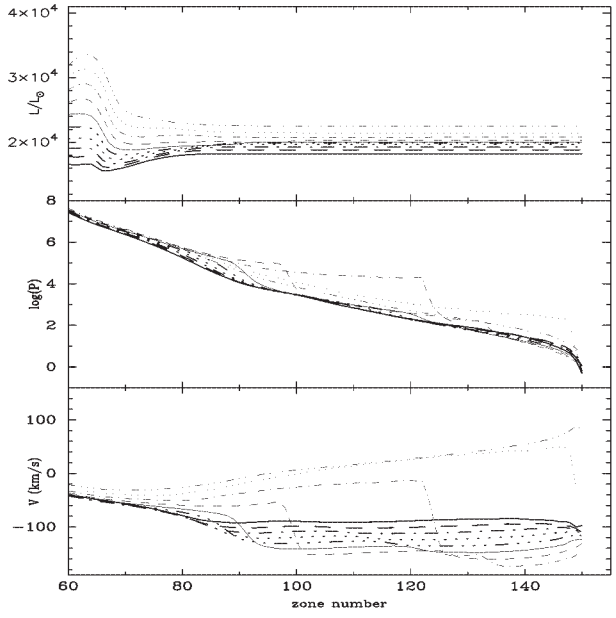


Figure 3: Time evolution of the profiles of luminosity (upper diagram), gas pressure (middle) and velocity (bottom) versus the number of the mass zone between the phases 0.69–0.87, corrsponding to the generation of the shock 1. Phase 0.69 refers to the thick solid curve, and phase 0.87 - to the thin three-dotted curve. The mass zone number 60 approximately corresponds to T=250 000 K, while the mass zone 150 corresponds to the surface

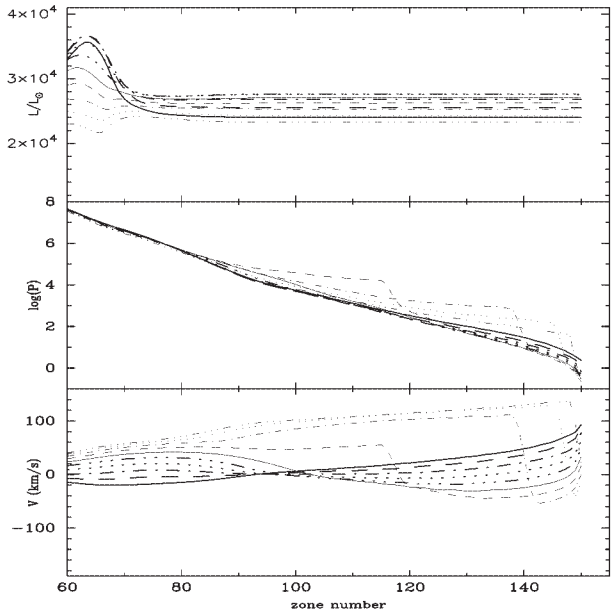


Figure 4: Same as in Fig. 3 for the phases 0.91–1.09, corresponding to the generation of the shock 2

starts rapidly increasing, but the radiation is effectively absorbed in the outer region of the Z-peak zone ($T = 200\,000$ K). From the phase 0.8 (the beginning of the "stillstand") until 0.95 this absorption is especially strong (see Figs. 3–4). This absorption creates an over-pressure above the Z-peak zone. After approximately the phase 0.75 the compression wave, provoked by this over-pressure, starts propagating outwards and shortly transforms into shock 1 (Fig. 3).

This shock enters the zone of He ionization, where it causes perturbations of temperature and density and, consequently, the increase of the opacity by a factor of 2. The strong radiative absorption in the region of the Z-peak and in the wake of the shock 1 is the cause of the observed bump in the light curve.

The shock 1 then increases in amplitude, up to 140 km/s, and reaches a compression rate of about 100. It rapidly passes through the atmosphere and escapes. After the escape of the shock 1 the outer envelope starts expanding, while the inner shells are still in compression. The expansion of the outer atmosphere is slow. The absorption in the Z-peak region is still about 11 000 $L_\odot$, but the luminosity from the inner region increases, so the total stellar luminosity starts increasing after the short bump. The accumulation of the thermal energy due to absorption in this zone continues. Near the phase 0.95 the compression starts expanding from the inner zones upwards (see Fig. 4) and a new shock 2 is formed in the helium ionization zone. At $\phi$=1.1 it arrives to the surface and escapes.

An important result from the above analysis is that both shock waves have origin in the region laying well below the photosphere and are due to the $\kappa$-mechanism

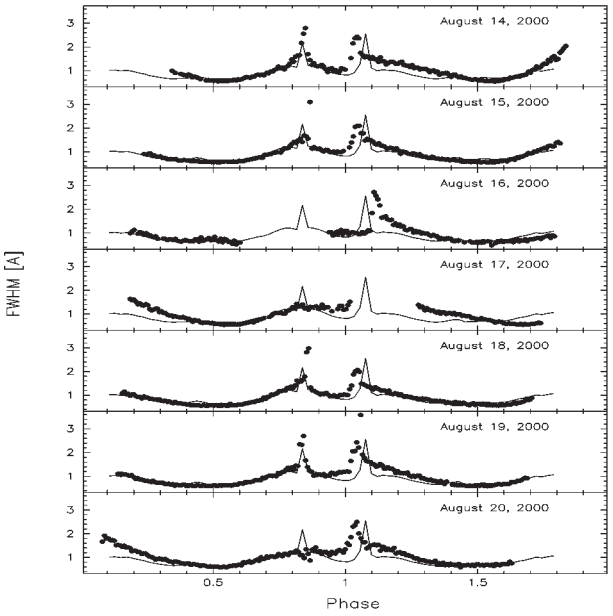


Figure 5: Theoretical (solid) and observational (points) FWHM of the Si III 4553 Å line. The comparison is presented for all seven consecutive nights, with the dates indicated in each diagram

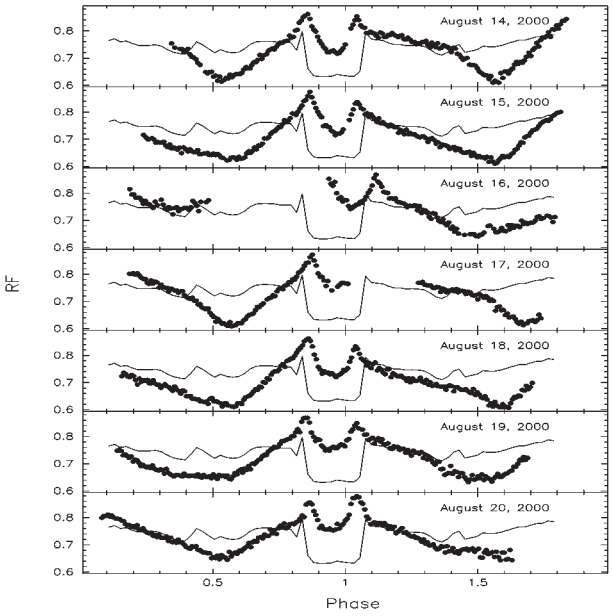


Figure 6: Same as in Fig. 5 for the radial velocities measured from the minima of the principal absorption component

in the Z-peak zone.

## 5. Line profiles: theory and observations

After the model has been generated, we calculated a series of snap-shots of the atmospheric structure (about 50 per pulsational period) in order to study the theoretical line profiles. The line transfer problem for each model atmosphere was resolved with the code of Fokin (1991) under the LTE assumption. For all phases we assume the same microturbulent velocity of 1 km/s, and we considered a projected rotation velocity of $v \sin i = 24$ km/s (Stankov et al. 2003).

In Figs. 5-6 we present the detailed comparison of different features of the predicted profiles versus the observational ones obtained in 7 consecutive nights in August 2000. Note that the theoretical curve is the same in each diagram, and is compared with the observed curves for different nights. These diagrams show, respectively, the FWHM (Fig. 5) and the radial velocities measured at the minima of the principal absorption components (Fig. 6).

Note that the observational curves are noticeably variable from cycle to cycle. If we fix some phases, we shall see that the discrepancy between the observed and predicted curves as well significantly varies from night to night. This behaviour cannot be explained by our model, because it is strictly periodic.

The radial velocity curves (Fig. 6) show very good agreement with the observations for almost all the nights. We note that the "stillstand" is rather an idealization, especially clearly seen in the curve of August 16: during this period the velocity varies significantly, a fact confirmed by our model.

Generally, the comparison is good and confirms the consistence of our model.

## 6. Conclusion

Our nonlinear model represents reasonably well the observed features of BW Vulpeculae. Two shocks are generated consequently - one at each phase of the observed velocity discontinuities, and not only one as previousely stated by Moskalik and Buchler (1994)). The physical origin of these shocks is suggested to be a strong radiative absorption in the zone of the "Z-peak". Also, the characteristic asynchroneous motions of the upper and lower envelope regions can contribute to the shock generation. We stress that both shocks are generated below the photosphere.

We found that a metallicity $Z = 0.02$ is too low, so that the observed amplitudes can be reproduced only with $Z = 0.03$. The linear analysis shows that the only driving zone in the models is that of the "Z-peak" of opacity at $\log T = 5.2 - 5.4$. Just above and below there are two regions of positive dissipation. LNA calculations show that the model with $Z = 0.03$ is unstable in the F-mode, while the $Z = 0.02$ model is only marginally unstable. We found that the lower damping zone becomes more effective as Z decreases from 0.03 to 0.02 which possibly explains lower amplitude

for Z=0.02. We suggest that other members of the $\beta$ Cepheid group, having much smaller amplitudes than BW Vul, probably have lower metallicity, as shown in our second model, identical except for $Z = 0.02$.

**References**

Aerts C., Mathias P., Van Hoolst T. et al.: 1995, *A&A*, **301**, 781.

Barry D.C., Holberg J.B., Forrester W.T. et al.: 1984, *ApJ*, **281**, 766.

Dziembowski W.A., Pamiatnykh A.A.: 1993, *MNRAS*, **262**, 204.

Fokin A.B.: 1990, *ApSS*, **164**, 95.

Fokin A.B.: 1991, *MNRAS*, **250**, 258.

Fokin A.B., Gillet D.: 1997, *A&A*, **325**, 1013.

Fokin A.B.: 2001, *In Stellar pulsation - nonlinear studies, ASSL series, ed. by M.Takeuti and D.D.Sasselov*, **257**, 103-136.

Heyndericckx D.: 1992, *PhD thesis, Katholieke Universiteit Leuven, Belgium.*

Horvath A. Gherega O. Farkas L.: 1998, *Rom. Astron. Journal*, **8**, 89.

Jeannin L., Fokin A.B., Gillet D., Baraffe I.: 1997, *A&A*, **326**, 203.

Lesh J.R., Aizenman M.L.: 1978, *ARA&A*, **16**, 215.

Moskalik P., Buchler J.R.: 1994, *in: L.A. Balona, H.F. Henrichs & J.-M. Le Contel (Eds) Pulsation, Rotation and Mass Loss en Early-Type Stars, IAU 162, Kluwer Academic Publishers, p.19.*

Stankov A., Ilyin I., Fridlund C.V.M.: 2003, *A&A*, **408**, 1077.

# ENRICHMENT OF THE GALACTIC DISK BY THE NEUTRON CAPTURE ELEMENTS (Ba and Eu)

T.I. Gorbaneva

Department of Astronomy, Odessa State University
T.G.Shevchenko Park, Odessa 270014 Ukraine

ABSTRACT. The abundances of Ba and Eu were determined for 38 red giant stars in the metallicity range $-0.6$ <[Fe/H] < $+0.25$ using the spectral synthesis technique. The spectra were obtained with spectrograph ELODIE (Haute Provence Observatoire, France), the resolwing power is 42000, S/N is more than 100. For the Ba and Eu lines the effects of hyperfine structure and isotope shifts are included, assuming the isotope ratios of the r-process component of the solar system material. Abundances of the n-capture element ( Ba and Eu) for 38 red giants with metallicities [Fe/H] from -0.6 to +0.25 and correlation of the [Ba/Eu] ratios with stellar metallicities are present. The [Ba/Eu] ratio reflects substantial production of Ba in the s-process for the stars with metallicity $-0.6$ <[Fe/H] < $+0.25$.

**Key words**: nucleosythesis: neutron captures; stars: abundances; stars: giants.

## 1. Introduction

Chemical elements heavier than the Fe peak (Z> 30) are formed in two processes of neutron capture: r-process and s-process (Burbidge et al. 1957). At the relatively low neutron densities ($N_n$=108 $cm^-3$ ; Pagel 1997), the time between their captures is more, than time of the $\beta$-decays. Such captures are refered to s-processes (slow). If the density of neutrons is rather high there are many neutron-captures between the $\beta$-decays, and such captures are refered to r-processes (rapid). According to the theory of evolution (Travaglio et al.1999), s-process nuclei are mainly synthesized during the thermally pulsing asymptotic giant branch phase of the low-mass stars (2-4 $M_\odot$). There is a necessary flux of neutrons for maintenance of a chain of s-process.

Theory proposes an existence of several quite different astrophysical sites for the operation of the two neutron-capture nucleosyntheses mechanisms. For the case of s-process, the two possible astrophysical environments are: a) the helium burning cores of massive stars (M> 10$M_\odot$). Then reaction $^{22}Ne(\alpha,n)^{25}Mg$ is responsible for the elements with atomic mass A< 90 (the "weak" component) (Peters (1968), Lamb et al. (1977), Sneden, Cowan (2003) and Truran et al. (2002)): b) The thermally pulsing helium shells of asymptotic giant branch stars. The reaction $^{13}C(\alpha,n)^{16}O$ produces neutrons that leads to the elements formation A> 90 (the "main" component) (Schwarzschild (1967), Busso et. al (1999)). However, the specific site of the r-process is an unsolved problem, but it is strongly suspected that Type II Supernovae play an important role. Truran et al. (2002) point out four possible sites, three of which occur in SNeII explosions.

Contributions from various processes are different at the different stages of the Galaxy evolution, the course of various elements with metallicity differs also. It allows one to trace the sources of the contribution to an enrichment of the ISM. If we can identify stellar environments in which either the s-process or r-process contributions dominate, we can use this information to constrain the detailed characteristics of the corresponding nucleosynthesis mechanism. If we can distinguish s-process and r-process elemental contributions, we can use stellar abundance data to trace the chemical evolution of such processes over the Galactic history.

In this paper, we present n-capture element abundances ( Ba and Eu) for 38 red giants with metallicities [Fe/H] from -0.6 to +0.25. Use of the high-resolution spectra (R=42000), the reliable stellar parameters and detailed structure of the Ba and Eu lines. Ba and Eu abundnces are determined and detect the trends in the behaviour of elemental ratios [Ba/Fe], [Eu/Fe] and [Ba/Eu]. A decrease of [Eu/Fe] and [Ba/Fe] with the metallicity increase have been obtained.

## 2. Observations and parameters

All the spectra used in this paper are extracted from the most recent version of the library of stellar spectra collected with the ELODIE echelle spectrograph at the Observatory de Haute-Provence by Soubiran et al. (1998) and Prugniel & Soubiran (2001). The per-

formances of the instrument mounted on the 193cm telescope, are described in Baranne et al (1996). A resolving power of 42 000 in the wavelength range $\lambda\lambda$ 3850–6800 ÅÅ. Spectrum extraction, wavelength calibration and radial velocity measurement have been performed at the telescope with the on-line data reduction software while straightening of the orders, removing of cosmic ray hits, bad pixels and telluric lines were performed as described in Katz et al (1998). The continuum level drawing and equivalent width measurements were carried out by us using DECH20 code (Galazutdinov 1992).

Highly precise temperatures ($\sigma = 10 - 15$ K) have been determined from line depth ratios (Kovtyukh et al. 2006). The spectral lines of high and low excitation potentials respond differently to the change in effective temperature ($T_{\rm eff}$). This method is independent of interstellar reddening and takes into account the individual characteristics of the star's atmosphere.

The surface gravity log $g$ was determined using two different methods, the method based on the ionisation balance for iron and a second method by fitting the wings of a Ca I line profole.

Microturbulent velocities $V_{\rm t}$ were determined by forcing the abundances determined from individual FeI lines to be independent of equivalent width.

### 3. Elemental abundances

Ba and Eu abundances are determined from the line profile fitting of the stellar spectra using the STARSP code developed by Tsymbal (1996). We have used the grid of stellar atmospheres from Kurucz (1993). The line list is extracted from Kurucz (1994) compilation, and it includes all the relevant atomic and molecular lines. Elemental abundances are derived from the BaII resonance line $\lambda$ 4554Å and from the EuII subordinate line $\lambda$ 6645Å. The atomic data for these lines were taken from Mashonkina & Gehren (2000). BaII and EuII ions considered here have the lines that show appreciable hyperfine structure. We adopt the hfs patterns of Mashonkina & Gehren (2000) for Ba II. Mashonkina & Gehren (1999). have shown, that for line Ba $\lambda$ 4554Å an account for the hyperfine structure is important. They have presented 3-component HFS model of this line. Oscillator strengths of these components are identical to those in the solar spectrum. Recent NLTE calculation for BaII and EuII have been carried out by Mashonkina & Gehren [1999], [2000]. They have shown that for the line II $\lambda$ 4554Å which we used in our calculations, NLTE effects are small for FeH$> -1.9$. For Eu $\lambda$ 6645Å the correction NLTE ranges from 0.04 dex to 0.06 dex. Therefore we did not take into account the NLTE effects in our calculations. The behavior of elements in our study with metallicity is shown in Fig. 1 and Fig. 2.

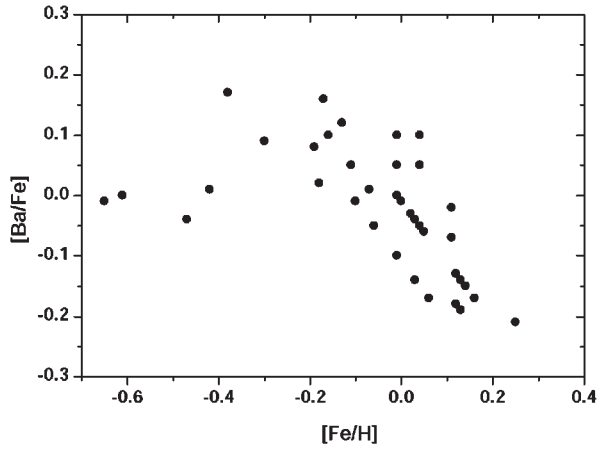


Figure 1: The run of [Ba/Fe] with [Fe/H]

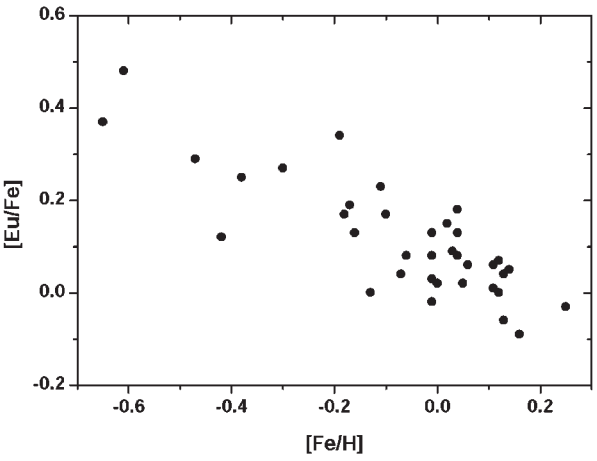


Figure 2: The run of [Eu/Fe] with [Fe/H]

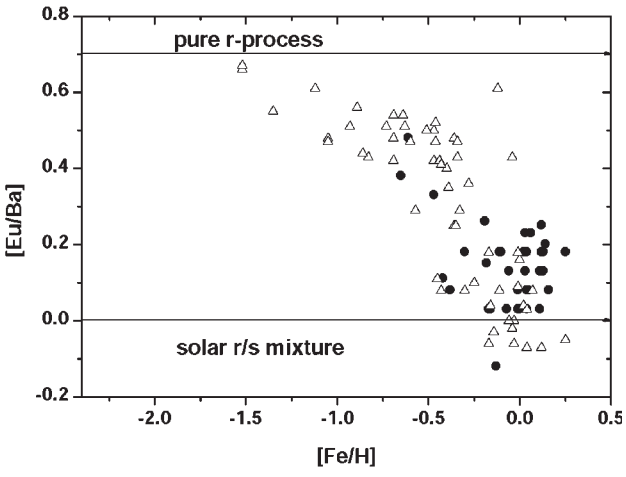


Figure 3: The run of [Ba/Eu] with [Fe/H]. Filled circles are from this paper open triangles are from Mashonkina (2001)

We observe in our sample of giants the trend of Ba/Fe and [Eu/Fe] versus [Fe/H] (Fig. 1, 2) similar to the that for disk stars collected in the work Burris et al. (2000) (see Fig. 5, Burris et al. (2000)).

Solar barium and europium abundances, $\log \varepsilon_{\mathrm{Ba},\odot} = 2.21$ and $\log \varepsilon_{\mathrm{Eu},\odot} = 0.53$, and van der Waals damping constants $C_6$ for the BaII and EuII lines were determined in the paper Mashonkina & Gehren (2000) from the solar line profile fitting.

The resulting mean Ba and Eu abundances are [Ba/Fe]=-0.02±0.11 and [Eu/Fe]=0.09±0.12. Europium is overabundant relative to barium with a mean value [Eu/Ba] = 0.11±0.08

## 4. Abundance ratios [Eu/Ba]

A comparison of Ba wit h Eu abundances shows the relative contributions of the r- s-process, since Ba may be product of the both processes. [Eu/Ba] abundance ratios are shown in Fig. 3. The contributions from the s- and r-process to the solar Ba abundance consist of 87% and 13%, respectively, according to Kappeler et al. (1989), 81% and 19% according to the data of Arlandini et al. (1999), 85% and 15% according to Burris et al. (2000). On the other hand the solar Eu is primarily a r-process product: 91% according to Cameron (1982) and Wisshak et al. (1996), and 97% according to Burris et al. (2000). The elemental abundances and the ratio of these two elements are presented in the Table1. The Ba and Eu abundances in Table1 can also be used to estimate the fraction of Ba produced by the r- and s-process in each star, using the assumptions that Eu is produced only by the r-process but Ba may be product in both processes.

[Eu/Ba] abundance ratios are shown in Fig. 3. The solar abundance ratio of Eu to Ba contributed by the r-process (Arlandini et al. 1999) relative to the total abundances, $[\mathrm{Eu/Ba}]_r = 0.70$, is indicated in Fig. 3 by solid line. Fig. 3 shows the [Eu/Ba] abundances ratios from our studies and the stars studied by Mashonkina & Gehren (2000, 2001). Using the deviation of the observed values of [Eu/Ba] from $[\mathrm{Eu/Ba}]_r = 0.70$, we can estimate the s-process contribution to Eu abundanse. For the our disk stars, the [Eu/Ba] values are all between 0.00 and 0.20. In the stars with metallicity about [Fe/H] $> -0.50$ the s-process contribution to Eu is significant.

Table 1: Abundance results for Ba and Eu

| HD | $T_{\mathrm{eff}}$ | log g | [Fe/H] | [Ba/Fe] | [Eu/Fe] | [Ba/Eu] |
|---|---|---|---|---|---|---|
| 2910 | 4756 | 2.7 | 0.12 | -0.18 | 0.07 | -0.25 |
| 4188 | 4809 | 2.7 | 0.04 | -0.05 | 0.13 | -0.18 |
| 6319 | 4650 | 2.3 | 0.06 | -0.17 | 0.06 | -0.23 |
| 6482 | 4738 | 2.4 | -0.11 | 0.05 | 0.23 | -0.18 |
| 10975 | 4881 | 2.4 | -0.19 | 0.08 | 0.34 | -0.26 |
| 11749 | 4679 | 2.4 | -0.10 | -0.01 | 0.17 | -0.18 |
| 11949 | 4708 | 2.3 | -0.16 | 0.10 | 0.13 | -0.03 |
| 15453 | 4696 | 2.4 | -0.07 | 0.01 | 0.04 | -0.03 |
| 15755 | 4611 | 2.3 | -0.01 | -0.10 | -0.0 | -0.08 |
| 15779 | 4821 | 2.7 | 0.02 | -0.03 | 0.15 | -0.18 |
| 16400 | 4840 | 2.5 | -0.01 | 0.05 | 0.08 | -0.03 |
| 17361 | 4646 | 2.5 | 0.12 | -0.18 | 0.00 | -0.18 |
| 18885 | 4722 | 2.5 | 0.16 | -0.17 | -0.09 | -0.08 |
| 19787 | 4832 | 2.75 | 0.14 | -0.15 | 0.05 | -0.20 |
| 25602 | 4693 | 2.4 | -0.42 | 0.01 | 0.12 | -0.11 |
| 25604 | 4764 | 2.7 | 0.13 | -0.14 | 0.04 | -0.18 |
| 26546 | 4743 | 2.25 | -0.01 | 0.00 | 0.03 | -0.03 |
| 26755 | 4630 | 2.2 | -0.06 | -0.05 | 0.08 | -0.13 |
| 27371 | 4955 | 2.7 | 0.11 | -0.07 | 0.06 | -0.13 |
| 28292 | 4453 | 2.1 | -0.18 | 0.02 | 0.17 | -0.15 |
| 28305 | 4925 | 2.55 | 0.11 | -0.02 | 0.01 | -0.03 |
| 28307 | 4961 | 2.7 | 0.12 | -0.13 | 0.00 | -0.13 |
| 31444 | 5080 | 2.75 | -0.17 | 0.16 | 0.19 | -0.03 |
| 33419 | 4708 | 2.3 | 0.00 | -0.01 | 0.02 | -0.03 |
| 33618 | 4590 | 2.3 | 0.05 | -0.06 | 0.02 | -0.08 |
| 34200 | 5055 | 2.8 | 0.04 | 0.05 | 0.08 | -0.03 |
| 34559 | 5010 | 2.9 | 0.04 | 0.10 | 0.18 | -0.08 |
| 37638 | 5093 | 2.8 | -0.01 | 0.10 | 0.13 | -0.03 |
| 40020 | 4670 | 2.3 | 0.13 | -0.19 | -0.06 | -0.13 |
| 42341 | 4655 | 2.6 | 0.25 | -0.21 | -0.03 | -0.18 |
| 43023 | 4994 | 2.6 | -0.13 | 0.12 | 0.00 | 0.12 |
| 45415 | 4762 | 2.53 | 0.03 | -0.04 | 0.09 | -0.13 |
| 46374 | 4661 | 2.3 | 0.03 | -0.14 | 0.09 | -0.23 |
| 46758 | 5003 | 2.9 | -0.30 | 0.09 | 0.27 | -0.18 |
| 53329 | 5012 | 2.8 | -0.38 | 0.17 | 0.25 | -0.08 |
| 54810 | 4669 | 2.4 | -0.47 | -0.04 | 0.29 | -0.33 |
| 64967 | 4864 | 2.55 | -0.65 | -0.01 | 0.37 | -0.38 |
| 67539 | 4781 | 2.45 | -0.61 | 0.00 | 0.48 | -0.48 |

## Conclusion

Using the spectra of the high quality, we have carried a detailed analysis of the abundances of Ba and Eu in the stars of the Galactic disk.

We observe in our sample of giants the trend of Ba/Fe and Eu/Fe versus Fe/H (Fig. 1, 2 ) similar to

the those for disk stars studied in the work of Burris et al. (2000) (see Fig. 5, Burris et al. (2000)).

The [Ba/Eu] ratio reflects substantial production of Ba in the s-process in the stars with metallicity $-0.6 <$[Fe/H] $< +0.25$. One can make a conclusion that the s-process prevailed in the synthesis of heavy elements at the time of disk stars formation.

Withing the metallicity domain of about -0.5 there is a jump of the [Eu/Ba] ratio, and this can indicate the decreasing contribution from the s-process and respective increasing of the r-process contribution in the Eu and Ba abundances of the metallicities [Fe/H] $< -0.50$.

**References**


Arlandini C., Kappeler F., Wisshak K., et al.: 1999, *ApJ*, **525**, 886.

Baranne A., Queloz D., Mayor M., et al.: 1996, *A&AS*, **119**, 373.

Burbidge E.M., Burbidge G.R., Fower W.A., Hoyle F.: 1957, *Rev. Mod. Phys.*, **29**, 547.

Burris D.L., Pilachowski C.A., Armandro T.E., et.al.: 2000, *ApJ*, **544**, 302.

Busso M., Gallino R., Wasserburg G.J.: 1999, *ARA&A*, **37**, 239.

Cameron A.G.W.: 1982, *Ap&SS*, **82**, 123.

Galazutdinov G.A.: 1992, *Prepr. SAO RAS*, **92**, 27.

Kappeler F., Beer H., Wisshak K.: 1989, *Rep. Prog. Phys.*, **52**, 945.

Katz D., Soubiran C., Cayrel R., et. al.: 1998, *A&A*, **338**, 151.

Kovtyukh V.V., Mishenina T.V.,Bienaymé O., et. al.: 2006, *Astron. Zh.*, **83**, 158.

Kurucz R.L.: 1993, CD ROM n13.

Lamb S., Howard W. M., Truran J. W., Iben I. Jr.: 1977, *ApJ*, **217**, 213.

Mashonkina L., Gehren T., Bikmaev I.: 1999, *A&A*, **343**, 519.

Mashonkina L.I., Gehren T.: 2000, *A&A*, **364**, 249.

Mashonkina L., Gehren T.: 2001, *A&A*, **376**, 232.

Pagel B.E.J.: 1997, *Nucl. and Chemic. Evol. of Galaxies (Cambridge University Press).*

Peters J.G.: 1968, *ApJ*, **154**, 225.

Schwarzschild M., Harm R.: 1967, *ApJ*, **150**, 961.

Sneden C., Cowan J.J.: 2003, *Science*, **299**, 70.

Soubiran C., Katz D., Cayrel R.: 1998, *A&AS*, **133**, 221.

Travaglio C., Galli D., Gallino R., et. al.: 1999, *ApJ*, **521**, 691.

Truran J.W., Cowan J.J., Pilachowski C.A., Sneden C.: 2002, *PASP*, **114**, 1293.

Tsymbal V.V.: 1996, *ASP Conf. Ser.*, **108**, 198.

Wisshak K., Voss F., Kappeler F.: 1996, in *Proc. 8th Workshop on Nuclear Astrophysics*, ed. W. Hillebrandt, Muller E. (Munich: MPI), **16**.

# ON THE NATURE OF ASYMMETRY OF THE LIGHT CURVES OF BM Cas – A LONG PERIOD ECLIPSING SUPERGIANT BINARY

P. Kalv, V. Harvig[1], T. Aas[1], I. Pustylnik[2]

[1] Tallinn University of Technology, Estonia
[2] Tartu Observatory, Estonia

ABSTRACT. We report results of the analysis of $UBVR$ light curves of the long period eclipsing binary BM Cas obtained between 1967 and 1996 in Tallinn observatory. The asymmetry of the light curves and color variations are discussed and interpreted in terms of a hot extended region close to the neck connecting the critical Roche lobes of the components.

**Key words**: stars:binaries:close - stars: individual: BM Cas

## 1. Introduction

A long period eclipsing binary BM Cas with a primary A5-A7 supergiant and invisible secondary component was an observational target for photometric study at Tallinn Observatory where a number of seasonal light curves of this peculiar system in UBVR colors were obtained between 1967 and 1996. A complete light curve (see Figure 1) was calculated according to

$$C = 2449051.17 + 197.275 * E - 2.847 \cdot 10^{-5} * E^2$$

Analysis of the O-C diagram based on these observations and a brief discussion of the observed properties of BM Cas as well as of its probable evolutionary history were published two years ago in our earlier paper (Kalv, Harvig, Pustylnik, 2005). Results of detailed spectroscopic investigation and of some photometric data of BM Cas by Fernie and Evans (1997) generally agree with our earlier conclusions about the probable range of physical parameters of the binary.

Here we summarize the main results of a semi-quantitative analysis of our seasonal light curves (some examples are demonstrated in Figures 2–6). Because of a pronounced intrinsic variability and asymmetry of the light curves as well as of anomalous radial velocity curves available only for the primary component up to now nobody proposed a quantitative model of BM Cas nor determined reliable physical parameters of the components and the binary orbit (an earlier detailed model assuming the extended scattering envelope elaborated by Barwig (Barwig 1976) contradicts the recent IUE data in UV which do not confirm the presence of circumbinary envelope claimed by Barwig).

## 2. Peculiarities of the $UBVR$ light curves

Individual $UBVR$ light curves manifest the following peculiarities:

*2.1. Temporal variations of the depths of both minima.*

There are significant differences between individual light curves in the depths of both minima and to a smaller extent in their duration. The average values of light in units of the total luminosity normalized to the local maximum at the bottom of the primary minimum range between 0.56 and 0.61 for the primary and between 0.86 and 0.89 for the secondary minimum in all four colors, the average semi-widths of the primary minimum range between $0.14P$ and $0.17P$. In some cases the primary minimum is even more shallow – the brightness at the bottom of the primary minimum 0.667 in B color and 0.70 in V was obtained from one partial light curve obtained in 1974.

*2.2 Sporadic displacements of the moment of the primary minimum.*

Sporadic displacements of the moment of the primary minimum from the predicted ephemerides amounting up to $0.02P$ have been detected (despite the fact that no significant systematic period variations have been found in our earlier paper). The same applies to the secondary minimum but because of a conspicuous asymmetry and scattering of observed points it is virtually impossible to give even the approximate numerical estimates.

*2.3 The absence of contribution to the total light from the secondary component.*

Spectroscopic data do not show the evidence for the presence of the spectrum of a companion either in the visible or UV (see Fernie and Evans 1997 for a more detailed discussion). Our multicolor photometric data

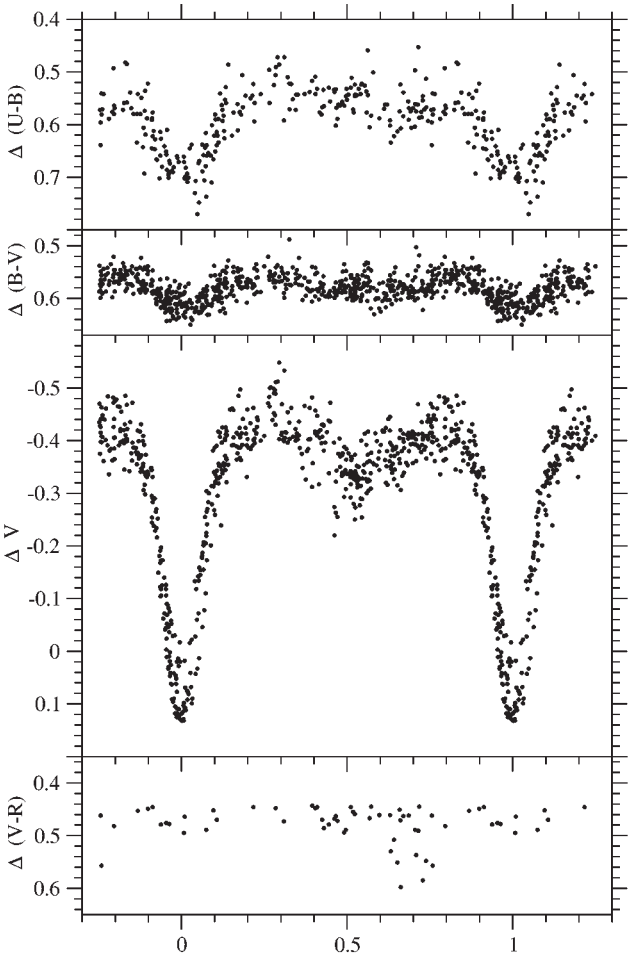


Figure 1: Light and colour curves of eclipsing binary system BM Cas (all observations). The mean–square–root error of a single measurement has been determined from the measurements of comparison and the check stars: $\sigma V = \pm 0.^{\mathrm{m}}009$ and $\sigma(B-V) = \pm 0.^{\mathrm{m}}01$.

supports this conclusion: a) assuming that the primary A5 supergiant is very close to its critical Roche lobe one can with a satisfactory accuracy reproduce the observed light variations as caused by a combined effect of the transient eclipse by a dark smaller body of an invisible secondary component and the ellipticity of the primary. The secondary minimum is caused solely by the ellipticity of the primary, b) within the uncertainties imposed by intrinsic variability the depths of both minima and their widths are roughly the same in all four colors.

### 3. Probable nature of asymmetry of the light curves and colour changes with phase

Over more than 25 years of our time series asymmetry of the seasonal light curves preserved in all colours the same pattern: the ascending branch dur-

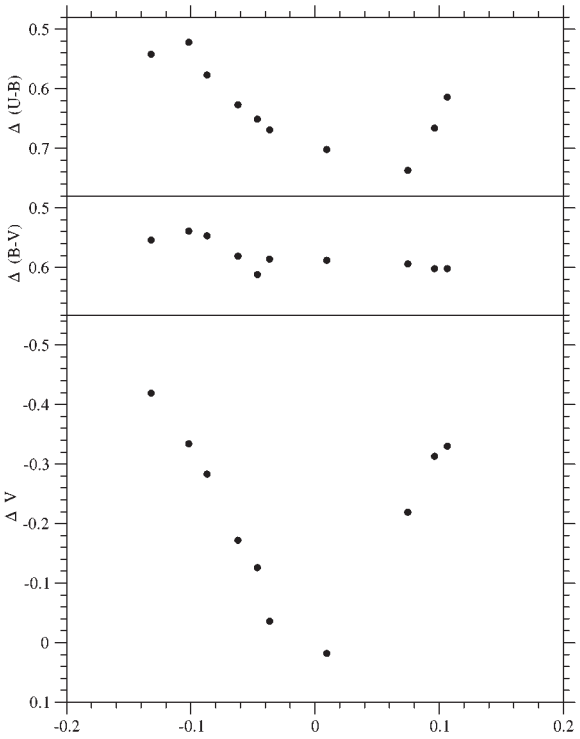


Figure 2: Light and colour curves of eclipsing binary BM Cas E=-19 (JD=2445303±40*d*).

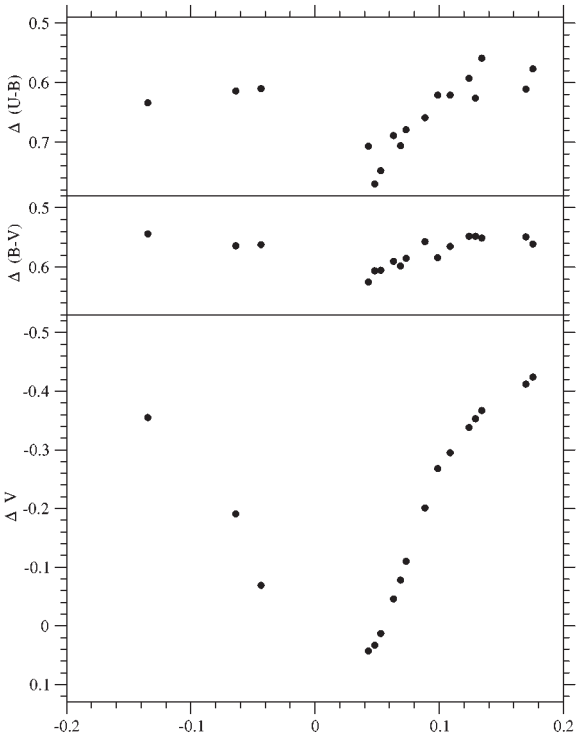


Figure 3: Light and colour curves of eclipsing binary BM Cas E=-11 (JD=2446884±40*d*).

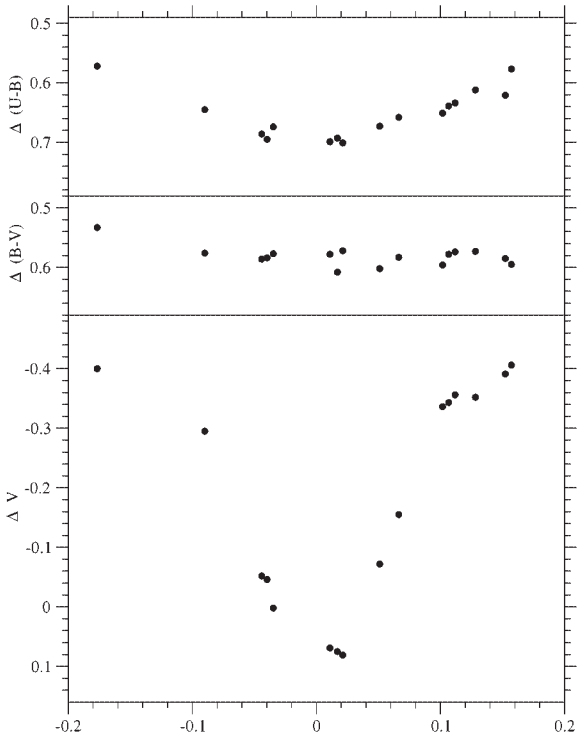


Figure 4: Light and colour curves of eclipsing binary BM Cas E=-10 (JD=2447079±40$d$).

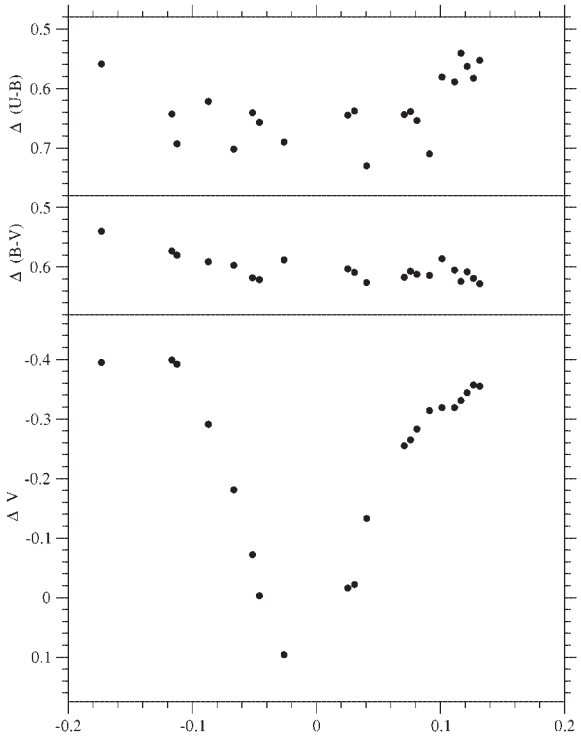


Figure 5: Light and colour curves of eclipsing binary BM Cas E=-9 (JD=2447274±40$d$).

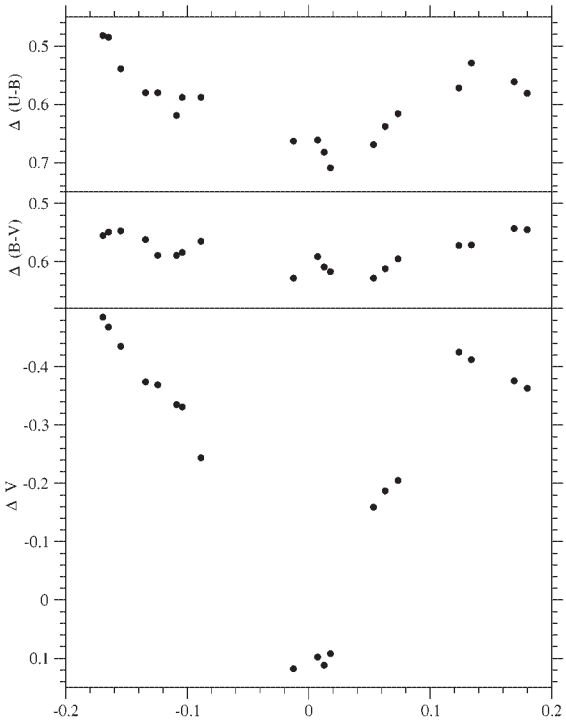


Figure 6: Light and colour curves of eclipsing binary BM Cas E=-8 (JD=2447472±40$d$).

ing primary minimum was systematically slightly more steep than the descending branch (a similar trend is in evidence in the published light curve of BM Cas by Fernie and Evans 1997) and statistically the maximum preceding the primary minimum is slightly (by $0.^{\rm m}01 - 0.^{\rm m}02$) higher than the following maximum (with the phase corresponding to the light maximum shifted from elongation – $0.75P$ to the orbital phase of $0.78P - 0.80P$).

We made an attempt to interpret both the observed pattern of asymmetry of the light curves and color variations from maxima to minima (see Figures 1–6, i.e. BM Cas looks more blue in the maximum light than in minimum, see also similar evidence from a brief note by Shao and Gaposchkin 1962). We postulated the presence of a rather extended, off–center hot region located close to the neck connecting the Roche lobes of both components superimposed upon A5 supergiant. Making use of the commercially available Binary Maker computer code we have found that the following parameters of the hot region result in the asymmetry of the light curve pretty similar to the observed pattern: the temperature contrast

$\Delta T/T_{1sg} \sim 0.2 - 0.25 (T_{1sg} = 8700K)$, the angular radius of the hot region

$R_{\rm sp} = 12^\circ - 15^\circ$, the central co-latitude $l = 88^\circ$, the central longitude $350^\circ$, inclination angle of orbit $i = 70.5^\circ$, the relative radii of the components $r1 = 0.438$ and $r2 = 0.338$ (in the units of semi–

major axis), the temperature of the invisible companion $T_2 = 4500K$. In relative measure (again in the units of semi–major axis of orbit) our value of $R_{\rm sp}$ is close to the radius of the cross–section at the inner Lagrangian point determined by the isothermal density drop–off of the gas stream (see formula in Meyer and Meyer–Hofmeister 1983). The same hot region can explain the small amplitude color changes up to

$\Delta(B-V) \sim 0.05 - 0.08$ from minima to maxima. In $U-B$ the amplitude of color excess amounts even to $0.^{\rm m}15$ and in the black body approximation of the hot source energy distribution we cannot match the observed color curves. This may be partially due to the influence of emission lines (H emission lines are present in BM Cas spectra, with maximum at the phase of the best visibility of the putative hot region, for more details see Barwig 1976) on the light curve in U.

*Acknowledgements.* Financial support of this investigation by the Grant 5760 of the Estonian Science Foundation is gratefully acknowledged.

**References**

Barwig H.D.: 1976, Spektroskopische Untersuchung des Bedeckungsveränderlichen BM Cassiopeiae. Inaugural- Dissertation zur Erlangung des Doktorgrades des Fachbereiches Physik der Ludwig-Maximilians-Univ. München.

Fernie J.D., Evans N.R.: 1997, The supergiant Binary BM Cas, PASP vol. 109, 541–548.

Kalv P., Harvig V., Pustylnik I.B.: 2005, BM Cas a long period eclipsing binary with a supergiant and common envelope, In: Zdenek Kopal binary star legacy, //eds. H.Drechsel and M.Zejda, Aph. and Space Sci., vol. 296, Nos 1–4, 457–460.

Shao C.Y., Gaposhkin S.: 1962, Supergiant Eclipsing Binary BM Cas, Astron. J. vol.67, 283.

Meyer F., Meyer–Hofmeister E.: 1983, A model for the standstill of the Z Camelopardalis variables, *A&A*, vol. 121, 29-34.

# NEW ECLIPSING BINARY IN ORION

A.V. Klabukova

Department of Astronomy, Odessa State University
T.G.Shevchenko Park, Odessa 65014 Ukraine

ABSTRACT. The original observatios, photometric elements, the phase light curve, moments of 14 weakening are presented.

**Key words**: Stars: binary: ecliption; stars: individual: NSV 1754.

The varyability of NSV 1754 = CSV 000453 was found by G. Hoffmeister (1944).

The star was observed on photografic plates of the Sky Patrol of Astronomical Observatory of Odessa State University. In an interval JD 2436526-2448926 143 estimations of brightness in rays pg are obtained.

The varyability of the star is confirmed. The period of the star was determinate with the Lafler and Kinman (1965) method. The brightnes of the comparison stars was determined by reducing to the standart SA 96.

The phase light curve is presented in Fig.1. The varyability type of the star is presumebly (EA).

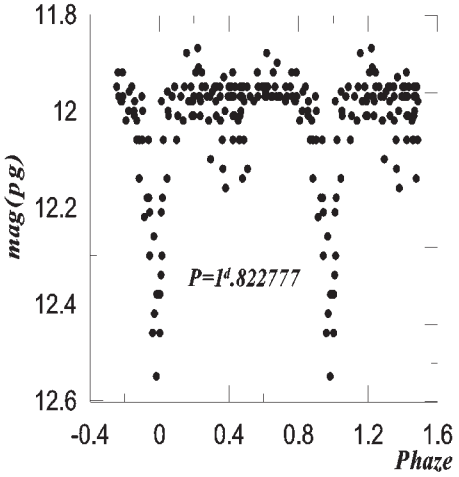


Figure 1: NSV 1754. Phase light curve corresponding to P=1.822777 days.

Table 1:

| $HJD_min24...$ | $E$ | $O-C$ |
|---|---|---|
| 36900.548 | 0 | 0.000 |
| 36964.290 | 35 | -0.055 |
| 38732.442 | 1005 | 0.003 |
| 39038.591 | 1173 | -0.075 |
| 42372.490 | 3002 | 0.035 |
| 44521.568 | 4181 | -0.011 |
| 44986.281 | 4436 | -0.106 |
| 45622.549 | 4785 | 0.013 |
| 47093.485 | 5592 | -0.032 |
| 47093.514 | 5592 | -0.003 |
| 47146.379 | 5621 | 0.001 |
| 47474.501 | 5801 | 0.024 |
| 47855.439 | 6010 | 0.001 |
| 48183.539 | 6190 | 0.001 |

In Table 1 the minimum points and deviations (O-C) from elements:

$$HJD_{min} = 2436900.548 + 1.^d822777 \times E$$

are listed.

In Table 2 the HJD and photographic magnitudes of the star are presented.

## References

Hoffmeister C.: 1944, AN **274**, 176.
Lafler J., Kinman T.D.: 1965, *Ap. J. Suppl.*, **11**, 216.

Table 2:

| HJD 24...d | $m_{pg}$ | HJD 24...d | $m_{pg}$ | HJD 24...d | $m_{pg}$ |
|---|---|---|---|---|---|
| 36542.379 | 11.95 | 39766.590 | 11.97 | 46079.346 | 11.97 |
| 36606.282 | 11.92 | 40183.447 | 12.14 | 46081.316 | 11.97 |
| 36844.570 | 11.97 | 40502.546 | 12.01 | 46090.269 | 11.95 |
| 36855.616 | 12.02 | 40868.555 | 12.00 | 46328.583 | 11.95 |
| 36900.548 | 12.38 | 40870.586 | 12.18 | 46357.540 | 12.01 |
| 36904.416 | 11.97 | 40967.295 | 11.97 | 46359.527 | 11.98 |
| 36933.375 | 12.21 | 40968.286 | 11.88 | 46360.547 | 12.06 |
| 36954.273 | 11.95 | 41219.590 | 12.06 | 46379.503 | 12.02 |
| 36959.319 | 11.92 | 41254.524 | 11.97 | 46380.492 | 11.96 |
| 36960.310 | 11.92 | 41355.254 | 12.22 | 46463.265 | 11.98 |
| 36964.290 | 12.42 | 41708.343 | 11.95 | 46711.587 | 11.95 |
| 36979.326 | 11.87 | 42310.588 | 12.06 | 46770.434 | 11.95 |
| 37227.591 | 11.92 | 42311.584 | 11.95 | 46771.419 | 12.10 |
| 37338.319 | 11.98 | 42331.523 | 12.12 | 46772.415 | 11.95 |
| 37366.241 | 11.98 | 42338.554 | 12.12 | 46772.440 | 12.00 |
| 37582.549 | 11.88 | 42340.558 | 11.95 | 46795.370 | 12.01 |
| 37637.429 | 11.95 | 42344.552 | 11.92 | 47092.518 | 12.02 |
| 37672.373 | 11.95 | 42363.492 | 11.96 | 47093.485 | 12.38 |
| 37942.578 | 11.97 | 42372.490 | 12.55 | 47093.514 | 12.38 |
| 37943.584 | 11.91 | 42423.335 | 12.02 | 47097.503 | 11.98 |
| 37945.593 | 12.01 | 43160.304 | 12.01 | 47146.379 | 12.38 |
| 37961.497 | 12.01 | 43166.301 | 12.14 | 47154.360 | 12.16 |
| 37969.541 | 11.97 | 44521.568 | 12.38 | 47176.312 | 12.01 |
| 37973.550 | 11.95 | 44524.569 | 11.97 | 47177.304 | 12.26 |
| 37974.542 | 11.92 | 44609.332 | 11.95 | 47208.239 | 12.18 |
| 37975.548 | 11.92 | 44612.321 | 11.98 | 47450.539 | 12.06 |
| 38084.248 | 11.97 | 44638.255 | 11.98 | 47450.566 | 12.14 |
| 38085.248 | 12.21 | 44877.572 | 11.96 | 47451.558 | 11.97 |
| 38292.559 | 11.90 | 44878.580 | 11.98 | 47474.501 | 12.30 |
| 38297.564 | 12.01 | 44883.564 | 11.95 | 47531.332 | 11.98 |
| 38303.585 | 11.95 | 44886.578 | 11.95 | 47834.513 | 11.97 |
| 38319.544 | 11.95 | 44887.551 | 11.98 | 47851.439 | 12.02 |
| 38374.471 | 11.97 | 44903.527 | 11.98 | 47855.439 | 12.38 |
| 38378.435 | 11.97 | 44907.505 | 11.98 | 47857.438 | 12.06 |
| 38405.370 | 11.97 | 44910.502 | 11.93 | 47860.419 | 11.97 |
| 38407.415 | 11.97 | 44957.379 | 11.95 | 47865.396 | 12.01 |
| 38441.291 | 11.97 | 44986.281 | 12.30 | 47917.280 | 12.18 |
| 38671.573 | 11.96 | 44996.250 | 11.95 | 47934.226 | 11.97 |
| 38707.514 | 11.95 | 45263.537 | 12.00 | 48158.594 | 11.95 |
| 38708.555 | 11.97 | 45351.300 | 11.97 | 48180.549 | 12.06 |
| 38732.442 | 12.38 | 45618.564 | 12.00 | 48181.533 | 12.06 |
| 38736.413 | 11.95 | 45619.575 | 12.00 | 48182.549 | 12.06 |
| 39036.577 | 12.01 | 45621.565 | 12.00 | 48183.539 | 12.46 |
| 39037.604 | 11.97 | 45622.549 | 12.34 | 48541.547 | 11.97 |
| 39038.591 | 12.46 | 45641.490 | 11.95 | 48541.571 | 12.06 |
| 39055.490 | 11.97 | 45699.340 | 12.02 | 48563.514 | 12.06 |
| 39059.581 | 11.97 | 46007.500 | 12.01 | 48926.513 | 11.97 |
| 39122.396 | 12.06 | 46030.407 | 11.97 | | |

# ABOUT THREE CATACLYSMIC VARIABLE STARS

A.V. Klabukova

Department of Astronomy, Odessa State University
T.G.Shevchenko Park, Odessa 65014 Ukraine

ABSTRACT. In order to detect the new outbursts of the three cataclysmic variable TV Crv, NSV 1775, NSV 895, their positions was scanned on the plates of the Odessa collection of the sky service obtained for the period 1958 - 1988. The new outbursts were detected for stars TV Crv, NSV 1725.

**Key words**: Stars: cataclysmic; stars: individual: TV Crv, NSV 1775, NSV 895.

## 1. TV Crv

The variable star type U Gem TV Crv was discovered by C.W. Tombaugh, about what was informed by Levy (1990). For the star 11 outbursts are revealed (Levy, 1990), in which the light of the variable reaches $12^m$. In a quiet condition the star has the light of $17^m$-$18^m$. Hudec R.(1992) revierved 107 plates of the Bamberg observatory taken in 1964-1967 and episodically in 1971-1974, but did not find new outbursts of the star.

In order to detect the outbursts of this variable its position was scanned on more then 316 plates of the Odessa collection of the sky service obtained for the period 1958 - 1988. On two plates, taken on the 23rd and 24th, April, 1963, the outburst of the variable was detected. The Julian dates of photos are 2438143.324 and 2438144.377. At the outburst the variable reached $12.^m1$ photocraphic macnitude.

The outbursts of the same brightness could be detected still more for 85 plates of the Odessa collection, on other plates the limiting stellar magnitude is more feeble $12.^m5$. It should be noted, that our photos of the given area of the sky nonuniformly cover the whole period of observations. So in 1961 there are 10 plates for the season of observations including 54 calendar days in succession, in 1962 - 11 plates for the season per 101 calendar days, in 1963 - 7 plates for the season per 78 calendar days. For other years there are only incidental photos from 1 up to 5 per year. Therefore it is difficult to draw a conclusion about outbursts of activity of the given star throughout all the period of observations.

## 2. NSV 1725

NSV 1725 = SVS 852 = CSV 441 -is the star presumably of UC type, discovered by Faddeyeva (Parenago, 1938). About 400 photos of the Odessa collection were reviewed, obtained for period 1958-1988. Two outbursts are revealed, stellar light in which reaches $10.^m5$ in pg-macnitude. Julian dates of photos are 2436574.306 and 2436855.612. Thus it confirms that this star is variable and refers to U Gem type.

## 3. NSV 895

NSV 895 = SVS 918 is the star found T. Hvan on the photos of the Moscow collection (Kholopov, 1953), presumably of UG type or nova, for which the outbursts on two plates reach $11.^m7$. At a minimum the star is more feeble $17.^m2$ in pg-magnitude (Kholopov, 1953). About 800 plates of the Odessa collection for period 1958-1988 were reviewed. In about 440 plates from the above, it would be possible confidently to determine an outburst (limiting stellar magnitude $13^m$ -$15^m$). New outbursts are not revealed. It is most probable that the star is of nova type.

## References

Levy O.H.: 1990, *JAU Circ.,* 4983.
Hudec R.: 1992, *IBVS,* 3706.
Parenago P.P.: 1938, *Peremennye Zvezdy,* **5**, 206.
Kholopov P.N.: 1953, *Peremenye Zvezdy,* **9**, N5, 334.

# THE INVESTIGATION OF THE CLASSICAL CEPHEID RT Aur PERIOD

A.S. Kosinsky, V.G. Tamello, I.J. Kushmar, I.S. Bryukhanov, A.S. Semenyuta, I.I. Balyuk

Amateur group of variable stars observers "Betelgeuse",
the Republic Center of Technical Creativity of Pupils,
Makaionak street, 12, Minsk 220023 Belarus, *betelgeize_astro@mail.ru*

ABSTRACT. The outcomes of the research into RT Aur period for the last 93 years are given in the article. New elements of changes in RT Aur brightness have been determined by the authors: $J.D.max = 2447890,265 + 3.7283116 * E$

**Key words**: Star: classical Cepheid RT Aur.

The research results of changes in the period of RT Aur brightness fluctuations (1985–2005) according to visual observations and measurements in the Odessa Photocollection negatives and in the Minsk Photocollection negatives (MPPLF) are represented in the paper. A set of epochs of RT Aur maximums, obtained by many professional astronomers in the 20th century were used in the research with a kind permission of Vitaliy P. Goransky (GAISh, Rossiya, Moskow).

The following members of the amateur group of variable stars observers "Betelgeuse" took part in the research: Ivan M. Sergey, Vladimir V. Schukin, Attila Kosa-Kiss, Valeriy D. Grigorenko,

Andrey J. Pogosyants, Alexey S. Kosinsky, Natalya A. Narkevich, Valentina G. Tamello,

Vyacheslav T. Mamedov, Igor V. Klochko, Ivan S. Bryukhanov, Jury B. Strigelsky, Ivan J. Kushmar, Alexey M. Gain, Roman A. Grabovsky, Andrey S. Semenyuta, Igor I. Balyuk.

The elements of changes in RT Aur brightness (General Catalogue of variable stars (37) have been used in the O-C research:

$$J.D.max = 2442361.155 + 3.728115 * E$$

Two selective (but not best) diagrams of changes in the star brightness obtained on the basis of visual observations and measurements in photonegatives are given below (fig. 1, 2).

Let us introduce the O-C diagram, the chart and the outcomes of the research, where the data of GAISh were used (fig. 3).

Ninety nine epochs of maximums, obtained from our own observations as well as observations of foreign astronomers were used during the research into RT Aur period (see References).

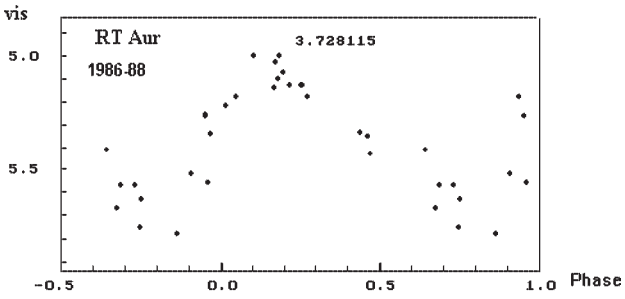


Figure 1:

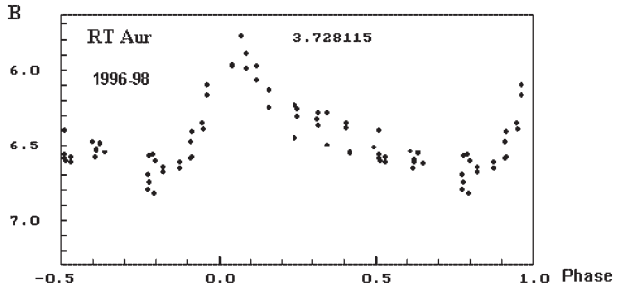


Figure 2:

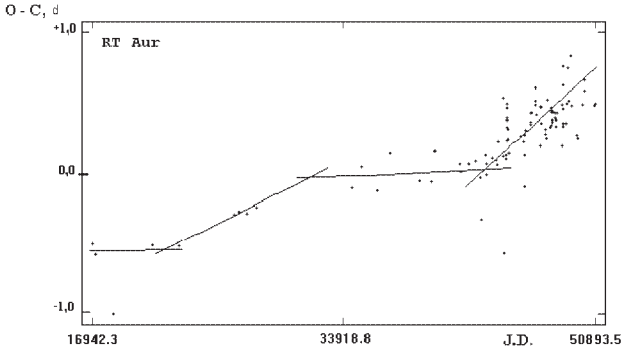


Figure 3:

The O-C diagram shows the spasmodic changes in the star period. Much earlier independent observations by German astronomers confirmed our assumptions that from the moment of RT Aur discovery three sharp spasmodic changes in the period have taken place. Sometimes considerable divergences of observed maximums from calculated O-C values are registered by our researches as well as German scientists. This fact can be presumably regarded as the evidence of some extraordinary chemical and physical changes, taking place inside the star, which is quite a rare occurrence for the stars of such variability type. On the basis of RT Aur observations, carried out by the group "Betelgeuse" in 1985–2005 and taking into account the RT Aur maximums from GAISh index the new elements of changes in RT Aur brightness have been established:

$$J.D.max = 2447890.265 + 3.7283116 * E,$$

where M - m = 0.3 p. Two diagrams of changes in star brightness, obtained from visual observations are given below (fig. 4 - all observations group "Betelgeuse" date back to 1985–2005; fig. 5 - observations, carried out by Andrey Semenyuta (Kazakhstan) and Igor Balyuk (Belarus) in 2005):

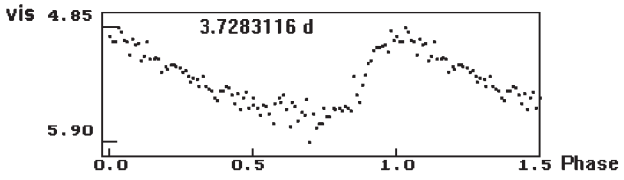


Figure 4: RT Aur 1985–2005, 14 observers

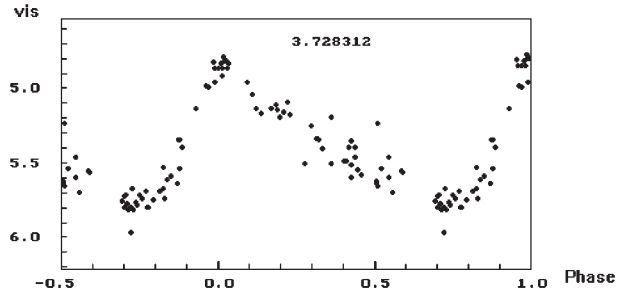


Figure 5: RT Aur 2005 (A. Semenyuta, I. Balyuk)

*Acknowledgements.* We are thankful to Vitaliy P. Goransky, Nicolai N. Samus, Valentin G. Karetnikov, Tatyana V. Puzevich for attention and help.

**References**

Hoffmeister C., Richter G., Wenzel W. Veranderliche Sterne. Sternwarte Sonneberg. Leipzig, 1990.
Kippenhahn R. Hundert Milliarden Sonnen. Geburt, Leben und Tod der Sterne. Piper Munchen Zurich 6. Auftgabe 1987.
Soloviev A.: 1922, *Mirov. Isw.*, 99.
Kukarkin B.: 1935, *NNVS*, **4**, 383.
Krebs C.: 1987, *AN*, **263**, 159.
Nielsen A. V.: 1939, *Aarchus Medd.*, 14.
Mergentaler J.: 1941, *A.J.*, **18**, No 3, 209.
Dufay J.: 1947, *AAp*, **10**, 80.
Grouiller H.: 1947, *AAp*, **10**, 85.
Marks A.: DNU 1, 1956 - Urania Ann. Sci. Suppb. No 1, 1956.
Wisniewski W.Z., Johnson H.L.: 1968, *Arizona Comm.*, **No 112**, 57.
Takase B.: 1969, *Tokyo Bull.*, **ser II**, **No 191**.
Schaltenbrand R., Tammann G.A.: 1971, *AsAp Suppl* **4**, 265.
Winzer J.E.: 1973, *A.J.*, **78**, 618.
Feltz K.A., Mc Namara D.H.: 1980, *PASP*, **92**, 609.
Szabados L.: 1977, *Budapest Mitt.*, **No 70**.
MVS 8, H. 5, 78, 1978.
Harris H.C.: 1980, Thesis.
Huebscher J., Lichtenknecker D., Mundry E.: 1985, *BAV Mitt.*, **No 39**.
Huebscher J., Lichtenknecker D., Meyer J.: 1986, *BAV Mitt.*, **No 43**.
Schmidt J.: 1985, *BAV Rundbrief*, **No 2**, 75.
Kohler, Ratz: 1985, *MVS* **10, H. 7**, 163.
Mofett T.J., Barnes III T.G.: 1984, *ApJ Suppl*, **55**, 389.
Ratz K., Ratz M.: 1983, *MVS* **10, H. 2**, 42.
Bryukhanov I.S.: 1987, *Variable Stars* **22, No 4**, 617-622.
GEOS NC 322, 1982, p. 1/3.
Budquest J.: 1981, *GEOS NC* **270**, p. 3/4.
MVS 9, H. 5, 163, 1983.
MVS 9, H. 3, 80, 1981 (Arbeitskreise "Veranderliche Sterne" DDR).
Williams: *JBAA* 15, 245, u. 270.; AN No 4021.
Marknick, Williams: JBAA 15, 245, u. 270.; AN No 4021.
Goldman H., Ratz M., Ratz K.: 1990, *MVS* **12, H. 3**, 51.
Ratz M., Shille K.: 1988, *MVS* **11, H. 7**, 164.
Goldman H., Ratz M., Ratz K., Hinzpeter A.: 1988, *MVS* **11, H. 7**, 150.
MVS 11, H. 1, 19, 1986.
Lafler J., Kinman T. D.: 1965, *Ap. J. Suppl.*, **11**, 216.
Kholopov P.N., Samus N.N. et al.: 1985, *General Catalogue of variable stars*, **v. I–III**.

# HIGH PRECISION EFFECTIVE TEMPERATURES OF F-K SUPERGIANTS AND CLASSICAL CEPHEIDS

V.V. Kovtyukh

Department of Astronomy, Odessa National University
T.G. Shevchenko Park, Odessa 65014 Ukraine, *val@deneb1.odessa.ua*

ABSTRACT. We present precise effective temperatures ($T_{\rm eff}$) of 110 F-K supergiants determined from the method of line depth ratios. For each star, we have measured the line depths a large number of spectral lines of low and high excitation potentials and established $\sim 100$ relations between $T_{\rm eff}$ and their ratios. These relations have been calibrated against previously published accurate temperature estimates. The range of application of the method is 4000–7000 K (F2–K4). The internal error for a single calibration is less than 110 K, while the combination of all 100 calibrations reduces the uncertainty to only 5–35 K (1 sigma). A big advantage of the line ratio method is its independence on interstellar reddening, spectral resolution, and line broadening due to rotation or microturbulence.

**Key words**: Stars: fundamental parameters; stars: effective temperatures; stars: supergiants; stars: classical cepheids.

## 1. Introduction

The method of the line depth ratios (R1/R2) is based on the use of a large number of paired spectral lines. The lines are paired to cover a large range of excitation potentials of the lower level. The low and high-excitation lines respond differently to the change of $T_{\rm eff}$, therefore the ratio of their depths (or equivalent widths) should be a very sensitive indicator of the temperature. The high-excitation lines vary much less with $T_{\rm eff}$ compared to the low-excitation lines.

In general, the strength of a given line depends, beside the temperature, on the large number of other atmospheric factors, like chemical abundance (or metallicity, [Fe/H]), rotation, micro- and macroturbulence, surface gravity log g, atomic constants, non-LTE conditions, etc. The rationing of lines allows to cancel those factors that affect all lines in the same way. These advantages may not apply to the strong lines which strength is dominated by the damping wings. Therefore only weak lines can be safely used with the line ratio technique.

The line depth ratio method has a long history. Among latest developments are the works by Gray and co-authors (Main Sequence, giants), Strassmeier & Schordan (2000, giants), Padgett (1996, T Tauri stars), etc. Despite the long history, the line ratio method has been only recently transformed into a form that is suitable for the practical use, as for example in the investigation of the chemical abundance analysis of supergiant, giants and Main Sequence (MS) stellar atmospheres. In a serie of papers, our group has improved the method. In Kovtyukh et al. (1998) and Kovtyukh & Gorlova (2000), 37 calibrations for $T_{\rm eff}$ were derived from high-dispersion spectra of supergiants and classical cepheids with effective temperatures from 4500 to 7000 K. The original Kovtyukh & Gorlova (2000) calibration depend upon the excitation temperature analysis of Fry & Carney (1997) combined with the photometric results of Kiss & Szatmary (1998). The current calibration uses the previous information combined with the excitation analysis results for supergiants of Luck & Bond (1989) and the 13-color photometry results of Bravo Alfaro, Arellano Ferro & Schuster (1997). Luck & Bond showed that their effective temperatures were consistent with the V–K calibration of Ridgway et al. (1980) and agreed well with J–K calibration especially at temperatures above 4600 K. This method is not totally dependent upon previous excitation analyses. More importantly, it has been demonstrated to yield consistent results as a function of phase for numerous Cepheids spanning periods from 3 to 47 days (Luck & Andrievsky 2004; Kovtyukh et al. 2005; Andrievsky, Luck & Kovtyukh 2005).

As a next step we derived similar calibrations for the MS stars, with temperatures 4000–6150 K (Kovtyukh et al. 2003; Kovtyukh, Soubiran & Belik 2004). From 600 line pairs we selected 105 with the smallest dispersions (less than 100 K each). This high precision indicates that these calibrations are largely insensitive to metallicity, surface gravity, micro- and macroturbulence, rotation and other individual stellar parameters. In Kovtyukh, Soubiran & Belik (2004), the discovery of a narrow gap (just 50 K wide, between 5560 and 5610

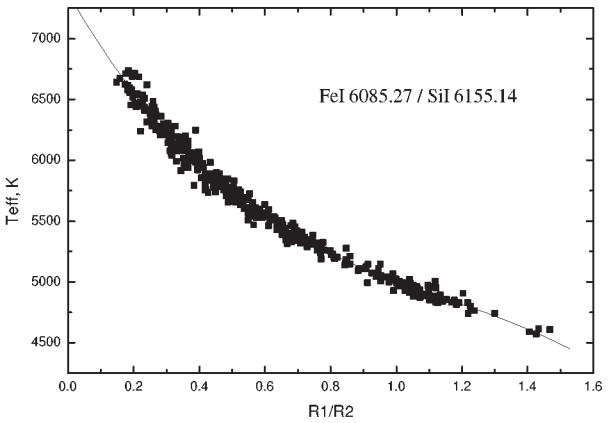


Figure 1: Example of the typical temperature calibrations derived in this work.

K) in the distribution of effective temperatures for 248 MS stars was a nice confirmation of the precision of the method. This gap is attributed to the jump in the penetration depth of the convective zone. The line ratio method has also been tested on giant stars (Kovtyukh et al. 2006). This latter work demonstrated how variations in $T_{\rm eff}$ at a 5–10 K level can be detected for a given star.

The effective temperature obtained from this new technique gives currently one of the most precisely determined fundamental stellar parameters – the relative precision is of the order of 0.1 percent.

## 2. Observations

The investigated spectra are part of the library collected at the Haute Provence Observatory (Soubiran et al. 1998) and they were obtained with the 193 cm telescope equipped with the ELODIE spectrometer (R=42000). The useful spectral range is 4400–6800 ÅÅ, signal-to-noise ratios are larger than 100. All the spectra have been reduced as described in Katz et al. (1998).

Also we used the spectra obtained with UVES at the VLT unit Kueyen (=VLT2). All supergiants are observed with two instrument modes Dichroic 1 and Dichroic 2, in order to cover almost completely the wavelength interval from 3000 to 10000 Å. The spectral resolution is about 80000, and for most of the spectra, the typical S/N ratio is 300–500 in the V band.

The further processing of spectra (continuum level location, measuring of line depths and equivalent widths) was carried out by us using the DECH20 software (Galazutdinov 1992). Line depths $R_\lambda$ were measured by means of a Gaussian fitting.

## 3. Construction of the temperature calibrations

Based on our previous experience, we first conducted an analysis of the potential atomic lines used for the temperature calibrations. We excluded ion lines and the high excitation lines (such as C, N, O transitions), that are sensitive to log g and therefore ambiguous for temperature determination (see Caccin, Penza & Gomez 2002). We primarily used lines belonging to the iron-peak elements (such as Si, Ti, V, Cr, Fe, Ni) because they have a negligible response to changes in log g, and a negligible star to star variation in element abundances.

Then, to begin the iteration process, an initial temperature has been assigned to each star. These temperatures will be a source of systematic uncertainties in the zero-point and in the slope of the final calibrations. They will also affect the internal precision of the calibrations. The choice of the initial temperature scale is therefore very important. Unlike dwarfs, there is no for the supergiants such a natural standard as the Sun. Many recent studies can be found in the literature with temperature scales for supergiants (Luck & Bond 1989; Luck & Wepfer 1995; Fry & Carney 1997; Bravo Alfaro, Arellano Ferro & Schuster 1997, Gray, Graham & Hoyt 2001, Yong et al. 2006). Using these temperatures, we constructed the first set of R1/R2 vs. $T_{\rm eff}$ calibrations. Each calibration was composed of the the lines with vastly different excitation energies of the lower level. We visually examined scattered plots for every ratio and retained only those that showed a clear tight correlation with $T_{\rm eff}$ (see Fig.1). An analytic fit was performed for these selected ratios to produce the first calibrations. By averaging temperatures calculated from these fits, we obtained a second $T_{\rm eff}$ approximation for each star. The random uncertainty has been reduced by 50–100 K. These improved values for $T_{\rm eff}$ have been iterated once again to produced the final calibrations.

The precision of a given calibration varies with $T_{\rm eff}$. We therefore provide for each calibration an allowed range of temperatures where it should be used.

The average internal accuracy of a single calibration (1 sigma) is 60–110 K (ranging from 60–65 K for the best and 100–110 K for the worst cases). Fig. 1 shows our typical calibration. In many cases the dependences could not be fitted with a continuous polynomial, therefore we tried other analytical functions: $T_{\rm eff} = ab^r r^c$, $T_{\rm eff} = ab^{1/r} r^c$, $T_{\rm eff} = ar^b$, $T_{\rm eff} = ab^r$, $T_{\rm eff}$=$a + b * ln(r)$. Here $a, b, c$ are constants and $r$ is the line ratio, $r$=R1/R2. The choice of the particular approximation was done according to the least square deviation.

In cases where R1/R2 was a non-monotonic function (i.e., a given value of R1/R2 corresponded to more

Table 1: High precise temperatures of the supergiants

| HD | $T_{\rm eff}$ | $\sigma$, K | N | error, K | HD | $T_{\rm eff}$ | $\sigma$, K | N | error, K |
|---|---|---|---|---|---|---|---|---|---|
| 000371 | 5083 | 52 | 34 | 9.0 | 147266 | 5078 | 123 | 34 | 21.1 |
| 000611 | 5405 | 117 | 78 | 13.2 | 151237 | 5808 | 140 | 43 | 21.3 |
| 003421 | 5300 | 84 | 80 | 9.4 | 152830 | 6754 | 159 | 36 | 26.5 |
| 004362 | 5301 | 103 | 83 | 11.3 | 159181 | 5181 | 61 | 72 | 7.2 |
| 004482 | 4935 | 122 | 51 | 17.0 | 164136 | 6797 | 134 | 25 | 26.9 |
| 005747 | 5044 | 137 | 35 | 23.1 | 171635 | 6151 | 87 | 79 | 9.8 |
| 008992 | 6331 | 81 | 73 | 9.5 | 172365 | 6018 | 222 | 36 | 36.9 |
| 009900 | 4620 | 53 | 27 | 10.3 | 172588 | 6803 | 258 | 71 | 30.6 |
| 009973 | 6836 | 124 | 73 | 14.6 | 174383 | 5713 | 99 | 88 | 10.6 |
| 010806 | 5049 | 89 | 34 | 15.3 | 176155 | 6474 | 85 | 38 | 13.7 |
| 011544 | 5145 | 60 | 34 | 10.3 | 179784 | 4975 | 35 | 34 | 6.0 |
| 015784 | 6606 | 118 | 36 | 19.7 | 180028 | 6307 | 115 | 72 | 13.6 |
| 016901 | 5509 | 70 | 89 | 7.4 | 180583 | 5986 | 71 | 35 | 12.0 |
| 017905 | 6476 | 165 | 24 | 33.7 | 182296 | 5054 | 47 | 33 | 8.1 |
| 018391 | 5756 | 142 | 66 | 17.5 | 185018 | 5398 | 89 | 34 | 15.3 |
| 020123 | 5160 | 54 | 61 | 6.9 | 185758 | 5367 | 91 | 67 | 11.1 |
| 020902 | 6705 | 84 | 68 | 10.2 | 186155 | 6839 | 148 | 7 | 56.0 |
| 026630 | 5309 | 58 | 67 | 7.1 | 187203 | 5750 | 113 | 26 | 22.1 |
| 031910 | 5401 | 103 | 86 | 11.1 | 188650 | 5649 | 186 | 69 | 22.4 |
| 032655 | 6755 | 144 | 53 | 19.7 | 189671 | 4919 | 59 | 32 | 10.5 |
| 034248 | 6077 | 171 | 70 | 20.5 | 190323 | 6133 | 122 | 35 | 20.6 |
| 036891 | 5089 | 59 | 70 | 7.1 | 190403 | 4978 | 102 | 31 | 18.4 |
| 042456 | 4821 | 86 | 62 | 10.9 | 190405 | 6071 | 251 | 30 | 45.8 |
| 044812 | 4931 | 80 | 67 | 9.8 | 193370 | 6467 | 85 | 31 | 15.3 |
| 045416 | 4826 | 74 | 58 | 9.7 | 194069 | 4916 | 48 | 30 | 8.7 |
| 045829 | 4547 | 59 | 36 | 9.8 | 194093 | 6227 | 70 | 32 | 12.3 |
| 048329 | 4583 | 46 | 40 | 7.3 | 195295 | 6780 | 71 | 75 | 8.2 |
| 048616 | 6528 | 93 | 64 | 11.7 | 195432 | 5907 | 132 | 38 | 21.4 |
| 050372 | 4860 | 72 | 53 | 9.8 | 195593 | 6567 | 95 | 31 | 17.1 |
| 052220 | 5605 | 67 | 90 | 7.1 | 198726 | 6097 | 81 | 86 | 8.8 |
| 053003 | 5499 | 113 | 81 | 12.5 | 199394 | 5082 | 125 | 34 | 21.5 |
| 054605 | 6564 | 83 | 69 | 10.0 | 200102 | 5312 | 93 | 33 | 16.2 |
| 057146 | 5126 | 48 | 68 | 5.9 | 201078 | 6338 | 73 | 64 | 9.2 |
| 062345 | 5004 | 85 | 62 | 10.8 | 202109 | 5060 | 113 | 33 | 19.7 |
| 067523 | 6558 | 137 | 76 | 15.8 | 202314 | 4996 | 75 | 33 | 13.0 |
| 074395 | 5247 | 64 | 75 | 7.4 | 204075 | 5262 | 91 | 71 | 10.8 |
| 077020 | 4911 | 68 | 59 | 8.9 | 204867 | 5431 | 65 | 76 | 7.5 |
| 079698 | 5241 | 105 | 72 | 12.3 | 205603 | 4989 | 59 | 29 | 10.9 |
| 084441 | 5281 | 92 | 66 | 11.3 | 206731 | 5037 | 63 | 32 | 11.1 |
| 090452 | 6890 | 99 | 68 | 12.0 | 206859 | 4912 | 37 | 63 | 4.7 |
| 092125 | 5336 | 99 | 84 | 10.8 | 208606 | 4766 | 60 | 31 | 10.8 |
| 097082 | 5557 | 48 | 87 | 5.2 | 209750 | 5199 | 57 | 65 | 7.1 |
| 099648 | 4967 | 75 | 63 | 9.5 | 210848 | 6238 | 160 | 82 | 17.6 |
| 101947 | 6578 | 188 | 65 | 23.4 | 211153 | 5132 | 132 | 34 | 22.6 |
| 104452 | 5663 | 248 | 32 | 43.8 | 214567 | 4950 | 84 | 57 | 11.1 |
| 109379 | 5124 | 99 | 69 | 11.9 | 214714 | 5416 | 178 | 66 | 21.9 |
| 114988 | 4972 | 173 | 25 | 34.5 | 215665 | 4900 | 70 | 54 | 9.6 |
| 117440 | 4736 | 62 | 50 | 8.7 | 216206 | 5029 | 39 | 32 | 6.8 |
| 125728 | 5009 | 99 | 34 | 17.0 | 216219 | 5758 | 184 | 78 | 20.8 |
| 125809 | 4861 | 57 | 59 | 7.4 | 217754 | 6860 | 172 | 72 | 20.2 |
| 134852 | 6650 | 197 | 37 | 32.3 | 218043 | 6625 | 128 | 29 | 23.9 |
| 136537 | 4978 | 56 | 62 | 7.1 | 221661 | 5034 | 116 | 33 | 20.2 |
| 139862 | 5086 | 106 | 35 | 17.8 | 223047 | 4864 | 39 | 54 | 5.3 |
| 142357 | 6397 | 123 | 24 | 25.2 | 224165 | 4857 | 34 | 32 | 6.1 |
| 146143 | 6072 | 92 | 89 | 9.8 | 225292 | 4974 | 74 | 34 | 12.7 |

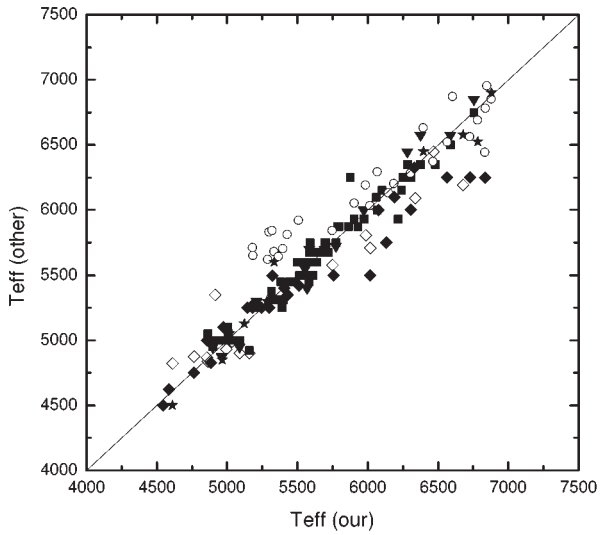


Figure 2: Comparison of our temperatures with estimates from the literature: filled squares – Fry & Carney 1997; open rhombuses – Bravo Alfaro, Arellano Ferro & Schuster 1997; open circles – Gray, Graham, Hoyt 2001; filled triangles – Yong et al. 2006; filled rhombuses – Luck & Bond 1989; stars – Luck & Wepfer 1995.

than one value of $T_{\rm eff}$), we have limited the range of application for temperatures to exclude this ambiguity. More details about the line ratio techniques can be found in Kovtyukh et al. (2006).

## 4. Results and summary

In Table 1 we report $T_{\rm eff}$ for 110 supergiants derived from our calibrations. Each entry includes the name of the star, mean $T_{\rm eff}$, standard deviation of the mean temperature, number of calibrations used, and 1 sigma error. Fig. 2 compares for 110 objects our temperatures with estimates from the literature.

The final precision we achieve is 5–35 K (1 sigma), for the spectra of R=42000, S/N=100–150. This can be further improved with higher resolution and larger S/N. We note that this error budget does not include the possible uncertainties that arise from the individual properties of stars, like magnetic field, metallicity, $V_{tur}$, v*sin*i, etc. When monitoring a given star however, these individual parameters remain fixed, which allows to detect temperature "variations" as small as 4–10 K.

The high accuracy of $T_{\rm eff}$ determination provided by the line ratio method allows in turn to achieve a high accuracy in [Fe/H] determination – down to 0.02–0.05 dex. The scatter of the points in Fig.1 arises mainly from the individual parameters of each star (like rotation, chemical composition, convection, binarity, etc.) rather than from the measurements errors of line depths (which are mostly due to the uncertainty of continuum placement). The averaging of temperatures obtained from 70–100 line ratios significantly reduces the uncertainty from a single calibration.

Summarizing, supergiant temperatures determined in this work using line ratio technique, are of high internal precision and agree well with the most accurate estimates from the literature.

*Acknowledgements.* The author thanks Dr. C. Soubiran for kindly provided Elodie spectra.

### References

Andrievsky S.M., Luck R.E., Kovtyukh V.V.: 2005, *AJ*, **130**, 1880.
Bravo Alfaro H., Arellano Ferro A., Schuster W.J.: 1997, *PASP*, **109**, 958.
Caccin B., Penza V., Gomez M.T.: 2002, *A&A*, **386**, 286.
Galazutdinov G.A.: 1992, *Prepr.SAORAS*, **92**, 28.
Fry A.M., Carney B.W.: 1997, *AJ*, **113**, 1073.
Gray D.F.: 1989, *ApJ*, **347**, 1021.
Gray D.F.: 1994, *PASP*, **106**, 1248.
Gray D.F., Baliunas S.L., Lockwood G.W., Skiff B.A.: 1992, *ApJ*, **400**, 681.
Gray D.F., H.L. Johanson H.L.: 1991, *PASP*, **103**, 439.
Gray D.F., Brown K.: 2001, *PASP*, **113**, 723.
Gray R.O., Graham P.W., Hoyt S.R.: 2001, *AJ*, **121**, 2159.
Katz D., Soubiran C., Cayrel R., Adda M., Cautain R.: 1998, *A&A*, **338**, 151.
Kiss L.L., Szatmary K.: 1998, *MNRAS*, **300**, 616.
Kovtyukh V.V., Gorlova N.I., Klochkova V.G.: 1998, *Astron.Lett.* **24**, 372.
Kovtyukh V.V., Gorlova N.I.: 2000, *A&A*, **358**, 587.
Kovtyukh V.V., Soubiran C., Belik S.I., Gorlova N.I.: 2003, *A&A*, **411**, 559.
Kovtyukh V.V., Soubiran C., Belik S.I.: 2004, *A&A*, **427**, 933.
Kovtyukh V.V., Mishenina T.V., Gorbaneva T.I., Bienaymé O., Soubiran C., Kantsen L.E.: 2006, *Astron.Rep.*, **50**, 134.
Kovtyukh V. V., Andrievsky S. M., Belik S. I., Luck R. E.: 2005, *AJ*, **129**, 433.
Luck R.E., Bond H.E.: 1989, *ApJSS*, **71**, 559.
Luck R.E. & Andrievsky S.M.: 2004, *AJ*, **128**, 343.
Luck R.E., Wepfer G.G.: 1995, *AnJ*, **110**, 2425.
Padgett D.L.: 1996, *ApJ*, **471**, 847.
Ridgway S. T.; Joyce R. R.; White N. M.; Wing R. F.: 1980, *ApJ*, **235**, 126.
Soubiran C., Katz D., Cayrel R.: 1998, *A&ASS*, 133, 221.
Strassmeier K.G., Schordan P.: 2000, *Astr.Nachr.*, **321**, 277.
Yong D., Carney B.W., de Almeida L., Pohl B.L.: 2006, in press (astro-ph 0512348).

# COLORIMETRY OF TWO FLARES ON EV LACERTAE FROM UBVRI OBSERVATIONS IN 2004

M.N. Lovkaya[1], B.E. Zhilyaev[2]

[1] Scientific-research Institute "Crimean Astrophysical Observatory", p. Nauchny, Crimea, Ukraine, 98409,Ukraine, *rita@crao.crimea.ua*
[2] Main Astronomical Observatory, NAS of Ukraine, 27 Akademika Zabolotnoho, 03680 Kyiv, Ukraine, *zhilyaev@mao.kiev.ua*

ABSTRACT. According to the fast UBVRI photometry data obtained during international synchronous observations of the flaring red dwarf EV Lac, a fine time structure of two flare events is investigated and occurrence of high-frequency oscillations (HFO) during a flare is confirmed. It is revealed that HFO appear at the earliest stages of the flare development. The periods of fluctuations are from several seconds up to tens seconds. Typical amplitudes amount to some hundredths of a magnitude in the U band. HFO lead to significant variations in colors of the pure flare radiation - up to one and more magnitude. The detailed colorimetric analysis allows to note changing of such characteristics of a flare as optical thickness, electron density and temperature during the flare development. In the brightness maximum a flare radiates as a black body with temperature approximately $18500 \pm 1500$ K. It is established that a flare is oscillating between the states of optically thick and optically thin in the Balmer continuum hydrogen plasma during the most part of its lifetime.

**Key words**: UBVRI photometry, Stars: flaring: stars: individual: EV Lac.

## 1. Introduction

Colorimetry is the crucial quantitative method in the analysis of radiation of flaring stars. Multicolor photometry allows to estimate such characteristics of radiating plasma as the effective temperature, electron density, and optical thickness. To estimate these parameters different authors have carried out simulation of color characteristics for various mechanisms of flare radiation. Theoretically, the monitoring of a star in the UBVRI bands during the flare lifetime enables one to receive a detailed picture of changes in flare plasma characteristics with time. However, colorimetry of flaring stars has not yet led to unequivocal conclusions about properties of the pure flare radiation. The main difficulties in interpretation of the colorimetry data are concerned with low time resolution (5...19 sec) and limited precision of observation in the U band ($\sim 0.15$ mag), whereas variations in color-indexes can amount to one and more magnitude during a few seconds (Zhilyaev et al., 2005).

Last years synchronous observations of flaring stars were carried out with the high time resolution (up to 0.1 sec) with several remote telescopes. The digital filtering technique has been applied to data processing to increase accuracy of brightness and colors estimations of flares. A new fact has been established - occurrence of high-frequency oscillations (HFO) during a flare (Zhilyaev et al., 2000; Zhilyaev et al., 2003). This factor was not investigated in early works on colorimetry. The combination of above approaches allows one to carry out the colorimetric analysis from the very onset of a flare till its fading.

Basic conclusions of the present work are: HFO appear at the earliest stages of the flare development. The periods of oscillations are from several seconds to tens seconds. Typical amplitudes amount to some hundredths of a magnitude in the U band. HFO lead to significant variations in colors of the pure flare radiation - up to one and more magnitude.

It is necessary to note, that recently HFO were found in flaring dwarf stars in the radio (Abada-Simon et al., 1995) and in the x-ray (Mitra-Kraev et al., 2005) too.

## 2. Observations and results

Observations of the flare star EV Lac were carried out in September, 2004 with the Synchronous Network of Telescopes involving telescopes of four observatories in Ukraine (the 1.25-m AZT-11 and 50", CrAO), Russia (the Peak Terskol 2-m), Greece (the Stephanion 76-cm) and Bulgaria (the Rozhen 2-m, and the Belogradchik 60-cm). For 14 nights of observations more than ten flares have been registered.

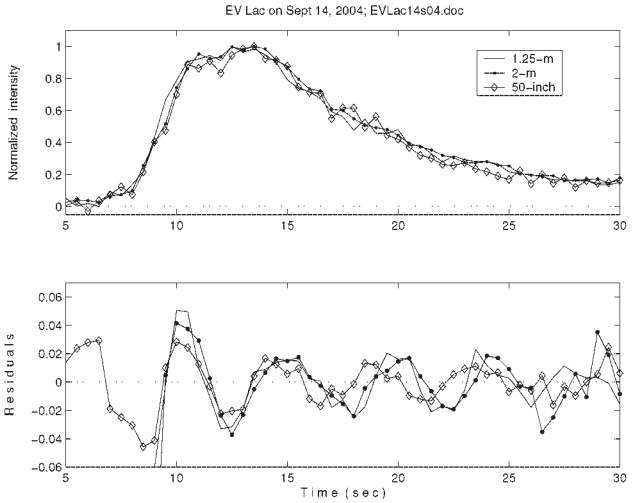


Figure 1: A flare event on EV Lac, September 14, 2004, 20:31 UT (max). See text.

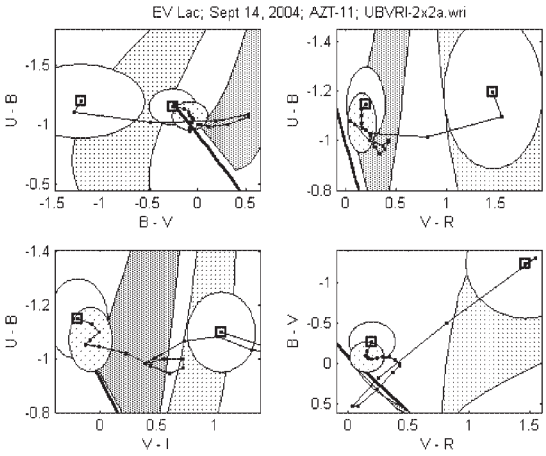


Figure 2: Color time tracks of the flare in EV Lac, September, 14th 2004.

In the present work we analyze two flares observed simultaneously on three telescopes synchronized up to 0.1 sec in UTC. A flare of EV Lac on September 14, 2004 ( maximum at 20:31 UT) was observed with three telescopes: the 2-m (Terskol), the 50" and AZT-11 (CrAO). The amplitude of a flare in the U band amounts to two magnitudes, duration about 40 sec.

Fig 1 shows fragments of light curves of the flare in the U band both before (top) and after (bottom) the high-frequency filtering. The light curves are normalized to unit intensity in a brightness maximum. One can see only weak signs of HFO in the raw photometric data. The bottom graph shows clearly a presence of HFO after corresponding high-frequency digital filtering of the light curves. The period of fluctuations is 4.5 sec, amplitude - a few hundredths of a magnitude. Obvious correlation in the data received simultaneously on remote telescopes evidences the reality of HFO. Presence of HFO is revealed in other spectral bands too. The power spectra of residuals obtained with the telescope AZT-11 in the U and I bands show low-coherent oscillations with periods of 4.5 and 6.3 sec, respectively. There is a clear shift in frequency between the oscillations registered in the U and I bands.

The UBVRI photometry data (AZT-11, CrAO) allow us to trace time variations of color-indices and to develop the time color tracks technique for flare plasma diagnostics and estimating its thermodynamic characteristics. The interval of time suitable for colorimetric analysis was limited to 20 sec because of low amplitude of a flare in the R and I bands, though the flare remained visible in the U band during some more 40 sec. Variations detected in color-indices during a short-term period of the flare lifetime amount to one magnitude and more.

Figure 2 shows time evolution of color-indices of the pure flare radiation. The beginning and the end of a flare are marked by squares. The 95% error ellipses in the beginning of a flare (b), in the maximum and in the end of a flare (c) are shown too. Markers on tracks follow with a time step of 1 sec.

To prepare the color-color diagrams the results of color-indices calculations for various sources of radiation were used (Straizys, 1977; Chalenko, 1999). The light gray area denotes the color characteristics of hydrogen plasma optically thin in the Balmer continuum with $T_e = 10000$ K and $N_e$ from $10^{14}$ to $10^{10}$ $cm^{-3}$, the deep gray area corresponds to optically thick plasma with $T_e$ from 15000 to 8000 K. The heavy black line notes the blackbody radiation. The flare beginning is close to the area occupied by radiation of a blackbody with T from 17000 to 22000 K. For 4 sec a flare reaches its maximum at temperature $T_{bb} = 18500$ K. Plasma of a flare appears opaque only near to a maximum of its brightness within several seconds. Then the tracks run to the area of hydrogen plasma optically thick in the Balmer continuum. The temperature of a flare drops to $T_e$ = 8000 - 10000 K, and for some seconds a flare passes in the area occupied by hydrogen plasma optically thin in the Balmer continuum with $T_e = 10000$ K and $N_e$ from $10^{14}$ to $10^{10}$ $cm^{-3}$.

All the sites in Ukraine, Russia, Greece and Bulgaria had registered the second flare event on September 12, 2004. The amplitude of a flare was about 1.5 magnitudes in the U-band, duration was about 150 sec.

Both the initial and smoothed data clearly show the presence of HFO on a descending part of a flare. The power spectra calculated from these light curves detect oscillations with periods about 17, 8 and 6 sec.

Figure 3 represents the light curves of a flare observed with 3 telescopes in CrAO, Bulgaria and Greece and high-frequency oscillations in brightness in the U band after elimination of the main flare light curves. These graphs reveal that HFO arise just before a flare,

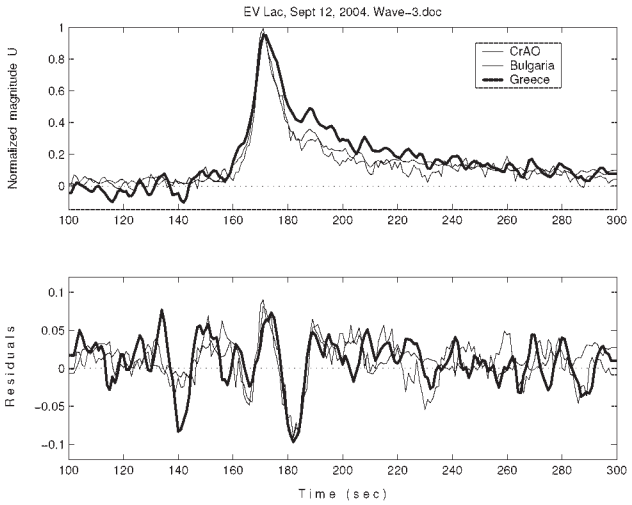


Figure 3: The light curves of a flare on EV Lac, September 12, 2004, observed with 3 telescopes in CrAO, Bulgaria and Greece. See text.

maybe provokes a flare; it lasts about one minute, its period is about 17 sec. The low-frequency UBV light curves and color-indices of the pure flare radiation show evidently oscillations with a period about of 17 sec (Figure 4).

The light curves in the R and I bands have been excluded from consideration because of intensive variations caused by HFO. On the (B-V) curve asterisks note peaks at the moments 12, 29, 46 sec from the accepted flare's onset. As we shall see below, in these points the track of a flare on the color-color diagram crosses the blackbody line.

Figure 5 represents a color time track of this flare. Markers on the track follow with a time step of 5 sec. According to the theoretical color-color diagrams (Chalenko, 1999), the flare's onset falls in the area corresponding to the radiation of hydrogen plasma optically thick in the Balmer continuum with $T_e \sim 10000$ K. In the same area the radiation of the photosphere heated by a rapid flow of electrons with energies 50, 100 and 200 keV is localized (the dashed, solid and dotted lines). During approximately 10 sec from the accepted onset the flare reaches a maximum and radiates as a blackbody with $T_{bb}$ = 17000 - 22000 K with the most probable value of 18500 K. Then the flare starts oscillating between the areas of the diagram occupied by hydrogen plasma optically thick and optically thin in the Balmer continuum. At the end of a flare (marked by a square) the track moves towards the area of radiation of optically thin hydrogen plasma with $T_e \sim 10000$ K.

Thick black circles correspond to peaks on the (B-V) color curve (see Fig 4) and fall to points where the flare track crosses the blackbody line. For the limited segment in the vicinity of a flare maximum

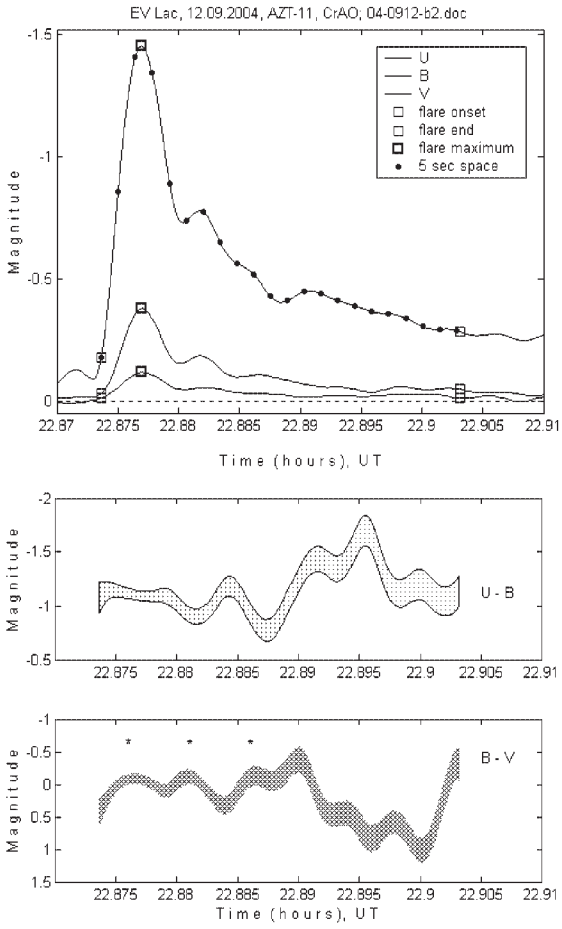


Figure 4: Low-frequency UBV light curves and the corresponding colors of the flare in EV Lac, September, 12th 2004.

it is possible to estimate the (V-R) color-indices too. The color-color diagram (U-B) - (V-R) confirms that a flare in its maximum radiates as a blackbody with temperature $\sim$ 18500 K.

## 3. Conclusion

The detailed colorimetric analysis of two flares on EV Lac has allowed to notice changes in optical thickness and electronic density during the development of a flare and to estimate temperature in the flare maximum. A new unknown earlier fact has been established: oscillations of plasma of a flare between the states of optically thick and optically thin in the Balmer continuum.

These oscillations have recently found a theoretical explanation (Kouprianova et al., 2004; Stepanov et al., 2005). HFO are connected with fast magnetoacoustic oscillations of magnetic coronal loops on a star. The theory enables to estimate the main parameters of the coronal loops (temperature, electron density and the typical sizes). This opens new prospects for studying

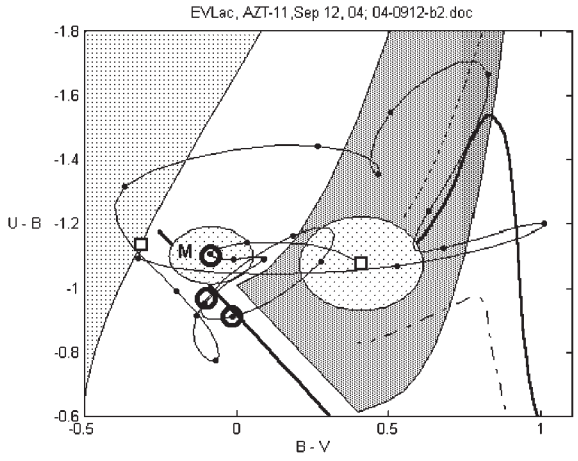


Figure 5: Color tracks of the flare from September, 12th 2004. Markers correspond to 5-s intervals. The beginning and the end of the flare are marked by squares. 95% error ellipses are shown at the beginning and at the maximum of the flare. Thick circles correspond to maxima on color curve B-V (asterisks in Figure 4). It is interesting, that in these points the track crosses the blackbody line.

the coronas of flaring stars, specific *"coronal seismology"*. The synchronous observations of flaring stars in the UBVRI-system with several remote telescopes with high time resolution may be a source of such a work.

## References

Abada-Simon M., Lecacheux A., Aubier M., and Bookbiner J.: 1995, *Lect. Notes Phys.,* **454**, 32.

Chalenko N.: 1999, *Astron. Reports,* **7**, 459.

Kouprianova E.G., Tsap Y.T., Kopylova Y.G., Stepanov A.V.: 2004, *IAU Symp. 223, Multi-Wavelength Investigations of Solar Activity, eds. Stepanov A.V. et al.,* 391.

Mitra-Kraev U., Harra L.K., Williams D.R., Kraev E.: 2005, *Astron. and Astrophys.,* **436**, 1041.

Stepanov A.V., Kopylova Y.G., Tsap Y.T., Kouprianova E.G.: 2005, *Pis'ma Astron. Zh.,* **31**, 684.

Straizys V.: *Multicolor Stellar Photometry, 1977, Mokslas Publishers, Vilnius.*

Zhilyaev B.E., Romanyuk Ya. O., Verlyuk I.A., Svyatogorov O.A., Khalack V.R., Sergeev A.V., Konstantinova-Antova R.K., Antov A.P., Bachev R.S., Alekseev I.Yu., Chalenko V.E., Shakhovskoy D.N., Contadakis M.E., Avgoloupis S.J.: 2000, *Astron. and Astrophys.,* **364**, 641.

Zhilyaev B., Romanyuk Ya., Svyatogorov O., Verlyuk I., Alekseev I., Lovkaya M., Avgoloupis S., Contadakis M., Seiradakis J., Antov A., and Konstantinova-Antova R.: 2003, *Kinematics and Physics of Celestial Bodies, Supplement,* **4**, 30.

Zhilyaev B., Romanyuk Ya., Verlyuk I., Svyatogorov O., Kaminsky B., Andreev M., Gershberg R., Lovkaya M., Avgoloupis S., Seiradakis J., Contadakis M.E., Antov A., Konstantinova-Antova R., Bogdanovski R.: 2005, *Astron. and Astrophys.,*(submitted).

# THE BEHAVIOR OF $\alpha$ – ELEMENTS ABUNDANCES IN THE THIN AND THICK DISKS OF THE GALAXY

T.V. Mishenina[1] , T.I. Gorbaneva[1], C. Soubiran[2], O. Bienayme[3], V.V. Kovtyukh[1], S.A. Korotin[1]

[1] Department of Astronomy, Odessa State University
T.G.Shevchenko Park, Odessa 270014 Ukraine, *tamar@deneb.odessa.ua*
[2] Observatoire Aquitain des Sciences de l'Univers,
CNRS UMR 5804, BP 89, 33270 Floirac, France
[3] Observatoire Astronomique de l'Universite Louis Pasteur, Strasbourg, France

ABSTRACT. We have carried out the detailed analysis of 350 high-resolution spectra of FGK dwarfs and giants. Abundances of Fe, Si, Ca and Ni have been determined under LTE approximation, whereas abundances of Mg have been determined under NLTE approximation. Spatial velocities with an accuracy better than 1 $\mathrm{km\,s^{-1}}$ , as well as orbits, have been computed for dwarfs (or all) stars. They have been used to define 2 subsamples kinematically representative of the thin disk and the thick disk in order to highlight their respective properties. A transition occurs at [Fe/H] $= -0.3$. Stars more metal-rich than this value have a flat distribution with $Z_{max} < 1$ kpc and $\sigma_W < 20$ $\mathrm{km\,s^{-1}}$ , and a narrow distribution of [$\alpha$/Fe] . There exist stars in this metallicity regime which cannot belong to the thin disk because of their excentric orbits, neither to the thick disk because of their low scale height. Several thin disk stars are identified down to [Fe/H] $= -0.80$. Their Mg enrichment is lower than thick disk stars with the same metallicity. Both the dwarfs and the giants show a decrease of [$\alpha$/Fe] with [Fe/H] in the thick disk.

**Key words**: Stars: fundamental parameters; stars: abundances; stars: kinematics; stars: atmospheres; Galaxy: stellar content.

## Introduction

In this paper we put particular attention to the transition between the thin disk and the thick disk and to the abundances of the $\alpha$-elements Mg and Si and the iron-peak element Ni. According to the current nucleosynthetic theory, $\alpha$-elements are being produced as a result of $\alpha$-capture reaction, taking place in the core of massive stars during their explosion as SN II (Burbidge et al. 1957). Fe is produced by both massive SN II and less massive SN Ia. If the percentage of massive stars in the earlier Galaxy was higher than today, one can predict that the $\alpha$/Fe ratio is going to change over time. A well established observational fact shows that in old metal-poor stars of the Galaxy, [$\alpha$/Fe] , in particular [Mg/Fe] , is overabundant relative to Sun's value (Wallerstein 1961; Gratton & Sneden 1987; Magain 1989; Nissen et al. 1994; Fuhrmann et al. 1995, etc). If the $\alpha$-element overabundance is a typical chemical pattern in halo stars in comparison with disk stars, there is a question whether there is a distinction in the Mg behaviour in other subsystems of the Galaxy, in particular in the thin and thick disks. Such a difference would have important consequences on the choice of the most probable scenario of formation of the thick disk (collapse, accretion etc.) and its timescale.

## 1. Observations, parameters and abundances

All the spectra used in this paper are extracted from the most recent version of the library of stellar spectra collected with the ELODIE echelle spectrograph at the Observatory de Haute-Provence by Soubiran et al. (1998) and Prugniel & Soubiran (2001). The performances of the instrument mounted on the 193cm telescope, are described in Baranne et al (1996). A resolving power of 42 000 in the wavelength range $\lambda\lambda$ 3850–6800 ÅÅ.

The continuum level drawing and equivalent width measurements were carried out by us using DECH20 code (Galazutdinov 1992).

Our group has improved the line-depth ratio technique to determine $T_{eff}$ (Kovtyukh et al. 2003). This method, relying on ratios of the measured central depths of lines having very different functional dependences on $T_{eff}$ , is independent of interstellar reddening and takes into account the individual characteristics of the star's atmosphere. For the most metal-poor stars, $T_{eff}$ was determined earlier (Mishenina & Kovthyukh

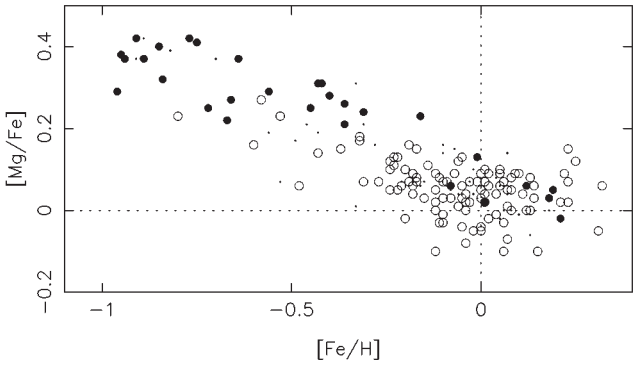


Figure 1: [Mg/Fe] vs [Fe/H] for the whole sample. Black dots indicate thick disk stars, open dots thin disk stars, small dots represent the unclassified stars.

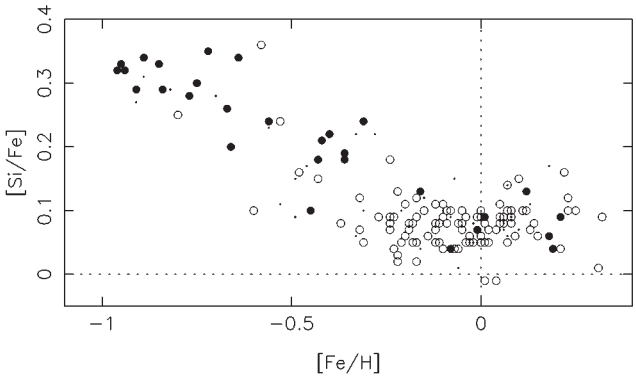


Figure 2: Same as Fig. ?? for Si.

2001). The $H_\alpha$ line-wing fitting was used for stars studied in this work.

The surface gravity log $g$ was determined using two different methods, the method based on the ionisation balance for iron and a second method by fitting the wings of a Ca I line profole.

Microturbulent velocities $V_t$ were determined by forcing the abundances determined from individual FeI lines to be independent of equivalent width.

Fe, Si, Ni abundances for dwarfs and Fe, Si, Ca, Ni, for giants were determined from an LTE analysis of equivalent widths using the WIDTH9 code and the atmosphere models by Kurucz (1993).

The determination of Mg abundance was carried out through detailed NLTE calculations using equivalent widths of 4 lines ($\lambda\lambda$ 4730, 5711, 6318, 6319 ÅÅ) and profiles of 5 lines ($\lambda\lambda$ 4571, 4703, 5172, 5183, 5528 ÅÅ).

NLTE abundances of Mg were determined with the help of a modified version of the MULTI code of Carlsson (1986) described in Korotin et al. (1999a,b).

## 2. Stellar kinematics, metallicity, elemental abundances

We have selected our sample to span the metallicity range $-1.0 <$[Fe/H] $< +0.3$ in order to define 2 subsamples representative of these two populations. A discrimination of thin disk and thick disk stars is possible using the fact that the two disks are known to be distinct by their spatial distribution and local density, and by their velocity, metallicity and age distributions.

We have computed the probability of each star, with a measured velocity (U,V,W), to belong to the thin disk ($Pr_1$) and to the thick disk ($Pr_2$).

Figs. 1, 2 show the trend, of the abundances of Mg and Si as a function of [Fe/H] for dwarfs. It can be seen that :

- there are a few thin disk stars with [Fe/H] $< -0.30$
- metal poor stars ([Fe/H] $< -0.60$) are all enriched in Mg and Si ([Mg/Fe] $> +0.20$, [Si/Fe] $> +0.15$)
- on the contrary at solar metallicity, the enrichment of Mg and Si does not exceed +0.20
- at a given metallicity thick disk stars have higher [Mg/Fe] on average than thin disk stars
- the dispersion of [Si/Fe] is remarkably small for [Fe/H] $> -0.30$ but quite high at lower metallicity
- [Mg/Fe] and [Si/Fe] decline with metallicity from about +0.40,+0.35 to 0.0, +0.08 respectively
- there are stars with thick disk kinematics at solar metallicities, their abundance trends follow the thin disk

Mg and Si are $\alpha$ elements which are supposed to be mainly produced in SNII. It can be seen in this plot that a transition occurs at [Mg/Fe] $\simeq +0.2$. Stars with [Mg/Fe] $< +0.2$ have a mean abundance of [Si/Fe] $=+0.08$ with a very low dispersion of $\pm 0.03$, lower than our error estimates. [Mg/Fe] is more dispersed ($\pm 0.06$) around the mean of [Mg/Fe] $=+0.05$. For stars with [Mg/Fe] $> +0.2$ the distribution is consistent with a linear correlation: [Si/Fe] =0.7 ; [Mg/Fe] +0.06 (rms=0.06).

### *2.1. The thin disk*

Several thin disk stars are found at low metallicity, down to [Fe/H] $= -0.80$. Reddy et al (2002) have found in their samples a significant number of stars with [Fe/H] $< -0.40$ that they identify as belonging to the thin disk. Our observations suggest that the distribution of [$\alpha$/Fe] in the thin disk is very narrow, specially for Si, at [Fe/H] $> -0.30$. On this point we are in perfect agreement with Reddy et al (2002) and Bensby et al. (2003). For the metal-rich part, we obtain as mean values and dispersions : [Mg/Fe] $=+0.05$, $\sigma_{[Mg/Fe]}$=0.07, [Si/Fe] $=+0.07$, $\sigma_{[Si/Fe]}$=0.03. Such a narrow chemical distribution implies that the stars formed from an homogeneous gas.

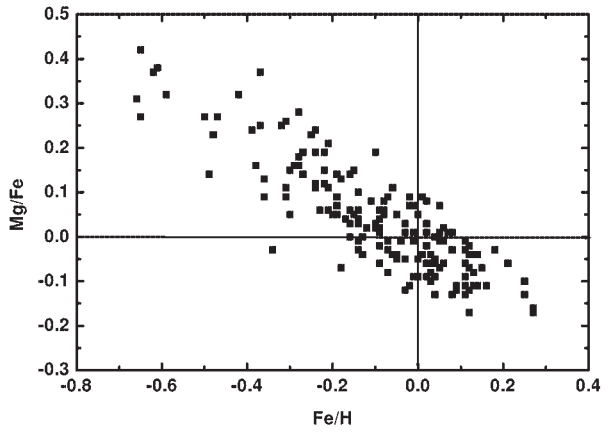


Figure 3: [Mg/Fe] vs [Fe/H] for giants.

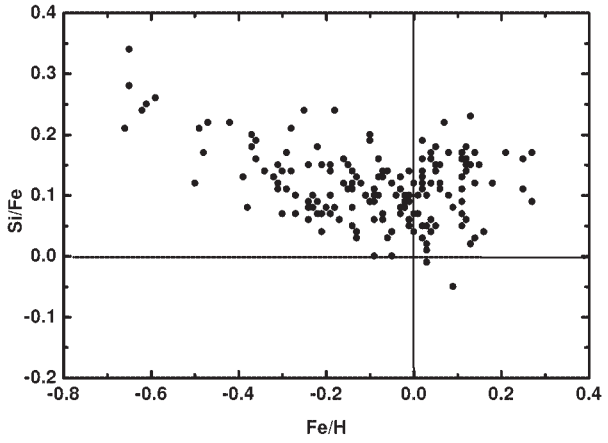


Figure 4: Same as Fig. 3 but for Si.

*2.2. The thick disk*

Having eliminated from the thick disk the 8 stars having high metallicity and a flat distribution, we see from Fig. 2 that [Mg/Fe] decreases from the halo value (+0.40) at [Fe/H] =–1.00 to +0.20 at [Fe/H] =–0.30. Si has the same behavior, decreasing from +0.35 to +0.17, with one deviating star HD 110897 having a lower enrichment in Si. These findings are nicely consistent with the trends found by Bensby et al. (2003) that they interpreted as the signature of the chemical enrichment by SNIa.

Fig. 3, 4 show the trend of the abundances of Mg and Si as a function of [Fe/H] for giants. A trend of [alpha/Fe] and Ni abundance with [Fe/H] for giants is a similar to one of dwarfs.

## Main results

1. 2 subsamples kinematically representative of the thin disk and the thick disk are defined. A transition occurs at [Fe/H]=–0.3.

2. Stars more metal-rich than this value have a flat distribution with Zmax<1 kpc and W<20 km/s, and a narrow distribution of [al/Fe].

3. There exist stars which cannot belong to the thin disk because of their excentric orbits, neither to the thick disk because of their low scale height.

4. Several thin disk stars are identified down to [Fe/H]=–0.80. Their Mg enrichment is lower than thick disk stars with the same metallicity.

5. The star formation in the thick disk stopped at [Fe/H]=–0.30, [Mg/Fe]=+0.20, [Si/Fe]=+0.17.

6. A vertical gradient in [alpha/Fe] may exist in the thick disk.

7. Both dwarfs and giants show a similar trend of [alpha/Fe] and Ni abundance with [Fe/H].

## References

Baranne A., Queloz D., Mayor M., et al.: 1996, *A&AS*, **119**, 373.

Bensby T., Feltzing S., Lundstrom I.: 2003, *A&A*, **410**, 527.

Burbidge E.M., Burbidge G.R., Fower W.A., Hoyle F.: 1957, *Rev. Mod. Phys.*, **29**, 547.

Carlsson M.: 1986, *Uppsala Obs. Rep.*, **33**.

Fuhrmann K., Axer M., Gehren T.: 1995, *A&A* **301**, 492.

Galazutdinov G.A.: 1992, *Prepr. SAO RAS*, **92**, 27.

Gratton R.G., Sneden C.: 1987, *A&A*, **178**, 179.

Idiart T.P., Thévenin F.: 2000, *ApJ*, **541**, 207.

Korotin S.A., Andrievsky S.M., Luck R.E.: 1999a, *A&A*, **351**, 168.

Korotin S.A., Andrievsky S.M., Kostynchuk L.Yu.: 1999b, *Ap&SS*, **260**, 531.

Kovtyukh V.V., Soubiran C., Belik S.I., Gorlova N.I.: 2003, *A&A*, **411**, 559.

Kurucz R.L.: 1993, CD ROM n13.

Kurucz R.L.: 1992, *The Stellar Populations of Galaxies, Eds. B. Barbuy, A. Renzini, IAU Symp.*, **149**, 225.

Magain P.: 1989, *A&A*, **209**, 211.

Mishenina T.V., Kovtyukh V.V.: 2001, *A&A*, **370**, 951.

Nissen P.E., Gustafsson B., Edvardsson B., Gilmore G.: 1994, *A&A*, **285**, 440.

Prugniel P., Soubiran C.: 2001, *A&A*, **369**, 1048.

Reddy B.E., Tomkin J., Lambert D.L., Prieto C.A.: 2002, *MNRAS*, **340**, 304.

Shimanskaya N.N., Mashonkina L.I., Sakhibullin N.A.: 2000, *ARep*, **44**, 530.

Soubiran C., Katz D., Cayrel R.: 1998, *A&AS* **133**, 221.

Soubiran C., Bienaymé O., Siebert A.: 2003, *A&A*, **398**, 141.

Wallerstein G.: 1961, *ApJS*, **6**, 407.

Zhao G., Gehren T.: 2000, *A&A*, **362**, 1077.

# ON THE MEAN DENSITY OF GALAXIES AND IDENTIFICATION OF STRUCTURES

E. Panko[1], P. Flin[2]

[1] Astronomical Observatory, Nikolaev State University
Nikolskaya, 24, Nikolaev 54030 Ukraine, *tajgeta@sp.mk.ua*
[2] Institute of Physics, Pedagogical University,
Swientokrzyska, 15, Kielce, 25-406 Poland, *sfflin@cyf-kr.edu.pl*

ABSTRACT. We discuss the difficulty of detecting of galaxy structures when the Voronoi tessellation technique is applied to two dimensional data. The problem relates to the determination of the mean density of objects in an investigated field. For data originating from plates with different limiting magnitudes there are subregions with totally different galaxy densities in the different part of investigated field. As a result galaxy structures being more numerous in more populated regions. The described effect is a general one, since all wide-field optical surveys have been made from plates with different magnitude limits.

**Key words**: Galaxy clusters; data analysis – Voronoi tessellation.

## 1. Introduction

Our project is to study a large sample of galaxy structures (Panko,& Flin, 2005a) the observational basis for our work being the Münster Red Sky Survey, hereinafter MRSS (Ungruhe, 1999). The MRSS contains scans of 217 plates of adjoining fields in the ESO Southern Sky Atlas R covering more that 5000 square degrees. The resulting catalogue includes 5,524,245 galaxies, with all possible sources of systematic error having been carefully studied. The catalogue is complete down to $r_F = 18^m.3$, although in individual ESO fields the faintest recorded magnitude can reach $19^m.5$ and less. The MRSS covers almost exactly the same region of the sky as the APM, which is tied to observations in the $B$ band.

We selected the Voronoi tessellation technique (hereinafter VTT) to search for galaxy structures (Icke & van de Weygaert, 1987; Zaninetti, 1989; Ramella et al., 1999, 2001). The VTT is completely non-parametric, and therefore sensitive to both symmetric and elongated clusters, allowing robust studies of non-spherically symmetric structures.

In the two-dimensional case, which is our approach, the VTT creates polygonal cells containing one seed each and enclosing the whole area closest to its seed. This natural partitioning of space by the VTT has been used to model the large-scale distribution of galaxies.

We performed a galaxy cluster search using the VGCF (Voronoi Galaxy Cluster Finder) program developed by Ramella et al. (2001); see also Ramella et al. (1999) for a description of the automatic procedure used for galaxy cluster identification in photometric galaxy catalogues. After some experimentation we selected appropriate values needed for suitable density contrast (Panko,& Flin, 2005b)

The application of the procedure yields the following parameters: the coordinates of the centre of the overdense region, the number of galaxies in the region, the estimated number of background galaxies, and the area of the structure. We have completed the identification of structures over the entire region investigated, taking into account all galaxies in the MRSS catalogue. We catalogue only structures having at least eight galaxies. There are 16,550 such structures.

## 2. Local density variations and structures search

For computational reasons the VTT analysis was performed after dividing the complete MRSS catalogue into separate portions. Each separate portion had the seven degree extension in declination of the survey, while the breadth in right ascension varied, depending on the declination of the investigated field. The values for the extent in right ascension ranged from 21 minutes through 36 minutes, up to 1 hour. Each region contains data from several ESO plates. The particular field discussed here is presented in Fig.1 The coordinates of the centre are: $23^h.65$ and $-22^o.5$, and it contains galaxies found on four adjoining ESO plates with very different limiting magnitudes.

Fig.1 presents the relation between the galaxy num-

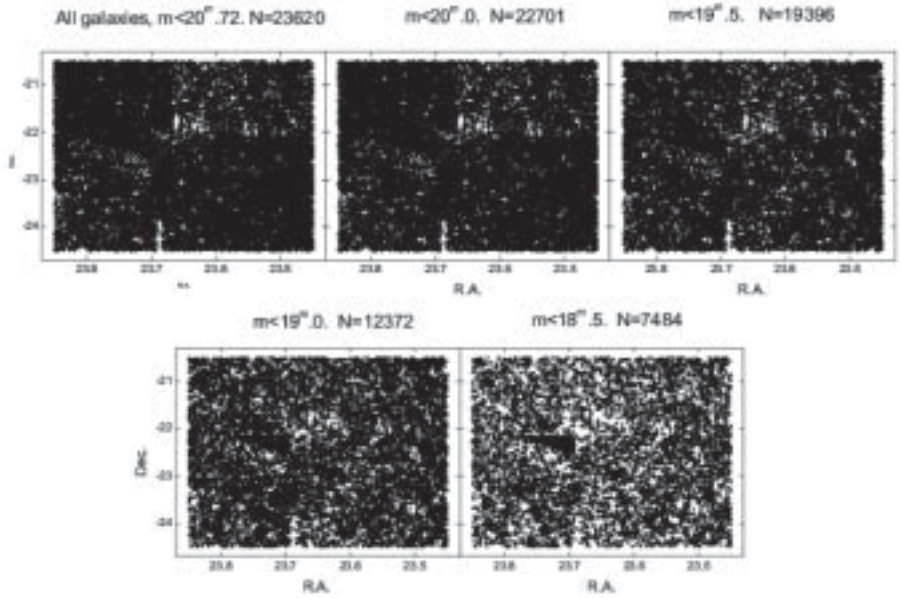


Figure 1: The variations in the local density of galaxies discussed here. In the upper part of the field the number density ratio from left and right is 1.78, 1.71, 1.23 0.95 and 0.85 respectively.

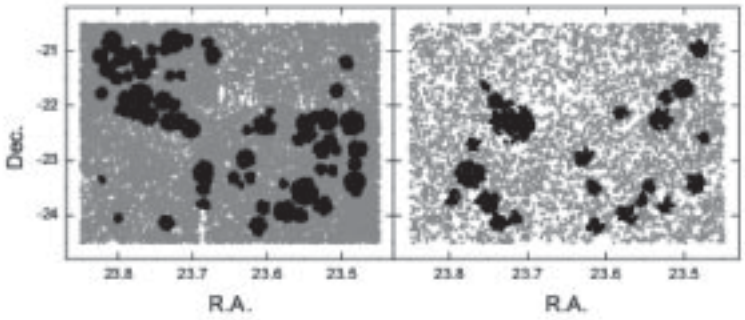


Figure 2: The galaxies which are identified as structure members (black dots). The limiting magnitude is 20.22 (left panel) and 18.5 (right panel). Background galaxies are shown as gray dots.

bers and the limiting magnitude considered. It is clearly seen that the number of objects detected on the plates is drastically different for a limiting magnitude of $20^m.22$ (Fig.1, first panel), although the plate boundaries are smoothed for a limiting magnitude of $18^m5$ (Fig.1, last panel). Note that this limiting magnitude is very close to the completeness limit of the catalogue.

The application of the VTT is very sensitive to the mean density of galaxies in the field. When the sample containing all galaxies in the region considered was investigated, we found 69 structures located as shown in Fig.2 (left panel). They are located almost exclusively in the high density regions.

We repeated the analysis for the same region using a limiting magnitude for the galaxies of $18^m.5$. In this instance we found 23 structures (Fig.2, right panel), of which only 15 had been detected previously when a fainter magnitude limit was considered.

## 3. Conclusions

It is obvious that a cluster finding algorithm involving the VTT depends strongly on the general density of galaxies. The algorithm uses the mean density of objects in the area considered. But that is a feature not only of the VTT but also of other automated techniques that are based on mean density estimation. The small differences among the various techniques are connected with the size of the area in which the background density is estimated, as well as the manner of counting background objects. Both the global and the local galaxy density are considered. Our remarks are valid for all techniques in which the galaxy density is computed.

The strange situation presented in our Fig.2 occurred where nearby regions with very different densities were joined together. Simultaneous consideration of low and high density regions yields a greater number of structures detected in more populated regions than in less numerous ones. For technical reasons it is not possible to evaluate a large section of the sky simultaneously, so it is always necessary to divide the entire analyzed region into smaller pieces. In such smaller regions it is possible to have plates with very different magnitude limits. Therefore it is safer to work only with objects lying above the statistically complete magnitude limit.

In such manner a homogeneous set of data is obtained. Please note, that in our example when the completeness limit was applied, 15 of 23 detected structures had also been detected to a fainter limiting magnitude. In the APM there are no structures in the region, which can be attributed to the dissimilar spectral coverage of the two surveys and the different technique of cluster finding.

Because of the change in mean density level in denser regions, the size of a structure (radius of the structure and its area, both measured in square arcseconds) will be smaller. The number of galaxies inside the structure will also be smaller, so that in some structures the number of galaxies drops below the level that allows them to be counted as structures (in our case eight galaxies). That introduces an inhomogeneity in the structure catalogue. In our case, we stress that the same effect occurs in all algorithms where the mean density is counted. Presumably automated cluster finding techniques do not always give indisputable results, as some believe.

## References

Icke V., van de Weygaert R.: 1987, *A&A*, **184**, 16.

Panko E., Flin P.: 2005a, in: *The Fabulous Destiny of Galaxies : Bridging Past and Present*, the proceedings of Marseille 2005 Meeting. Ed. V. le Brun, (in press).

Panko E., Flin P.: 2005b, in: *Astrophysics and Cosmology after Gamow – Theory and Observations*, the proceedings of Gamow Memorial International Conference GMIC'100. Ed. S.Silich (in press).

Panko E., Flin P.: 2006, *A&ATr.*, (in press).

Ramella M., Nonino M., Boschin W., Fadda D.: 1999, in *ASP Conf. Ser.* **176**, Observational Cosmology: The Development of Galaxy Systems, ed. G. Giuricin, M. Mezzetti, P. Salucci (San Francisco: ASP), 108.

Ramella M., Boschin W., Fadda D., Nonino M.: 2001, *A&A*, **368**, 776.

Ungruhe R.: 1999, *Ph.D. Thesis*, Astron. Institute Univ. Münster, Germany. (MRSS).

Zaninetti L.: 1989, *A&A*, **224**, 345.

# STARS WITH VIGOROUS CONVECTION ENVELOPES AND RESULTS ON GENERAL MAGNETIC FIELD OBSERVATIONS

S.I. Plachinda

Crimean Astrophysical Observatory, Nauchny, Crimea 98409 Ukraine,
*plach@crao.crimea.ua*

ABSTRACT. Existence of the GMF on convective stars with vigorous convective envelopes confirms a conclusion that the GMF is a real phenomenon and reflects properties of a stationary global magnetic field, Origin Magnetic Field, of the Sun', convective star', radiative interior onto its surface. The presence of a variability of the longitudinal magnetic field measurements on $\epsilon$ Gem throughout the night is suspected.

**Key words**: stars: atmospheres, convection, activity; magnetic field

| Computed result | Actual observation |
|---|---|
| $9.^y5$ | $\sim 9.^y5 \div 10.^y5$ |
| $13.^d62$ | $13.^d62$ |
| $9.^d02$ | $9.^d03$ |
| $27.^d42$ | $27.^d42$ |
| $27.^d70$ | $27.^d72$ |
| $28.^d14$ | $28.^d14$ |

Table 1: Actual and computed periods for GMF of the Sun as a star

## 1. Introduction

The first results of the General Magnetic Field (GMF) measurements of the Sun as a star were published by A. Severny (1969). The value of the GMF of the Sun as a Star (GMFSS) varies with the period of sunspots cycle: maximal solar activity - maximal GMF amplitude; minimal solar activity - minimal GMF amplitude (Kotov et al., 1998). This picture represents, to first order, beating of two main neighbour frequencies, 1/26.93 and 1/27.14 (Plachinda, 2004b), which are produced by differential rotation of latitude belts with most contribution to the registered signal (equatorial and active region areas of the Sun). Using these frequencies one can calculate main prominent periods in the power spectrum for GMF of the Sun as a star including period of activity cycle (Table 1). One of the initial periods is due to a rigid rotation of radiative zone, and the second one is produced by differential rotation. Hence, Origin Magnetic Field of the Sun radiative zone is captured by moving matter of the convective zone and transported to the surface, where beating of two main frequencies produces observing picture. What mechanism of macro-organizing of the magnetic fields which are captured by moving matter and transported to the surface? Such possibility give us the law of parameter correlations of self-organizing structures of the open thermodynamic system: "In the thermodynamics of open systems, a star as a whole is a dissipative system of the greatest scale, in which global magnetic fields are self-organized due to the energy of rotation and convective motions, while dissipative systems are realized in small-scale structures due to the energy of the carrier of the deficit of photospheric radiation resulting in stellar flares and other local phenomena. Probably, this general synergetic approach will give a key to understanding the various manifestations of the solar-type activity on main-sequence stars." (Gershberg, 2005).

## 2. Observations

The program of systematic measurements of GMF on slowly rotating stars with convective envelopes was initiated at Crimea in 1989. The observations and data reduction were carried out using 2.6m Shajn telescope, Stokesmeter, coude spectrograph and "'Flip-Flop"' Zeeman Measurements Technique (Plachinda and Tarasova, 1999; Plachinda, 2004a).

In terms of Babcock' and Leighton' phenomenological magneto-kinematic model of the solar cycle and in terms of standard $\alpha$-$\Omega$ dynamo theory, there are only two main components of large-scale magnetic field on the Sun: toroidal magnetic field and axisymmetric poloidal field. Both toroidal (strong) and poloidal (weak) fields change its polarity with a period of $\sim$22 ys. Toroidal magnetic field lies in the base of the convective zone and manifests itself when magnetic loops emerge on the surface in bipolar active regions, reaching peak values during maximum of spot activity. The axisymmetric poloidal field lies under the photosphere

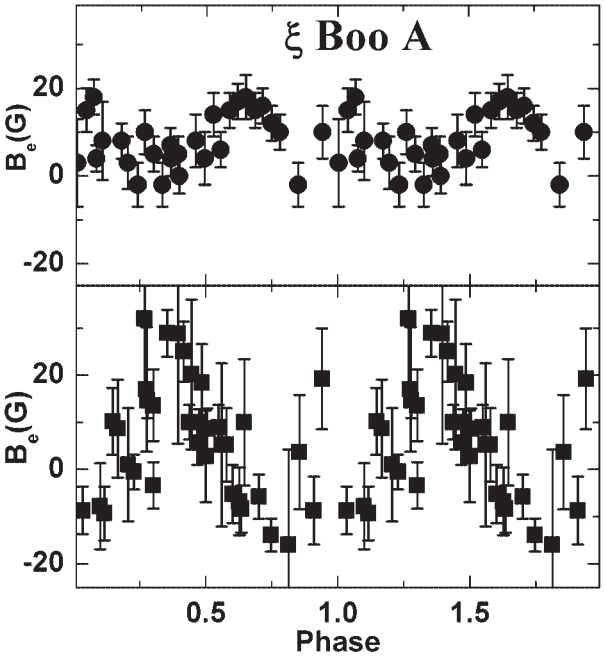


Figure 1: GMF of the $\xi$ *Boo A*

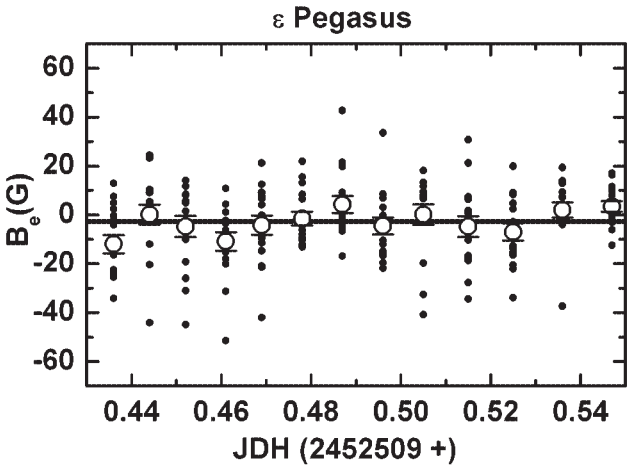


Figure 2: $\epsilon$ *Peg:* the example of absence of the significance discrepancy between different longitudinal magnetic field measurements throughout the night. The solid straight line represents magnetic field mean value $B_e$ = -2.7 G.

and changes its polarity with a period of ~22 yr as well, but reaching peak values of about 1-2 G on rotation poles during minimum of spot activity. It is believed today that the underlying cause of the solar activity cycle is the interplay between poloidal magnetic field, differential rotation, and convection that is illustrated by the most developed Babcock' and Leighton' phenomenological model of the solar cycle. According to aforesaid, what is the origin of the GMF?

Today, the presence of weak general magnetic field (up to some dozen Gausses) for 21 convective stars (F9-M3 spectral types and I-V luminosity classes) is detected (Plachinda, 2004a; Plachinda, 2005). For two solar-like stars variations of the GMF as a function of the stellar rotation has been determined: for more active and more young star than the Sun $\xi$ Boo A (G8 V) with $P_{rot}$ = 6.198 d, and for old solar-like star 61 Cyg A (K5 V) with $P_{rot}$ = 36.617 d. For $\xi$ Boo A GMF variations as a function of rotational period was confirmed using MuSiCoS and Stokesmeter by Petit et al. (2005) (see Figure 1, where GMF variations are shown as a function of rotational period: first panel - Stokesmeter, MuSiCoS, Pic du Midi, 2003; second panel - Stokesmeter, Crimea, 1990; 1998-1999 and Multislit magnetometer observations (Brown and Landstreet, 1981; Borra et al., 1984). The bottom curve shows domination of the dipole component contrary to the top curve for 2003 year, which demonstrates the presence of quadrupole component. Analogue behaviour of the GMF on the Sun is present.

Owing to properties of GMFSS (Plachinda and Tarasova, 2000), especially because there is a balance of positive and negative magnetic fluxes, $\Phi_+/\Phi_- = 0.99$, in agreement with Maxwell equation $\vec{\nabla} \bullet \vec{B} = 0$, we suppose that the GMF is real nonaxisymmetric large-scale field on the Sun as on other convective stars.

The radius of stars increases as they evolve out of the main sequence. For convective giants the radii are tens of times the sun's radius and for convective supergiants hundreds of times. In the case of a dipole configuration when the star size increases the field can be decrease as the cube. In the convective giant stage the GMF as the global magnetic field of the radiative zone of a star will be reduced by a factor of $10^3 - 10^5$. In the case of supergiants, this coefficient will be even larger, $10^5 - 10^7$. If a giant is an evolved sun-like dwarf then the global field of the radiative zone beneath of the tachocline of the star would be less than a tenth of a Gauss and undetectable. In this case, as in the case of supergiants, we can suppose that the detected field on the stars surface is probably the product of the operation of dynamo mechanisms. On the other hand, if a giant is an evolved magnetic star with a high initial magnetic field at the poles ($10^4$ G) then its global field in the radiative core may reach tens of Gauss and can be detectable. In the case of supergiants the magnitude of the field of the former magnetic star in the radiative core is a small fraction of a Gauss and will be undetectable. Therefore, in most cases, the fields which have been detected on giants and supergiants is probably the product of the operation of dynamo mechanisms.

Figure 2 and Figure 3 for $\epsilon$ Peg and $\epsilon$ Gem illustrate of both the absence and presence of a variability of the longitudinal magnetic field throughout the night. In this case of $\epsilon$ Gem, probably, the process of emergence

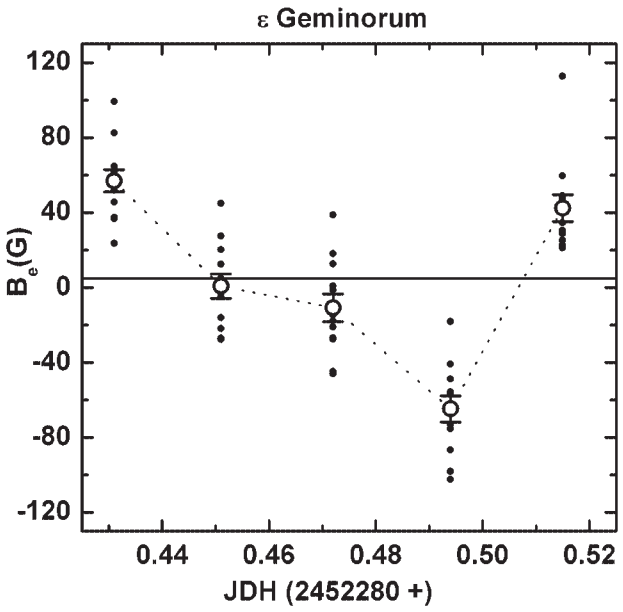


Figure 3: $\epsilon$ *Gem:* the significance discrepancy between different longitudinal magnetic field measurements throughout the night. The solid straight line represents magnetic field mean value $B_e = 4.9$ G.

of active region on the surface was registered as it was detected for 61 Cyg A (Plachinda, 2004b).

Existence of the GMF on convective stars with vigorous convective envelopes confirms a hypothesis that the GMF is a real phenomenon and reflects properties of a stationary global magnetic field, Origin Magnetic Field, of the Sun', convective star', radiative interior onto its surface.

*Acknowledgements.* The author is thankful to Roald Gershberg for helpful discussion.

### References

Borra E.F., Edwards G., & Mayor M.: 1984, *Astrophys. J.*, **284**, 211.

Brown D.N., & Landstreet J.D.: 1981, *Astrophys. J.*, **246**, 899.

Gershberg R.E.: 2005, *"Solar-type Activity in Main-Sequence Stars"*, Springer, p. 431.

Kotov V.A., Scherrer P.H., Howard R.F., Haneychuk V.I.: 1998, *Astrophys. J. Suppl. Ser.*, **116**, 103.

Petit P., Donati J.-F., Auriere M., Landstreet J.D., Lignieres F., Marsden S., Mouillet D., Paletou F., Toque, N., Wade G.A.: 2005, *MNRAS*, **361**, 837.

Plachinda S.I.: 2005, *Astrophysics*, **48**, 9.

Plachinda S.I.: 2004a, *NATO Science Series*, **161**, 351.

Plachinda S.I.: 2004b. In: *"Multi-Wavelength Investigations of Solar Activity"*. IAU Symposium **223**, 689.

Plachinda S.I. & Tarasova T.N.: 1999, *Astrophys. J.*, **514**, 402.

Plachinda S.I. & Tarasova T.N.: 2000, *Astrophys. J.*, **533**, 1016.

Severny A.B.: 1969, *Nature*, **224**, 53.

# THE ORIGIN OF BRIGHTNESS VARIATIONS IN BC CYGNI

M. Rohanidazegan[1], D. G. Turner[1], E. N. Pastukhova[2], L. N. Berdnikov[2]

[1] Department of Astronomy and Physics, Saint Mary's University
Halifax, Nova Scotia B3H 3C3, Canada, *mrohani@ap.smu.ca, turner@ap.smu.ca*

[2] Sternberg Astronomical Institute, 13 Universitetkij Prosp.
Moscow 119899, Russia, *lberdnikov@yandex.ru*

ABSTRACT. The variability of the type C semi-regular (SRC) M3.5 Ia supergiant variable BC Cyg is examined with reference to measurements of its photographic $B$ magnitude derived from 866 archival plates in the Harvard and Sternberg collections and eye estimates of its visual $V$ magnitude made by members of the AAVSO. The star is the brightest member of the cluster Berkeley 87, so it has a well established reddening, distance, and age. BC Cyg exhibits interesting features in its century-long baseline of brightness variations that relate to pulsation and evolution: an $0^m.5$ increase in $\langle B \rangle$ over the past century in conjunction with a decrease in pulsation period from $\sim 700^d$ to $687^d$. Associated colour changes imply that the star is hottest when brightest visually or photographically, coolest when faintest visually or photographically. Despite the increase in $\langle B \rangle$, the star's luminosity appears to have decreased over the past century, presumably as a result of stellar evolutionary effects.

**Key words**: stars: variable: other — stars: late-type — stars: individual (BC Cyg).

## 1. Background

Type C semi-regular variables (SRC) constitute a group of 55 stars in the *General Catalogue of Variable Stars* (Kholopov et al. 1985) that, in contrast to the SRA and SRB variables, include some of the most massive and exotic stars in the Milky Way, all having reached the red supergiant stage of evolution. A prime example is Betelgeuse ($\alpha$ Ori, spectral type M1-2 Ia-Ibe), its light variations having been followed since the early 1800s. The origin of the variability in such stars is not fully understood, although pulsation and rotation of bright or dark regions across the visible hemisphere are believed to play an important role.

The SRC variable BC Cygni is an M3.5 Ia supergiant displaying moderate amplitude variability that is located near the edge of the young cluster Berkeley 87 lying in a heavily-obscured region of Cygnus (Turner & Forbes 1982). Because of its likely cluster membership, the age ($8 \times 10^6$ years), original mass ($\geq 20\ M_\odot$), space reddening ($E_{B-V}(\mathrm{B0}) = 1.55 \pm 0.01$), and distance (1.1 kpc) of BC Cyg are known reasonably well.

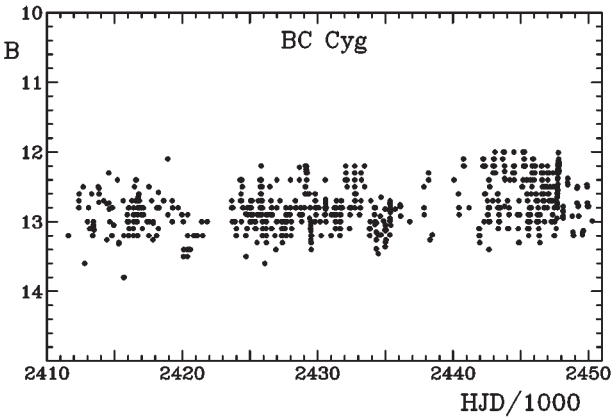


Figure 1: Combined eye estimates of photographic magnitude $B$ for BC Cyg from plates in the Harvard and Sternberg collections.

A major obstacle to a full understanding of the physical mechanism(s) responsible for light variations in SRC variables is a lack of extensive temporal data on their brightness changes, which tend to be semi-repeatable with long-term excursions in average brightness over time scales of several hundreds of days or more. We have collected a large database of brightness estimates for BC Cyg that provides some clues on what may be responsible for its variability.

## 2. Observations

An extensive set of brightness data for BC Cyg was constructed using eye estimates of its photographic $B$ magnitude relative to a reference sequence of stars in Berkeley 87, as obtained from 688 patrol series plates in the Harvard College Observatory Photographic Plate Collection as well as from 178 plates in the collection of the Sternberg Institute. Visual observations are also available (Waagen 2005) from recent estimates by ob-

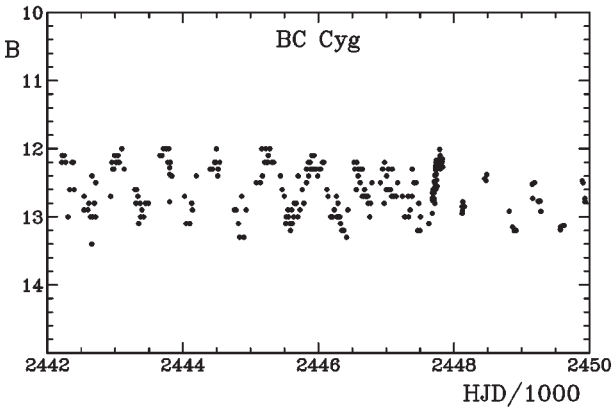


Figure 2: A smaller time segment of the data plotted in Fig. 1 illustrating the regular cyclical variations in BC Cyg.

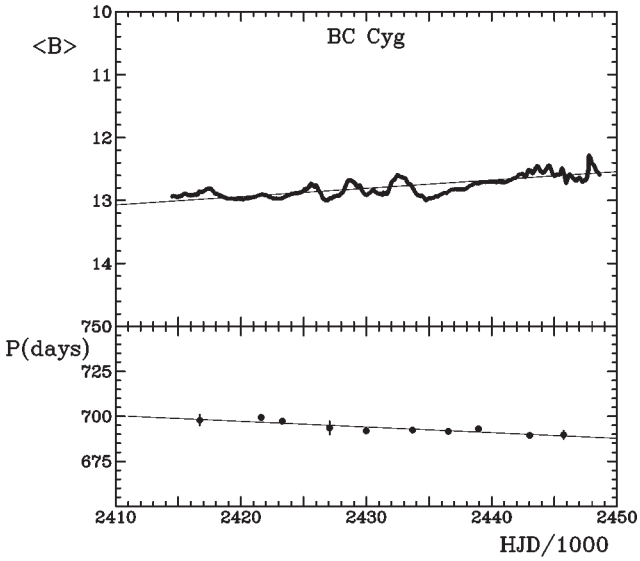


Figure 3: a) A plot of 50-point mean $\langle B \rangle$ magnitudes for BC Cyg from the data of Fig. 1 (top); b) estimates for the pulsation period of the star over restricted time intervals covering the same temporal interval (lower).

servers belonging to the American Association of Variable Star Observers (AAVSO).

The $B$ data are illustrated in Fig. 1, all adjusted to the Harvard system. The regular cyclical nature of the star's brightness changes is more apparent when the data are restricted to less extensive time intervals, as in Fig. 2.

### 3. Analysis

An interesting feature of the light variations in BC Cyg, illustrated in Fig. 3, is their long-term behaviour. The mean $\langle B \rangle$ magnitude of BC Cyg has increased by $\sim 0^{\rm m}.5$ over the past century (Fig. 3a), while the primary period of variability for the star has decreased monotonically over the same time interval (Fig. 3b), from $P = 700^{\rm d}$ in 1900 to $P = 687^{\rm d}$ at present, a rate of decrease of $3^{\rm h}$ per year.

From AAVSO visual eye estimates, which appear to be reasonably close to Johnson system $V$ magnitudes, it is possible to track changes in the colour of BC Cyg as it brightens and fades, as illustrated in Fig. 4. The analysis requires a combination of visual eye estimates with photographic magnitudes estimated from survey plates, both of which are subject to uncertainties of about $\pm 0^{\rm m}.1$ to $\pm 0^{\rm m}.2$. To the extent that the 66 data points selected to be nearly coincident in time represent the general trend when averaged, as in Fig. 4, it appears that the star gets redder as it gets fainter, bluer as it brightens. The implication is that BC Cyg is hottest when it is brightest photographically, coolest when it is faintest photographically.

We have used the above information in conjunction with the star's known space reddening and distance to track the periodic changes observed for the star in an H-R diagram. The conversion of $B$ and $V$ magnitudes and colours into $T_{\rm eff}$ and $\log L/L_{\odot}$ depends directly on the effective temperatures and bolometric corrections adopted for M supergiants. The present calculations rely upon the parameters tabulated by Lee (1970).

In the H-R diagram of Fig. 5, dotted lines lines indicate the location of the Cepheid instability strip, while solid relations represent theoretical stellar evolutionary tracks for stars with original masses of 5 $M_{\odot}$, 10 $M_{\odot}$, and 25 $M_{\odot}$ and $Z = 0.01$. The parameters for BC Cyg in 1900 at light maximum, light minimum, and mean light are shown by filled circles, those for 2000 by open circles. Over the past century it appears that BC Cygni has evolved downwards along the red supergiant branch towards lower luminosities, as confirmed by its gradually decreasing pulsation period (Fig. 3b), which is presumably tied to a diminishing mean radius.

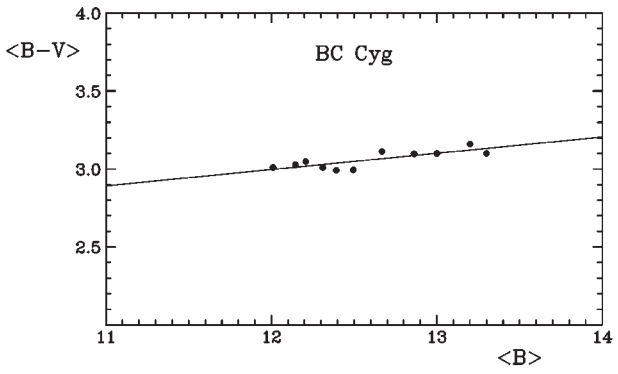


Figure 4: The observed colours of BC Cyg as a function of the star's photographic magnitude as derived from averages of AAVSO visual estimates with photographic estimates of the star made within roughly ten days of each other.

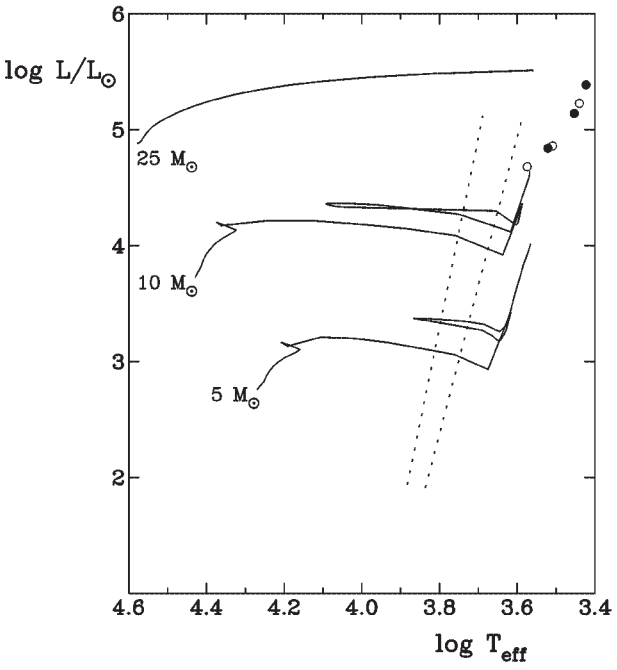


Figure 5: A theoretical H-R diagram showing evolutionary tracks for stars of 5 $M_\odot$, 10 $M_\odot$, and 25 $M_\odot$ and $Z = 0.01$, the region of the Cepheid instability strip (dotted lines), and the estimated parameters of BC Cyg over its pulsation cycle around 1900 (filled circles) and 2000 (open circles).

Although the mean $B$ magnitude of BC Cyg increased over the past century, its bolometric luminosity actually decreased according to the adopted bolometric corrections and effective temperatures inferred from mean $B$-$V$ colours. Such features require independent confirmation. Existing stellar evolutionary models cannot replicate the observed changes in the star's parameters, according to the results of Fig. 5.

The regular periodic nature of the star's brightness variations is clearly tied to pulsation, as evident from the fact that BC Cyg, as well as SRC variables in Per OB1, follow a period-luminosity relation similar to that of Cepheids (Turner 2005).

## 4. Discussion

The photographic magnitude of BC Cyg increased by $\sim 0^{\rm m}.5$ over the past century, but the star's bolometric luminosity apparently decreased by about the same amount over that interval, if the observed colour changes are accurate. The luminosity decline has been associated with an increase in the star's effective temperature and a decrease in mean radius, as evidenced by a period decrease for its $700^{\rm d}$ pulsations. If the associated colour changes and assigned bolometric corrections are correct, the star is most luminous when it is faintest visually and photographically.

As recognized roughly fifty years ago by Struve (1959), "It appears that studies of period change are by far the most sensitive test available to the astronomer for detecting minute alterations in the physical characteristics of a star." That has been demonstrated previously to be true for Cepheid variables, which are yellow supergiants, but it also applies to the red supergiant variables belonging to the SRC class.

The primary brightness variations in BC Cyg display the regularity of pulsation, which was tested using simple models for the interior of the supergiant in conjunction with adiabatic pulsation calculations. The same technique was followed by Stothers (1969) in his modeling of M supergiants 36 years ago, under the assumption that the complex superadiabatic region near the surfaces of such stars is essentially insignificant relative to the adiabatic interior. The short-term cyclical variations in all SRC variables are similarly implicated to arise from pulsation. The longer-term brightness changes in BC Cyg, on the other hand, may be tied to evolutionary changes in the star.

BC Cygni is an important SRC variable since its cluster membership provides basic information about its reddening, luminosity, and evolutionary mass. The collection of a century-long baseline of data on its brightness variations provides a wealth of material for analyzing the nature of the star's variability. It is clearly useful to obtain similar information for other SRC variables if we are to understand in detail the mechanisms responsible for the full range of their light variations as well as to track their exact behaviour in the astrophysical H-R diagram.

*Acknowledgements.* We acknowledge with thanks the variable star observations from the AAVSO International Database contributed by observers worldwide and used in this research.

## References

Kholopov, P.N., et al.: 1985, *General Catalogue of Variable Stars*, 4th Edition (Moscow: Nauka).
Lee, T.A.: 1970, *ApJ*, **162**, 217.
Stothers, R.: 1969, *ApJ*, **156**, 541.
Struve, O.: 1959, *Sky & Telescope*, **18**, 309.
Turner, D.G.: 2005, *Odessa Astron.Publ.*, **18**, this conference.
Turner, D.G., Forbes, D.: 1982, *PASP*,**94**, 789.
Waagen, E.O.: 2005, Observations from the AAVSO International Database, private communication.

# MONITORING OF SPECTRAL VARIATIONS OF MIRA-TYPE AND SEMIREGULAR VARIABLE STARS

G.M. Rudnitskij

Sternberg Astronomical Institute, Moscow State University
13 Universitetskij prospekt, Moscow, 119992 Russia, *gmr@sai.msu.ru*

ABSTRACT. The results of monitoring of a sample of late-type variable stars (Mira Ceti-type and semiregulars) are reported. Since 1980 a sample of 60 stars has been observed in the maser line of the $H_2O$ molecule at a wavelength of 1.35 cm. These observations are performed on the RT-22 radio telescope of the Pushchino Radio Astronomy Observatory (Moscow Region). Since 1994 optical spectra of some of these stars have also been monitored on the 1.25-meter telescope of the Crimean Laboratory of the Sternberg Astronomical Institute. Regularities in the spectral behavior of the stars are discussed. Variations of the circumstellar $H_2O$ masers correlate with the visual light curves (AFOEV and AAVSO data) with a time lag of 0.3–0.4$P$ ($P$ is the star's period). Flares of the H$\alpha$ emission noted in R Leo, U Aur, R Cas, and R LMi were followed 1.5–2 years later by corresponding flares of the $H_2O$ masers. These phenomena are interpreted as a consequence of propagation of a shock wave driven by stellar pulsation. Alternatively, the shock can be produced by motion of a low-mass satellite (a planet or a brown dwarf) in the inner layer of the circumstellar envelope. The effects of such a satellite on the spectrum and light curve of the primary star are discussed.

**Key words**: Stars: AGB and post-AGB; variables: others; masers; radio lines: stars; stars: individual: U Aur, S CrB.

## 1. Introduction

Long-period variable (LPV) stars are of great interest, since they represent the final stage in the evolution of solar-type stars. They represent one of the most numerous group among variable stars (several thousands, according to the latest surveys, e.g., NSVS[1]). Their periods (or light cycles) $P$ range from $\sim 100^d$ to $\sim 600^d$. At the LPV stage the stars actively lose mass at a rate of $\sim 10^{-7}$–$10^{-5} M_\odot$/year. The lost material forms extended circumstellar gas–dust envelopes hosting molecular maser radio sources. Several hundred LPVs are known to be sources of maser radio emission in molecular lines (OH, $H_2O$, SiO). This emission is highly time-variable, especially in the $6_{16}$–$5_{23}$ $H_2O$ rotational line at $\lambda = 1.35$ cm. To understand the nature of the $H_2O$ maser variability, our team has begun monitoring of a sample of LPVs in the $H_2O$ line and optical spectrum. Periodic appearance of optical emission lines may suggest the presence of shock waves, which determine the LPV photometric and spectral variations. To connect the LPV variations in the optical and microwave ranges, we have undertaken long-term multiwavelength monitoring of sample of stars that includes several tens of Mira-type and semiregular variables. Here I report some results of this monitoring together with a model explaining particulars of LPV behavior.

## 2. Observations

Radio observations in the $H_2O$ line at $\lambda = 1.35$ cm have been performed since 1980 on the 22-meter radio telescope at Pushchino Radio Astronomy Observatory (Astro Space Center of the Lebedev Institute of Physics, Russian Academy of Sciences) jointly with PRAO colleagues. We use a 1.35-cm wavelength receiver with a helium-cooled FET amplifier and a 128-channel filter-bank spectrometer with a resolution of 0.1 km/s. Since December 2005 we also use for spectral analysis of the signal a 2048-channel autocorrelator with a total bandwidth of 12.5 km/s and velocity resolution of 0.082 km/s. Intervals between consecutive observing sessions normally do not exceed 1–2 months.

Since 1994, our team has been monitoring a sample of about 30 Miras in the H$\alpha$ line, see Esipov et al. (1999) and references therein. For optical spectroscopy, we use a diffraction spectrograph with a maximum resolution of 0.25 Å/pixel. An echellé spectrograph with a resolving power of 10,000 has been tested. The spectra are recorded with ST-6 and ST-8 Santa Barbara Instruments Group[2] CCD cameras (Table 1). This instrumentation is in operation on the 125-cm telescope

[1] http://skydot.lanl.gov/nsvs/red_variables.php

[2] http://www.sbig.com/

at the Crimean Laboratory of the Sternberg Astronomical Institute.

Table 1: CCD cameras utilized in the observations

| Camera | $\lambda\lambda$, Å | $\Delta\lambda$, Å |
|---|---|---|
| ST-6I | 4000–11,000 | |
| 600 lines per mm | 5700–7700 | 5 or 2.5 |
| 1200 lines per mm | 6000–7000 | 2.5 or 1.25 |
| ST-6V | 4000–11,000 | –"– |
| ST-8 | | |
| 1200 lines per mm | 6300–6700 | 0.25 |

In the radio continuum, we have observed a sample of 34 Miras and semiregular variables at $\lambda = 6$ and 3 cm on the Australia Telescope Compact Array in Narrabri (Chapman & Rudnitskij 1998). Our sample included mostly southern Miras and semiregulars as well as some well-known objects in common with our $H_2O$/H$\alpha$ sample ($o$ Cet, U Ori, W Hya, R Aql). However, the result was negative: only upper limits on the flux density were determined, from 0.1 to 0.4 mJy.

## 3. Results

Figures 1, 2 illustrate the behaviour of U Aur and S CrB in the visual light, H$\alpha$, and $H_2O$ lines. The effect we observe is typical for many stars of the sample. The curve of the integrated $H_2O$ line flux follows the visual light curve with some phase delay $\Delta\varphi \sim 0.3$–$0.4P$, where $P$ is the stellar period. However, maximum visual–$H_2O$ correlation may have place not promptly, within the same light cycle, but several periods later, as we have found in RS Vir (Lekht et al. 2001).

We have traced the evolution of the H$\alpha$ emission in about 30 stars (R Aql, R Leo, R Cas, U Her, $\chi$ Cyg, and others, Table 2). The appearance of the emission is not regular, not all light cycles are accompanied by it. The emission flared at different light phases $\varphi$ of the stars, from minimum to maximum, although phases $\varphi \sim 0.4$–$0.5$ seem to be preferred. Some stars showed rather erratic behaviour of the H$\alpha$ emission. Some others, during our monitoring interval, displayed isolated bursts of the H$\alpha$ emission, followed (about a year and a half later) by a flare of the $H_2O$ maser radio emission. These stars are R Leo (see Esipov et al. 1999 for details), R Cas, and U Aur. We have been tracing their $H_2O$ maser history since early 1980s (Berulis et al. 1983), when they were rather strong $H_2O$ emitters, but soon faded and remained silent in the $H_2O$ line until 1997–1998. Then the probably shock-stimulated flares happened, see model by Rudnitskij & Chuprikov (1990). Interpreting this in the framework of our model (see Section 4), this may be a periastron episode of a planet in a highly eccentric orbit with a period $P \sim 15$ years.

Table 2: Long-period variables monitored in 1994–2005 in the $H_2O$ and H$\alpha$ emission lines

| Name | Type | $P$, d | $H_2O$ | Notes |
|---|---|---|---|---|
| R Aql | M | 284 | + | $H_2O^a$ |
| RR Aql | M | 395 | + | $H_2O^b$ |
| U Aur | M | 408 | + | |
| RX Boo | SRb | 340 | + | $H_2O^a$ |
| R Cnc | M | 362 | – | |
| R Cas | M | 430 | + | $H_2O^c$ |
| T Cas | M | 445 | – | |
| Y Cas | M | 413 | + | $H_2O^l$ |
| $o$ Cet | M | 332 | – | |
| S CrB | M | 360 | + | |
| V CrB | M | 358 | – | C star |
| R Crt | SRb | 160 | + | $H_2O^a$ |
| S Crt | SRb | 155 | + | $H_2O^a$ |
| W Cyg | SRb | 131 | – | |
| $\chi$ Cyg | M | 408 | – | S star |
| RY Dra | SRb | 331 | – | C star |
| T Dra | M | 422 | – | C star |
| RU Her | M | 485 | – | |
| T Her | M | 165 | – | |
| U Her | M | 406 | + | $H_2O^{a,d}$ |
| W Hya | SRa | 361 | + | $H_2O^{a,e}$ |
| R Leo | M | 310 | + | $H_2O^{f,g}$ |
| R LMi | M | 372 | + | |
| RW LMi | SRa | 640 | – | C star |
| U Ori | M | 368 | + | $H_2O^{a,h}$ |
| R Peg | M | 378 | + | |
| S Per | SRc | 822 | + | $H_2O^m$ |
| VX Sgr | SRc | 732 | + | $H_2O^n$ |
| R Tri | M | 267 | + | |
| RS Vir | M | 354 | + | $H_2O^i$ |
| RT Vir | SRb | 155 | + | $H_2O^{a,k}$ |
| R UMa | M | 302 | – | |

*References to our observations in the $H_2O$ line:*
[a]Berulis et al. (1983); [b]Berulis et al. (1998);
[c]Pashchenko & Rudnitskij (2004);
[d]Kudashkina & Rudnitskij (1988);
[e]Rudnitskij et al. (1999); [f]Rudnitskij (1987);
[g]Esipov et al. (1999); [h]Rudnitskij et al. (2000);
[i]Lekht et al. (2001); [k]Lekht et al. (1999);
[l]Rudnitskij & Pashchenko (2005);
[m]Lekht et al. (2005);
[n]Rudnitskij & Pashchenko (1999).

As for the radio continuum survey, we hoped to find, in addition to the visual–$H_2O$ and H$\alpha$–$H_2O$ correlations, a radio continuum–$H_2O$ correlation: the increases in the $H_2O$ maser flux were supposed to be due to amplification of the varying underlying stellar continuum. The H$\alpha$–radio continuum correlation could also be of interest. The result was negative. The only star we could detect in the centimeter-wave radio continuum was the symbiotic Mira R Aqr, which is a well-known radio source (Dougherty et al. 1995 and references therein). The system R Aqr consists of a Mira variable with $P = 387^{\rm d}$ and presumably a white dwarf in an eccentric orbit with $P_{\rm orb} = 44$ years. Our result (integrated flux $S(6\ {\rm cm}) = 17.2$ mJy,

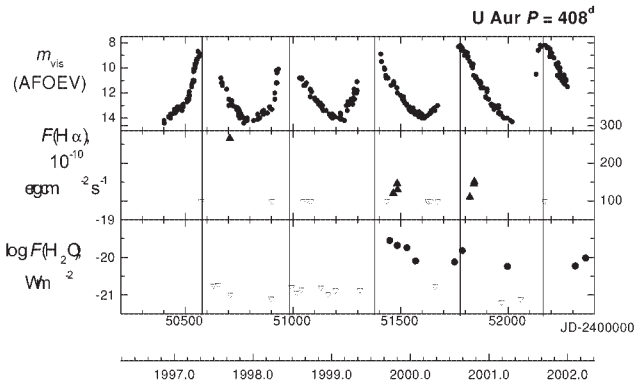


Figure 1: The data for the Mira variable U Aur: (a) visual light curve (AFOEV), (b) absolute flux in the H$\alpha$ emission line, (c) integrated flux in the $H_2O$ radio line.

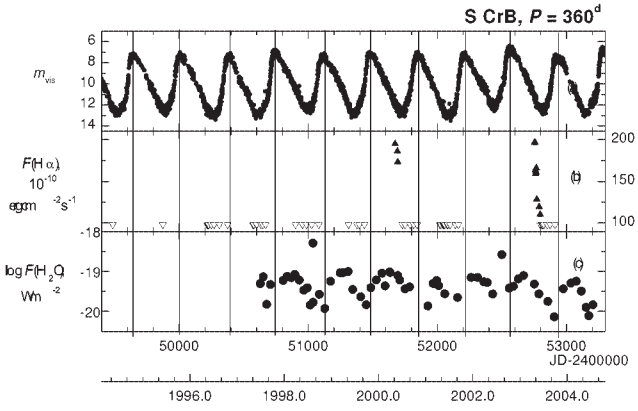


Figure 2: Same as in Fig. 1, but for the Mira variable S CrB.

$S(3\text{ cm}) = 15.9$ mJy) is quite consistent with the MERLIN result of Dougherty et al. (1995), 16 mJy at $\lambda = 6$ cm. This emission is produced by the common nebular envelope of the system R Aqr, its flat spectrum is consistent with that of an optically thin plasma cloud and is not related to the photosphere of the Mira component. The main conclusion of this experiment is that radio continuum from Miras is much weaker than expected for a postshock layer of ionized gas at shock velocity 15–20 km/s (required to produce strong H$\alpha$ emission). One possible explanation is the presence of a slightly ionized "radio photosphere" (Reid & Menten 1997) that absorbs the radio continuum but lets out the optical emission freely.

### 4. The model for the observed variations

It is usually assumed that light variations of Mira-type stars are due to stellar pulsations. The pulsations produce strong shocks that ionize the stellar atmospheric gas thus exciting optical emission lines. However, our observations as well as those of other authors (e.g., Knapp et al. 1995, Reid & Menten 1997) have not detected strong radio continuum that would necessarily accompany the optical emission. One explanation is the "radio photosphere" of Reid & Menten (1997).

I propose an alternative hypothesis, which was initially published in the reports of Rudnitskij (2000, 2002). A similar idea was put forward independently by Berlioz-Arthaud (2003). Details can be found also on the Russian-language Astronet Web page (Rudnitskij 2005). The hypothesis explains the behavior of the optical emission lines across a Mira cycle and, probably, the photometric variability.

It is supposed that the optical line emission originates in a local source at the surface of the Mira atmosphere. This source can be a fireball around a nearby companion—a planet or a brown dwarf revolving in an orbit just outside the atmosphere, at a distance of about 1 AU from the stellar center. Its orbital velocity ($\sim 30$ km/s for the central mass $\sim 1M_\odot$) is highly supersonic. Estimates show (Rudnitskij 2002) that the conical shock around and behind the companion emits enough H$\alpha$ quanta to account for the observed line fluxes shown in Figures 1 and 2. Moreover, the total brightness variations of a Mira can explained to a considerable extent by the "fireball" effect. Figure 3 shows the location of the companion's orbit with respect to the star and to the sky plane. Figure 4 presents model light curves due to the fireball radiation. At the right the projection of the orbit onto the sky plane is shown together with the assumed star and orbit parameters (asterisks mark the periastron). The amplitude of the model light curve in the $V$ band can reach $2^m$, which may be adequate for "regular" semiregulars (such as the quasi-periodic SRc star W Hya), but is somewhat low for Miras with visual amplitudes $\Delta m > 2.5^m$. However, this simplified model so far does not take into account secondary effects such as hard radiation of the shock, which reduces opacity around the fireball, thus uncovers deeper atmospheric layers and adds to the brightness variation. Another effect can be tidal excitation of nonradial pulsations by the motion of the companion in the atmosphere. These effects are to be considered in forthcoming publications. Finally, the trailing shock from the fireball reaches the masering region in the circumstellar envelope and causes an increase in the $H_2O$ maser line flux.

The model describes well by purely geometrical effects any shape of the star's light curve. This is achieved by fitting several parameters (stellar mass $M_*$, stellar radius $R_*$, orbit inclination to the sky plane $i$, periastron longitude $\omega$, semimajor axis $a$, eccentricity $e$). Especially interesting light curves are obtained in the case of eccentric orbits—asymmetry, bumps on the ascending/descending branches, and even double maxima (see Fig. 3), as observed, e.g., in the classical Miras R Cen and R Nor.

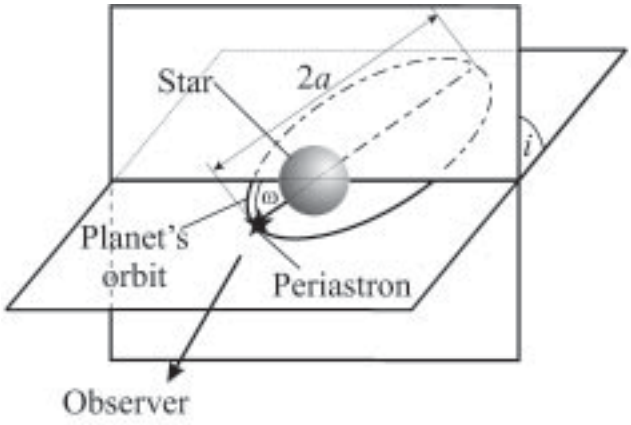


Figure 3: Parameters of the planetary orbit: $2a$ is the major axis, $\omega$ is the periastron longitude, $i$ is the angle of inclination to the sky plane.

Irregularities in the brightness variation, which are rather typical in Miras (retarded or advanced maxima as compared to the mean light elements, different heights of the maxima), can be due to a superposition of a chaotic light-curve component. The Miras' light curves are known to consist of two addenda, regular and chaotic (Whitney 1984, Klyus 1988, Cannizzo et al. 1990). The latter component arises from intrinsic (rather erratic) stellar pulsation, whereas the regular component is imposed by the companion's orbital motion. In this hypothesis semiregular variables possess only this chaos; they have no companion in a suitable orbit to maintain the regular Mira-type variation.

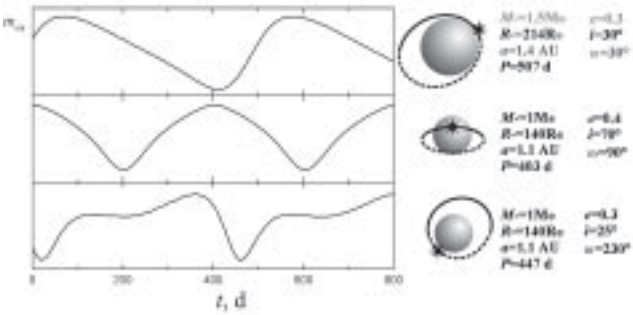


Figure 4: Model light curves for different parameters of the companion's orbit (see text).

Interestingly, the model explains also the period–luminosity dependence for Miras. Many versions of this relationship can be found in the literature, beginning from the classical paper of Clayton & Feast (1969), who gave this dependence in a tabular form ($P$ *versus* $M_V$) for Miras in the Large Magellanic Cloud. Newer works usually give this dependence as $M = -m \log P + n$ (where $m$ and $n$ are some constants) and use infrared stellar magnitudes. The advantages of this approach are that (*a*) amplitudes of Miras' light variations and maximum heights vary from cycle to cycle in the infrared much less than in the visual, (*b*) in the infrared the effect of interstellar extinction (which is usually difficult to take into account for such distant objects as Miras) is much less. Recently Knapp et al. (2003) derived the period – $K$-band absolute magnitude relationship as

$$M_K \propto -3.39(\pm 0.47) \log P. \qquad (1)$$

The period–luminosity dependence in Miras is usually attributed to their pulsation properties. The "planetary" model of the Mira-type variability discussed in this paper, too, yields the correct value for the slope of the period–luminosity relation. Indeed, the star's luminosity $L \propto R_*^2$ and its absolute magnitude $M \propto -5 \log R_*$. On the other hand, if we accept that the star's period $P$ is the period of revolution of a planet at the outskirts of the stellar atmosphere, then, according to Kepler's third law, $P \propto R_*^{3/2}$, and

$$M \propto -3.33 \log P, \qquad (2)$$

in accordance with, e.g., relationship (1). The bolometric correction, mass, and effective temperature of the star affect this relationship rather weakly.

Moreover, the "planetary" hypothesis predicts a verisimilar value of the "pulsation constant", though in this case no actual pulsation is involved. The period $P$ of revolution of a planet at distance $R_*$ from the stellar center (at the outer boundary of its photosphere) depends on the stellar mass $M_*$ as

$$P = 2\pi \sqrt{\frac{R_*^3}{GM_*}}. \qquad (3)$$

The quantity in the radicand is inversely proportional to the mean density of the star $\rho_*$. This precisely matches the formula for the pulsation constant:

$$Q = P(M_*/\mathrm{M}_\odot)^{1/2}(R_*/\mathrm{R}_\odot)^{-3/2}, \qquad (4)$$

For $M = 1\mathrm{M}_\odot$ and $R_* = 1$ AU we find $Q = 0.116$ d, which corresponds to the main-tone pulsation. This was shown by Berlioz-Arthaud (2003).

## 5. Conclusions

Our long-term monitoring of a sample of Miras has confirmed the correlation between the stars' visual brightness and integrated $H_2O$ maser flux. The model for $H_2O$ maser variability in late-type giants assume a direct impact of a moderate-velocity ($v_{\rm sh} \sim 5$–$10$ km/s) shock, reaching the masering region in the circumstellar envelope (Rudnitskij & Chuprikov 1990). The delay between the optical and $H_2O$ maxima depends on the shock travel time and may be as long as a few stellar periods (Lekht et al. 2001). The shock model is supported by H$\alpha$-line monitoring: appearance of strong

Balmer emission is a diagnostic for the early stage of shock propagation in the stellar atmosphere; as the weakened shock reaches the $H_2O$ masering region at a few stellar radii outside, it results in an appropriate maser increase.

However, the model of a spherical shock, driven by the stellar pulsation and embracing the entire stellar surface, may be not valid. In this case the Balmer emission should be accompanied by emission in the radio continuum of the entire stellar disk that should be observable at centimeter waves. We could not detect in the radio continuum even the stars previously known to be radio continuum sources (*o* Cet, R Aql, W Hya, Knapp et al. 1995, Reid & Menten 1997), though the sensitivity was sufficient (typically 0.1–0.3 mJy at the $3\sigma$ level). The upper levels obtained imply that strong spherical shocks with front velocities $v_{\rm sh} \geq 15$–$20$ km/s do not exist in Miras or they may be invisible at microwaves, because they do not propagate above the radius of the "radio photosphere", $r_{\rm ph} \sim 2R_*$ (Reid & Menten 1997), strongly absorbing the radio emission, but transmitting the optical emission.

An alternative to the pulsation-driven shock is proposed. The Balmer emission comes from a local source—fireball surrounding a nearby companion (brown dwarf or planet) revolving around the expanded red giant. The fireball is undetectable at microwaves because of its small angular size. The model accounts well for the appearance of the optical emission lines, it also reproduces the variations of the $H_2O$ maser, the shape of the visual light curves, and the period–luminosity dependence for Miras.

*Acknowledgements.* The author is grateful to V.F. Esipov for the optical spectroscopy data, to M.I. Pashchenko, E.E. Lekht, S.V. Rottar, V.A. Samodurov, I.A. Subaev, and A.V. Tolmachev for help with the $H_2O$ observations, to Jessica M. Chapman for joint *ATCA* observations. This work was supported by the Ministry of Industry and Science of the Russian Federation on the RT-22 radio telescope (facility registration number 01-10) and by the Russian Foundation for Basic Research (project code 06-02-16806). This research made use of the visual observations of the Association française des observateurs d'étoiles variables (AFOEV) from the SIMBAD database of the Centre des données astronomiques de Strasbourg (France).

## References

Berlioz-Arthaud P.: 2003, *Astron. Astrophys.*, **397**, 943.

Berulis I.I., Lekht E.E., Pashchenko M.I., Rudnitskij G.M.: 1983, *Astron. Zh.*, **60**, 310.

Berulis I.I., Lekht E.E., Munitsyn V.A., Rudnitskij G.M.: 1998, *Astron. Zh.*, **75**, 394.

Cannizzo J.K., Goodings D.A., Mattei J.A. 1990: *Astrophys. J.*, **357**, 235.

Chapman J.M., Rudnitskij G.M. 1998: *Asymptotic Giant Branch Stars, IAU Symp. 191 Poster Session*, #P4-01.

Clayton M.L. & Feast, M.W. 1969, *MNRAS*, **146**, 411.

Dougherty S.M., Bode M.F, Lloyd H.M. *et al.* 1995, *MNRAS*, **272**, 843.

Esipov V.F., Pashchenko M.I., Rudnitskij G.M., Fomin S.V.: 1999, *Pis'ma Astron. Zh.*, **25**, 775.

Klyus I.A. 1988: *Peremennye Zvezdy*, **22**, 697.

Knapp G.R., Bowers P.F., Young K., Phillips T.G.: 1995, *Astrophys. J.*, **455**, 293.

Knapp G.R., Pourbaix D., Platais I., Jorissen A.: 2003, *Astron. Astrophys.*, **403**, 993.

Kudashkina L.S., Rudnitskij G.M.: 1988, *Peremennye Zvezdy*, **22**, 925.

Lekht E.E., Mendoza-Torres J.E., Pashchenko M.I., Berulis I.I.: 1999, *Astron. Astrophys.*, **343**, 241.

Lekht E.E., Mendoza-Torres J.E., Rudnitskij G.M., Tolmachev A.M.: 2001, *Astron. Astrophys.*, **376**, 928.

Lekht E.E., Rudnitskij G.M., Mendoza-Torres J.E., Tolmachev, A.M.: 2005, *Astron. Astrophys.*, **437**, 127.

Pashchenko M.I., Rudnitskij G.M.: 1999, *Astron. Zh.*, **76**, 363.

Pashchenko M.I., Rudnitskij G.M.: 2004, *Astron. Zh.*, **81**, 418.

Reid M.J., Menten K.M. 1997: *Astrophys. J.*, **476**, 327.

Rudnitskij G.M.: 1987, *Circumstellar Matter. Proc. 122 Symp. IAU*, Dordrecht: Reidel, 267.

Rudnitskij G.M.: 2000, *The Impact of Large-Scale Surveys on Pulsating Star Research. IAU Coll. 176, ASP Conf. Ser.*, **203**, 384.

Rudnitskij G.M.: 2002, *Publ. Astron. Soc. Australia*, **19**, 499.

Rudnitskij G.M.: 2005, *http://www.astronet.ru/db/msg/1202883.*

Rudnitskij G.M., Chuprikov A.A.: 1990, *Astron. Zh.*, **31**, 853.

Rudnitskij G.M., Pashchenko M.I.: 2005, *Pis'ma Astron. Zh.*, **31**, 853.

Rudnitskij G.M., Lekht E.E., Berulis I.I.: 1999, *Pis'ma Astron. Zh.*, **25**, 467.

Rudnitskij G.M., Lekht E.E., Mendoza-Torres J.E., *et al.*: 2000, *Astron. Astrophys. Suppl. Ser.*, **146**, 385.

Whitney C.A. 1984: *JAAVSO*, 13, 31.

# THE CCD CAMERA WITHOUT COOLING

O.Sh. Shahrukhanov

Department of Astronomy, Odessa State University
T.G.Shevchenko Park, Odessa 65014 Ukraine

ABSTRACT. The device with the parameters taking one's intermediate stand between the standard TV and CCD cameras with cooling is developed. This camera works without cooling. Accumulation time can be established in the limits from 1 up to 16 TV frames. The results of trial measurements and possibilities for using of the given device are illustrated in this work.

**Key words**: Devices: CCD cameras

## 1. Introduction

In modern astronomical observations the CCD cameras with cooling Peltie elements have a broad distribution, that enables to accumulate the signal of observing object during long time. For the fast processes researches the cameras working in the TV standard with accumulation time of 40 milliseconds have been used. These cameras do not require cooling, that considerably simplifies their design and makes them much more economically on the expendable power. The block diagram of the device, possibilities to use it in the various fields of astronomy and the results of trial observations are discussed.

## 2. Device's structure and observations

For this device author has an attempt to keep the preferences of the both types cameras. For the author's device the accumulation time could be set within the limits of 1 up to 16 TV frames with step-type behaviour in one TV frame (from 40 up to 640 milliseconds). An information's input from the camera is carried out in the format of TV signal. This fact gives the possibility to use the camera as well with computer and videomonitor, respectively, and it is very important for the objects guiding in a manual mode. This device has high profitability (its power expend is about 1,2 Volt.), and it allows to supply it from the independent sources. For example, in the field conditions the camera can work from the storage battery of the automobile.

Possibilities of the using of this device are extensive enough. Let's consider some of them.

1. Sky objects photometry: it is possible to observe the objects with quickly brightness variability. Preferences in comparison with TV cameras, – higher sensitivity, and for the cooling ones, – faster informations input.

2. Atmosphere's researching. The range of accumulation times allows to receive stable fibrous structure around the stars, caused by the atmospheric turbulence effects. From the research of the given structures it is possible to determine their characteristical frequencies and other parametrs.

3. Guiding. Guiding of the objects by the using oh this camera is possible as in the automatic mode (at presence of computer system of telescope guiding), and in the manual one with the observer's visual control (it is especially important for old telescopes which work without computer's guiding systems).

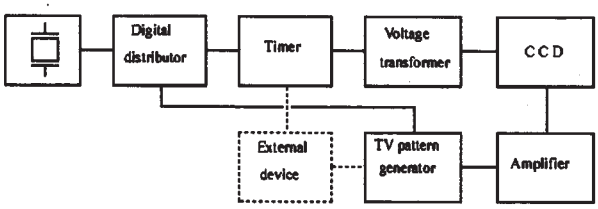


Figure 1: Block diagram of the device

The block diagram of the device is represented in Figure 1.

Digital distributor forms the series of the signals required for the matrix control and for the output signal conversion.

Timer operates by the process of accumulation. For this case it formats the signals of the previous block being depended on the information coming in from the outside device or from the panel of the manual control's block.

Voltage transformer converts input signals by the level of voltage what could be need for the CCD matrix control.

Amplifier strengthens a signal from the matrix output both for amplitude and for current.

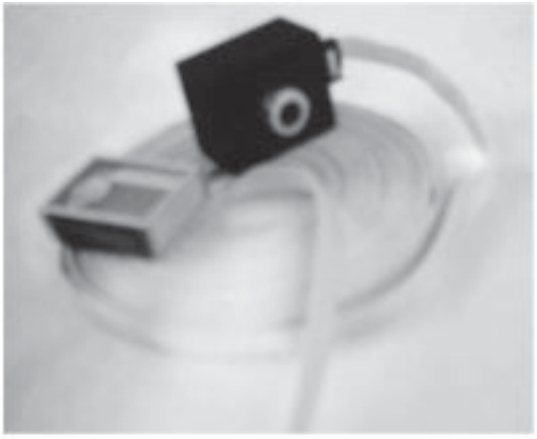

Figure 2: CCD device without cooling

TV pattern generator translates the amplified signal to the standard of the televisional one. As the outside devices could be a computer (if a digital processing is required, and control of the device or a telescope too) or the videomonitor if is need the visual control (guiding, visual search of the objects etc.).

Trial observations were carried out on the territory of the Astronomical Observatory of Odessa National University, situated in the central part of the city of Odessa. At that an objective lens with diameter of inlet 5 cm, and focal length 8 cm.

At maximal time of accumulation (16 TV of the staff) the sensitivity of this CCD matrix allows to observe the objects of 10.5 mag without additional information processing.

An appearance of device is given in Figure 2.

# THE FLUCTUATIONS IN THE IRAS DISTRIBUTION

R.B. Shatsova, G.B. Anisimova

Rostov Pedagogical University, *galina@iubip.ru*

ABSTRACT. The great fluctuations in the infrared sky are situated along the meridians of Universal Sky Net.

It is related also to the large structures. So the edge of the zone of avoidance of galaxies over $IRAS_{60}$ and $IRAS_{100}$ for long extension coincides to the Γ meridian, perpendicular to the ecliptic E. The Large Magellanic Cloud is situated near the southern pole of ecliptic. The IR radiation of the zodiacal belt, discovered by Hauser, is confirmed. Perhaps, it is obliged not only and not so much to a zodiacal light of the Solar system.

**Key words:** IRAS, structure of Galaxy, Universal Sky Net.

One can distinguish both regular and accidental components in the distributions of stellar and nonstellar matter. The concentrations to the plane and to the centre of Galaxy, to the Gould Belt and others are considered as the regular ones. And the deflexions from them are attributed to the accidental fluctuations.

The fluctuations, which own the certain predicted characteristics, must be excluded from the number of accidental ones. Such predictions give, in particular, the regular multi-polar Universal Sky Net (USN). A lot of its poles are the known in astronomy points. Every C-pole has the intersection of its own bunch of meridians. There are known in astronomy circles among them.

USN permits to join almost all well known in astronomy elements into the united net and to find the regularities in their mutual orientation.

USN is built on the basis of:

1. One of known circles (for instance, ecliptic – E)
2. The fastened point (for instance, $\eta$ - the intersection of ecliptic E with the Galactic equator – MW)
3. The net is branching in the poles by the empiric rule

The common USN geometry was described in (Shatsova & Anisimova, 2003; 2004). The used in this article net elements (the bunches of meridians in $\xi$, $\eta$, $\zeta$ poles), are shown in Fig. 1, 2 and Table 1.

The equation for k- meridian of the bunch in C-pole is presented in the used here polar coordinate system ($\Omega$, $\rho$):

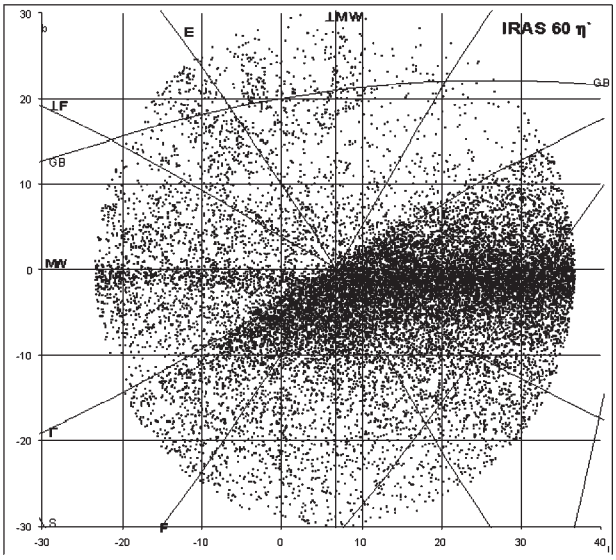


Figure 1: The position of IRAS sources $\lambda = 60m\mu$ in the pole $\eta$ and the USN meridians

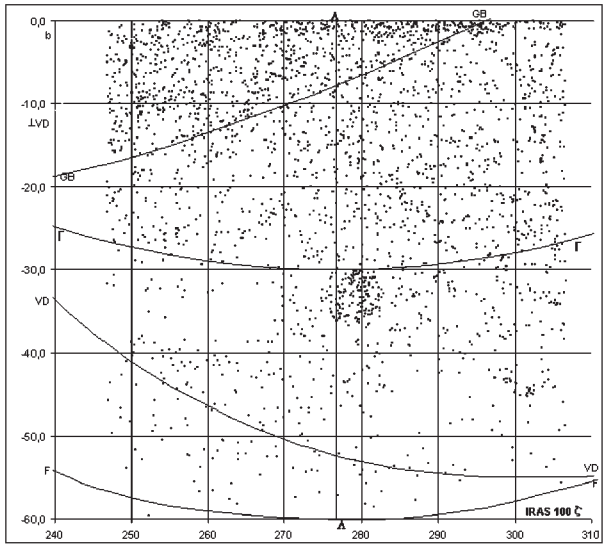


Figure 2: The position of IRAS sources $\lambda = 60m\mu$ in the pole $\zeta$ and the USN meridians

| Pole | Meridians | | | Pole | Meridians | | | Pole | Meridians | | |
|---|---|---|---|---|---|---|---|---|---|---|---|
| $\xi$ | $k$ | sym-bol | $\Omega$ | $\eta$ | $k$ | sym-bol | $\Omega$ | $\zeta$ | $k$ | sym-bol | $\Omega$ |
| m=4 | 0 | $\Lambda$ | 0 ° | m=6 | 0 | $\perp$MW | 0 | m=2 | 0 | $\Lambda$ | 0 |
| $l$=96. ° 7 | 1 | S | 45 ° | $l$=186.7 | 1 | E | 30 | $l$=96.7 | 1 | $\Gamma$ | 90 |
| $b$=-60 ° | 2 | E | 90 ° | $b$=0 ° | 2 | $\perp$F | 60 | $b$=30 ° | | | |
| | 3 | $\perp\Gamma$ | 135 | | 3 | MW | 90 | | | | |
| $\lambda$=0 ° | | | | $\lambda$=90 ° | 4 | $\Gamma$ | 120 | $\lambda$=0 ° | | | |
| $\beta$=0 ° | | | | $\beta$=0 ° | 5 | F | 150 | $\beta$=90 ° | | | |

Table 1: The USN elements are presented: the poles - coordinates (galactic-(l,b) and ecliptical-( $\lambda, \beta$)), and the number of meridians, intersecting in this poles (m); the meridians - the symbol and the positional angle $\Omega$ of each meridian

$\Omega_C = \Omega_0 + k\pi/m_C$, (1)
where $k$=0, 1 ,..., $m_C$ -1, $m_C$ - the number of meridians in the bunch: $m_\xi$ =4, $m_\eta$ =6, $m_\zeta$ =2.

The positional angle $\Omega$ is measured off the direction to the North Galactic Pole $\Pi_{MW}$ to the side of increase of galactic longitudes $l$, $\rho$ - the radius-vector or the angular polar distance along the great circle.

In this work we examined the IRAS data (IRAS Point Source Catalog, 1985) in two waves (60 and 100 m$\mu$) in classes 2 and 3 in the sky regions around ($\xi$, $\eta$, $\zeta$) poles in radius 30 ° and the opposite poles ($\xi$‘, $\eta$‘, $\zeta$‘), that is about 40% of the sky. The IR radiation is connected with the dust shells of the stars, nebulaes and the galaxies.

Each element of USN has not only the geometrical sense, but also reflects some peculiarities of cosmic structures.

The two examples over the IRAS data is shown here.

1. $IRAS_{60}$ in the region of $\eta$‘ pole, situated near the centre of the Galaxy (l=0 ° , b=0 ° ), (Fig.1).

The meridians $\Gamma$, MW and E are very clearly seen here. The great circle $\Gamma$ passes through the celestial and ecliptic poles, and the solstices. The IR map shows a triangle of very dense dust. $\Gamma$ is exactly its hypotenuse for the length of tens degrees. The optical map shows, that this line is the edge of the zone of avoidance of galaxies (de Vaucouleurs, 1959). The MW meridian passes along the radius of the region along the northern edge of the narrower dense galactic zone. The E meridian outlines the right edge of the zodiacal IRAS concentration.

It is remarkable, that the edge's lines coincide the meridians, and their intersection - $\eta$‘ pole of USN.

The edge locations form the effect of density asymmetry. The $\Gamma$ and E sides of lower density are turned to the I quadrant, and of higher density are turned to the III quadrant. The quadrants have no symmetry relatively MW, moreover, MW zones raise the density in II and IV quadrants. Hence it follows the density asymmetry around the pole itself. So MW and $\Gamma$ meridians are at the edges of large-scale structures. And E, F, $\perp$F and $\perp$MW are at the edges of smaller density fluctuations.

The connection of IRAS distribution with the USN net is the sign of regularity and, hence, it is not accidental.

2. $IRAS_{100}$ in the region of the southern ecliptical pole - $\zeta$‘ (Fig. 2)

Only two USN circles intersect here - $\Gamma$ and $\Lambda$. $\Lambda$ also passes through the galactic poles. Large Magellanic Cloud (LMC), having strong IR radiation, is near this pole. $\Gamma$ and $\Lambda$ touch the core of LMC. The internal LMC structures are parallel to $\Gamma$ and $\Lambda$ (Efremov, 1989, Fig. 21). The bright LMC halo asymmetrically surrounds $\zeta$‘, but there is larger ($\approx$10 ° ) and more symmetrical to $\zeta$‘circle – the parallel to E near the pole. We see the density jumps on $\Gamma$, $\Lambda$ and especially on GB (Gould Belt), creating the asymmetry of density in the quadrants.

These and other poles are situated in the centers of chosen regions, within $\rho$=30 ° . It is natural to examine the distribution of point IRAS sources in polar coordinates ($\Omega$, $\rho$). The coordinates ($\Omega$, $\rho$) can be obtained from (l, b):

$$tg\Omega = \frac{\sec b_c \cdot \sin(l-l_c)}{tgb - tgb_c \cdot \cos(l-l_c)}$$
$$\sin\rho = \frac{\cos b}{\sin\Omega} \cdot \sin(l-l_c) \quad (2),$$

where ($l_c$, $b_c$) – the coordinates of C pole (see Table 1).

The polar net is divided into the cells $S_i$ ($\Delta\Omega$=5 ° , $\Delta\rho$=5 ° ). The object numbers $n_i$ and the corresponding density – $d_i = n_i/S_i$ are counted in each cell .

As we examine the accidental components, we must exclude from $d_i$ the regular component - the mean $d(b)$ in the region at latitude $b$, that reflects first of all the galactic concentration. For each region and each IRAS wave length we obtained the histograms of $\Delta d_i = d_i$–$d$ in the cells of sectors in function of $\Omega$ (or a symbol of meridian) for each interval of $\rho_j$. There are positive and negative deflexions.

The example for the region of $\eta$ pole, $IRAS_{100}$ is presented in Fig.3.

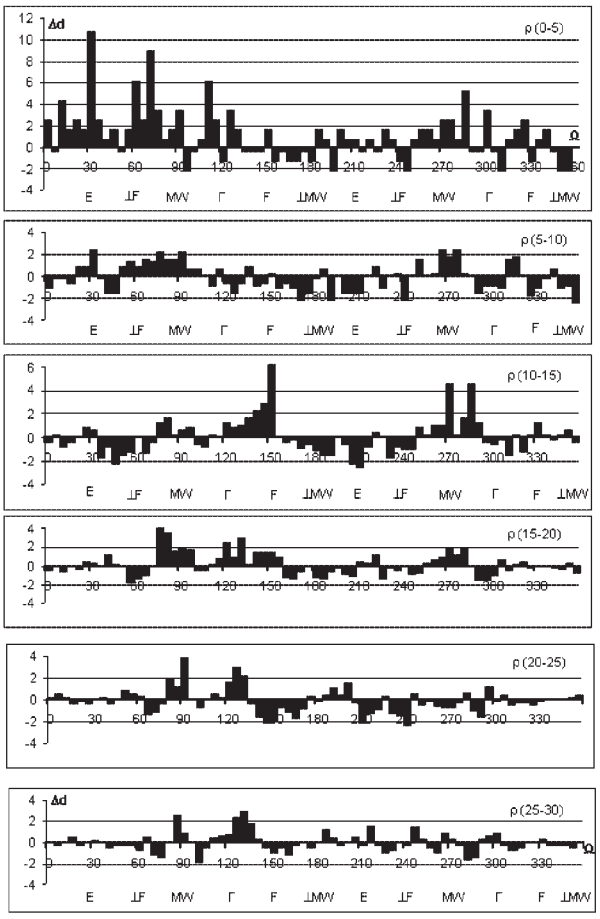


Figure 3: The example of $\Delta d$ histogram for different $\rho$ intervals around the $\eta$ - pole for $IRAS_{100}$

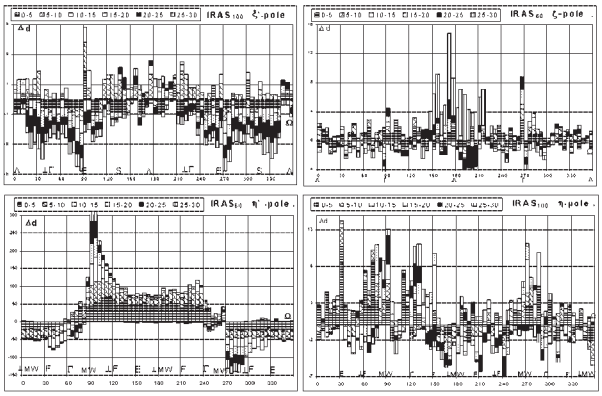

Figure 4: The examples of IRAS $\Delta d$ histograms in function ($\Omega$, $\rho$)

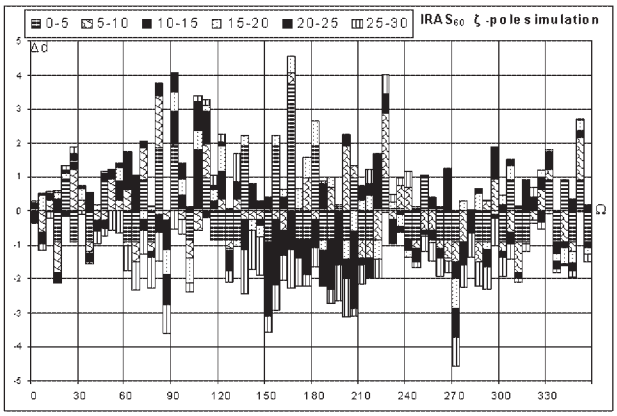


Figure 5: The distribution of density excess ($\Omega$, $\rho$) for IRAS simulation $\lambda = 60m\mu$ in the $\zeta$-pole

$\Delta d$ depends systematically on $\Omega$. The largest density jump from $\Omega$(0-130 $^\circ$) sector to $\Omega$(130-250 $^\circ$) sector is seen near the pole, at $\rho$=0-5 $^\circ$. The density jumps from $\Delta d > 0$ to $\Delta d < 0$ reduce at the other $\rho$, the sector borders varies slightly, but the contrast is remained. The $\Delta d > 0$ peaks, as a rule, lie at the meridians, and $\Delta d < 0$ corresponds to the space between the meridians.

Fig. 4 shows the examples of the combined histograms. For compactness, $\Delta d(\rho_j)$ are presented for different $\rho_j$ at every $\Omega$ in each histogram, but it does not mean the summing up.

The largest fluctuations along the meridians, corresponding $\Omega_i$ and $\Omega_i$+180 in all divisions of the material are given in Table 2, where $\Delta d_{max}(\Omega)$ is the density excess and in brackets ($N$) – the number of cells, having $\Delta d > 0$.

The joint analysis of Fig. 3-4 and Table 2 confirms the conclusions, obtained from Fig. 1-2 analysis. But, the numerical comparison can be done only inside the same region. And than one can do the qualitative comparison between the different regions.

Table 2 shows the connection of the density fluctuations with the majority of the USN meridians. Hence, the interpretation given by Hauser (1995) as a zodiacal light of the Solar system is doubtful. It was obtained in particular over $IRAS_{12}$ and $IRAS_{25}$ data for one meridian – E. The connection of USN with the galactic and extragalactic structures was discussed in (Shatsova & Anisimova, 2004).

We made the accidental simulations in conditions of galactic concentration. The number of points, equal the number of real objects were scattered accidentally inside each zone on latitude $\Delta b$=10 $^\circ$. The ($\Omega$, $\rho$) distribution was obtained over the same procedure as for the real objects. There is no peculiarities in the simulated distribution, only the MW concentration and the peculiarity of the formula (2) tg$\Omega = \infty$, for $\Omega$=90, 270. The example is shown in Fig. 5.

The main conclusions:

1. It is confirmed the predicted by USN the similar regularity in the distribution of fluctuations and large-scale structures: the density excess along the meridians and its deficit between the meridians and near the net's

Table 2: Maximal deflections of IRAS density from mean density

| | **IRAS 60** | | | | | | **IRAS 100** | | | | | | |
|---|---|---|---|---|---|---|---|---|---|---|---|---|---|
| | $\Lambda$ | $\perp\Gamma$ | E | S | $\|\|$(S) | | $\Lambda$ | $\perp\Gamma$ | E | S | $\|\|$(S) | | |
| $\xi$ | 1,2 (7) | 2,1 (3) | 2,1 (5) | 1,9 (5) | 4 (5) | | 1,2 (6) | 1,1 (3) | 2,0 (3) | 1,9 (4) | 3,9 (5) | | |
| $\xi$‘ | 2,0 (7) | 1,9 (5) | 2,0 (6) | 0,6 (6) | | | 1,7 (7) | 1,9 (5) | 1,9 (6) | 1,6 (5) | | | |
| | $\perp$MW | E | $\perp$F | MW | $\Gamma$ | F | $\perp$MW | E | $\perp$F | MW | $\Gamma$ | F | $\|\|(\Gamma)$ |
| $\eta$ | 4 (6) | 8 (5) | 11 (5) | 8 (11) | 8 (8) | 6 (7) | 4,5 (6) | 11 (7) | 9 (6) | 4,5 (11) | 6 (7) | 6 (7) | 5,5 (3) |
| $\eta$‘ | 50 (4) | 50 (4) | 75 (5) | 60 (6) | 45 (7) | 50 (3) | 50 (4) | 50 (3) | 70 (5) | 60 (6) | 45 (4) | 70 (4) | |
| | $\Lambda$ | $\perp\Gamma$ | LMC | | MW | GB | $\Lambda$ | $\perp\Gamma$ | LMC | | MW | GB | |
| $\zeta$ | 10 (9) | 3 (10) | | | 5,5 (5) | | 7 (7) | 3,4 (9) | | | 5 (8) | | |
| $\zeta$‘ | 13 (6) | 16 (5) | 20 (5) | | 4,4 (4) | 5,0 (4) | 12 (7) | 6,8 (7) | 12,5 (5) | | | 2,5 (4) | |

poles. The existence of unknown before meridians F, $\perp F$, $\perp\Gamma$ and S is confirmed over these features.

2. It is noticed the unknown peculiarities of the USN elements: the meridians and the poles are situated at the edges of sky belts, where the density jumps take place. This asymmetry leads to the division of the space into the sectors of different density.

3. The connection of the majority of IRAS fluctuations and the USN elements means that the fluctuations of density are not accidental. The same follows from the obtained simulations.

4. There is no qualitative differences for $IRAS_{60}$ and $IRAS_{100}$ distribution, only in details.

As the positive fluctuations along the meridians and the negative between them were predicted, then the observed such fluctuations are not accidental.

**References**

Shatsova R.B., Anisimova G.B.: 2003, *Astrofizica*, **46**, 319.

Shatsova R.B., Anisimova G.B.: 2004.

*IRAS Point Source Catalog, Washington*, 1985.

G. de Vaucouleurs: 1959, *Soviet Astron Zh*, **36**, 977.

Efremov Y.N.: 1989, *Sites of star formation in galaxies.*

Hauser M.G.: 1995, *IAU Sympos*, **168**.

# THE PROTOPLANETARY SYSTEM FORMATION AS A RESULT OF THE MERGING OF CLOSE BINARY STAR CONSISTING OF THE LOW MASS PRE–MS STARS

F.V. Sirotkin, V.G. Karetnikov

Astronomical observatory, Odessa National University

ABSTRACT. The mechanism of protoplanetary system formation as a result of a merge of binary star consisting of the low mass ($0.5 - 1M_{\odot}$) preMS stars is considered. During the merging the more massive component is destroyed. The substance of the destroyed component forms spiral gaseous arm and circumstellar disk. The protoplanetary embryos (clouds) with masses about 2-5 $M_j$ are forming as the result of division of the spiral arm. The rotation of the circumstelar disk, clouds and star are in plane. The formed clouds are on the eccentric ($e > 0.3$) orbits.

**Key words**: computational fluid dynamics, binary star, protoplanetary system

## 1. Introduction

The degree of the stars multiplicity (number of systems divided by a number of stars) in the solar neighborhood is more than 57 % (Duquennoy 1991) and probably is underestimated. The probability of discovery of not found yet component always exists. Such components are discovered gradually with an increase of an accuracy of observations and use of other methods of observation and data processing. Thus, *it is possible to consider that the multiplicity of observed star is the lower limit of real star multiplicity.* The multiplicity of preMS stars twice exceeds the multiplicity of solar type MS stars (Köhler 1998).

The basic parameter determining properties of binaries is the specific angular moment of the protostellar cloud. The angular moment distribution of binaries of various types is continuous. The lower limit of the specific angular moments range of observable binaries is $\sim 2 \cdot 10^{18}$ $cm^2c^{-1}$ (Masevich, Tutukov 1988). It extends to the specific angular moments range of the planetary systems $10^{17} - 10^{21}$ $cm^2c^{-1}$ (Goodman and all 1993). Thus, the range of the angular moment of binaries overlaps the range of the angular moment of protostellar systems. The angular moment of binaries with brown dwarfs extends to the specific angular moment range of the planetary systems (Tutukov 2002). Thus, the distribution of the binaries and planetary systems on the angular moment is continuous. It allows assuming, that the *binaries with the extreme small (transitive between binary and planetary systems) angular moment can exist.*

Binary stars with semiaxis $A$ that satisfy equation:

$$A/R_{\odot} < 6(M/M_{\odot})^{1/3} \qquad (1)$$

where $M = M_1 + M_2$ is mass of system, nearly are not observed (Popova 1982) (see fig. 1). During contraction to the main sequence the binaries with semiaxis which are satisfying equation (1), will have common envelopes, because the components will have radii about $3 - 5R_{\odot}$ (Stahler 1993).

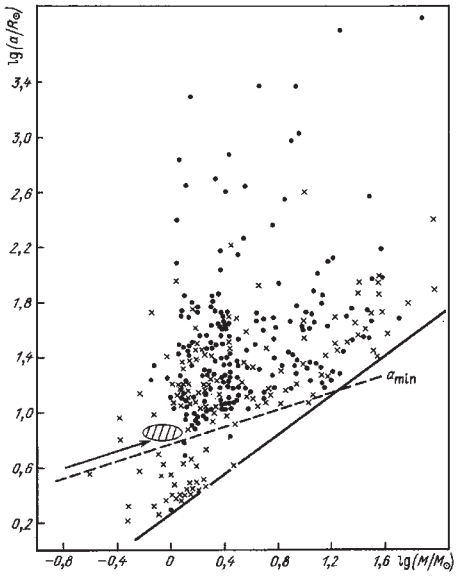


Figure 1: The semiaxes - primary component mass distribution (Masevich, Tutukov 1988) for spectroscopic binaries. A shaped line corresponds to equation 1. The shaded oval corresponds to considered binaries.

The considered stars have deep convective envelopes (Palla, Stahler 1993). And binaries can lose the angular momentum by stellar wind with rather small loss of

system mass (Krajcheva 1978). As the result of a loss of the angular moment the orbital separation can decrease and mass transfer in such systems can occur. If the mass transfer ratio is high, then system can merge. This mechanisms of angular moment loss is actual for stars with low ($< 1.5M_\odot$) mass. For more massive stars, the time interval on which they are convective, is much shorter (Palla, Stahler 1993)

During last years hundreds planetary systems are discovered. The comparison of extrasolar planets and planets of solar system shows, that the extrasolar planets can have masses about $0.1 - 10M_J$ and can have orbits with higher eccentricity (0.69 for HD 89744) and semiaxis in the range 0.2 - 10 a. u. *The presence of wide range of parameters of observable extrasolar planets allows to assume that mechanisms of formation of planetary systems another than for solar system can exist.*

The standard mechanism of planetary systems formation is its formation from systems with circumstellar disks. The probability of detection of the disk practically linearly grows with age of stars. The observation of stars in young clusters shows that the quantity of stars with disks decreases from 80-90 % in clusters with age $0.3 - 1 \cdot 10^6$ years is up to 3 % in clusters with age $\sim 3 \cdot 10^7$years (Haisch etc. 2001). Thus, *the presence of disks around young stars is the same widespread phenomenon as their multiplicity.*

The noted observation facts allows to assume, that disks around some protoplanet systems could be produced in the merging binaries. This merging possible as a result of angular moment loss by stellar wind, interaction of system with the common envelope and other processes.

We suppose that the planetary system forms step by step in the following processes:

1. The close binary star formation. $M_{1,2} < 1.5M_\odot$, $M_2/M_1 \sim 1$
2. The loss of angular moment by stellar wind or interaction with common envelope.
3. Merging of binary star. The formation of the circumstellar disk
4. The mass transfer and angular moment transfer along the circumstellar disk and between star and circumstellar disk under the viscous friction.
5. The formation of protoplanetary embryos

## 2. Method

In the case of polytropic state equation:

$$P = K\rho^\gamma, \tag{2}$$

where $\gamma$ is the ratio of specific heats (in present calculations $\gamma = 5/3$), $K$ is the entropy function, the equation of motion of a compressible fluid can be written in the form:

$$\frac{\partial \rho}{\partial t} + \nabla \cdot (\rho \vec{v}) = 0 \ , \tag{3}$$

$$\rho \frac{\partial K}{\partial t} + \rho(\vec{v} \cdot \nabla)K = -\frac{\gamma - 1}{\rho^\gamma} \Im \ . \tag{4}$$

$$\frac{\partial \vec{v}}{\partial t} + (\vec{v} \cdot \nabla)\vec{v} = -\frac{1}{\rho}\nabla P - \vec{F}, \tag{5}$$

where $\rho$ is the density, $\vec{v}$ the velocity, $P$ pressure, and the $\Im$ the energy loss function which comprises all nonadiabatic sources and sinks of energy.

In SPH (Lucy 1977, Gingold & Monaghan 1977), these equations of motion are solved using Lagrangian formulation in which the gas is partitioned into fluid elements. A subset of these fluid elements are selected and represented by particles. In SPH these subset is chosen so that the particle mass density is proportional to the fluid density, $\rho$. This means that $\rho$ can be estimated from the local density of particles at later times if the system is updated according to the equations of hydrodynamics.

Since the number of particles is finite, it is necessary to include a "smoothing"procedure to interpolate between them to represent the fields as continuous quantities. If each particle has a mass $m_j$ then the smoothed density is given by

$$\rho(\vec{r}) = \sum_{i=1}^{N} m_i W(|\vec{r} - \vec{r}_i|, h), \tag{6}$$

where $h_i$ is the smoothing length, and $W(r, h)$ is the smoothing kernel which satisfies the following conditions:

$$\int W(r - r', h)dr' = 1, \tag{7}$$

$$\lim_{h \to 0} W(r - r', h) = \delta(r - r'). \tag{8}$$

The calculations presented here were performed using the Gaussian kernel

$$W(r, h) = \frac{\exp(-r^2/h^2)}{\pi^{3/2}h^3}, \tag{9}$$

In the implementation used here the components of a binary system have their own fixed smoothing length. The primary component is described by $N_p$ particles with smoothing length $h_p$ and mass $m_p = M_1/N_p$. The secondary component is described by $N_s$ particles with smoothing length $h_s$ and mass $m_s = M_2/N_s$, $N_s = N - N_p$, where $N$ is the total number of particles. For this case the SPH form of the equation (6) is

$$\rho_i = \sum_{j=1}^{N} m_j W_{ij}, \tag{10}$$

$$W_{ij} = W(r_{ij}, h_i)/2 + W(r_{ij}, h_j)/2 \tag{11}$$

where $\rho_i$ is the smoothing density at the point $\vec{r}_i$, and $r_{ij} = |\vec{r}_i - \vec{r}_j|$.

SPH form of the equation (3) is the following

$$\frac{d\vec{v}_i}{dt} = -\sum_{j=1}^{N} m_j \left(\frac{P_i}{\rho_i^2} + \frac{P_j}{\rho_j^2}\right) \cdot \nabla_i W_{ij} - \\ -G\sum_{j=1}^{N} \frac{M(r_{ij})}{r_{ij}^2}\frac{\vec{r}_{ij}}{r_{ij}} + \vec{a}_i^{visc} \qquad (12)$$

$$M(r_{ij}) = 4\pi m_i \int_0^{r_{ij}} r^2 W(r,h) dr,$$

where $G$ is the Newtonian gravitation constant. The second term in equation (12) is the gravitational forces, $\vec{a}_i^{visc}$ is the viscous forces. The standard artificial viscosity is employed (Monaghan 1992):

$$\vec{a}_i^{visc} = \sum_{j=1}^{N} m_j \Pi_{ij} \nabla_i W_{ij}, \qquad (13)$$

where

$$\Pi_{ij} = \frac{-\alpha\mu_{ij}c_{ij} - \beta\mu_{ij}^2}{\rho_{ij}} \qquad (14)$$

$$\mu_{ij} = \begin{cases} \dfrac{\vec{v}_{ij}\cdot\vec{r}_{ij}}{h(r_{ij}^2/h^2+\eta^2)}, & \vec{v}_{ij}\cdot\vec{r}_{ij} < 0 \\ 0, & \vec{v}_{ij}\cdot\vec{r}_{ij} \geq 0 \end{cases} \qquad (15)$$

and $\vec{v}_{ij} = \vec{v}_i - \vec{v}_j$,$\vec{r}_{ij} = \vec{r}_i - \vec{r}_j$, $c_{ij} = c_i - c_j$ is the average sound speed of particles $i$ and $j$, $h_{ij} = (h_i + h_j)/2$, $\rho_{ij} = (\rho_i + \rho_j)/2$. The numerical simulation is performed with constant $\alpha = 0.5$, $\beta = 1$, $\eta = 0.001$.

Ignoring any sources of entropy other than artificial viscosity, the smoothed equation(4) for the entropy function $K$ is

$$\frac{dK_i}{dt} = \frac{\gamma - 1}{2\rho_i^{\gamma-1}} \sum_{j=1}^{N} \Pi_{ij} m_j \vec{v}_{ij} \cdot \nabla_i W_{ij} \qquad (16)$$

The solution of the equations (10),(12),(16) is determined by a choice of the initial conditions. The construction of initial conditions can be divided into three steps:

- The first step is the construction of internal structure of each component as a star in the state of hydrostatic equilibrium.
- The second step is to take into account the rotation of each component and tidal forces operating between them.
- The last step is the coordinate transformation and establishing of the initial velocities of particles.

At the first step the models were constructed by placing particles down randomly and then solving equation (12) in the presence of frictional dumping to achieve a stationary equilibrium (Gingold and Monaghan 1977).

At the second stage we take into account rotation and tidal forces. For each binary component the tidal forces were estimated considering another companion as a point mass.

At the last step we make transformation of coordinates. For the primary component this transformation of coordinates can be written as follows':

$$\vec{r}_i = \vec{r}_i + \vec{r}_{cm_1} \ , \ \vec{v}_i = \vec{\Omega} \times \vec{r}_i \ , \ i = 1...N_p, \qquad (17)$$

and for the secondary one:

$$\vec{r}_i = \vec{r}_i + \vec{r}_{cm_2} \ , \ \vec{v}_i = \vec{\Omega} \times \vec{r}_i \ , \ i = N_p + 1...N, \qquad (18)$$

where $\vec{r}_{cm_1}$ is the primary component's center of mass, $\vec{r}_{cm_2}$ is the secondary component's center of mass. The initial angular velocity $\vec{\Omega}$ was set in units of the Keplerian angular velocity $\vec{\Omega}_K$:

$$\vec{\Omega} = k_\Omega \vec{\Omega}_K, \quad |\vec{\Omega}_K| = \sqrt{\frac{GM}{(2A)^3}} \qquad (19)$$

where $M = M_1 + M_2$. In close binaries, the tidal distortion of a star by its companion gives rise to a perturbation of the external gravitational field which in turn causes a secular motion of the line of the apses (Stern 1939):

$$\frac{d\omega}{dt} = \left(\frac{R_1}{A}\right)^5 \Omega_K q k_2 15 (1-e^2)^{-5} \left(1 + \frac{3e^2}{2} + \frac{e^4}{8}\right) \qquad (20)$$

where $q = M_2/M_1$ is the ratio of component masses, $e$ is the orbital eccentricity, $\omega$ is the longitude of the periastron. The apsidal-motion constant $k_2$ depends on the internal structure of the star and measures the extent to which mass is concentrated towards the stellar center. For the preMS stars along their vertical part of the evolutionary track the apsidal-motion constant is typically of the order of $10^{-1} - 10^{-2}$. For systems with circular orbits this means that the angular velocity higher than the Keplerian angular velocity (i.e. $k_\Omega > 1$). To estimate parameter $k_\Omega$ one can use the following formula

$$k_\Omega = 1 + \frac{0.22 q^{7.71}}{32.13 q^{7.46} + \ln(1 + q^{6.48})}. \qquad (21)$$

This formula is correct in case if the orbital eccetntriciry is zero, the primary component fill its Roche lobe, the secondary component is point mass and the ratio of specific heats $\gamma$ equals to 5/3.

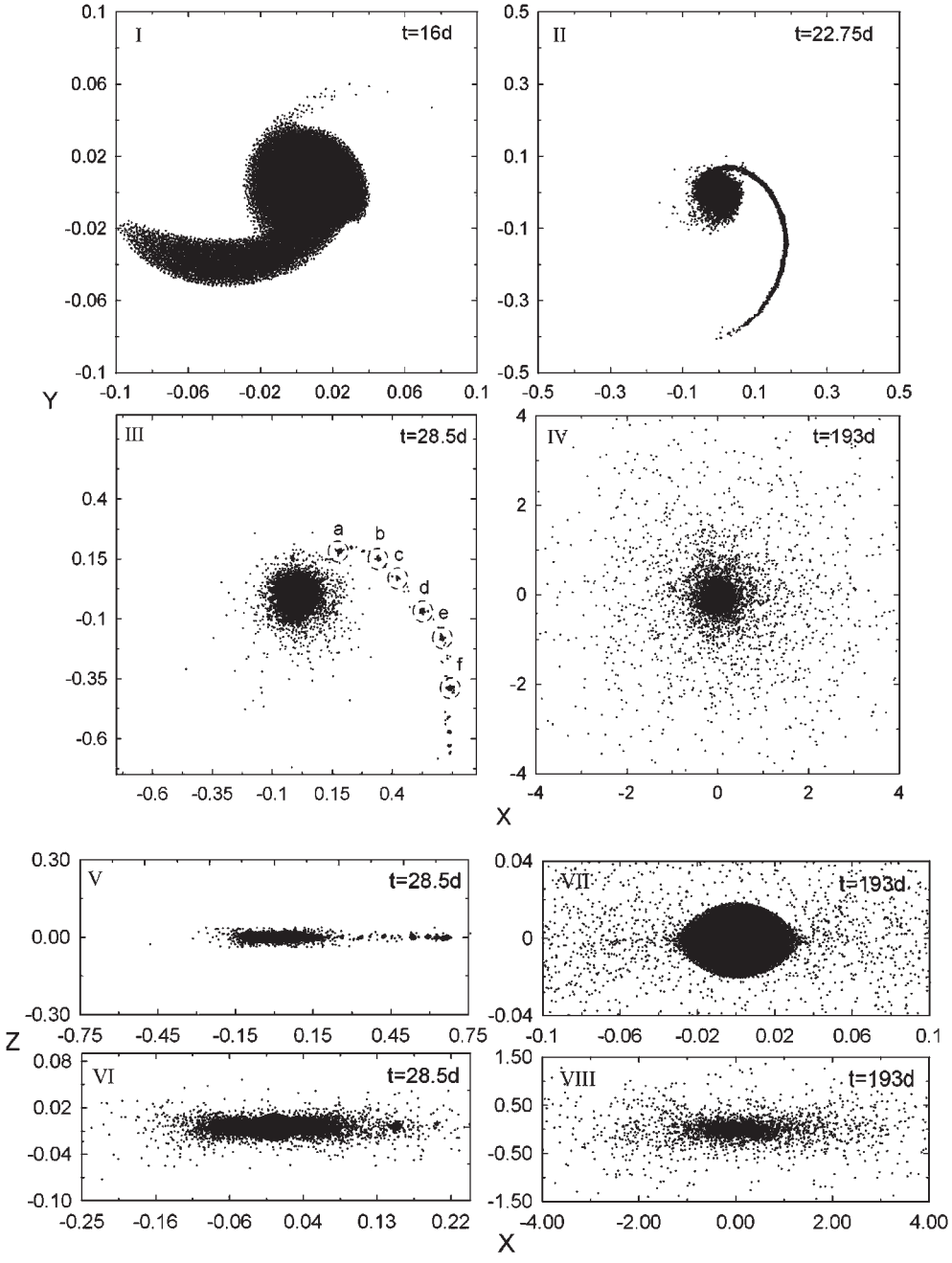


Figure 2: There are particle positions at the various moments of time in the orbital plane (I-IV), and in the XOZ plane(V-VIII). The dotted line on the figure (III) border the formed clouds. The moment of time is marked on each figure. Distances are in units of a.u.

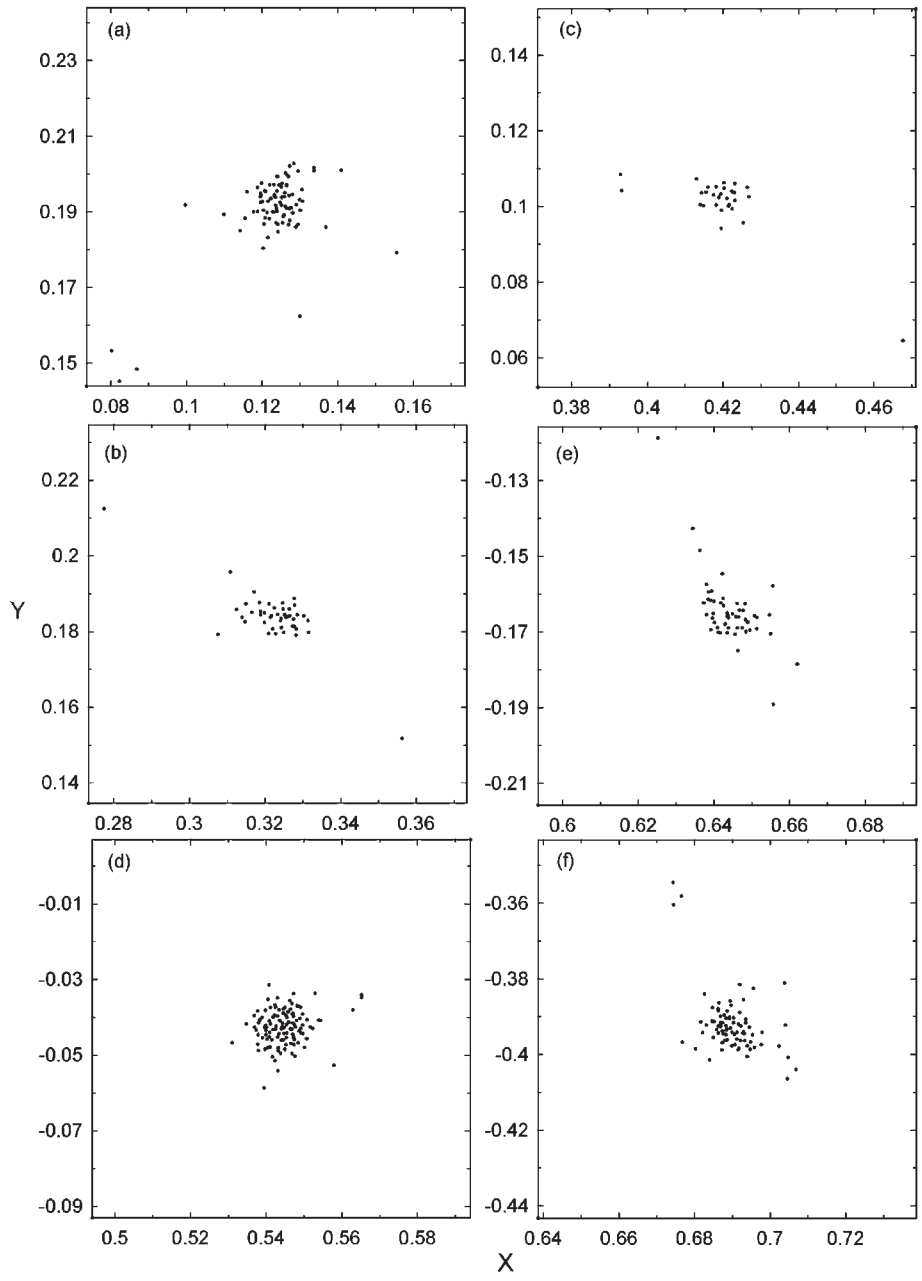


Figure 3: The particle positions which correspond to formed clouds. The marking of pictures corresponds to the marking of clouds on fig. 2.III.

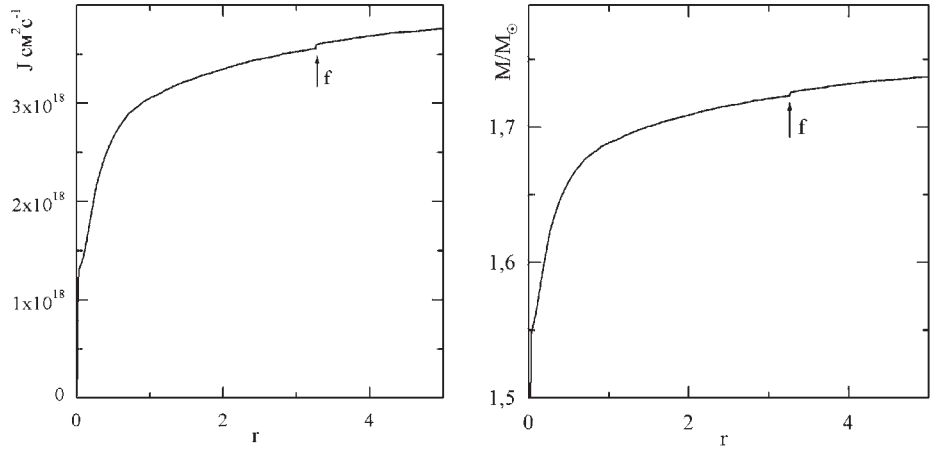


Figure 4: Left figure is angular moment - radius distribution in the orbital plane. Right figure is mass - radius distribution in the orbital plane. Radius is in units of a.u.

### 3. Results

We choose the following limits of binaries parameters which satisfy the observation data and at which the merging of binary star are probably:

1. The age of binary star should be less, or is comparable with the age of such Tauri stars.
2. The binary's mass is $M_{1,2} < 1.5M_\odot$
3. The ratio of component masses is in the range of $0.5 < q < 1$.
4. The specific angular moment is about $10^{18} - 10^{19}$ $cm^2c^{-1}$
5. The semiaxis is $A < 7.3R_\odot$
6. The binaries components should be close to filling its Roche lobe.

| Cloud marking | Mass ($M_J$) | semiaxis | eccen. |
|---|---|---|---|
| a | 3.16 | ... | ... |
| b | 1.69 | ... | ... |
| c | 1.14 | ... | ... |
| d | 4.26 | 0.3 | 0.5 |
| e | 2.02 | $\sim 0.5$ | 0.6 |
| f | 2.98 | $\sim 3$ | 0.6-0.7 |

Table 1: Some clouds parametrs. See fig 2.II

The calculation with the following parameters of binary star was performed: $M_1 = 0.9M_\odot$, $M_2 = 0.85M_\odot$, $R_1 = 4.6R_\odot$, $R_2 = 4.4R_\odot$, $A = 6R_\odot$. The primary component was approximated using $Np = 27000$ particles and secondary component $Ns = 3000$ particles. Size of the smoothed length for a primary component is $h_p = 0.045R_1$ and for secondary component is $h_s = 0.045R_2$

The integration was performed up to the moment of time $t = 220d$ with an average time step $\Delta t = 3d$. The mass transfer will begin at the time moment $t = 3d$, when components are in the periastron. Through 4-5 periods the rate of mass transfer grows so, that the primary component begins to overflow its Roche cavity. The matter of the primary component begins to flow out of the Roche cavity through an external La-grange point, forming the spiral arm (fig. 2,I-VI).

The most part of primary component matter accrete by the secondary component. The rest of the matter forms the circumstellar disk, which is $\sim$ 12% of the system mass.

The spiral arm divides on clouds of planetary ($< 5M_J$) masses. The masses of these clouds depend on distance up to the central star (see tab. 1, fig. 2.II).They are on the orbits with high eccentricity $e > 0.3$. The most of these clouds accrete on the star or become a part of circumstellar disk. The direction of clouds rotation coincides with a direction of star rotation. The disk has radius is approx 4 a.u. The inner layers of the disk matter (closer to the star) are on circular orbits, and the external layers are on the eccentric orbits. As a result of circumferential pressure, which arises at friction of adjacent cylindrical layers rotating with different angular velocities, the transfer of mass and angular moment in a radial direction exists. Destruction and accretion to the disk of the formed clouds results an increase of velocity of radial expansion of the disk. The direction of the disk rotation coincides with a direction of teh star rotation. Disk and clouds contain 12 % of the system mass and 64 % of the angular moment of the system (see fig. 4). Mass of the formed star is $1.54M_\odot$, equatorial radius is $6.5R_\odot$. The relation of polar radius to equatorial radius is approx 1/2.

The specific angular moment of system is $3.86 \cdot 10^{18}$ and was invariable during integration. The full system

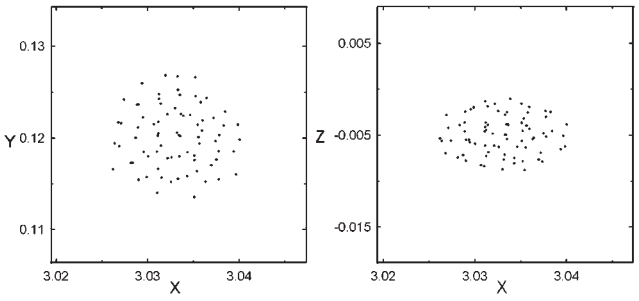


Figure 5: There is particle positions for the cloud "$f$"on the orbital plane $t = 220d$.

energy has changed less than 1% from its initial value.

## 4. Conclusion

1. As a result of a merge of the binary star, consisting from low mass preMS of stars, the basic structures of planetary systems can be formed: the central star, the circumstellar disk and compact cloud of the planetary masses.

2. Clouds are formed occurs in time about hundreds orbital periods of initial binaries from the spiral arm, formed during merging.

3. The clouds are on the orbits with semiaxis $< 5$ a.u. and high eccentricity. Masses of clouds are 2 - 5 $M_J$, that is in the good agreement with masses of observed planets.

4. For an explanation of the observable super planets eccentricity is not required of additional mechanisms. It is possible to explain this eccentricity as residual from received at the moment of clouds formation. The initial eccentricity can be reduced by dissipation of kinetic energy in the tides and interaction of clouds with disk.

5. A star devours embryos that form in the spiral arm, resulting in bursts of luminosity. This explains the variations of luminosity of a class of young stars known as the FUOrs.

## References

Duquennoy A. & Mayor M.: 1991, *Astron. Astrophys.*, **248**, 485.

Köhler R. & Leinert Ch.: 1998, *Astron. Astrophys.*, **331**, 997.

Masevich A.G., Tutukov A.V.: 1988, *Evoliutsija zvezd: teorija i nabliudenija.*

Tutukov A.V.: 2002, *Azh*, **79**, 762-767.

Popova E.I., Tutukov A.V., Yungelson L.R.: 1982, *Sov. Astron. Lett.*, **8**, 160-162.

Stahler S.W., Palla F.: 1993, *Astrophys. J.*, **418**, 414-425.

Krajcheva Z.T., Popova E.I., Tutukov A.V., Yungelson L.R.: 1978, *Azh*, **55**, 1176-1189.

Haisch K.E., Lada E. A.: 2001, *Astrophys. J.*, **533**, L153-156.

Lucy L.B.: 1977, *Astron. J.*, **82**, 1013.

Gingold R.A., Monaghan J.J.: 1977, *Mon. Not. R. Astron. Soc.*, **181**, 375-389.

Monaghan J.J.: 1992, *Annu. Rev. Astron. Astrophys.*, **30**, 543-574.

# THE DETERMINATION OF PERIODS AND THE DEFINITION OF VARIABILITY TYPE OF NEW VARIABLE STAR IRAS 17583+5150

A.P. Solonovich, I.S. Bryukhanov

Amateur group of variable stars observers "Betelgeuse",
the Republic Center of Technical Creativity of Pupils,
Makaionak street, 12, Minsk 220023 Belarus, *betelgeize_astro@mail.ru*

ABSTRACT. The measurements of brightness of the star IRAS 17583+5150 discovered using the Odessa observatory negatives are discussed in the article. The proposed types of these stars are IRAS 17583+5150 – type SRB (SRC).

**Key words**: Variable Star, type SRB (SRC).

### The history of research

The analysis of photo-electric measurements series of "HIPPARCOS" experiment allowed Roger W. Sinnott to state in the electronic version of "Sky & Telescope" magazine that the new variable star GV Dra is of EA type (Sinnott, 2000a; 2000b). The same assumption has also been made by Sergey E. Guryanov in the "Zvezdochet" magazine. While measuring the brightness of the star GV Dra Ivan S. Bryukhanov using the Odessa Photocollection negatives discovered optical variability of the star Tyc 2 3523 1519 1 or alternatively IRAS 17583+5150 or else IRC+50275 or HD 164645. Viewing in the Minsk Photocollection negatives (MPPLF) in V rays Alexander P. Solonovich confirmed the variability of the star IRAS 17583+5150.

### IRAS 17583+5150

Ivan S. Bryukhanov has discovered optical variability of the star Tyc 2 3523 1519 1 (or alternatively IRAS 17583+5150 or else IRC+50275 or HD 164645, spectrum Mc) in the Odessa Photocollection negatives. The measurements were carried out using only the negatives of the Odessa observatory where the maximal amplitude of star brightness fluctuations is 7.4m–8.9m in V rays. The map and the stars for comparison in a visual range for IRAS 17583+5150 (fig. 1).

Ivan S. Bryukhanov's visual estimations of brightness of the star IRAS 17583+5150 were carried out using Neiland-Blazko method in 567 photographic plates.

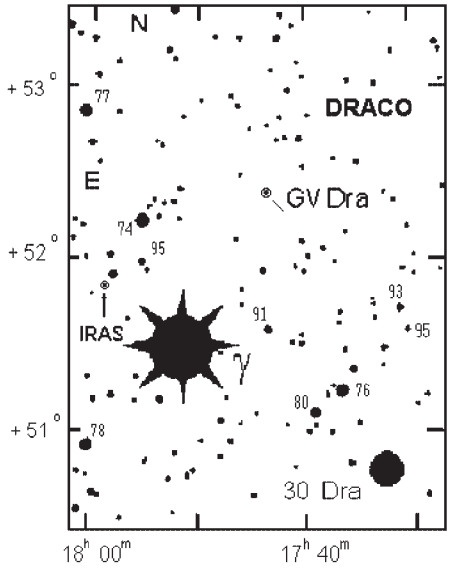


Figure 1: Map and stars of comparison IRAS 17583+5150 and GV Dra (Sinnott, 2000a; 2000b)

The determination of period or cycles of star brightness fluctuations was carried out by Ivan S. Bryukhanov using Lafler-Kinman method.

Taking into account the instability of star brightness fluctuations Ivan S. Bryukhanov applied the method of "cutting" the whole set of measurements into separate smaller intervals with the view of determining the brightness fluctuations periodicity.

The set of measurements of star brightness was divided by the researcher into 2 intervals: the early observations from 2436432 to 2441898 JD, the amplitude of fluctuations is from 8.m1 up to 8.m9 in V rays; the observations from 2442243 to 2449221 JD, the amplitude of fluctuations is from 7.m4 up to 8.m7 in V rays.

In the interval from 2436432 to 2441898 JD shorter intervals were taken for the determination of brightness

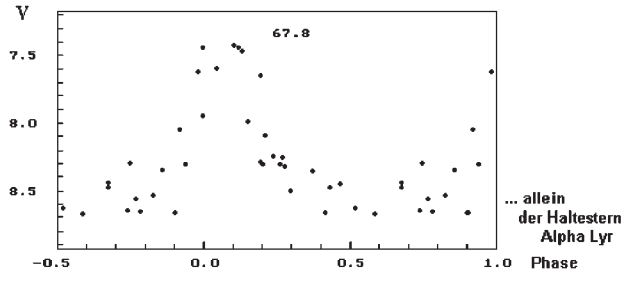


Figure 2: 2442573–2445879 J.D.

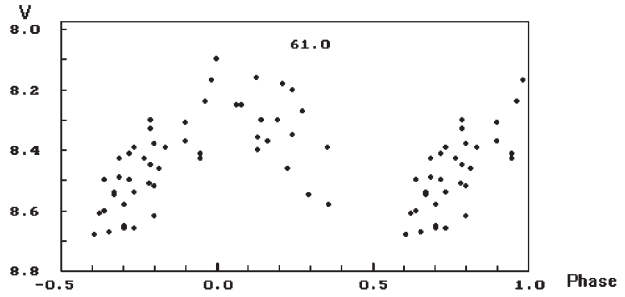


Figure 3: 2436779–2437173 J.D.

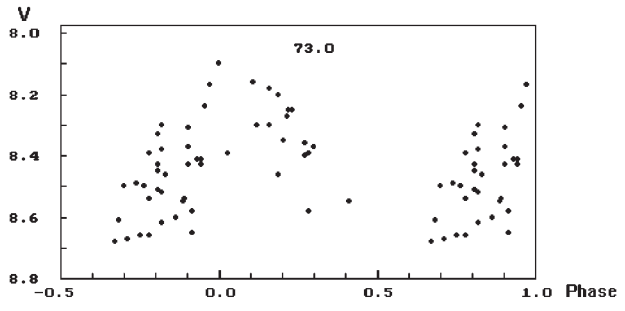


Figure 4: 2436779–2437173 J.D.

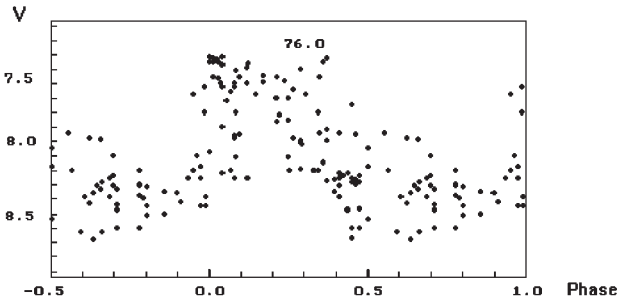


Figure 5: 2444694–2447022 J.D.

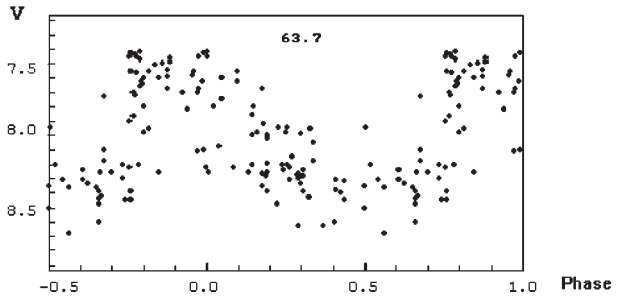


Figure 6: 2444694–2446655 J.D.

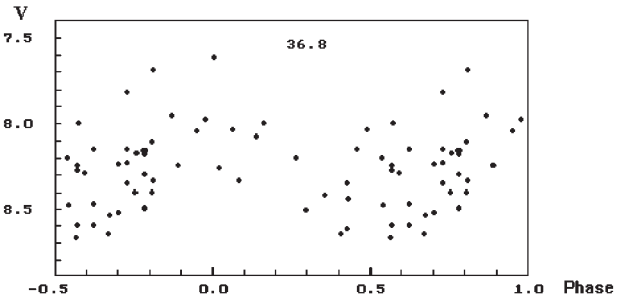


Figure 7: 2446936–2448036 J.D.

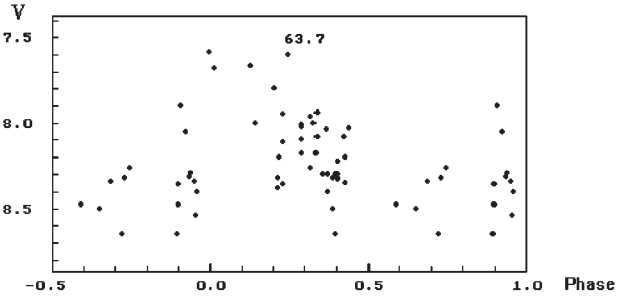


Figure 8: 2448061–2449221 J.D.

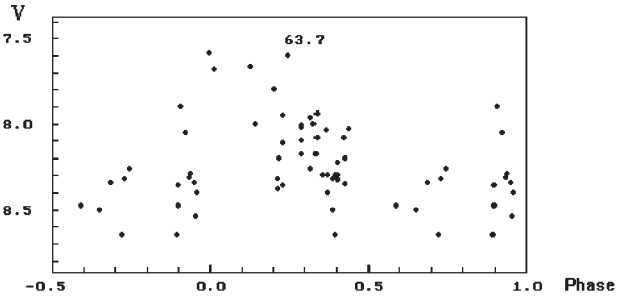


Figure 9: 2442573–2445879 J.D.

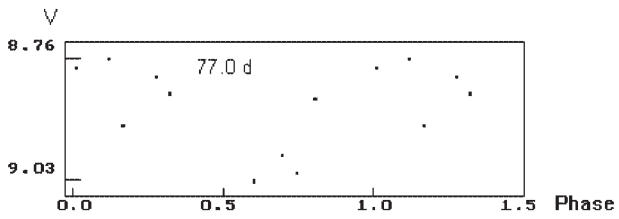


Figure 10: 2449840–2450201 J.D.

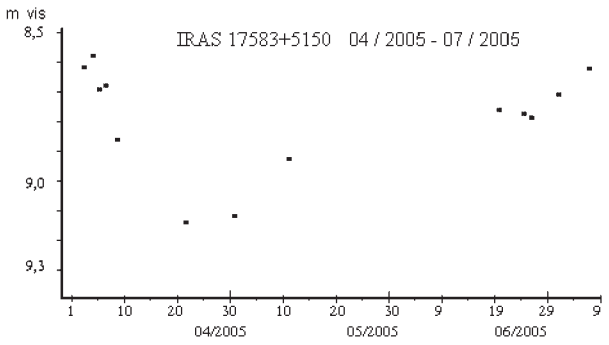


Figure 11: Observer Ivan S. Bryukhanov

fluctuations cycles of IRAS 17583+5150:

- 2436779–2437173 J.D. The cycle 61,0 d is clearly observed; possible cycles are 52,0 d and 73,0 d.

- 2437079–2437173 J.D. The cycle 65 - 66 d. is clearly observed.

In the interval from 2442243 to 2449221 JD shorter intervals were taken for the determination of brightness fluctuations cycles of IRAS 17583+5150:

- 2442243–2444052 J.D. Chaotic brightness fluctuations (?) or cycles 227 d (?) and 21.5 d (?) can be also observed.

- short interval 2444694–2446655 J.D. The cycles 63.7 d, 76.0 d are observed.

- 2446936–2448036 J.D. Chaotic brightness fluctuations (?) or cycle 36,8 d (?) are observed.

- 2448061–2449221 J.D. The cycle 63,7 or 66 d is clearly observed.

The conclusion is that the most clearly observed in different intervals of measurement series is the cycle 65±10 days, and these cyclic fluctuations are sometimes interrupted by chaotic brightness fluctuations.

The 8 most successful diagrams of brightness fluctuations of IRAS 17583+5150 in V rays in different time intervals are given below (fig. 2, 3, 4, 5, 6, 7, 8, 9):

Visual estimations with the use of the Minsk Photocollection negatives (MPPLF) in V rays carried out by Alexander P. Solonovich resulted in his obtaining in the interval 2449840–2450201 J.D. the diagram of change in brightness fluctuations of IRAS 17583+5150 with the cycle 77 d. within 8.6–9.1 V limits (fig. 10). A visual patrol of IRAS 17583+5150 was carried out by Ivan S. Bryukhanov in April–July 2005 (fig. 11.)

Long and exact photo-electric and visual measurements of IRAS 17583+5150 brightness are required for confirmation or refutation of variability type.

*Acknowledgements.* We are thankful to Nikolai N. Samus, Valentin G. Karetnikov, Alexandr I. Pichun and Tatyana V. Puzevich for consultations and help in work.

**References**

Gur'yanov S.E.: 2000, *Zvezdochet*, **4**.

Lafler J., Kinman T.D.: 1965, *Ap. J. Suppl.*, **11**, 216.

Sinnott R.W.: 2000a, http://skyandtelescope.com/observing/objects/variablestars/article_291_1.asp.

Sinnott R.W.: 2000b, http://skyandtelescope.com/observing/objects/variablestars/article_292_1.asp.

# THE QUEST FOR DISCOVERING EXTRAGALACTIC CEPHEIDS

László Szabados

Konkoly Observatory, Hungarian Academy of Sciences,
H-1525 Budapest XII, PO Box 67, Hungary, *szabados@konkoly.hu*

ABSTRACT.

Chronology of studying extragalactic Cepheids is summarized, and the census of known classical Cepheids and their metal-deficient siblings, the anomalous Cepheids is taken. Up to now (August 2005) about 11000 Cepheids have been revealed in 74 galaxies. Cepheids belonging to the Milky Way galaxy only represent about 6 per cent of the total Cepheid sample.

**Key words**: Stars: variable: Cepheid; Stars: variable: extragalactic

## 1. Introduction

Cepheid variables have been in the forefront of observational astronomy for more than two centuries. The first Cepheids were discovered in 1784 when Edward Pigott (1785) revealed variability in the brightness of $\eta$ Aquilae and John Goodricke (1786) pointed out periodic changes in the brightness of $\delta$ Cephei.

One century later, astrophotography became an efficient tool for searching for brightness variability of stars. From 1891 on, hundreds of Cepheids were found in the Magellanic Clouds, based on photographic observations carried out at the Harvard Southern Station in Arequipa (Peru). These historic observations led to the discovery of the famous period-luminosity relationship. Existence of this P-L relation raised Cepheids among the primary distance indicators in establishing the cosmic distance scale.

Another important consequence of these photographic observations is that more Cepheids have been known in either Magellanic Cloud than in our own Galaxy from the beginning of the 20th century. For the sake of historical truth, however, one has to keep in mind that the Magellanic Clouds were not considered to be external galaxies until Edwin Hubble's discovery about nature of the "spiral nebulae". Hubble's seminal result was also achieved with the help of Cepheid variables.

The first external galaxies beyond the Magellanic Clouds known to contain Cepheid variables were M31 and M33 (Hubble 1925a), and NGC 6822 (Hubble 1925b). Discovery of Cepheids in more remote galaxies was extremely difficult in the subsequent decades because those variables had to be detected near the magnitude limit of the photoplates, even if involving the largest available telescopes in the search.

Nearly coinciding with the two hundredth anniversary of discovering the first Cepheids, a new and much more efficient (with respect to photography) wide-field imaging was introduced in astronomy: the CCD era commenced.

In addition to the CCD technique, Hubble Space Telescope (HST) gave another impetus to the projects aimed at discovering and studying extragalactic Cepheids. One of the Key Projects to be carried out with the HST was the determination of the Hubble constant via the precise calibration of the P-L relationship for Cepheids and involving various secondary distance indicators. The detailed description of this calibration and the actual value of the Hubble constant are beyond the scope of this paper, the interested reader is referred to the summary paper by Freedman et al. (2001).

Besides this Key Project, another major survey was performed during the first decade of the operation of the HST. In this project the Hubble constant was determined by calibrating the absolute magnitude of Type Ia supernovae, and the distance to the host galaxies was derived from the Cepheids revealed in the galaxies studied. The final review of this HST related experiment (carried out by Saha, Tammann, Sandage, and their co-workers) is forthcoming.

Researchers dealing with Cepheids concentrated on the reliable calibration of the P-L relation, properly correcting for interstellar extinction (both foreground and in the host galaxy), and metallicity dependence of the Cepheid luminosities, and no survey was published on the census of known Cepheids in the last decade. The latest summary on the observations of extragalactic Cepheids (Jacoby et al. 1992) contains only information available before the launch of the HST.

A state-of-the-art compilation on the census of extragalactic Cepheids has been, therefore, long overdue. Authors of research papers on Cepheids, being unaware of the exact value, usually seriously underestimate the number of galaxies known to contain Cepheids, if such information is mentioned at all.

## 2. Census of classical Cepheids

For the time being, Cepheids are known in 74 galactic systems. Table 1 is a chronology of finding the first Cepheids in various host galaxies.

In Table 1, the main eras of Cepheid discoveries are separated by horizontal lines. The *classic era* terminated with Hubble's discoveries was followed by a long gap. In the *second* flourishing period Cepheid-hosting galaxies were added to the list at an average rate of one galaxy every second year. The *third era* of extragalactic Cepheid discoveries commenced with the use of HST. It has to be emphasized, however, that ground based optical telescopes were also efficiently used for finding new Cepheids in external galaxies, so the increased rate – about 3 additional galaxies each year (!) – is not solely due to the use of the HST. Quite recently, however, the role of the HST is diminishing in the Cepheid discovery projects.

Some other key events in studying extragalactic Cepheids are also mentioned in Table 1. These remarks appear in brackets following the designation of the relevant extragalactic system. Such milestones are the early discovery of the first anomalous Cepheid (1950), finding the first Cepheids beyond the Local Group (1968), the first Cepheids revealed by applying CCD technique (1986), and the first Cepheids found in the Virgo Cluster (1994).

Nowadays, the new intention of the Cepheid surveys is to reveal as many Cepheids as possible in the nearest galaxies (of various metallicity), in order to carry out a reliable determination of the P-L relationship and to study its universality and dependence on chemical composition. It is, therefore, the number of extragalactic Cepheids which shows an enormous increase recently, instead of the number of the Cepheid-bearing galaxies. Two major optical wide field surveys contributing to the increase of the known extragalactic Cepheids are the projects DIRECT (see Bonanos et al. 2003, and references therein) and Araucaria (Pietrzynski and Gieren 2004).

In order to take a census of known Cepheids, a thorough search was performed in the Cepheid related literature. The results have been summarized in a separate table (posted during the conference). An updated version of the full table will be published in a monograph on Cepheids to be published by Springer (Szabados 2007). That comprehensive table contains information on the number of known Cepheids, the type of the host galaxy, and its membership in galaxy aggregation.

This census was taken for *classical* (i.e. Population I) and the so-called *anomalous Cepheids*. According to the recent evolutionary and pulsation model calculations (Caputo et al. 2004), the anomalous Cepheids are the extreme metal-deficient counterparts of the classical Cepheids. Anomalous Cepheids have been found in numerous dwarf spheroidal galaxies of the Local Group, and also in the metal-poor subsystems of several nearby galaxies which contain classical Cepheids. Owing to their short (0.4-2.4 day) pulsation period, anomalous Cepheids are of lower luminosity than the classical Cepheids which typically pulsate with a longer period. The current photometric magnitude limit does not allow to find anomalous Cepheids beyond the Local Group.

The other varieties of Cepheids have been disregarded here. Type II (formerly Population II) Cepheids clearly differ from classical and anomalous Cepheids in their general properties (mass, internal structure, evolutionary phase).

A shortcoming of this census is that the actual number of known classical Cepheids cannot be given exactly for the nearest galactic systems: in the case of our own Galaxy and the two Magellanic Clouds a lower limit can only be given.

As to the Milky Way galaxy, the problem is caused by the ambiguity hidden in the classification scheme: the known Galactic Cepheids are divided into 6 groups according to the typological classification used by the GCVS: DCEP, DCEPS, CEP, CEP(B), CWA, and CWB. Types DCEP and DCEPS are classical Cepheids of normal and small amplitude, respectively, while double mode (beat) Cepheids belong to the CEP(B) type. When taking the census of Galactic Cepheids, only variables classified as DCEP, DCEPS, and CEP(B) have been considered as classical Cepheids. CWA and CWB stars which denote Type II Cepheids, obviously are not considered here. Stars classified as CEP are, however, problematic because the available information does not allow to decide whether they belong to classical or Type II Cepheids – or they are Cepheids at all. It would be, therefore, unjustified to include them among the classical Cepheids in the census, irrespective of the fact that majority of them may be insufficiently studied classical Cepheids.

The number of known Galactic classical Cepheids was determined from the electronic version of the GCVS, taking into account some recently published additional information. V1359 Aql, V382 Car, V641 Cen, and AF Cru classified as classical Cepheids have been excluded because they turned out not to be Cepheids recently. Moreover, V553 Cas is in fact a classical Cepheid (Berdnikov et al. 1996) misclassified in the GCVS. Evidently several Cepheids in the constellation Doradus, Hydrus, and Tucana located in fact in the Magellanic Clouds have been disregarded. The two known anomalous Cepheids in our Galaxy, BL Boo and XZ Ceti, have been also taken into consideration. Thus the total number of known classical and anomalous Cepheids in our Galaxy is 605. Classification for additional 321 variables (indeterminate types CEP and CEP:) as Cepheids needs confirmation.

Table 1: Chronology of finding the first Cepheids in various host galaxies

| Year | Galaxy |
|---|---|
| 1784 | Milky Way |
| 1904 | Small Magellanic Cloud, Large Magellanic Cloud |
| 1925 | NGC 6822, M31, M33 |
| 1950 | Sculptor (the first anomalous Cepheid) |
| 1967 | Ursa Minor |
| 1968 | NGC 2403 (first Cepheids beyond the Local Group), Leo II |
| 1971 | IC 1613 |
| 1976 | Draco |
| 1978 | Leo I |
| 1982 | Sextans A |
| 1984 | M81, NGC 300 |
| 1985 | Fornax, Sextans B, WLM |
| 1986 | M101 (first Cepheids revealed by CCD-photometry), Carina |
| 1988 | NGC 247, NGC 3109, NGC 7793 |
| 1990 | NGC 147, NGC 185, DDO 216 |
| 1992 | NGC 205, IC 4182 |
| 1994 | NGC 4571 (first Cepheids in Virgo Cluster), NGC 5253, DDO 69 |
| 1995 | M96, NGC 2366, DDO 155, Sagittarius, Sextans |
| 1996 | M100, NGC 925, NGC 4496A, NGC 4536, NGC 4639, IC 10 |
| 1997 | M95, NGC 3621 |
| 1998 | NGC 2090, NGC 2541, NGC 4414, NGC 7331, DDO 50, DDO 187 |
| 1999 | M66, M91, M106, NGC 1326A, NGC 1365, NGC 3198, NGC 3319, NGC 4535, NGC 4603, NGC 4725 |
| 2000 | NGC 1425 |
| 2001 | NGC 2841, NGC 3982, NGC 4527 |
| 2002 | IC 342, And III, And VI |
| 2003 | M83, NGC 1637 |
| 2004 | NGC 4395, And II, Phoenix |
| 2005 | NGC 3370 |

Strangely enough, the classification is easier for extragalactic Cepheids. This situation is due to the fact that photometric data bear information on the shape of the light curve (whose knowledge may not be enough for an adequate classification) and on the mean brightness of the star. Unaware of the distance to an individual Galactic Cepheid, its luminosity cannot be deduced from the photometric data alone. For an extragalactic Cepheid, however, the known distance of the galaxy and the mean brightness of the star allow the determination of the luminosity of the Cepheid, and from the known P-L relationships one can decide whether this value corresponds to a classical or a Type II Cepheid. As to anomalous Cepheids, the situation is not so easy, because their lower luminosity makes their identification more difficult in external galaxies.

Census of the Cepheids in both Large and Small Magellanic Clouds is also uncertain. Ambiguity in the number of Cepheids belonging to Magellanic Clouds is caused by a reason different from the case of our Galaxy. Being the nearest extragalactic systems known to contain Cepheids, Magellanic Clouds are very popular targets, and several major observational projects were carried out without cross-identifying the hundreds of new Cepheids discovered in these independent surveys. The number of Cepheids found and studied in the main microlensing projects is listed in Table 2. Prior to these microlensing projects, 1169 variables were classified as classical Cepheids by the editors of the GCVS in the LMC, and 1167 classical and 35 anomalous Cepheids have been catalogued in the SMC. The huge number of the Magellanic Cepheids (and the small number of the indeterminate Cepheids) is mainly due to Henrietta Swan Leavitt's and the two Gaposchkins'

Table 2: Number of Cepheids discovered/studied in the Magellanic Clouds during the major microlensing projects

| Project | Cepheids in LMC | SMC |
|---|---|---|
| EROS | 290 | 590 |
| MACHO | ∼1800 | ∼2000 |
| OGLE | 1335 | 2048 |

indefatigability. The MACHO data indicate that there are hundreds of anomalous Cepheids among the newly discovered variables in the LMC (Alcock et al. 1999). For denoting the anomalous Cepheids, the abbreviation BLBOO was introduced in the fifth volume of the latest edition of the GCVS, containing the extragalactic variable stars (Samus 1995).

A simple summation of the number of Cepheids ever discovered in either Magellanic Cloud would largely overestimate the actual number of known Cepheids because of the independent rediscoveries of many variables. It is known, for example, that the MACHO sample contains 551 Cepheids already discovered on the early Harvard plates (Alcock et al. 1999). Another example is given by Efremov (2003) who performed a careful cross-identification of the Cepheids discovered during various surveys in two open clusters of the LMC. Unfortunately a complete cross-identification of the Cepheids revealed by various microlensing projects is still missing, but the EROS team has tackled to this work. Taking a risk of mistake, I estimate that the number of known classical Cepheids is about 3000 in each of the Magellanic Clouds.

Ranking the galaxies according to their known Cepheid content, the record holder is the SMC, the second is the LMC, M31 is the third, M33 is the fourth, and the Milky Way Galaxy is placed only fifth. As a matter of fact, the number of known Cepheids in M31 obtained in the census may be a lower limit, too. An et al. (2004) published some important results of the POINT-AGAPE microlensing survey, and it is obvious from their Figure 8 that there are hundreds of Cepheids among the 35 000 variable stars detected in the Andromeda nebula. However, the incomplete information on these variables does not allow to include these Cepheids in the census.

By now (2005 August) *4273 Cepheids* have been detected *beyond the Magellanic Clouds*, 2144 of which are in Local Group member galaxies, and 401 Cepheids in various galaxies belonging to the Virgo Cluster. All these statistical data imply that *Galactic Cepheids represent about 6 per cent of the total Cepheid sample.*

This compilation clearly shows importance of the discovery and study of extragalactic Cepheids.

*Acknowledgements.* Compilation of the tables was largely facilitated by the use of the on-line databases SIMBAD (CDS, Strasbourg), and the NASA Astrophysics Data System. Financial support from the Hungarian OTKA grant T046207 is acknowledged. The author is indebted to the conference organizers for including this contribution in the scientific program of the meeting in the author's absence.

**References**

Alcock C., Allsman R. A., Alves D. R., et al. (The MACHO Collaboration) 1999, *AJ*, **117**, 920

An J. H., Evans N. W., Hewett P., et al. (The POINT-AGAPE Collaboration) 2004, *MNRAS*, **351**, 1071

Berdnikov L. N., Vozyakova O. V., & Ignatova V. V. 1996, *IBVS*, No. 4398

Bonanos A. Z., Stanek K. Z., Sasselov D. D., Mochejska B. J., Macri L. M., & Kaluzny, J. 2003, *AJ*, **126**, 175

Caputo F., Castellani V., Degl'Innocenti S., Fiorentino G., & Marconi M. 2004, *A&A*, **424**, 927

Efremov Yu. N. 2003, *Astron. Rep.*, **47**, 1000

Freedman W. L., Madore B. F., Gibson B. K., et al. 2001, *ApJ*, **553**, 47

Goodricke J. 1786, *Phil. Trans. R. Soc., London*, **76**, 48

Hubble E. P. 1925a, *Obs*, **48**, 139

Hubble E. P. 1925b, *ApJ*, **62**, 409

Jacoby G. H., Branch D., Ciardullo R., et al. 1992, *PASP*, **104**, 599

Pietrzynski G. & Gieren W. 2004, in Variable Stars in the Local Group, Proc. IAU Coll. 193, eds. D. W. Kurtz & K. R. Pollard, ASPC 310 (San Francisco: ASP), p. 87

Pigott E. 1785, *Phil. Trans. R. Soc., London*, **75**, 127

Samus N. N. (ed.) 1995, General Catalogue of Variable Stars, Vol. 5, Kozmosinform, Moscow

Szabados L. 2007, Cepheids, Springer

# IS POLARIS LEAVING THE CEPHEID INSTABILITY STRIP?

D. G. Turner

Department of Astronomy and Physics, Saint Mary's University
Halifax, Nova Scotia B3H 3C3, Canada, *turner@ap.smu.ca*

ABSTRACT. Although Polaris is generally regarded as an overtone pulsator that may soon switch to pulsation in the fundamental mode, it is argued that the variable is actually crossing the instability strip for the first time and is in the process of leaving the instability strip altogether. The luminosity of Polaris inferred from its optical F3 V companion, as well as from A, F, and G-type stars lying within a few degrees of it and populating a group main sequence coincident with that for Polaris B, is $\langle M_V \rangle = -3.07 \pm 0.04$ s.e., consistent with fundamental mode pulsation. The star's rate of period increase, 4.5 s yr$^{-1}$, is also consistent with predictions from stellar evolutionary models for a fundamental mode pulsator crossing the instability strip for the first time, and its location redward of strip center agrees with similar predictions supporting a bluer instability strip for such stars. The onset of a much-reduced and irregular pulsation amplitude that began shortly after 1963–1966, when there was a glitch in the star's O–C data, suggests that the process of leaving the instability strip may have begun at that time. High quality photometric and radial velocity data for Polaris show no evidence for a second periodicity in its light signal that might indicate overtone pulsation. In summary, Polaris seems most likely to be a Cepheid that is crossing the instability strip for the first time and is now beginning the lengthy process of departing the instability strip altogether.

**Key words**: stars: variable: Cepheids — stars: individual (Polaris).

## 1. Introduction

The North Star, Polaris ($\alpha$ UMi), as well as being the brightest and closest of 40 Cepheids visible without optical aid, is one of the most intriguing, extensively discussed, frequently studied, and perhaps misinterpreted objects in the sky. Its light variability was suspected a century and a half ago by Seidel (1852) and Schmidt (1857), as well as by Pannekoek in the 1890s (Pannekoek 1913), from visual comparisons with $\beta$ UMi, and was confirmed in a photographic study by Hertzsprung (1911). The light amplitude a century ago was small, only $0^{\rm m}.11 \pm 0^{\rm m}.01$, and has decreased in recent years. In the *General Catalogue of Variable Stars* it was originally listed as a Type II Cepheid, although it is definitely a Type I pulsator.

Many current ideas about the nature of Polaris are tied to the parallax derived for it by the *Hipparcos* mission (ESA 1997). But a recent investigation of the evolutionary period increase in the star reaches different conclusions (Turner et al. 2005). This paper summarizes the known properties of the star in order to clarify the true nature of the variable.

## 2. Companion Stars

Polaris is a stellar triple, with an unseen AF-type dwarf orbiting it every 29.6 yrs according to radial velocity observations, and an F3 dwarf, 19 arcsec distant, sharing its space motion (Kamper 1996; Weilen et al. 2000). Two fainter optical companions may also be part of the system, but would be of very late spectral type if *bona fide* members (Fernie 1966).

The optical companion to Polaris is an F3 V dwarf (Turner 1977) that can be used to establish the reddening and distance of the Cepheid (Gascoigne & Eggen 1957; Fernie 1966; McNamara 1969; Turner 1977; Turner 1984). But existing photometry for Polaris B is often contaminated by stray light from the much brighter Cepheid. Photometry by McNamara (1969) indicates that his data may be unaffected by that influence. He finds $V = 8.60$ for Polaris B, a result confirmed from CCD imaging by Kamper (1996).

Table 1: Properties of Polaris B.

| V | B–V | U–B | Data Source |
|---|---|---|---|
| ··· | 0.41 | ··· | Gascoigne & Eggen (1957) |
| ··· | 0.42 | 0.01 | Fernie (1966) |
| 8.60 | 0.41 | 0.01 | McNamara (1969) |
| 8.60 | ··· | ··· | Kamper (1996) |
| ··· | 0.42 | ··· | Turner et al. (2005) |
| 8.60 | 0.42 | 0.01 | Best Values |
| Sp.T. | F3 V | | Turner (1977) |

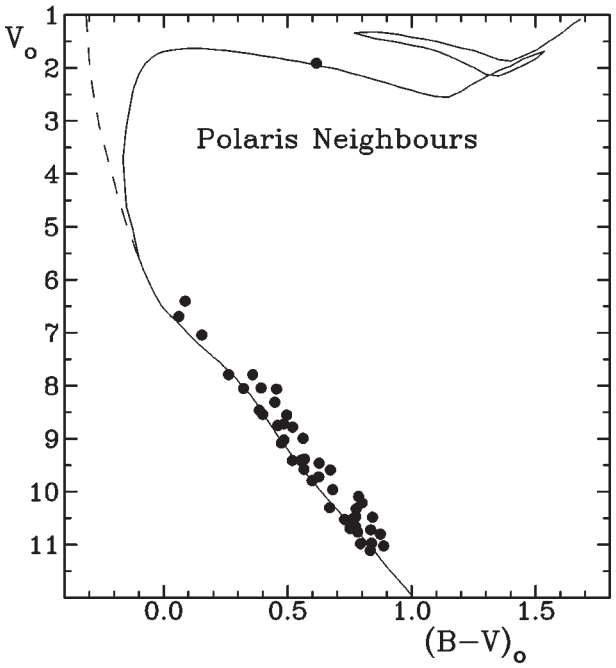


Figure 1: Unreddened colors and magnitudes for A, F, and G-type stars in the field of Polaris ($E_{B-V}$ = 0.02) along with a ZAMS fit for $V_0 - M_V = 4.98$. The isochrone corresponds to log $t$ = 7.9, the dashed line to the ZAMS.

Table 1 gives the results of a new analysis of existing photometry for the companion after adoption of $V$ = 8.60 for the star. Existing observations include the transformed $PV$ data of Gascoigne & Eggen (1957), Fernie's (1966) $UBV$ observations (by private communication) newly reanalyzed, McNamara's (1969) Strömgren photometry adjusted to the system of Schmidt (see Turner et al. 1987) and transformed to the $UBV$ system (Turner 1990), and new $BV$ observations obtained in connection with the study by Turner et al. (2005).

The various adjusted observations agree well, and in conjunction with the star's F3 V spectral type, imply a reddening of $E_{B-V}$ = 0.02 ± 0.01 s.e. and $V_0 - M_V = 5.02 \pm 0.07$ s.e. to the system, or $d = 101 \pm 3$ pc. The *Hipparcos* parallax for Polaris implies a larger distance of $d = 132 \pm 8$ pc, which is inconsistent with the adopted zero-age main-sequence (ZAMS) luminosity for Polaris B. The implied absolute magnitude for Polaris is $\langle M_V \rangle = -3.09 \pm 0.07$ s.e. as tied to the companion, and $\langle M_V \rangle = -3.68 \pm 0.14$ s.e. according to the *Hipparcos* parallax. The predicted luminosity for fundamental mode pulsation is $\langle M_V \rangle = -2.93 \pm 0.08$, and $\langle M_V \rangle = -3.40 \pm 0.08$ for first overtone pulsation (Turner 1992).

It may be possible to refine those estimates, since there is evidence suggesting the existence of a loose group of A, F, and G-type stars lying within three

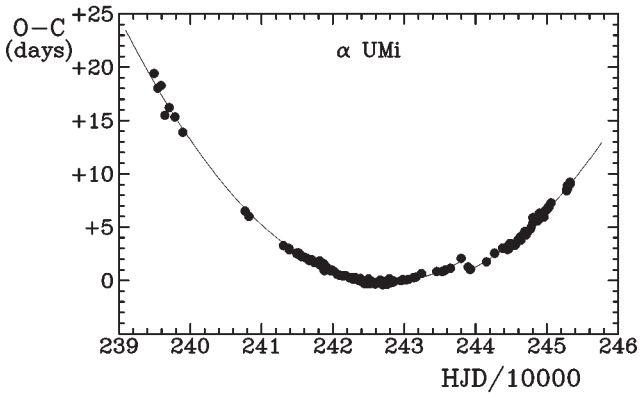


Figure 2: O–C data for Polaris from 1844 to 2004 obtained from the analysis of photometric and radial velocity observations and corrected for the star's orbital motion. The plotted curves depict the parabolic trend of the data resulting from evolutionary effects. A glitch occurs between 1963 and 1966.

degrees of Polaris that may constitute the remains of a sparse cluster containing the Cepheid (Turner et al. 2005). Polaris B is a very likely member of the group. The implied distance modulus for the cluster from ZAMS fitting of *Hipparcos* $BV$ data for likely group stars, including the results of Table 1 for Polaris B and adopting its reddening for the group, is $V_0 - M_V = 4.98 \pm 0.04$ s.e., or $d = 99 \pm 2$ pc, as illustrated in Fig. 1. The implied luminosity for Polaris is $\langle M_V \rangle = -3.07 \pm 0.04$ s.e., consistent with fundamental mode pulsation. The implied age of the group is $\sim 8 \times 10^7$ yr when Polaris is included as a member.

### 3. Period Changes

The rapid period changes in Polaris have a lengthy history (see Turner et al. 2005), and are consistent with a period increase amounting to 4.5 s yr$^{-1}$. Fig. 2 illustrates the regularity of the parabolic (evolutionary) trend in the O–C data once the times of maximum light and minimum radial velocity have been adjusted for light travel time in the unseen binary system and the displacement between light and radial velocity curves for the star (see Turner et al. 2005). The rate of period increase agrees closely with predictions from published stellar evolutionary models for a Cepheid crossing the instability strip for the first time (Turner et al. 2006), as illustrated in Fig. 3. The brief glitch in the O–C data between 1963 and 1966 is a puzzle, but, if attributed to the assimilation of a 7 Jovian mass planet, provides an additional argument that Polaris is a first crosser.

At roughly the same time as Polaris was experiencing a glitch in its pulsational period increase, the star's

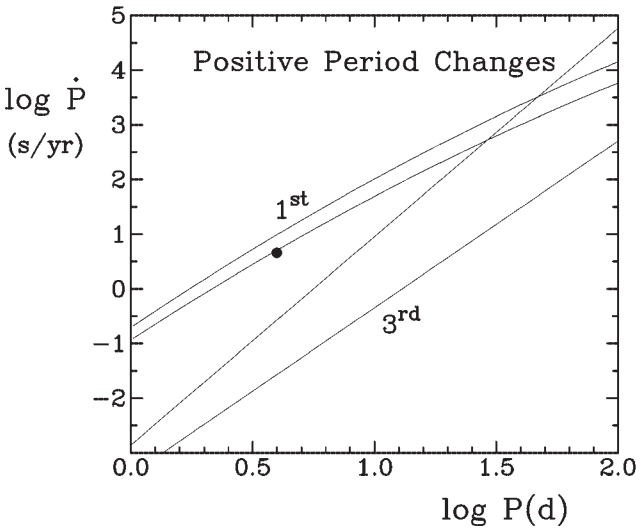


Figure 3: Expected period changes for Cepheids in first and third crossings of the instability strip as predicted from stellar evolutionary models. The bands denote the range of model predictions for the rates of period change, while the point is the observed result for Polaris.

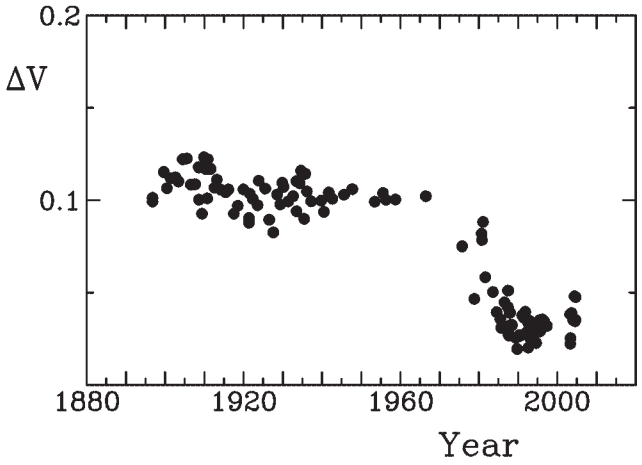


Figure 4: Observed secular trends in the amplitude of visual brightness variability for Polaris.

light amplitude began a marked decline from previous levels, as illustrated in Fig. 4. The light amplitude $\Delta V$ is presently irregular, and varies slowly on a cycle-to-cycle basis, but always at levels between $0^{\rm m}.02$ and $0^{\rm m}.05$ (Evans et al. 2004; Turner et al. 2005). The abrupt change in character of the star's pulsation amplitude around 1970 suggests that at that time it may have undergone a sudden change in the manner in which it is crossing the Cepheid instability strip.

The atmospheric composition of Polaris (Usenko et al. 2005) displays the usual characteristics of a gas that has been associated with hydrogen burning via the CNO cycle, but that cannot be tied to its instability strip crossing mode, for example by arguing that atmospheric contamination from the stellar core is produced by dredge-up during evolution through the red supergiant stage. As noted by Maeder (2001), the observed atmospheric signatures of CNO burning are found in many intermediate-mass stars near the terminal stages of hydrogen burning, and can be matched to models of meridional mixing in rapidly rotating stars. Additionally, many current stellar evolutionary models for intermediate-mass stars predict that convection in the outer layers of red supergiants does not penetrate deep enough to produce atmospheric contamination through dredge-up. The observed atmospheric signatures of CNO burning in Cepheids certainly display no obvious trends that can be tied to instability strip crossing mode (Turner & Berdnikov 2004).

## 4. Pulsation Mode

A number of factors have conspired to imply that Polaris is an overtone pulsator. First, the *Hipparcos* parallax implies a luminosity well in excess of that for fundamental mode pulsation. Second, the intrinsic color of Polaris for overtone pulsation places it on the blue side of the instability strip, consistent with the location of double-mode and overtone Cepheids. Lastly, arguments are made occasionally that the signature of incipient fundamental mode pulsation may be detected in its light and/or radial velocity variations.

Regarding the last point, observations of Polaris are notoriously difficult to obtain, and in most data samples one can find examples of spurious observations that may have deleterious effects on period-finding routines. Seasonal effects and the 29.6-yr orbital motion of Polaris about its unseen companion can also conspire to create alias periods in periodogram analyses for the star.

An exception appears in the tellurically-calibrated CCD eschelle radial velocity measurements of Kamper & Fernie (1998), which are of very high precision and accuracy. Fig. 5 presents a periodogram analysis of the *residuals* from Kamper & Fernie's measures after fitting the main signal to the known 4-day pulsation period of Polaris and accounting for seasonal effects on the zero-point for the measures as well as orbital motion about the companion. Kamper & Fernie cite a minimum uncertainty for the observations of about $\pm 0.004$ km s$^{-1}$, which is depicted by the level of the dotted line in Fig. 5. The frequencies corresponding to pulsation periods of 4 and 5.7 days are indicated, the latter being the appropriate period for fundamental mode pulsation if the observed periodicity is that for first overtone pulsation.

It can be seen that there is no residual signal in the data of any significance, particularly around a

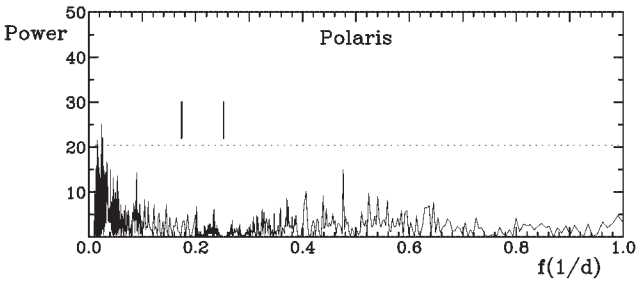


Figure 5: A periodogram analysis for the radial velocity observations of Kamper & Fernie (1988) adjusted for seasonal and orbital variations in zero-point and prewhitened by the removal of the sinusoidal 4-day periodicity in the data. The dotted line depicts the strength of a signal generated by uncertainties in the observations, and vertical lines denote the frequencies corresponding to periods of $5^{\rm d}.75$ (left) and $4^{\rm d}.00$ (right).

putative fundamental mode period of 5.7 days. The prewhitening of the radial velocity data is also seen to remove all evidence for the primary 4-day periodicity in the velocities. It seems clear that Polaris does not exhibit any unambiguous evidence for overtone pulsation, as also confirmed by the high precision photometric observations of the star by Evans et al. (2004) using the star camera on the *Wide Field Infrared Explorer* satellite.

## 5. Discussion

Taken together, all of the various observed characteristics of Polaris can be attributed to fundamental mode pulsation in a Cepheid that is crossing the instability strip for the first time and seems likely to be in the process of leaving it on the cool (redward) side. The intrinsic colors of Polaris place it slightly redward of center in the instability strip observed for other Galactic Cepheids, but outer-layer convection tends to damp out pulsation in first crossers much more efficiently than in stars in higher strip crossing modes (Alibert et al. 1999). There is therefore no ambiguity between the star's location in the H-R diagram and the conjecture that it is a first-crossing, fundamental-mode pulsator.

Of greater interest is the possibility of using Polaris as a Galactic calibrator for the Cepheid period-luminosity relation. The star's unique characteristics — closest and brightest Cepheid, one of only a few stars identified as likely first crossers, extremely small light amplitude, and imminent departure from the instability strip — distinguish it from all other Galactic Cepheids known to belong to open clusters. It therefore seems imperative to study the space motions of the stars around Polaris in order to establish if they are physically associated with the Cepheid, as is the case for its optical F3 V companion.

## References

Alibert, Y., Baraffe, I., Hauschildt, P., Allard, F.: 1999, *A&A*, **344**, 551.
ESA: 1997, *The Hipparcos and Tycho Catalogues*, ESA SP-1200 (ESA: Noordwijk).
Evans, N.R., Buzasi, D., Sasselov, D.D., Preston, H.: 2004, *BAAS*, **36**, 1429.
Fernie, J.D.: 1966, *AJ*, **71**, 732.
Gascoigne, S.C.B., Eggen, O.J.: 1957, *MNRAS*, **117**, 430.
Hertzsprung, E.: 1911, *Astron.Nach.*, **189**, 89.
Kamper, K.W.: 1996, *JRASC*, **90**, 140.
Kamper, K.W., Fernie, J.D.: 1998, *AJ*, **113**, 996.
Maeder, A.: 2001, *Ap&SS*, **277**, 291.
McNamara, D.H.: 1969, *PASP*, **81**, 68.
Pannekoek, A.: 1913, *Astron.Nach.*, **194**, 359.
Schmidt, J.F.J.: 1857, *Astron.Nach.*, **46**, 293.
Seidel, L.: 1852, *IIK1.D.K.Akad.Wiss.München*, **6**, 564.
Turner, D.G.: 1977, *PASP*, **89**, 550.
Turner, D.G.: 1984, *JRASC*, **78**, 229.
Turner, D.G.: 1990, *PASP*, **102**, 1331.
Turner, D.G.: 1992, *AJ*, **104**, 1865.
Turner, D.G., Berdnikov, L.N.: 2004, *A&A*, **423**, 335.
Turner, D.G., Leonard, P.J.T., English, D.A.: 1987, *AJ*, **93**, 368.
Turner, D.G., Savoy, J., Derrah, J., Abdel-Sabour Abdel-Latif, M., Berdnikov, L.N.: 2005, *PASP*, **117**, 207.
Turner, D.G., Abdel-Sabour Abdel-Latif, M., Berdnikov, L.N.: 2006, *PASP*, **118**, in press.
Usenko, I.A., Miroshnichenko, A.S., Klochkova, V.G., Yushkin, M.V.: 2005, *MNRAS*, **362**, 1219.
Weilen, R. Jahreiss, H., Dettburn, C., Lenhardt, H., Schwan, H.: 2000, *A&A*, **360**, 399.

# THE NATURE OF THE TYPE C SEMI-REGULAR VARIABLES

D. G. Turner

Department of Astronomy and Physics, Saint Mary's University
Halifax, Nova Scotia B3H 3C3, Canada, *turner@ap.smu.ca*

ABSTRACT. The type C semi-regular (SRC) variables are M-type supergiants like Betelgeuse that undergo regular periodic brightness fluctuations superposed upon seemingly irregular trends. Many of the 55 recognized Milky Way M-type supergiants belonging to the class are multi-periodic, with radial pulsation almost certainly the source of their primary short-period luminosity changes. Noted here are additional characteristics of the stars, not supplied in the GCVS, that can be recognized in their growing archival inventories: amplitude for both long-term and short-term light variability increasing with luminosity, regular changes in mean brightness possibly tied to evolution, and a period-luminosity relation in need of further observational corroboration. As the immediate stellar precursors to many Type II supernovae and as auxiliary standard candles for the extragalactic distance scale, SRC variables are in need of more extensive observational studies to elucidate their many intriguing properties.

**Key words**: stars: variable: other — stars: late-type.

## 1. Introduction

Semi-regular variables are defined in the *General Catalogue of Variable Stars* (GCVS, Kholopov et al. 1985) as luminous stars of late spectral type that exhibit noticeable periodicity in their light changes accompanied by variations of a more irregular type. Type C semi-regulars, or SRC variables, are a small subset of the class restricted to M-type supergiants, typically of luminosity classes Ia to II. They may be related to the LC class of slow irregular variables in the GCVS that also comprise late-type supergiants.

There are 57 SRC variables in the GCVS, and 72 LC variables, compared with 490 classical Cepheids and 188 Cepheids of uncertain classification. This order of magnitude difference in numbers evident in the GCVS does not reflect the true space densities of the two types of stars. According to Pierce et al. (2000) and Jurcevic et al. (2000), long period variables, and SRCs in particular, are much more common than Cepheids in most galaxies, are more luminous than Cepheids, and also obey a period-luminosity relation that makes them inherently valuable distance indicators. The problem is that red supergiants tend to be relatively little studied and less well understood than their yellow supergiant kin. Complete light curves are not available for many of them.

Cool M-type supergiants are fairly rare massive stars that display the physical properties of highly evolved objects with progenitor masses of less than about 20 $M_{\odot}$ according to stellar evolutionary models by Meynet et al. (1993). The upper luminosity limit is established by the fact that more massive stars cannot evolve into the red supergiant region, but remain as hotter stars until their eventual explosion as Type II supernovae. The upper limit to red supergiant masses and luminosities is a recognizable feature in the H-R diagrams for luminous stars in other galaxies (Humphreys 1987).

Although it is expected that all M supergiants will eventually explode as Type II supernovae (Chevalier 1981), two of the most spectacular such events in recent years, SN 1987A in the Large Magellanic Cloud and SN 1993J in M81, apparently originated from B3 I and G8-K5 I progenitors with masses of $\sim$18 $M_{\odot}$ and $\sim$17 $M_{\odot}$, respectively (Sonneborn et al. 1987; Aldering et al. 1994). Presumably there was some evolution towards the hot side of the H-R diagram prior to the explosions, although the details are uncertain. If expectations are correct for existing members of the M supergiant population of the Milky Way, then it seems essential to learn more about the role played by SRC variables in the late stages of stellar evolution, since they are the likely progenitors of many future Type II supernovae in the Galaxy. The rapid rate of evolution for massive M supergiants assures that such events will continue to occur in the not-too-distant future. A detailed knowledge of the properties of individual members of the SRC class may therefore have fairly immediate applications.

## 2. Observational Characteristics

Observational data on the light curves of SRC variables are often limited owing to the long temporal cycles in their brightness levels. The American Association of Variable Star Observers (AAVSO) maintains

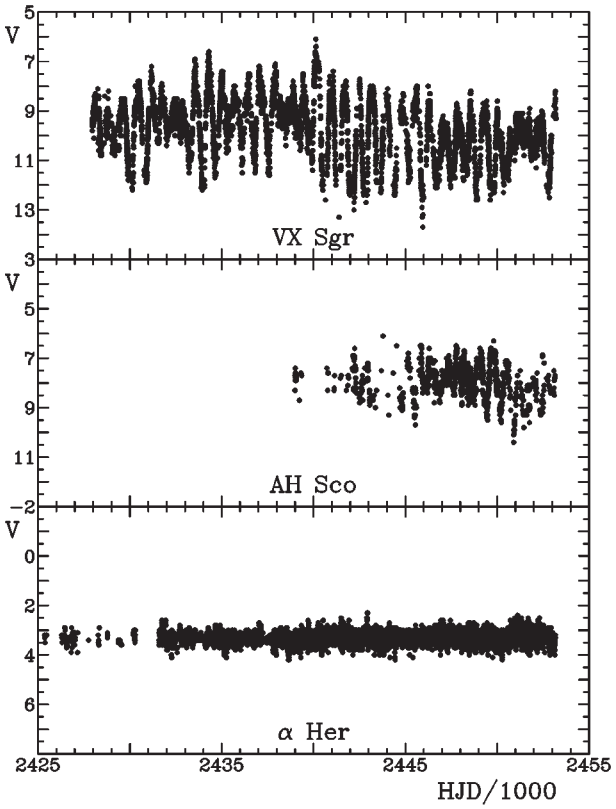


Figure 1: Light curves for the SRC variables VX Sgr, AH Sco, and $\alpha$ Her constructed from AAVSO visual observations (Waagen 2005).

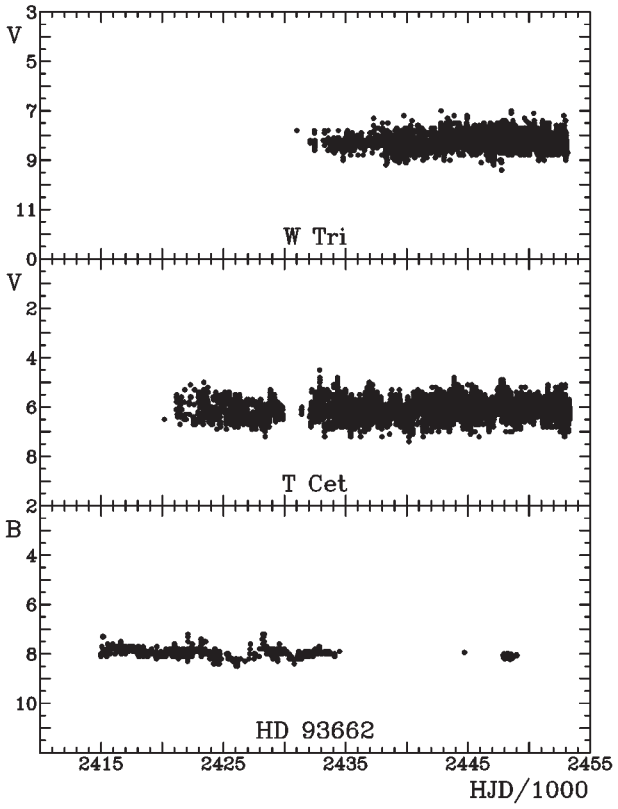


Figure 2: Light curves for the SRC variables W Tri and T Cet constructed from AAVSO visual observations (Waagen 2005), and for the bright M giant HD 93662 from photographic observations (Turner et al. 2005).

extensive databases for a large fraction of listed variables, and they provide instructive information about the light characteristics of individual class members.

Light curves, from Waagen (2005), are illustrated in Figs. 1 and 2 for a sample of SRC variables, all plotted at identical scales to illustrate the dependence of light amplitude on luminosity class for the stars. The nature of the amplitude dependence is illustrated in Fig. 3, and is tied to information available from AAVSO observers and spectral types in the GCVS. Note how light amplitudes increase as surface gravity decreases (towards type Ia supergiants, with emission-line Ia supergiants considered here to be more luminous), a natural consequence of an effect tied to the ability of radial pulsation to counteract the force of gravitational attraction at the star's surface.

Note in Fig. 1 the regular cyclical variations ($P = 757^{\rm d}$) of VX Sgr (M4-10 Iae) superimposed upon longer-term variations in mean light level. The regular cyclical variations ($P = 769^{\rm d}$) of AH Sco (M4-5 Ia-Iabe) are similar to those of VX Sgr, but of smaller amplitude. The star is also less luminous. The variations ($P = 116^{\rm d}$) in $\alpha$ Her (M5 Ib-II) are of small amplitude and the brightness level is essentially constant. The driving force for the variability is less effective against gravity in $\alpha$ Her than in more luminous M supergiants.

Note in Fig. 2 that the variations ($P = 592^{\rm d}$) in W Tri (M5 II) are small, and the mean light level of the star is relatively stable. The light variability ($P = 288^{\rm d}$) of T Cet (M5-6 II) displays an amplitude closer to that of class Iab SRC variables than class Ib-II stars. Finally, the star HD 93662 (M1 II) has $P = 5756^{\rm d}$ (Turner et al. 2005), but does not display the cyclical nature typical of SRC variables. Its variability is more typical of starspot or chromospheric activity. A similar object may be the newly-discovered SRC variable BD+20°1171, which appears to display light fluctuations on an even longer time scale (Brukhanov 2001).

Another source of archival observational data is the Harvard College Observatory Photographic Plate Collection, which contains images dating from roughly 1890 to the mid 1990s. Harvard plates are relatively untapped for the study of SRC variables to our knowledge, but are very useful for obtaining information on light variability and period changes in members of the class less frequently observed by AAVSO members.

Examples are shown in Fig. 4 for the southern SRC variables CL Car (M5 Ia), which has $P = 512^{\rm d}$, and IX Car (M2 Iab), which has $P = 357^{\rm d}$. Note how the

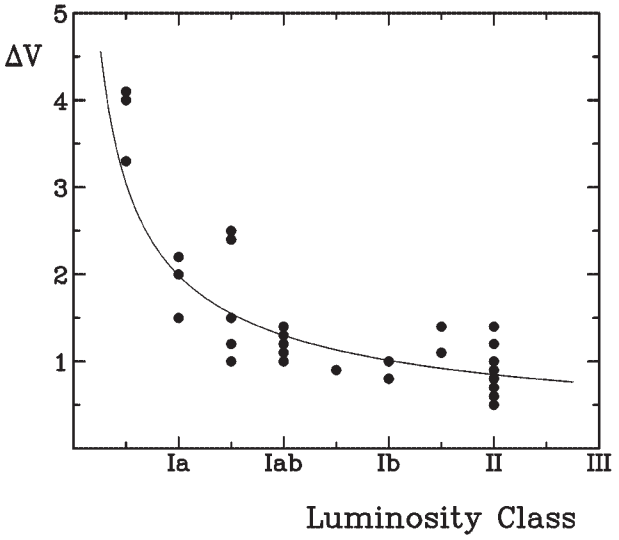


Figure 3: The trend in pulsational $V$ amplitude as a function of spectroscopic luminosity class for SRC variables, as derived from AAVSO observations and GCVS data. Emission-line type Ia M supergiants are assumed to be more luminous than regular Ia supergiants. A possible trend line is illustrated.

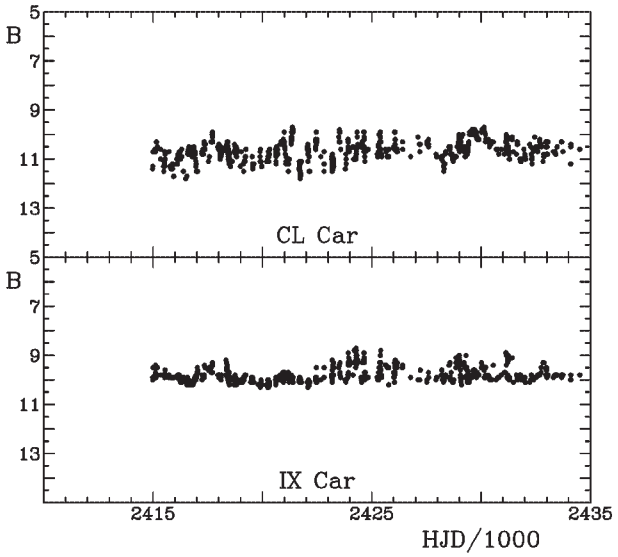


Figure 4: Light curves for the SRC variables CL Car and IX Car constructed from eye estimates off plates in the Harvard College Observatory Photographic Plate Collection.

photographic amplitude of IX Car increases as the star brightens. A separate study of the northern SRC variable BC Cyg in the open cluster Berkeley 87 is presented by Rohanidazegan et al. (2005).

### 3. Pulsation in the SRC Variables

Stothers (1969) used stellar evolutionary models to confirm pulsation as the origin of variability in M supergiants, noting the existence of a period-luminosity relation for cluster and association members. Glass (1979) found that SRC variables in the Large and Small Magellanic Clouds also follow a *PL* relation, which was confirmed using data for additional LMC SRC variables by Feast et al. (1980). Wood et al. (1983) used a deeper survey of long period variables in the LMC and SMC to separate M supergiant variables from variables belonging to the asymptotic giant branch (AGB). As noted by Wood et al. (1983), the masses of M supergiant variables are clearly much larger than those of AGB variables.

Kinman et al. (1987) further developed the usefulness of SRC variables as extragalactic distance indicators, and noted that those in the LMC follow the same *PL* trend as SRC variables in M33, making them excellent distance indicators. The most recent use of SRC variables as standard candles has included studies by Pierce et al. (2000) and Jurcevic et al. (2000) to reestablish a Galactic calibration of the *PL* relation to determine the distances to the LMC and M33.

It is possible to establish a period-luminosity relation for SRC variables using the few that are members of open clusters and associations, but the optical calibration relies heavily on the adopted scale of effective temperatures and bolometric corrections. Infrared calibrations are provided in the references cited above. An optical calibration tied to M supergiants in the region of h and $\chi$ Persei (Per OB 1) and Berkeley 87 is presented in Fig. 5. The relationship is similar to the *PL* relation for Galactic Cepheids, but displays more scatter. The calibration sample may contain a few objects that are not physical members of Per OB1, or perhaps some M supergiants pulsate in overtone modes. Further tests are needed to resolve the problems inherent in the existing sample. A *PL* relation for SRC variables predicted from period-radius and effective temperature relations is included for reference purposes in Fig. 5.

### 4. Discussion

Existing information on SRC variables is relatively incomplete because of the limited availability of observational data for them covering time intervals of a century or more. Uncertainties about class members raise a number of as-yet-unanswered questions. Do all SRC variables pulsate, or are there other mechanisms at work causing variability, particularly in low amplitude variables? Does circumstellar dust and/or gas play a role? Do luminous SRCs pulsate in the fundamental mode, or do some pulsate in overtone modes? What causes the slow changes in mean brightness of stars like BC Cyg, VX Sgr,and S Per? Is there a bet-

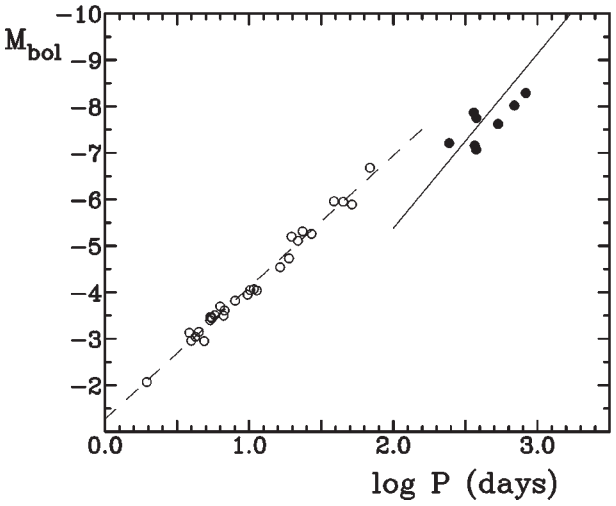


Figure 5: A period-luminosity relation for SRC variables in Per OB1 and Berkeley 87 (filled circles) constructed from $BV$ data for the stars in conjunction with their known reddenings. Shown for comparison is the Galactic calibration of the Cepheid period-luminosity relation (open circles). The solid line is a calibration based upon theoretical considerations, the dashed line a fit for cluster Cepheids.

ter method of classifying the SRC variables to account for differences in the nature of their variability?

Future work should probably include continuous spectroscopic or infrared observations of SRC variables over complete pulsation cycles to confirm the apparent colour changes, detailed light curves for SRC variables in a larger sample of open clusters, possibly the construction of more advanced pulsation models for red supergiants, and the development of a larger sample of SRC variables with comprehensive, that is, 100-year baseline, light curves. The last noted is possible through additional archival studies.

*Acknowledgements.* We acknowledge with thanks the variable star observations from the AAVSO International Database contributed by observers worldwide and used in this research.

**References**

Aldering, G., Humphreys, R.M., Richmond, M.: 1994, *AJ*, **107**, 662.

Brukhanov, I.S.: 2001, *Odessa Astron.Publ.*, **14**, 124.

Chevalier, R.A.: 1981, *Fund.Cosmic Phys.*, **7**, 1.

Feast, M. W., Catchpole, R.M., Carter, B.S., Roberts, G..: 1980, *MNRAS*, **193**, 377.

Glass, I.S.: 1979, *MNRAS*, **186**, 317.

Humphreys, R.M.: 1987, *PASP*, **99**, 5.

Jurcevic, J.S., Pierce, M.J., Jacoby, G.H.: 2000, *MNRAS*, **313**, 868.

Kholopov, P.N., et al.: 1985, *General Catalogue of Variable Stars*, 4$^{\text{th}}$ Edition (Moscow: Nauka).

Kinman, T.D., Mould, J.R., Wood, P.R.: 1987, *AJ*, **93**, 833.

Meynet, G., Mermilliod, J.-C., Maeder, A.: *A&AS*, 98, 477.

Pierce, M.J., Jurcevic, J.S., Crabtree, D.: 2000, *MNRAS*, **313**, 271.

Rohanidazegan, M., Turner, D.G., Pastukhova, E.N., Berdnikov, L.N.: 2005, *Odessa Astron.Publ.*,**18**, this conference.

Sonneborn, G., Altner, B., Kirshner, R.P.: 1987, *ApJ*, **323**, L35.

Stothers, R.: 1969, *ApJ*, **156**, 541.

Turner, D.G., Forbes, D., van den Bergh, S., Younger, P.F., Berdnikov, L.N.: 2005, *AJ*, **130**, 1194.

Waagen, E.O.: 2005, Observations from the AAVSO International Database, private communication.

Wood, P.R., Bessell, M.S., Fox, M.W.: 1983, *ApJ*, **272**, 99.

# ON THE PHOTOMETRY OF CC ANDROMEDAE

S.N.Udovichenko

Astronomical Observatory, Odessa National University
T.G.Shevchenko Park, Odessa 65014, Ukraine
*udovich@farlep.net*

ABSTRACT.

The photometric observation of $\delta$ Scuti star CC Andromedae using the 48 cm telescope with CCD photometer and the V filter of the UBV system at the Astronomical Observatory of Odessa National University have been made. The calculations of the time series data by using a new program Period04 (Lenz and Breger,2004) for multiple-frequency analysis, a seven-frequency solution has been developed. Also, the new frequency analyses for observation CC Andromedae made by Fitch in 1956 and 1957 have a seven-frequency solution, although Fitch (1967) give a six-frequency solution. The new frequency values closely fits all data of observations. The mode identification shows, that most frequencies correspond to radial and nonradial modes.

**Key words:** Delta Scuti – stars: individual (CC And).

CC And (SAO 36605) is $\delta$ Sct variable star spectral type F3 IV-V. The variability was found by Eggen and Linblad in 1952. The main pulsation period of 0.1249078 was determined in 1953 by Wilson and Walker (1956). Fitch(1960) made observations (27 nights) of the star with V filter from 1956 to 1957, finding four pulsating frequencies. Fitch (1967) analyzed the data set again and find six frequencies. From 1957 to 1984 any observations could not found in literature. In 1984 Fu Jian-ning and Jiang Shi-Jang was found seven frequencies from photoelectric observations at Beijing. (6 nights)

To study the possible variation of the star frequencies, a new observations of CC And were made in Astronomical Observatory of Odessa National University.

The main parameter of variable and comparison stars: variable – CC And, V=8.8, F3IV-V, B-V=0.33, Vsin i=20km/s; comparison – SAO 36623, V=8.1, G5.

The photometric observation of CC And were made using the 48 cm reflector with the f/4.5 Newtonian focus and CCD photometer with V filter of UBV system. The CCD photometer was created using CCD chip, hermetic housing and thermoelectric (Peltier) cooler, wich provide a temperature difference between the crystal and the environment of about -40$^o$C– -50$^o$C.

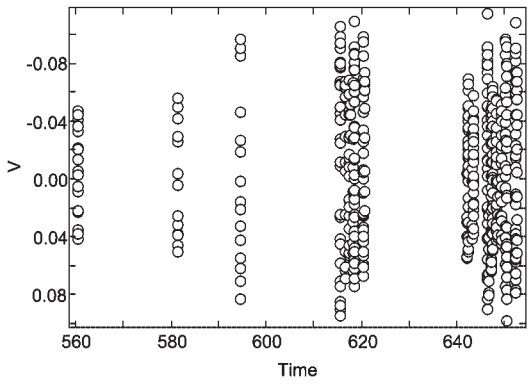


Figure 1: The all data set of observations of CC And

The exposure time and duty cycle were 50 sec and 10 sec, respectively. Evening and morning twilight flat-field frames were obtained for each night to flatten the raw CCD frames. For CCD differential photometry a program was used that performed CCD control, image processing, and aperture photometry. The procedures for the aperture photometry are composed of the dark-level and flat-field corrections and determination of the instrumental magnitude and precision. In order to fix the star at the same position in the exposed field during the observing run, guiding and careful adjustment were applied. The mean measurement error was about 0.007 - 0.01 mag.

About 1500 frames of observations CC And according control stars were measured and differential magnitudes were corrected for the atmospheric extinction and normalized by subtracting the mean of differential magnitudes for each night in order to correct the long-term instrumental drift. Than each observation was take as a mean of three measurements. The all set data of observations are shown in Fig 1. The resulting observed light curves CC And for each night are shown in Fig. 2. The full circles denote the observed data, solid curves represent the analytic light curves computed with seven frequencies obtained in the present

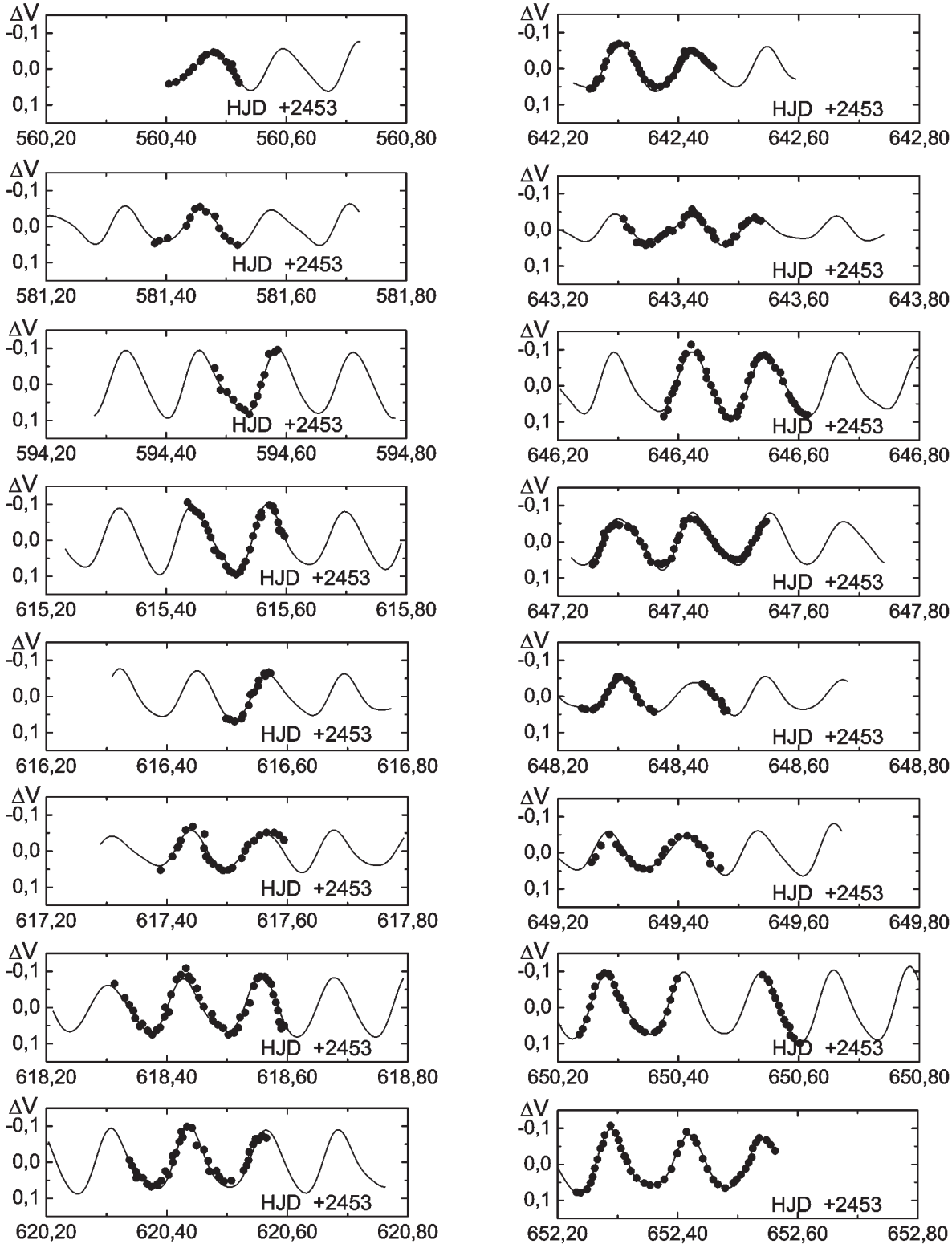


Figure 2: Light curves of CC And. The V-mag differens normalised to zero. The fit of seven-frequency solution is shown by the solid curves.

work.

The frequency analyses were performed using a new package of computer programs with single-frequency and multiple-frequency techniques by using utilize Fourier as well as multiple-least-squares algorithms (program Period04, Lenz and Breger, 2004). The power spectra of all data set shown in Fig. 3. It can be seen that the data set has seven reliable frequencies. For these seven frequencies the resulting fit curve were constructed. Table 1 shows the amplitudes and frequencies of Fourier analysis calculated for Fitch's observations (1960, 1967) and this work observations by using the program mentioned above.

Table 1: The frequencies and amplitudes of CC And
a) From photoelectric observations by Fitch, calculations by Fitch

| Frequency 1960, c/d | Amplitude mag | Frequency 1967,c/d |
|---|---|---|
| F1=8.00591 | 0.070 | F1=8.0059 |
| F2=7.81480 | 0.033 | F2=7.8148 |
| F3=16.01182 | 0.008 | F3=8.1010 |
| F4=15.82071 | 0.006 | F4=13.3462 |
| | | F5=16.0118 |
| | | F6=15.8207 |

b) The same observations
Program Period04

| Frequency c/d | Fr.sigma c/d | Amplit. mag | Am.sigma mag |
|---|---|---|---|
| F1=8.0058948 | 0.000006 | 0.069626 | 0.000305 |
| F2=7.8147856 | 0.000012 | 0.032910 | 0.000305 |
| F3=8.1010496 | 0.000040 | 0.010428 | 0.000305 |
| F4=13.346232 | 0.000047 | 0.008940 | 0.000305 |
| F5=7.9021857 | 0.000051 | 0.008171 | 0.000305 |
| F6=16.011999 | 0.000062 | 0.006694 | 0.000305 |
| F7=15.820949 | 0.000065 | 0.006437 | 0.000305 |

c) For this work, (Udovichenko, 2006),
Program Period04

| Frequency c/d | Fr.sigma c/d | Amplit. mag | Am.sigma mag |
|---|---|---|---|
| F1=8.005672 | 0.000061 | 0.062334 | 0.000643 |
| F2=7.814758 | 0.000146 | 0.026259 | 0.000643 |
| F3=8.096911 | 0.000390 | 0.009865 | 0.000643 |
| F4=13.34652 | 0.000444 | 0.008667 | 0.000643 |
| F5=16.01105 | 0.000548 | 0.007023 | 0.000643 |
| F6=9.939581 | 0.000700 | 0.005496 | 0.000643 |
| F7=15.81965 | 0.000738 | 0.005216 | 0.000643 |

The residuals between the observations and the theoretical light curves for seven frequencies are about 0.01 mag. Table 1 shows that amplitudes and frequencies F1 - F4 are very closely to Fitch's result. The frequencies F5, F7 are also of similar order that Fitch's

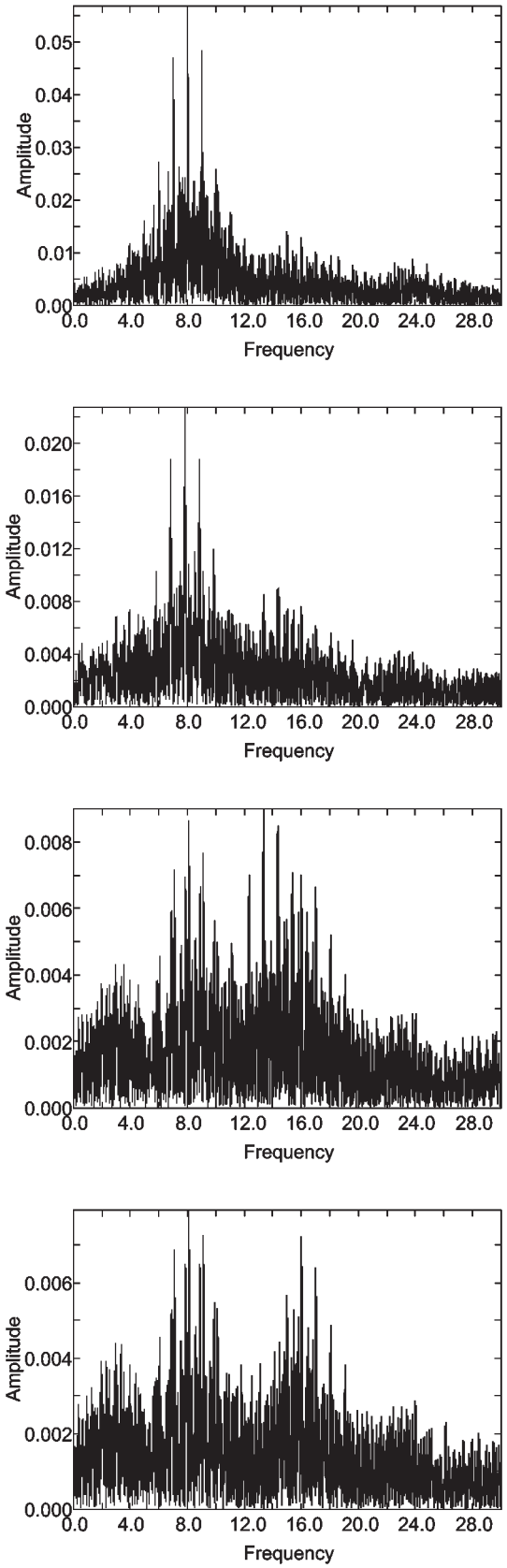


Figure 3: Power spectra CC And for frequencies F1-F4

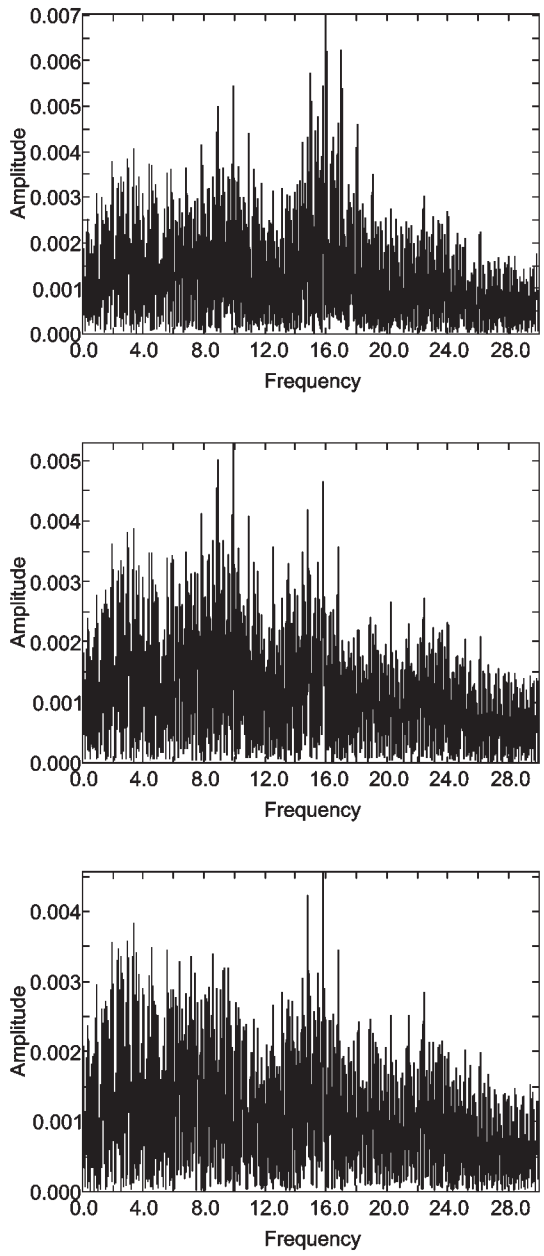


Figure 4: Power spectra CC And for frequencies F5-F7

frequencies F6, F7. The newly discovered frequency F6 (9.939581) has not large amplitude (0.005496), slightly less that frequency F5 (7.90218) from Fitch's observations.

If we can suggest that the biggest amplitude is the radial mode, then using the theoretical rations (Stellingwerf, 1979) we find that F1/F4=0.5998 and F4/F7=0.8436 agree with theoretical rations. Then, the pulsation modes of F1, F4 and F7 belong to the fundamental, the second overtone and third overtone, respectively. For another hand, the differences between some of the seven frequencies: F1-F2, F6-F7, F1-F5, F3-F1 can occur as equal-spacing effect of frequencies, when the frequency split corresponding to nonradial pulsation modes caused by the star's rotation. In this case F4 is a radial pulsation mode, but F1,F2,F3,F5,F6,F7 are nonradial pulsation modes. And CC And is a pulsator with multiple nonradial pulsation modes and a slow rotational velocity.

## References

Fitch W.S.: 1960, *Astroph.J*, **132**, 701.
Fitch W.S.: 1967, *Astroph.J*, **148**, 481.
Fu Jian-ning and Jiang Shi-yang: 1995, *Astron. Astroph. Sup. Ser.*, **110**, 303.
Lenz P., Breger M.: 2004, *Comm. in Asteroseismology*, **144**, 41.
Lindblad O.P., Eggen O.J.: 1953, *PASP*, **65**, 291.
Stellingwerf R.F.: 1979, *Astroph.J*, **227**, 935.

# PERIODS OF SMALL-AMPLITUDE CEPHEID Y OPH.

I.A. Usenko

Department of Astronomy, Odessa National University
T.G.Shevchenko Park, Odessa 65014 Ukraine, *igus@deneb1.odessa.ua*

ABSTRACT. Fourier analysis of all 299 *RV* data for Y Oph collected during last century displayed its mean pulsational period of 17.123024 days with two equidistanted ones, - 17.965158 and 16.355637 days, respectively. The ratio of these periods is near 0.92 with corresponding beat one near 370 days assumes nonradial pulsation of this Cepheid. Furthermore the analysis results provide an availability of one or more companions with orbital periods of 8424.1, 3361.3 days and more. Pulsational period and its amplitude undergo periodical changes, connected, probably with orbital periods, mentioned above.

**Key words**: Stars: radial velocities; Cepheids: nonradial pulsations; Cepheids: companions; Cepheids: Y Oph

## 1. Introduction

Classical Cepheid Y Oph is one of most attractive variable stars for investigations. At first, belonging to small-amplitude Cepheids group (DCEPS) it shows the phenomenon of pulsational amplitude decrease during almost one century, like the famous one $\alpha$ UMi (Polaris) (Fernie et al., 1995). At second, its pulsational period undergoes some changes, increased and decreased periodically (Szabados, 1989). At third, Y Oph belongs to spectroscopic binaries, having, probably a companion with orbital period from $1222.^d5$ (Szabados, 1989) to $2612^d$ (Abt & Levy, 1978), respectively. Y Oph come the second rank among the classical Cepheids by the number of their measured *RV* data. Unfortutunately, these data have been obtained during last century very irregularly: in the first decade (Albrech, 1907), in the thirties (Sanford, 1935), in the fifties (Abt, 1954), in the end of sixties, during the seventies and half of the eighties (Abt & Levy, 1978; Barnes et al., 1987; Beavers & Eittter, 1986; Coulson & Caldwell, 1985; Evans & Lyons, 1986; Lloyd Evans, 1980; Wilson et al., 1989). And for the nineties there are Berdnikov's set of 1995-1997 (Berdnikov, 2000), in which has been added the author's *RV* values (14 ones), based on McDonald spectra, obtained in the same time lag. So, totally there are 299 *RV* values covered almost one century.

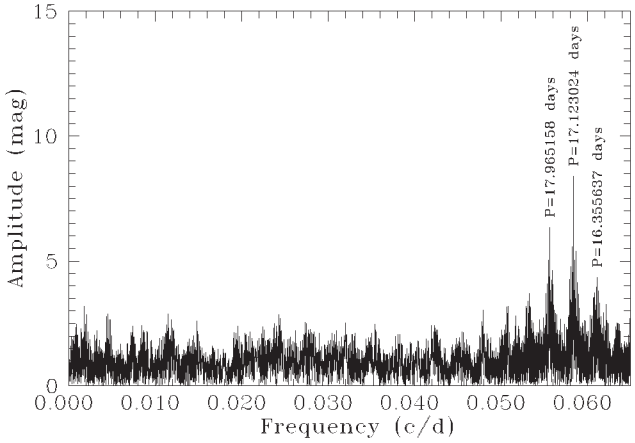


Figure 1: Fourier amplitude spectrum of Y Oph for pulsational period

The author's task consisted in the specification of pulsational and orbital periods using the Fourier analysis, and analyzing of pulsational period and amplitude changes during the last century.

## 2. Results

For analysis has been used PERIOD 98 program (Sperl, 1998) which allows to search for and fit sinusoidal patterns within a time series of data containing huge gaps. PERIOD 98 used tecniques Fourier and Fast Fourier analysis with minimization of residuals of sinusoidal fits to the data.

### *2.1. Pulsational periods*

A Fourier amplitude spectrum was obtained over the frequency range 0-1 $d^{-1}$ at a resolution of 0.00002 $d^{-1}$ (see Figure 1). At that, the highest amplitude 8.419 corresponds to frequence of 0.058401 $d^{-1}$, or 17.123024 days, respectively. At that the zero-point ($\gamma$ - velocity) is equal to -7.094 km/s. It is very noticeable that there is two frequences with high amplitudes (6.364 and 5.059) equidistanted from the main one by 0.0028 $d^{-1}$, - 0.0556633 $d^{-1}$ and 0.061141 $d^{-1}$, or 17.965158 and 16.355637 days, respectively.

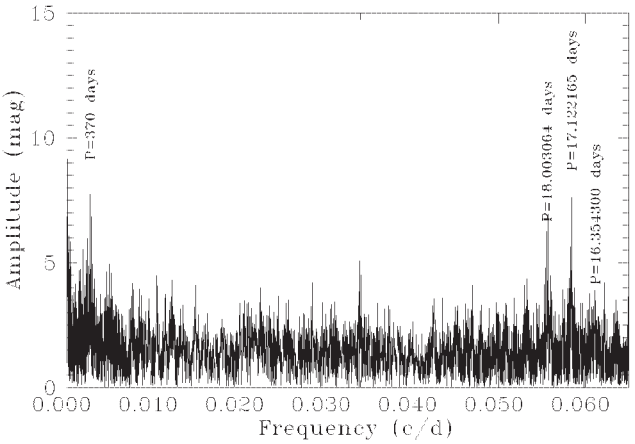


Figure 2: Fourier amplitude spectrum for residual velocities of Y Oph for pulsational period

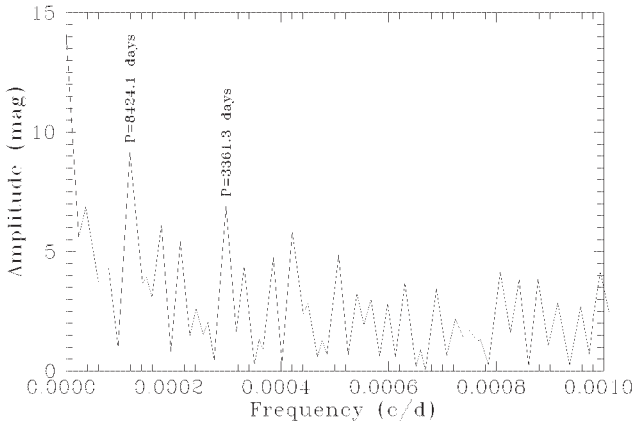


Figure 3: Fourier amplitude spectrum for residual velocities of Y Oph for orbital periods

Since the dominant period of Y Oph has been obtained, a Fourier search for additional periods was performed on the residual velocities. As seen in Figure 2 there are the same frequences of 0.05840383 $d^{-1}$ (amplitude 8.29059), 0.0555461 $d^{-1}$ (amplitude 6.25873) and 0.061146 $d^{-1}$ (amplitude 3.7445), that correspond well to periods mentioned above. But it is interesting that the period ratio is about 0.92, whould result in a beat period near 370 days. Nevertheless a such peak is present (see Figure 2). Therefore, if these observed periods correspond to the different modes then Y Oph is a nonradial pulsator.

*2.2 Orbital periods*

As seen in Figure 1 it is difficult to indify any frequences that could be correspond to the orbital period values, mentioned above. But in Figure 3, presenting the results of Fourier amplitude spectrum for residual velocities, are evident two values for 8424.1 and 3361.3 days, although the highest peak get to zero value. This fact could be explain by the presence of possible one more companion with longer orbital period.

*2.3. Changes in the pulsational period and amplitude*

Fourier search has been made for *RV* data, obtained by Albrecht (1907), Sanford (1935) and fresh data corresponded for the set of 1995-1997, to determine the pulsational period and amplitude values. These results, combined into Szabados (1989) and Fernie et al.(1995) ones, are given in Table 1. As seen, the periodic changes of the pulsational period and amplitude are evident.

Table 1: Changes of the pulsational period of Y Oph

| HJD Interval | Period, days | Ref. | $RV_{amp}$, $km^{-1}$ | Ref. |
|---|---|---|---|---|
| 2416977 - 2417445 | 17.978836 | 1 | 18.4 | 3 |
| 2421768 - 2427553 | 17.126137 | 1 | 19.2 | 3 |
| 2432781 - 2433106 | 17.113288 | 2 | 16.1 | 3 |
| 2434733 - 2435281 | 17.126813 | 2 | 16.8 | 3 |
| 2435281 - 2435691 | 17.111255 | 2 | 17.5 | 3 |
| 2439014 - 2439682 | 17.127643 | 2 | 21.8 | 3 |
| 2440778 - 2446601 | 17.126908 | 2 | 14.7 | 3 |
| 2450245 - 2451095 | 17.120887 | 1 | 16.5 | 1 |

1 - this work; 2 - Szabados (1989); 3 - Fernie et al. (1995).

## 3. Conclusions

1. Fourier analysis of all *RV* data displayed the mean pulsational period of 17.123024 days and two equidistanted ones, - 17.965158 and 16.355637 days, respectively.

2. The ratio of these pulsational periods is near 0.92 and the corresponding beat period near 370 days is presented in Fourier amplitude spectrum. This ratio value assumes nonradial pulsation of Y Oph.

3. These Fourier analysis data provide an availability of one or more companions with orbital periods of 8424.1 and 3361.3 days. The presence of companion with longer period do not except.

4. Pulsational period and its amplitude undergo periodical changes connected, probably with orbital motions of one or more companions.

**References**

Adelman S.J., Philip A.G.D., Adelman C.J.: 1996, *MNRAS,* **282**, 953.
Abt H.A.: 1954, *PASP,* **66**, 65.
Abt H.A. & Levy S.G.: 1978,*PASP,* **90**, 1888.
Albrecht S.: 1907, *Lick Obs. Bull.,* **4**, 130.
Barnes T.G., Moffett T.J. & Slovak M.H.: 1987, *ApJS,* **65**, 307.
Beavers W.I. & Eitter J.J.: 1986, *ApJS,* **62**, 147.
Berdnikov L.N.: 2000, *private communication.*
Coulson I.M. & Caldwell J.A.R.: 1985, *South Afr. Obs. Circ.,* **No.9**, 5.
Evans N.R. & Lyons R.: 1986, *AJ,* **93**, 436.
Fernie J.D., Khoshnevissan M.H., & Seager S.: 1995, *AJ,* **110**, 1326.
Lloyd Evans T.: 1980, *South Afr. Obs. Circ.,* **1, No.5**, 257.
Sanford R.F.: 1935, *ApJ,* **81**, 140.
Sperl M.: 1998, .
Szabados L.: 1989, *Budapest Mitt.,* **11, No.94**, 39.
Wilson T.D., Carter M.W., Barnes T.G., van Citters G.W., & Moffett T.J.: 1989, *ApJS,* **69**, 951.

# POLARIS, SMALL-AMPLITUDE CEPHEID WITH UNIQUE PHYSICAL PECULIARITIES

I.A. Usenko,[1], A.S. Miroshnichenko,[2], V.G. Klochkova,[3], V.E. Panchuk[3]

[1] Department of Astronomy, Odessa National University
T.G.Shevchenko Park, Odessa 65014 Ukraine, *igus@deneb1.odessa.ua*
[3] Ritter Observatory, University of Toledo
Toledo, OH 43606 USA, *asm0910@yahoo.com*
[3] Special Astrophysical Observatory, Russian Academy of Sciences
Nizhnij Arkhyz, Karachaevo-Cherkessia, 369167 Russia *valenta@sao.ru; panch@sao.ru*

ABSTRACT. We present the results of our analysis of spectroscopic observations of $\alpha$ UMi (Polaris) obtained in 1994 (5 spectra) and 2001–2004 (30 spectra) and frequency analysis of all Polaris *RV* data collected during last 120 years. This analysis has confirmed the proposition about its overtone pulsations in first and second overtones with $P_2/P_1 = 0.81$, i.e. Polaris is double-mode Cepheid (DMC). Moreover, there are the presence of modes splitting for pulsations in these overtones caused by the presence of the three companions at the least with orbital periods of 48.6, 29.91 and 19.44 years, respectively. Since Polaris is located near the blue edges of the Cepheid instability strip for the fundamental mode and first overtone, and an abrupt decrease of the pulsational amplitude and its recent increase could be due to its binarity.

**Key words**: Stars: radial velocities; Cepheids: overtone pulsations; Cepheids: companions; Cepheids: $\alpha$ UMi

## 1. Introduction

As it has been mentioned in paper of Usenko et al. (2005) there are some specific features of Polaris which testify about its pecuilar character:

1. Abrupt decrease of its pulsational amplitude during fourty years (5–6 $\mathrm{km\,s^{-1}}$ before 1950 (Roemer 1965) to 0.05 $\mathrm{km\,s^{-1}}$ in the 1990's (Fernie, Kamper, & Seager 1993)) and the beginning of one's increase during last 5-6 years (Hatzes & Cochran 2000).

2. According to fresh results of Turner et al. (2005) based on $O-C$ data of photometric and radial velocity estimates collected more than a hundred and fifty years, the pulsational period of Polaris has increased of $4.45\pm0.03$ $\mathrm{s\,yr^{-1}}$ during the interval 1896-1958, - as an evidence of Polaris' redward crossing of Cepheids instability strip (hereafter CIS). Since 1963 the period's increase has slow down to $4.28\pm0.73$ $\mathrm{s\,yr^{-1}}$, at that in stepwise during three years.

3. Preceding frequency analyses of radial velocity data sets of 1987-88 (Dinshaw et al. 1989) and 1992-93 (Hatzes & Cochran 2000) revealed besides the main pulsational period of 3.97 day a presence of additional one of 45.3 or 40.2 days, respectively. This period's presence has been explained by the Polaris rotation, availability of cool or macroturbulent velocity spots, or else of nonradial pulsations.

## 2. Observations and frequency analysis

In 39 spectrograms were obtained by authors during 1994-2005 using 1 m telescope of Ritter Observatory, University of Toledo, Ohio, USA; 2.1 m telescope of McDonald observatory, Texas, USA; 6 m telescope of SAO RAS, Russia. DECH 20 package (Galazutdinov 1992) allows to make the measurements of radial velocities after the using of a thorium-argon lamp for the wavelength calibration. To avoid the differnces in velocities caused by the Doppler effect across full spectral range, we used the measuring the shifts in each spectral order with subsequent averaging to produce velocities. Obtained radial velocity data are given in Table 1.

Before the searching for Polaris periodicities we have collected all the radial velocity data obtained by different authors during the researching period of 1896-2004. These data were taken from Roemer (1965), Schmidt (1974), Arellano Ferro (1983), Kamper et al. (1984), Dinshaw et al. (1989), Fernie et al. (1993), Kamper (1996), Kamper & Fernie (1998), Hatzes & Cochran (2000) papers. Including our 39 estimates we have in total, 2118 *RV* values. Next step was using the PE-

Table 1: Observational data of $\alpha$ UMi

| HJD 2400000+ | Number of orders | $RV$ (km s$^{-1}$) | $\sigma$ | NL |
|---|---|---|---|---|
| 49512.615 | 9 | -13.28 | 1.23 | 126 |
| 49579.824 | 9 | -14.21 | 1.21 | 116 |
| 49603.853 | 15 | -13.35 | 0.93 | 152 |
| 49637.792 | 9 | -14.97 | 1.05 | 132 |
| 49648.810 | 9 | -14.38 | 1.07 | 130 |
| 51240.612 | 22 | -18.26 | 2.81 | 302 |
| 51360.538 | 22 | -16.51 | 2.36 | 317 |
| 51361.536 | 22 | -14.53 | 2.68 | 275 |
| 52192.858 | 28 | -16.88 | 0.81 | 281 |
| 52416.655 | 9 | -16.53 | 1.17 | 138 |
| 52417.616 | 9 | -17.67 | 1.45 | 145 |
| 52421.679 | 9 | -17.85 | 1.32 | 109 |
| 52426.667 | 9 | -18.18 | 1.28 | 121 |
| 52427.650 | 9 | -17.35 | 3.06 | 119 |
| 52435.634 | 9 | -16.53 | 1.18 | 142 |
| 52441.673 | 9 | -16.78 | 1.08 | 112 |
| 52514.575 | 18 | -20.39 | 0.92 | 270 |
| 52515.588 | 25 | -15.33 | 0.86 | 391 |
| 52782.543 | 26 | -14.53 | 2.68 | 275 |
| 52833.741 | 9 | -21.64 | 1.30 | 100 |
| 52837.678 | 9 | -21.59 | 2.07 | 104 |
| 52839.746 | 9 | -23.97 | 2.00 | 111 |
| 52861.560 | 20 | -17.76 | 0.73 | 279 |
| 52867.562 | 20 | -17.75 | 0.79 | 251 |
| 52869.570 | 20 | -16.62 | 0.76 | 247 |
| 52891.600 | 26 | -16.38 | 0.89 | 384 |
| 52952.700 | 9 | -19.19 | 3.37 | 112 |
| 52986.692 | 9 | -18.48 | 2.89 | 125 |
| 52986.709 | 9 | -17.86 | 2.67 | 107 |
| 53005.595 | 9 | -16.50 | 3.13 | 141 |
| 53015.167 | 20 | -17.79 | 0.88 | 279 |
| 53019.108 | 20 | -17.28 | 0.82 | 266 |
| 53072.165 | 20 | -17.81 | 0.64 | 251 |
| 53072.631 | 20 | -18.02 | 0.77 | 291 |
| 53073.622 | 20 | -17.52 | 0.80 | 278 |
| 53162.191 | 20 | - 9.52 | 0.64 | 309 |
| 53246.192 | 20 | -16.50 | 0.73 | 281 |
| 53285.167 | 20 | -17.08 | 0.85 | 304 |
| 53367.091 | 27 | -20.51 | 3.84 | 261 |

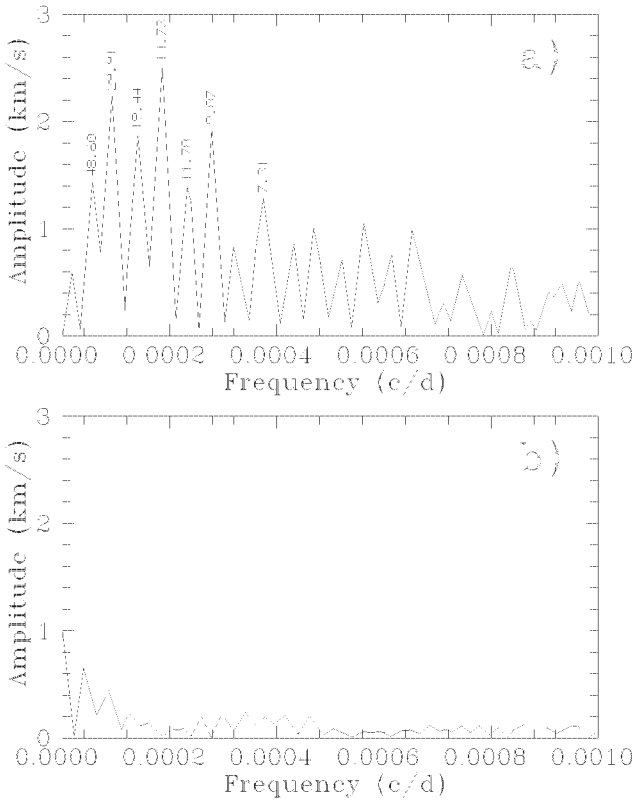


Figure 1: Fragment of Fourier amplitude spectrum of Polaris over a narrow frequency range corresponding to orbital periods (a) and to its spectral window (b).

RIOD 98 program (Sperl 1998) which allows to search for and fit sinusoidal patterns within a time series of data containing huge gaps. PERIOD 98 used tecniques Fourier and Fast Fourier analysis with minimization of residuals of sinusoidal fits to the data.

A Fourier amplitude spectrum was obtained over the frequency range 0-1 d$^{-1}$ at a resolution of 0.00002 d$^{-1}$. At that, the highest amplitude 2.504 corresponds to frequence of 0.0001862 d$^{-1}$, or 5378.77 days (14.73 years), respectively (see Figure 1). At that the zero-point ($\gamma$ - velocity) is equal to -15.446 km s$^{-1}$.

### *2.1 Orbital periods*

As seen in Figure 1: (a),- the highest peaks are located near zero frequence mark, - their frequences correspond to the longest periods, which could be interpret as orbital ones (see Table 2). And the results of spectral window (b) for these frequences confirm their truth.

As seen from Table 2, the highest amplitude frequencies $f_{O2}$ and $f_{O4}$ corresponds well to long since known orbital period (29.9 yr according to Dinshaw et al. 1989) and half of one, respectively. Frequency $f_{O7}$ make up a quarter of orbital period. At the same time we obtained two divisible frequences $f_{O3}$ and

Table 2: Possible orbital periods of $\alpha$ UMi

| No. | Frequency (c/d) | Amplitude ($km\,s^{-1}$) | Period (days/years) |
|---|---|---|---|
| $f_{O1}$ | 0.00005573 | 1.43374864 | 17750.01/48.60 |
| $f_{O2}$ | 0.00009247 | 2.23957558 | 10923.08/29.91 |
| $f_{O3}$ | 0.00014060 | 1.86965268 | 7100.00/19.44 |
| $f_{O4}$ | 0.00018620 | 2.50423271 | 5378.77/14.73 |
| $f_{O5}$ | 0.00023307 | 1.38833452 | 4303.04/11.78 |
| $f_{O6}$ | 0.00027867 | 1.92205718 | 3604.06/9.87 |
| $f_{O7}$ | 0.00037494 | 1.27912952 | 2669.17/7.31 |

Table 3: Possible pulsational periods of $\alpha$ UMi

| No. | Frequency (c/d) | Amplitude ($km\,s^{-1}$) | Period (days) |
|---|---|---|---|
| $f_{P1}$ | 0.25188093 | 0.80356599 | 3.970129896 |
| $f_{P2}$ | 0.25189359 | 0.75975109 | 3.969930253 |
| $f_{P3}$ | 0.25191766 | 0.94085008 | 3.969550986 |
| $f_{P4}$ | 0.25198733 | 1.22003231 | 3.968453520 |
| $f_{P5}$ | 0.25201773 | 0.88336295 | 3.967974809 |
| $f_{P6}$ | 0.31057769 | 0.45598194 | 3.219806273 |
| $f_{P7}$ | 0.31058276 | 0.57387475 | 3.216513541 |
| $f_{P8}$ | 0.31093616 | 0.49965752 | 3.216094234 |
| $f_{P9}$ | 0.05876390 | 0.73047045 | 17.017250819 |
| $f_{P10}$ | 0.05885130 | 0.62139714 | 16.991978218 |

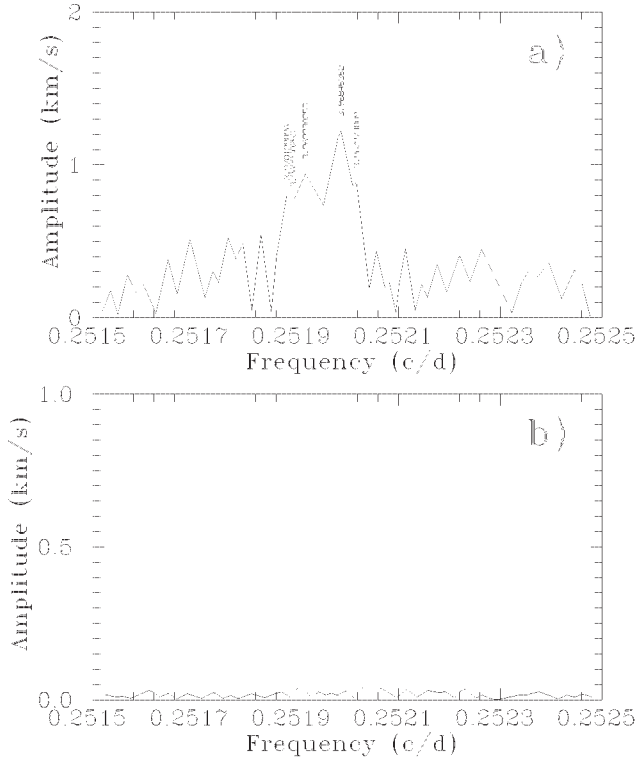


Figure 2: Fragment of Fourier amplitude spectrum of Polaris over a narrow frequency range corresponding to main pulsational period (a) and to its spectral window (b).

$f_{O6}$, thereas the reduction ratio of $f_{O1}/f_{O5}$ is closely approximated to 4. It follows that Polaris system has probably, in addition, some more orbital periods. If 19.44 - years period could be interpret as orbital one of Jovian-like body (Hatzes & Cochran 2000) then 48.6 - years period seems to be mysterious. Probably quite we have to do with presence of more cool companion than known one of later on $F4V$ spectral type (Evans et al. 2002).

*2.2 Pulsational periods*

3.97 - days pulsational period (frequency near to 0.25 c/d) is seen clearly in Figure 2. But we can see more surprising picture.

Judging from this figure it is clearly visible frequence splitting. Like in first subsection we represent these frequences in tabular form (see Table 3).

So, the single highest amplitude peak corresponds to pulsational period of 3.96845352 days ($f_{P4}$). Let suppose to consider it to be the main period. Then the presence of more high frequences the left of it could be explain by following. If we can consider the reliable orbital period of 29.91 yr as a *beat period*, then a sum of its frequence with one of main pulsational period gives the total frequence of 0.251894879 c/d, i. e. it corresponds well with the observed one $f_{P2}$ from Table 3! This unexpected fact finds the confirmations in case if the orbital periods of 48.6 and 19.44 yrs we would be consider as the beat periods too: the expected

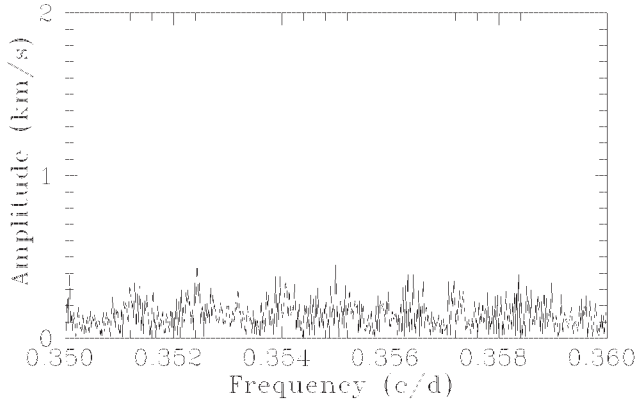


Figure 3: Fragment of Fourier amplitude spectrum of Polaris over a narrow frequency range corresponding to pulsational period in fundamental tone.

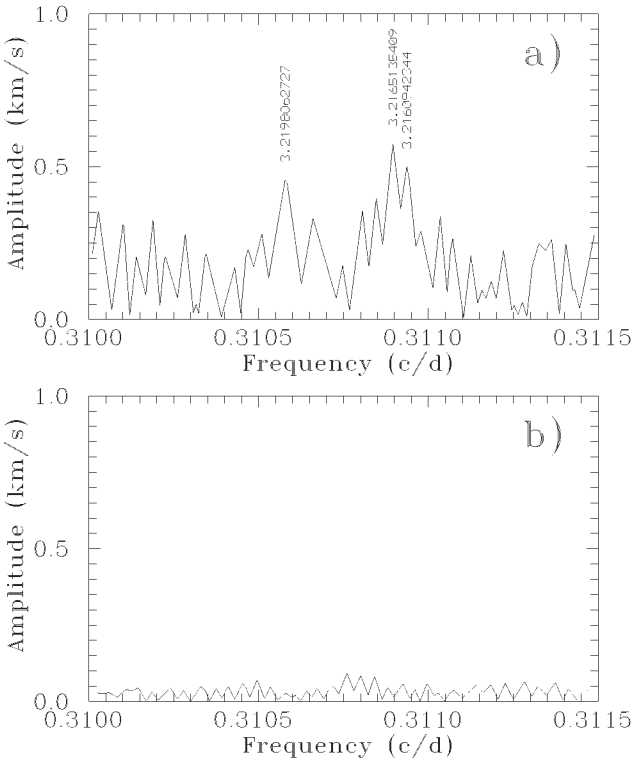


Figure 4: Fragment of Fourier amplitude spectrum of Polaris over a narrow frequency range corresponding to pulsational period in second overtone (a) and to its spectral window (b).

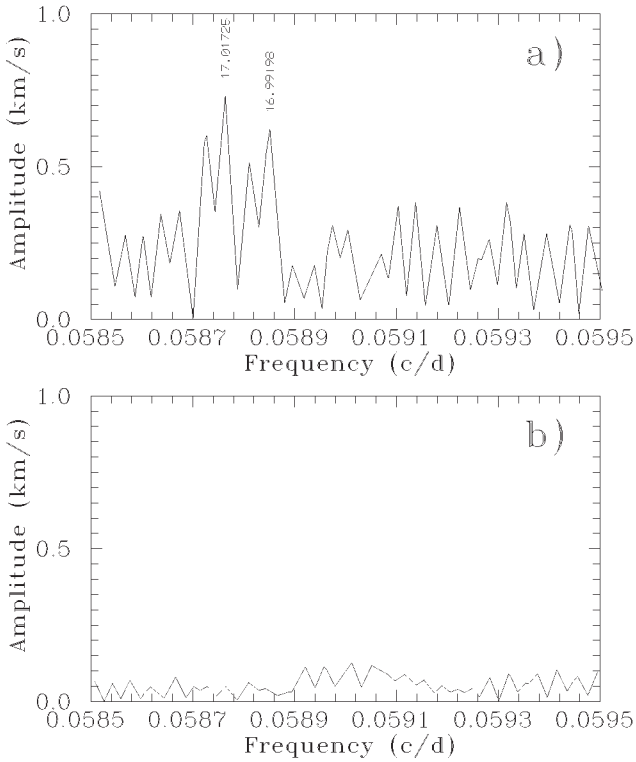


Figure 5: Fragment of Fourier amplitude spectrum of Polaris over a narrow frequency range corresponding to beat pulsational period between the first and second overtones (a) and to its spectral window (b).

frequences are 0.251930991 c/d and 0.251846727 c/d, respectively. They have a good agreement with observed ones of $f_{P3}$ and $f_{P1}$ from Table 3. A presence of frequence $f_{P5}$ is still unaccounted.

Next but very important step in our investigations was to determine the mode of observed pulsational period. Usenko et al. (2005) have founded that radii and distances obtained from interferometry and HIPPARCOS parallaxes correspond well to pulsational in *first overtone*. Having a plenty of radial velocity values we could be try to found the presence of different modes in our Fourier amplitude spectrum. On the assumption of observed period of 3.968453520 day is *fundamental* one and $P_1/P_0 = 0.71$, an espected frequency lies near 0.3549 $d^{-1}$. As seen from Figure 3, there are not any so significant frequences, whose could be correspond to value, mentioned above.

If this observed period corresponds still to *first overtone* pulsation and $P_2/P_1 = 0.81$ then we would make an attempt to search for the traces of frequences, corresponded to *second overtone*, - near 0.311 $d^{-1}$. And these traces were detected (see Figure 4).

Judging from Figure 4 there are three noticeable peacks with the highest amplitudes, - $f_{P6}$, $f_{P7}$ and $f_{P8}$ (see Table 3). If we take the highest amplitude period of 3.216513541 day (corresponds to frequency $f_{P7}$) and divide it by 0.81, we obtain the period of 3.96845 day, i.e. $f_{P4}$ from Table 3. The same operation for frequency $f_{P8}$ gives the period of 3.97013 day, - $f_{P1}$ from Table 3. Therefore, frequences $f_{P7}$ and $f_{P8}$ correspond to *second overtone* pulsations, and like in the previous case there are mode splitting caused by companions presence. At that the period of 3.216513541 day is conventional due to posiible Jovian-like body, mentioned above, with period of 19.44 yr. Frequence $f_{P6}$ is very unusial, because its presence does not connect with any of observed orbital periods.

In order to confirm the fact of existence for pulsations in second overtone, it is enough to detect the *beat period* between it and first one. An expected period lies in the ranges of 16.5 - 17 days. As seen from Figure 5 there are two highest peaks with frequences $f_{P9}$ and $f_{P10}$ (see Table 3), which correspond to periods of 16.99 and 17.02 days, respectively. It is marvellously, but last value agrees with 17.03 days one, founded by Hatzes & Cochran (2000)! Although these authors have supposed this period corresponds to the beat period between *fundamental* and *first overtone* modes and inasmuch as the fundamental one of 5.6 day did not detected, they considered 17.02 days period as a false one.

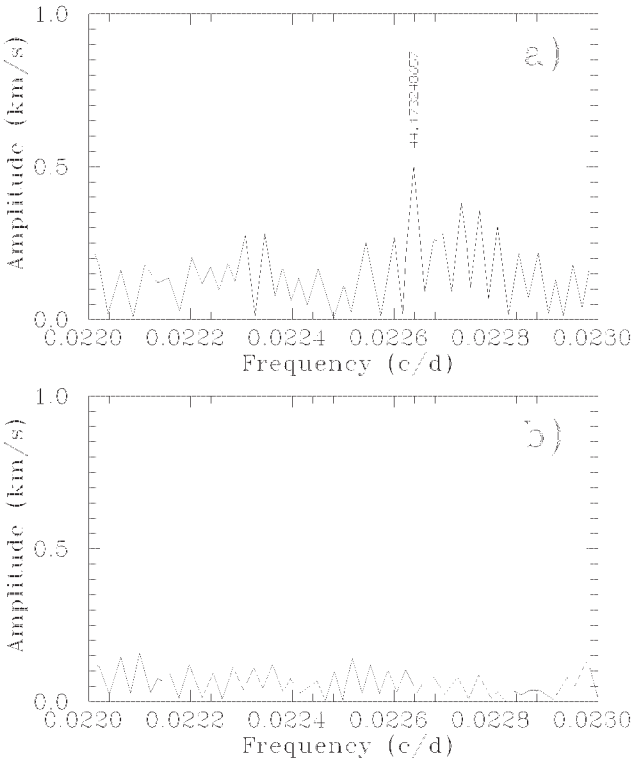


Figure 6: Fragment of Fourier amplitude spectrum of Polaris over a narrow frequency range corresponding to 45-days period (a) and to its spectral window (b).

*2.3 45-days period*

An existence of this unusual period was announced firstly by Dinshaw et al. (1989). An application of Fourier analysis for residual velocities displayed a strong peak on the periodogram at a frequency of 0.022 $d^{-1}$ and amplitude near 0.4 $km\,s^{-1}$. This result corresponded to the period of 45.3±0.2 days. Later Hutzes & Cochran (2000) confirmed this one, but the result was 40.2±0.7 days with the same amplitude. To check these results we have applied the same procedure for residual velocities. The resulting Fourier periodogram is given in Figure 6.

As seen, the highest peak corresponds to frequency of 0.022638136 $d^{-1}$ with amplitude 0.5 $km\,s^{-1}$, or period of 44.173249 days that has an exellent coincidence with the result of Dinshaw et al. (1989). There are any traces of 34.3 days (0.02915 $d^{-1}$) period's presence, detected earlier by Hatzes & Cochran (2000).

## 3. Summary

1. Changes of pulsational period for Polaris both periodical and spasmodic, can be explained by presence at the least of three companions;
2. Suspected orbital periods of 18.6 and 19.44 yrs are quite reliable.
3. Polaris belongs to double-mode Cepheids (DMC), at that its pulsation in fundamental tone is absent and there are pulsations in *first* and *second overtones* only with $P_2/P_1 = 0.81$ that agrees well with results of theory for classical Cepheids.
4. The presence of second overtone to be confirmed by the existence of *beat period* between it and *first* one.
5. Polaris modes splitting for pulsations in first and second overtones caused by the presence of three companions at the least.
6. The period of 44.173 days closed to 45-days one detected by Dinshaw et al. (1989) is quite reliable.

## References

Arellano Ferro A.: 1983, *ApJ,* **274**, 555.
Dinshaw N., Matthews J.M., Walker G.A.J., Hill G.M.: 1989. *AJ,* **98**, 2249.
Evans N.R., Sasselov D.D., & Short C.I.: 2002, *ApJ,* **567**, 1121.
Fernie J.D.: 1966, *AJ,* **71**, 731.
Fernie J.D., Kamper K.W., & Seager S.: 1993, *ApJ,* **416**, 820.
Galazutdinov G.A.: 1992, *Preprint SAO RAS* **No.92**.
Hatzes A.P., Cohran W.D.: 2000, *AJ* **120**, 979.
Kamper K.W., Evans N.R., and Lyons R.W.: 1984, *JRASC,* **78**, 173.
Kamper K.W.: 1996, *JRASC,* **90**, 140.
Kamper K.W., Fernie J.D.: 1998, *AJ* **116**, 936.
Roemer E.: 1965, *ApJ,* **141**, 1415.
Schmidt E.G.: 1974, *MNRAS,* **167**, 613.
Sperl M.: 1998, *PERIOD 98,* program.
Turner D.G., Savoy J., Derrah J., Sabour M.A., Berdnikov L.N., 2005, *AJ,* Usenko I.A., Miroshnichemnko A.S., Klochkova V.G., Yushkin M.V.: 2005, *MNRAS,* **362**, 1219.

# MAGNETISM OF WHITE DWARFS
## (intermediate results of a survey for kilogauss magnetic fields in white dwarfs)

G. Valyavin [1],[2], S. Bagnulo[3], S. Fabrika[2], A. Reisenegger[4], G.A. Wade[5], Inwoo Han[1], D. Monin[6]

[1] Korea Astronomy and Space Science Institute, 61-1, Whaam-Dong, Youseong-Gu, Taejeon, Republic of Korea 305-348
[2] Special Astrophysical Observatory,Russian Academy of Sciences, Nizhnii Arkhyz, Karachai Cherkess Republic, 357147, Russia
[3] European Southern Observatory,Alonso de Córdova 3107, Santiago, Chile
[4] Departamento de Astronomía y Astrofísica, Pontificia Universidad Católica de Chile, Casilla 306, Santiago 22
[5] Physics Department, Roual Military College of Canada, Kingston, Ontario, Canada
[6] Dominion Astrophysical Observatory, 5071, West Saanich Road, Victoria, British Columbia, V9E 2E7,Canada

ABSTRACT. We shortly present intermidiate results of a survey for weak magnetic fields among degenerate stars (white dwarfs and hot subdwarf stars). Kilogauss upper limits of longitudinal magnetic fields are presented for several brightest DA white dwarfs and new candidates to magnetic degenerates are found. We discuss our findings in the frame of 25% fractional incidence of white dwarf magnetism in the kilogauss region. The complete version of this presentation will be published in the **Astrophysical Journal**.

**Key words**: Stars: white dwarfs: subdwarfs: magnetic stars; stars: individual: WD1036+433, WD1647+591, WD1105-048.

### 1. Introduction

The investigation of white dwarf stars (WDs) is of fundamental importance for the understanding of stellar and galactic evolution, as WDs represent the final evolutionary stage of more than 90% of all stars. Nowadays we believe that the general properties and evolution of white dwarfs are fairly well understood. However, there are several important problems that still need to be properly addressed, especially those connected with the origin of the group of about one hundreed isolated magnetic white dwarfs (MWDs, Liebert & Sion, 1979; Angel, et al., 1981; Putney, 1999; Liebert, et al., 2003). Latest conclusions about progenitors of the MWDs (Liebert et al., 2003; Wickramasinghe & Ferrario, 2005) or about evolution of their magnetic fields which is likely seen in observations (Liebert & Sion, 1979; Valyavin & Fabrika, 1999; Liebert et al., 2003) form two main problems to be studied in the frame of stellar magnetism. The first problem is related to the origin of the MWDs. Earlier studies (Angel, et al., 1981) suggested that MWDs are descendants of magnetic Ap/Bp stars. More recent studies, however, have suggested that the progenitors are not restricted to this class (Liebert et a., 2003; Wickramasinghe & Ferrario, 2005). The second problem is associated with the evolution of a global magnetic field during a WD's life: it has been shown (Liebert & Sion, 1979; Valyavin & Fabrika, 1999; Liebert et al., 2003) that the magnetic field exhibits some peculiar features during the WD life time. One of them is that WDs with strong fields show a tendency to increase in fractional incidence with age, in contradiction to the hypothesis that WD magnetic fields decay with time.

The implications of the above studies are extremely significant. Unfortunately, *they are based on a highly biased and limited sample of strongly magnetic WDs*, and therefore they are still controversial and require better statistics. It appears quite likely that the fraction of MWDs (as compared to the total population of known WDs) will increase significantly if high-precision spectropolarimetric surveys are conducted. For the better understanding of the WD magnetic field origin, it is also important to extend the observations to a group of pre-WD hot subdwarf stars (Elkin, 1996), the magnetic nature of which is still not well studied.

The required accuracy of magnetic field measurements is about 1 kG or better. For these reasons, we are carrying out an observational program with the 6 m and 8 m Russian and European telescopes. Here, we present some new results from our survey (Valyavin et al., 2003) for kilogauss magnetic fields among isolated degenerate stars.

## 2. Observational strategy

Our observations are aimed at studying a random sample of WDs in a limited space volume with an accuracy of magnetic field measurements of about 1-2 kG and better. To answer the question of *whether WD magnetic field evolution can be detected in observations*, it is important to extend field measurements with uniform accuracy to the whole range of WD masses and temperatures. All types from the hottest (youngest) WDs to the coolest (oldest) degenerates of DA8-9 spectral classes are present in our list, in order to provide the survey with appropriate statistics.

With the aid of the 6 m telescope (BTA), we searched for circular polarization in cores of the hydrogen lines of the brightest ($V < 14$ mag) northern hot (young) WDs and WDs of intermediate temperatures. The cooler (and older) WDs, however, can not be studied well with this telescope. These stars are intrinsically fainter and have weaker Balmer absorption features that make it difficult to study them polarimetrically with the necessary field measurement accuracy. In order to minimize this observational bias, we have extended our list toward observations with the VLT of a random sample of southern WDs with $T_{\rm eff} < 9000$ $K$. These observations, when completed, will make it possible to determine the fractional incidence of magnetism in the low-field regime among WDs of different ages. Our full list consists of 40 isolated WDs of different masses and temperatures. In this paper, we report observations of the 8 brightest WDs in our target list for the 6 m telescope.

## 3. Observations and data reduction

The observations were carried out at the 6 m Russian telescope from 2003 to 2005 in the course of about 9 observing nights shared with other observational programs. The observations are now obtained using the updated prime-focus spectrograph-polarimeter UAGS (R $\sim$ 2000, H$\alpha$ region). The instrument and observational technique are described in detail by Naydenov et al. (2002).

In polarimetric observations of each star, we obtain series of short, consecutive exposures at two orthogonal orientations of the quarter-wave plate (the sequence of its position angles is $+45°, -45°, -45°, +45°$). Assuming *a priori* that the time-scale of possible variability of the longitudinal magnetic field could be as short as a few minutes, we usually set the integration time of each exposure to 60-300 s, depending on stellar magnitude and sky conditions.

For longitudinal magnetic field measurements, we initially use cross-correlation analysis of the displacement between positions of the H$\alpha$ line in spectra of opposite circular polarizations (see Valyavin et al., 2005 and references therein). Applying this method to the series of short time exposures, we then analyze rows of the longitudinal field values to rule out a possible variability of the magnetic field on longer time scales (tens of minutes and longer). After the determination of these scales for each star, we combine spectra of equal orientations of the quarter-wave plate into longer equivalent exposures and build Stokes $I$ and $V$ profiles as described by Valyavin et al. (2005). Finally, we obtain the longitudinal field determinations from the Stokes $I$ and $V$ profiles through the weak-field approximation, as described by Bagnulo et al. (2002).

## 4. Results

Results of longitudinal magnetic field measurements are summarized in Table 1, where column 1 is the name of the WD, column 2 is the spectral class, column 3 is the Julian Date of the midpoint of the observation, column 4 is the exposure time, and columns 5-6 report the measurements and uncertainties of the longitudinal magnetic fields as obtained using the weak-field approximation.

Six targets of our list (WD0009+501, WD0644+375, WD0713+584, WD1105-048, WD1134+300, WD1647+591) have already been observed by Schmidt & Smith (1995); Valyavin et al. (2003); Aznar Cuadrado et al. (2004). In order to minimize the probability to observe a possible zero crossover of the longitudinal magnetic field due to rotation, we repeated the observations of these WDs.

Two targets in our list (WD1105-048 and WD1036+433) showed longitudinal magnetic fields by the presence of weak circular polarization in the H$\alpha$ cores of their spectra. **WD1036+433** is the brightest ($V = 11.22$) weak-lined hot subdwarf star. In three observations of this degenerate in different nights, the longitudinal magnetic field was detected once at more than the $3\sigma$ level ( see Table 1 ). **WD1105-048** is, in comparison, a well-studied, ordinary DA3 WD discovered recently as magnetic by Aznar Cuadrado et al. (2004). The longitudinal magnetic field of this star was found to be variable, varying from about -1 to -4.6 kG. In this study, we confirm the magnetic nature of this degenerate star.

Table 1: Determination of the mean longitudinal field obtained as explained in § 3.

| Name WD | SP | JD -2400000 | Exp sec | $B_l$ *kG* | $\sigma$ *kG* |
|---|---|---|---|---|---|
| 0501+527 | DA1 | 53004.49 | 3600 | -3.9 | 2.8 |
| 0644+375 | DA2 | 53004.59 | 4020 | +1.9 | 1.8 |
| 0713+584 | DA4 | 53003.53 | 7100 | +0.6 | 0.8 |
| | | 53003.61 | 7100 | +0.8 | 1.0 |
| | | AVER | | +0.7 | 0.6 |
| 1036+433 | sdO | 53005.49 | 6000 | +9.6 | 2.6 |
| | | 53005.63 | 5000 | +5.9 | 2.8 |
| | | 53422.34 | 5500 | -1.1 | 3.2 |
| | | AVER | | +5.5 | 1.6 |
| 1105-048 | DA3 | 53006.54 | 3600 | -7.9 | 2.6 |
| | | 53007.55 | 7200 | -4.8 | 2.3 |
| | | 53007.64 | 3100 | +0.1 | 2.7 |
| | | AVER | | -4.4 | 1.4 |
| 1134+300 | DA3 | 53004.64 | 1800 | +8.9 | 4.5 |
| | | 53006.62 | 3600 | +3.5 | 2.7 |
| | | AVER | | +4.9 | 2.3 |
| 1647+591 | DAv4 | 53194.47 | 3600 | −2.9 | 3.4 |
| | | 53195.46 | 3600 | -8.7 | 3.2 |
| | | 53422.59 | 5100 | -0.5 | 2.8 |
| | | AVER | | -3.8 | 1.7 |

## 5. Discussion

We have presented new observations of kilogauss longitudinal magnetic fields in 6 WDs and 1 hot subdwarf. We confirm the magnetic nature of WD1105-048 and find a new candidate weak-field magnetic hot subdwarf, WD1036+433. Kilogauss upper limits are presented for the other 5 WDs. Here, we formally estimate the fraction of kilogauss MWDs as 17% (1/6) that is consistent with the estimate of Aznar Cuadrado et al. (2004) (25%). Note, that practically the same estimate of the frequency of kilogauss MWDs has been done using the magnetic field function technique (Fabrika & Valyavin, 1999). Based on these results, one might speculate that the MWDs are not a unique class of degenerate stars, but rather represent the strong-field tail of a continuous distribution of field intensities.

The 10 % fraction of megagauss MWDs (Liebert et al., 2003), in comparison to 25 % for kilogauss fields, supports this idea. This conclusion, however, could be more definite if framed in terms of surface magnetic fields (mean field modulus, $B_s$) since our study is based on observations of only the longitudinal component $B_l$ of the field, which is smaller than $B_s$ in all cases. In case of a dipolar geometry, the difference may be as much as 3 times and higher, depending on the orientation of the dipole to the line of sight. Furthermore, the large-scale magnetic field structure of the weak-field MWDs may be different from dipolar, giving a very strong observational bias to the underestimation of the incidence of WD magnetism in the polarimetric observations. Therefore, the above conclusion about the incidence of magnetism below 1 kG can only be considered as a lower limit.

*Acknowledgements.* GV is grateful to the Korean MOST (grant M1-022-00-0005) and KOFST for providing him an opportunity to work at the KAO through Brain Pool program. GAW acknowledges Discovery Grant support from the Natural Sciences and Engineering Research Council of Canada. AR acknowledges FONDECYT (grant 1020840).

### References

Angel J.R.P., Borra E.F., Landstreet J.D.: 1981, *ApJ Supplement*, **45**, 457.

Aznar Cuadrado R., Jordan S., Napiwotzki R., Schmid H.M., Solanki S.K., Mathys G.: 2004, *A&A*, **423**, 1081.

Bagnulo S., Szeifert T., Wade G.A., Landstreet J.D., Mathys G. 2002, *A. & A*, **389**, 191.

Elkin V.: 1996, *A&A*, **312L**, 5.

Fabrika S.N., Valyavin G., : 1999, *11th. European Workhop on White Dwarfs, ASP Conf. Series*, **196**, 214. J.E. Solheim, E.G. Meistas ed.

Liebert J., Sion E.M.: 1979, *Astrophysical Letters*, 20, 53.

Liebert J., Bergeron P., Holberg J.B.: 2003, *A. J.*, **125**, 348.

Naydenov I.D., Valyavin G.G., Fabrika S.N., et al.: 2002, *Bull. Spec. Astrophys. Obs.*, **53**, 124.

Putney A.: 1999, *11th. European Workhop on White Dwarfs, ASP Conf. Series*, **196**, 195. J.E. Solheim, E.G. Meistas ed.

Schmidt G.D., Smith P.S.: 1995, *Ap. J.*, **448**, 305.

Schmidt G.D., Grauer A.D.: 1997, *Ap. J.*, **488**, 827.

Valyavin G., Fabrika S.N.: 1999, *11th. European Workhop on White Dwarfs, ASP Conf. Series*, **196**, 206. J.E. Solheim, E.G. Meistas ed.

Valyavin G.G., Burlakova T.E., Fabrika S.N, Monin D.N.: 2003, *Astronomy Reports*, **47**, 589.

Valyavin G., Bagnulo S., Monin D., Fabrika S., Lee B.-C., Galazutdinov G., Wade G., Burlakova T.: 2005, *A.& A.* , **439**, 1099.

Wickramasinghe D.T., Ferrario Lilia: 2005, *MNRAS*, **356**, 1576.

# ON THE LIFE AND SCIENTIFIC ACTIVITY OF PROFESSOR A.Ya.ORLOV ($125^{th}$ anniversary of birthday)

M.Yu.Volyanska, V.G.Karetnikov, O.E.Mandel

Department of Astronomy, Odessa State University
T.G.Shevchenko Park, Odessa 65014 Ukraine

Figure 1: A.Ya.Orlov

Corresponding Fellow of the Academy of Sciences of the USSR (1927), Member of the Academy of Sciences of Ukraine (1939), Meritorious Science Worker of the Ukr.SSR (1951) Alexandr Yakovlevich Orlov (April 6, 1880 – January 28, 1954) was the most authoritative expert in the field of explore of fluctuations of latitude and movement of poles of the Earth, one of the founders of geodynamics – science, which studies the Earth as a complex physical system subjected to the influence of the external forces. A.Ya.Orlov was also an outstanding gravimetrist who developed new methods of gravimetry and created gravimetric maps of Ukraine, European part of Russia, Siberia and Altai and bound them in a uniform network.

A.Ya.Orlov was born in Smolensk in the family of a clergyman. In 1894 he arrived in Voronezh and entered classical gymnasium, after graduation from it in 1898 he entered the faculty of Physics and Mathematics at the Petersburg University. There he studied astronomy under the guidance of the well-known scientists – professors S.P.Glazenap, A.M.Zhdanov, private-associate professor A.A.Ivanov, astronomer N.A.Tachalov. In summer of 1901, being the student of the University, he worked in Pulkovo observatory. In 1902 upon graduation from the University with the first degree diploma he was retained at the University to prepare for a professorial rank and was sent for training abroad.

In 1903-1904 years he studied mathematics, mechanics and astronomy in the Sorbonne University (France). First half of 1905 he spent in Germany, where he worked on geophysics, mostly, on seismology at Goettingen, and autumn of 1905 he trained in Sweden. On returning home at the end of 1905 he took the position of the assistant in the Astronomical observatory of the Yurjev University (nowadays, the Institute of Astrophysics and Physics of Atmosphere of Academy of Sciences of Estonia in Tartu, before Yurjev).

In 1907 he was appointed to the post of the calculator at the Pulkovo observatory, where he conducted observations of stars on a large zenith-telescope to study the fluctuations of a pole, and in 1908 was elected the astronomer-observer at the Astronomical observatory of the Yurjev University, where he engaged in researches of deformations of the globe under action of lunar attraction.

In 1910 A.Ya.Orlov has maintained the Master thesis in the Petersburg University and in the same year he was elected a member of the Permanent Seismic commission at the Russian Academy of Sciences. The commission sent A.Ya.Orlov on the International seismological congress that took place in 1911, in Manchester (England). Here A.Ya.Orlov was elected the member of the International Committee on study of deformations of the Earth and in the same year he visited the York observatory in the USA to study the photos of comets.

In 1912 A.Ya.Orlov participated in the expedition to Western Siberia on the rivers Irtysh, Obi and Biya from Tobolsk up to Bijsk, the purpose of expedition was measurement of gravity in the different points of Siberia. In the same 1912 on behalf of the International Seismic Bureau he organizes the construction of the Gravimetric Station in Tomsk, where the observations with horizontal pendulums above a lunar attraction had already begun in 1913.

A new stage came in the life of A.Ya.Orlov in 1912 – he was invited to take a post of the head of the Chair of Astronomy and the Director of the Astronomical observatory of the Imperial Novorossiysk (nowadays the Odessa National) University; and the following years of his life and activity were connected with Odessa.

There his talent of the scientist and organizer revealed itself completely. From that moment the basic activity of A.Ya.Orlov took place in Ukraine, where he was a director of six observatories, two of which (Poltava gravimetric and the Main Astronomical Academy of Sciences of Ukr.SSR) he founded.

In the Odessa period of his life lasting more than 20 years, from December 1912 till February 1934, A.Ya.Orlov left a deep trace both in the preparation of the astronomical staff, and in science, as the Director of the Observatory, which thanks to him became a powerful scientific establishment of not only All-Ukrainian, but it is possible to say, A1l-Union importance. It came as a result of his extremely labour – intensive and very important researches both in Ukraine, and in Russia – in Siberia.

A.Ya.Orlov had been working for 8 years, from 1912 to 1920, as the Head of the Chair of Astronomy of the University. In 1920 the Novorossiysk University was closed and divided on several institutes. However, A.Ya.Orlov during such a short period of his teaching in the University succeeded to prepare such famous scientists as Z.N.Aksentjeva, V.A.Albitsky, I.I.Witkovsky, V.S.Zhardetsky, D.V.Pyaskovsky, N.M.Stojko, and N.V.Zimmerman.

A.Ya.Orlov also made a wholesome influence and on the Petersburg students V.P.Tsesevich and V.V.Sharonov coming to Odessa for summer observations, which would later became outstanding scientists (V.P.Tsesevich in 1944-1983 years was the Head of the Chair of astronomy and Director of Astronomical observatory of the Odessa University). Then A.Ya.Orlov wrote and published the textbooks: "Lectures on Spherical astronomy" and "The Course of Theoretical Astronomy".

In 1913 A.Ya.Orlov carried out vast reorganization work in the Odessa Astronomical Observatory, showing qualities of a wise leader. The Odessa Observatory, created by heroic efforts of A.K.Kononovich with almost complete absence of resources, was at that time in a bad condition. A.K.Kononovich, who was very sick in the last years of his life, could not give so much attention to the Observatorys businesses, as earlier. The scientific interests A.K.Kononovich lay in the field of astrophysics, and the Observatorys activity developed in an astrophysical direction. After the death of A.K.Kononovich in 1910 the management of the Observatory was entrusted to the professor of physics M.P.Kasterin, who was loaded with work even without that and could not give due attention to the Observatory.

Understanding perspectives of the astrophysical researches, A.Ya.Orlov did not restrain former directions of works, however, being interested in the development of astrometric researches, he achieved an increase of staff, he invited the graduates of the Novorossiysk University, who would subsequently become the known scientists – N.M.Lyapin, M.V.Vasnetsov, to work in the Observatory; he has left at the Chair of astronomy a university graduate N.V.Zimmerman, eventually, a well-known astrometrist ; then D.V.Pyaskovsky, subsequently a professor of the Kiev University.

A.Ya.Orlov founded a scientific library in the Odessa Astronomical Observatory and organized reduction of the large numbers of observations saved in the Observatory. In particular, an 18-year's series of observations of solar spots was reduced, and a special method of calculations was developed, giving reliable results. From these observations the elements of solar equator were determined and the movement of the spots on latitude was investigated. It is necessary to note, that A.Ya.Orlov was distinguished by the careful preparation of the organization of the observations and same careful and without delays processing of them.

A lot of attention A.Ya.Orlov paid to putting the tool park of the Observatory in order and especially to the restoration of the Repsolds meridian circle, that was made in 1862 (was received by the Observatory in 1871) and which was not used for more than 30 years. A talented university mechanic I.A.Timchenko was involved in the works of restoration of the circle, and executed them with greatest diligence and ingenuity. As a result, the meridian circle became one of the best telescopes of such type in the country, and it is still in the working order nowadays.

It was necessary for A.Ya.Orlov to put the building of the Observatory and the adjacent territory in order. For all this money was required. A.Ya.Orlov succeeded in persuading the officials of the Department of Science of the necessity of modernization of the Odessa Observatory, and some modest means were distributed and spent reasonably. The observatory building was reconstructed and received a completed architectural shape; an artful fencing was built around the observatory. The refractor of Cook, acquired in 1886, was sent for reconstruction to England.

The large employment as the Observatory Director and the Professor of the University did not prevent A.Ya.Orlov from continuing scientific researches. In 1915 he completed a capital work, and the doctor thesis, entitled: "Results of the observations above lunar-solar deformations of the Earth", was maintained at the Petrograd University. That work abounded in the original and valuable considerations about prospects and methods of research; a new method of the processing of observations by means of harmonic analysis, developed by A.Ya.Orlov, was given in it. The method he applied subsequently to researches of a number of variable stars. Continuing gravimetric research, A.Ya.Orlov made two expeditions on Altai in 1916 and 1917, where he determined value of the acceleration of gravity in 9 points.

In that period A.Ya.Orlov was the acknowledged leader of astronomical and geophysical researches in

Ukraine. It was no wonder, that at that time he was invited and taken as the Professor and the Director of the Astronomical observatory on the staff of the Kiev University (unfortunately, no detailed information was kept on his work at the Kiev University), and in 1920 A.Ya.Orlov was elected by the ordinary academician of the Ukrainian Academy of Sciences (UAS) created by V.I.Vernadsky.

A.Ya.Orlov was not "the room scientist", he took alive interest in the problems of the city, in which he lived and worked. Landslips were a great trouble for Odessa at that time; they brought the large harm to a coastal part of city. A.Ya.Orlov joined actively in the work of "Commission on struggle with landslips" and in March, 1913 he made the report in the Permanent Central seismic commission "About struggle with landslips in Odessa". Level measurements at the coast of Odessa were executed within the framework of that work under a management A.Ya.Orlov. And further A.Ya.Orlov accepted active participation in reaching the decision on essential practical tasks.

At the liquidation of the Novorossiysk University the Chair of astronomy was abolished as well, and the Astronomical Observatory was recognized by an independent establishment under the name of the Odessa State Astronomical Observatory of Peoples commissariat of the Education of Ukraine. It came as a result of the fact that the Observatory overgrew the frameworks of the University division and, especially, divisions of any of educational institutes, into which the Novorossiysk University was split. And the Observatory joined in the execution of the important state tasks at once.

For the restoration of the economy destroyed during World and Civil wars and intervention, in conditions of the international isolation the organization of the astronomical editions, realization of astronomic and geodetic works was required. A.Ya.Orlov organized for the Naval department restoration of a geodetic network from Dniester up to Dnieper, undertook the edition of "Astronomical calendar" (1919-1923), and then "Naval astronomical annual" (1921-1924), extremely necessary for the restored fleet by the Black sea. A.Ya.Orlov began to issue "Circular of the Odessa astronomical observatory" (1921-1927) as the continuation to the issued earlier "Transactions of the Astronomical observatory of the Novorossiysk University" (1914-1915). But, as any big scientist, A.Ya.Orlov was engaged by the global problems connected to the movement of poles and tide deformations of the Earth ever more, for which study the network of stations and observatories was necessary.

Understanding the necessity of the development of astronomical researches for Ukraine, the academician UAS A.Ya.Orlov undertook actions on association of researches and put forward an idea of creation the Central astronomical observatory in Kanev area in Ukraine and created an Astronomical Computing Bureau at the Ukrainian Academy of Sciences. However soon, the Presidium UAS liquidated the bureau without A.Ya.Orlov knowledge, and A.Ya.Orlov announced (1921) leaving the UAS in a mark of the protest. After a years delays and trials his application on leaving the UAS was satisfied in 1922.

However A.Ya.Orlov did not leave the idea of the creation of the central observatory in Ukraine and in 1921 sent to the Peoples Commissariat of the Education of Ukraine a number of letters on the transformation of the Odessa astronomical observatory into the Main state astronomical observatory of Ukraine. He manages to receive the necessary decision, the form and seal and to begin work of the Main observatory, which, probably, was not long (in the Odessa regional state archive ORSA, Fund -1395, List 1, 97, 1921 – only a few documents signed by A.Ya.Orlov with impressions of this seal were kept).

A.Ya.Orlov tried not only to prepare the necessary scientific staff, but also to involve young scientists already presented themselves in a good light the work of the observatory. When he was the director of the observatory I.D.Androsov, a known geodesist, N.M.Mikhalsky, a celestial mechanic, B.V.Novopashenny, an eminent astrometrist were invited to work. During directorate by A.Ya.Orlov in Odessa there came many well-known astronomers and astronomers-amateurs, also many scientists, which graduated from the Novorossiysk University earlier, for example, N.N.Donich. Undoubtedly, thanks to the attentive attitude of A.Ya.Orlov to the amateurs of astronomy we are obliged by the appearance in the science one of the greatest physicist and astrophysicist of the century G.A.Gamov, working for him for some time by the calculator, and also V.P.Glushko, an Academician of the Academy of Sciences of the USSR, in those years an amateur in he astronomy visiting the Odessa astronomical observatory, and other scientists. Let's note that A.Ya.Orlov was the first chairman of council of the Odessa branch of an All-Union Astronomical-Geodetical Society.

In 1922 and 1924 A.Ya.Orlov carried out a trip in Tomsk and Irkutsk in extremely difficult conditions and brought from there the gravimetric equipment to Odessa. We remind you that the gravimetric station organized in Tomsk by A.Ya.Orlov in 1913 still worked. In Odessa he determined a gravimetric point, included in the international catalogues; a fundamental mark of a highest, "zero" class was established used till now by the expeditions of scientific ships.

In 1924, during his directorate of the Odessa astronomical observatory, A.Ya.Orlov was elected the Dean of the Geodetic faculty of the Military Engineering Academy and in the same 1924 the gravimetric study of the Moscow abnormal station area was organized by him, which was completed the following year with success under the direct guidance by A.Ya.Orlov. In 1924

the Seismic commission of the Academy of Sciences of the USSR entrusted A.Ya.Orlov again with a management of observations in the USSR on deformations of the Earth.

In 1922-1928 years A.Ya.Orlov carried out works on the study of tides in the Black Sea, on the study of influence of the Moon on speed and direction of the wind. The measurements were carried out in Odessa, Sevastopol, and Poti. The researches by A.Ya.Orlov discovered that even in that practically closed reservoir, that the Black Sea is, a tidal wave exists with amplitude of 33 mm with an error of 1 mm. The initial phase was determined with an error of only 3 degrees. Thus, the fluctuations of the sea level achieve 6 cm at the coast of Odessa. It convinced A.Ya.Orlov of the irrationality of the creation a continental earth-tidal gravimetric station in Odessa, for the pendulums would have been influenced by the real-life sea tide. In that connection he puts forward the offer on the creation of the Gravimetric observatory in Poltava in 1924 and realization of the gravimetric survey in Ukraine.

The Poltava gravimetric observatory was founded by A.Ya.Orlov in 1926 for all-round study of gravity and for observations of latitude on a zenith-telescope. It was equipped with the first-class devices and was supplied with the scientific staff. In the autumn of 1926 A.Ya.Orlov went to Nizhniy Novgorod on behalf of the Academy of Sciences of the USSR for a choice of a place for an academic gravimetric station. As the result of his scientific merits the Director of the Odessa astronomical and the Poltava gravimetric observatory A.Ya.Orlov was elected the Corresponding Fellow of the Academy of Sciences of the USSR in 1927. In 1928 he was elected the honourable member of the Society of the amateurs of natural sciences in Moscow. A.Ya.Orlov was the Director of the Poltava observatory in 1926-1934 and in 1938-1951 years with an interval, when he worked in Moscow.

That extremely fruitful Odessa period of A.Ya.Orlovs life and activity came to an end in 1934 with his departure to Moscow, where he began to work in the P.K.Sternberg State astronomical institute (GAISh) of the Moscow University. There he organized a gravimetric branch GAISh (in Kuchino) and became its Head. In 1936 he was elected the member of the International Latitude Commission. In 1937 he was nominated the astronomer of the Moscow Geodetic Institute and in the same year was elected the member of the management of the Moscow branch of an All-Union Astronomical-Geodetical Society.

In October, 1938 A.Ya.Orlov returned to Ukraine and was appointed the Director of the Poltava Gravimetric Observatory. That year he addresses the Presidium of Academy of Sciences of Ukr.SSR with a letter about the necessity of the creation of an Academic Central Observatory near Kiev. The decision on the creation was accepted and A.Ya.Orlov was offered the development of the scientific program. As a result of those actions the Ukrainian astronomical committee was formed and the considerable means for purchase of instruments and scientific researches were allocated.

Figure 2: On the photo: the Director of the observatory A.Ya.Orlov with graduates from the Novorossiysk University (autumn 1916(?)). From the left to the right: V.A.Albitsky, A.M.Rybakov, D.V.Pyaskovsky, N.M.Lyapin, A.Ya.Orlov, I.I.Witkovsky, V.S.Zhardetsky, N.N.Donich, and N.M.Stojko-Radilenko.

That activity resulted in the fact that 1939 A.Ya.Orlov was elected the Academician of the Academy of Sciences of Ukr.SSR (repeatedly) and it was also entrusted to him to head the Carpathian Observatory (1939-1941 years). Then A.Ya.Orlov (1941) carried out a trip to the Far East (Blagoveshchensk) for the organization of the Far East Latitude Station, the project he offered in 1932.

The construction of the academic observatory in Kiev was postponed because of the war, but in 1943, after the deliverance of Kiev, A.Ya.Orlov returned to the questions of the observatory construction and in 1944 he was nominated as the director of the Main Astronomical (Goloseev) Observatory of the Academy of Sciences of Ukr.SSR, which he headed till 1948, and then in 1950-1951 years.

The results of the latitude observations by A.Ya.Orlov are stated in the book "Service of latitude", issued in 1958, and three volumes "Elected works" by A.Ya.Orlov were published in 1961. In the cities, where A.Ya.Orlov worked, the scientific conferences – so-called "The Orlov memorial readings" are held regularly, every 6 years. The first readings were carried out on the centenary from A.Ya.Orlovs birthday, the third readings were held in Odessa in 1992. The Orlov readings took place in 1998 and in 2004.

Everything, that we know about Alexandr Yakovlevich Orlov, chief of the Odessa astronomy in 1912-

1934 years, years of realization of the huge and rather labour-capacious works not only at our university and observatory, but also in Russia, and in Ukraine, speaks about an extraordinary versatile, active, purposeful and efficient man, easy on the rise, an initiator of the new and perspective scientific directions. He was the Person, which was not afraid for the sake of the science to offer both a post, and a rank of the academician of the UAS, and other advantages. The results of his works are significant, so our gratitude for it to him is infinite.

A.Ya.Orlov was married, had six children. There is information that he was related with well-known Vitte family.

# THE COOL GALACTIC R Coronae BOREALIS VARIABLE DY Persei

L. Začs

Institute of Atomic Physics and Spectroscopy, University of Latvia
19 Rainis blvd., Riga, LV-1586, Latvia, *zacs@latnet.lv*

ABSTRACT. DY Per (CGCS 372) was suspected to be an R CrB star based on the photometry by Alksnis (1994). Subsequent photometric monitoring revealed a number of sudden light declines typical for R CrB variables superimposed on the 792-day cycle of long-period light variations (Alksnis et al. 2002). However, the temperature of this star is much lower than average for other R CrB stars. Moreover, the luminosity of DY Per was suspected to be lower than usually for R CrBs. Keenan & Barnbaum (1997) estimated $T_{\rm eff} \simeq 3500$ K using the standard criteria of spectral classification and a giant luminosity. DY Per was classified as R8, C4,5, C5,4p, and C-Hd 4.5 $C_2$ 6 (Keenan & Barnbaum 1997). Alcock et al. (2001) revealed four stars similar to the Galactic variable DY Per among eight RCBs discovered in the Large Magellanic Cloud.

**Key words**: Stars: carbon; stars: winds, outflows; (stars:) circumstellar matter; stars: individual: DY Per

The imaging photometry of DY Per was taken with the Lulin 1-meter telescope (LOT), equipped with a Princeton Instruments PI 1300B CCD camera. High-resolution spectra for DY Per and the comparison star U Hya were obtained with the coudé échelle spectrometer MAESTRO fed by the 2m telescope at the Observatory on the Terskol Peak in Northern Caucasus equipped with a CCD detector with a resolving power of ∼45 000.

An inspection of the high-resolution spectrum of DY Per observed near the light maximum relative to the normal carbon star U Hya shows that neutron-capture elements are not enhanced while the features due to atomic carbon are strong, in agreement with that for typical R CrB stars. The metallicity was found to be nearly solar. The isotopic $^{13}$CN lines are not enhanced in the spectrum of DY Per relative to $^{12}$CN. Unfortunately the spectral regions around $H_\alpha$ and $H_\beta$ are very crowded to clarify the level of hydrogen deficiency in the atmosphere of DY Per.

A significant changes are seen in the profiles of sodium D lines between two seasons of observations. At least five components are resolved. Averaged D1&D2 heliocentric velocities of these components on 2002 (phase 0.77) and 1990 (phase 0.15) are (−197.3, −143.0, −57.0, −36.7, −12.8) km s$^{-1}$ and (−214.4, −157.8, −56.8, −36.6, −10.4) km s$^{-1}$, respectively. Thus two the most blueshifted components display changes both in the radial velocity and shape while three components near the stellar velocity of DY Per seems to be non- variable. The blueshifted components apparently are formed in the clouds of gas and dust ejected by DY Per. The rest revealed components originate in the stellar atmosphere and interstellar medium.

A close nearby star was detected about 2.5 arcsec from DY Per using CCD images during the recent deep light decline. The carbon star DY Per itself is much redder than the companion so a clear separation is seen in the B band. At longer wavelengths DY Per starts to outshines the companion. The presence of such companion was not revealed during more than 10 years of the photometric monitoring, however, it was supposed by Alksnis (1994) to interpret the variations of the observed colour indices. This anonymous companion, with observed colour indices (B-V)=1.35 and (V-R)=0.87, may be a foreground K 2–4 dwarf.

The complete paper was published in Astronomy & Astrophysics (see Začs et al. 2005).

*Acknowledgements.* This research has been supported by grant 05.1863 from the Latvian Council of Science. The Mutual Fund of scientific collaboration among Taiwan (ROC), Latvia and Lithuania is thanked for support.

## References

Alcock, C., Allsman R.A., Alves D.R., et al.: 2001, *ApJ*, **554**, 298.

Alksnis A.: 1994, *BaltA*, **3**, 410.

Alksnis A., Larionov V.M., Larionova L.V., et al.: 2002, *BaltA*, **11**, 487.

Keenan P.C., Barnbaum C.: 1997, *PASP*, **109**, 969.

Začs L., Chen W.P., Alksnis O., et al.: 2005, *A&A*, **438**, L13.

# THE SPECTROSCOPY OF THE PULSATING CARBON STAR R Lep

L. Začs, O. Alksnis

Institute of Atomic Physics and Spectroscopy, University of Latvia
19 Rainis blvd., Riga, LV-1586, Latvia, *zacs@latnet.lv*

ABSTRACT. The first results of detailed spectroscopy are presented for carbon Mira R Leporis. This long-period variable is undergoing deep fadings, apparently caused by dust formation around the star. High-resolution CCD spectra were observed for two seasons. The heliocentric photospheric radial velocity was found to be +32.6 and +38.4 km $s^{-1}$, respectively. Blueshifted emissions from the circumstellar gas are seen.

**Key words**: Stars: carbon; stars: oscillations; (stars:) circumstellar matter; stars: individual: R Lep

## 1. Introduction

Carbon-rich variable stars are thought to be near the end of the asymptotic giant branch evolution just prior to planetary nebula formation. Many of them are losing mass. Mira variables have visual light amplitudes more than 2.5 mag, emission lines in their spectra at certain phases, and periods in the 80 to 1000 days range. The variability characteristics of carbon stars differ greatly from one to another. There is a group of stars (R For, R Lep and R Vol, etc.) which lose mass in an apparently erratic way.

R Lep is a bright carbon Mira. It has a late spectral type of C 7,6e and a pulsation period of 432 days. From the extensive visual observations available for this star, Mattei & Foster (2000) find that its period of pulsation is slowly increasing. Whitelock et al. (1997) reproduced the light curve of R Lep with a sum of a 20,000 days sinewave and its first harmonics, plus a 438 d sinewave plus the first harmonic. They presented evidence that carbon-rich dust ejection occurs in a preferred direction, possibly from the equator and noted some similarity with R Coronae Borealis stars. Polarimetric observations clearly established the intrinsic polarization and its variability in R Lep (Raveendran 2002). Careful analysis is required to study this phenomenon in detail.

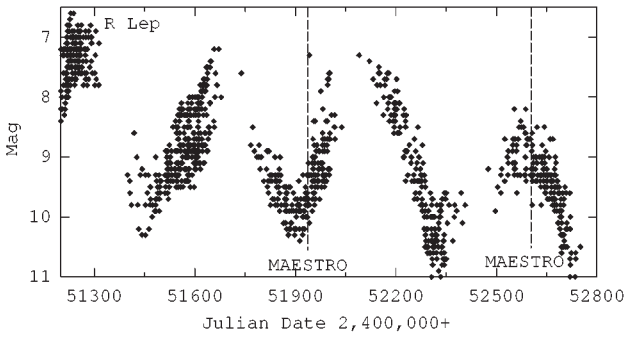


Figure 1: Light variations of R Lep according to the AAVSO data. The moments of high-resolution spectroscopic observations are indicated by the dashed lines.

## 2. Observations and results

High-resolution spectra for R Lep and the comparison star U Hya (C 7,3) were obtained with the coude echelle spectrometer MAESTRO fed by the 2-m telescope at the Observatory on the Terskol Peak in Northern Caucasus equipped with a CCD detector with a resolving power of 45,000. Two spectra were observed by F.Musaev on 26 January 2001 (JD2451936) and on 26 November 2002 (JD2452604) near the minima and maxima of periodic light pulsations (see Fig. 1). The spectra covered region from about 3600 to 10,200 Å in 85 wavelength bands overlapping shortward of $H_\alpha$. Each region spanned from 50 to 140 Å. The reduction of spectra were performed with the standard DECH20T routines. The basic data for both stars from literature are provided in Table 1.

An inspection of the high-resolution spectra of R Lep shows that a large number of strong $C_2$ and CN lines dominate over all the analyzed spectrum, blending significantly with the atomic absorption lines. However, a limited number of relatively uncontaminated atomic (molecular) lines were selected to measure radial velocity and check metallicity. Our analysis shows that the lines of the iron-peak elements in R Lep are of similar strength with those in U Hya. The radial velocity

Table 1: The basic data for R Lep and the comparison star U Hya.

| Star | R Lep | U Hya |
|---|---|---|
| l,b (deg) | 214, -31 | 260, +38 |
| Sp.type | C 7,6e | C 7,3 |
| Var.type, P | M, 432 d | SRb, 450 d |
| $M_{bol}$ | -4.79 (-3.6) | -4.0 |
| $T_{eff}$ | 2390 K | 2825 |
| $[Fe/H]$ | +0.2 | -0.1 |
| C/O | 1.03 | 1.04 |
| $^{12}C/^{13}C$ | 62 | 32 |

(RV) for R Lep was measured using about 30 relatively clean and symmetric atomic absorption lines selected over the whole spectral region in both spectra. In addition about 30 uncontaminated CN lines were selected for RV measurements. No significant difference was found in the velocity derived from atomic or molecular lines. The heliocentric correction was calculated to be $-19.7$ and $+2.9$ km s$^{-1}$, respectively. Thus the mean heliocentric stellar $RV_{\odot}$ was found to be +32.6 (2001) and +38.4 km s$^{-1}$ with a standard deviation of the mean value of about 0.4 km s$^{-1}$. The difference between the photospheric radial velocities derived for two seasons seems to be significant. The change could be the result of pulsations in this Mira variable.

The resulting spectra for the region around Na I D12 lines along with that for the typical carbon star U Hya are presented in Fig. 2. Most significant changes between two seasons in this region are seen in the sodium lines. While on January 2001 typical absorption lines of D12 are visible, on November 2002 the overlap of emission(?) and sharp absorption appeared near to the line cores. These sharp absorption features are blueshifted with an averaged D1&D2 velocity of $-25.6$ km s$^{-1}$ relative to the photospheric velocity. It is clear that such features are formed in the circumstellar matter ejected by R Lep. Significant changes between two seasons were found also in another strong (resonance) lines: the Balmer $H_{\alpha}$ & $H_{\beta}$, K I at 7698 Å, Ca II at 8542 (see Fig. 3) atomic, and $C_2$ molecular lines.

*Acknowledgements.* This research has been supported by grant 05.1863 from the Latvian Council of Science. We acknowledge with thanks the variable star observations from the AAVSO International Database contributed by observers worldwide and used in this research.

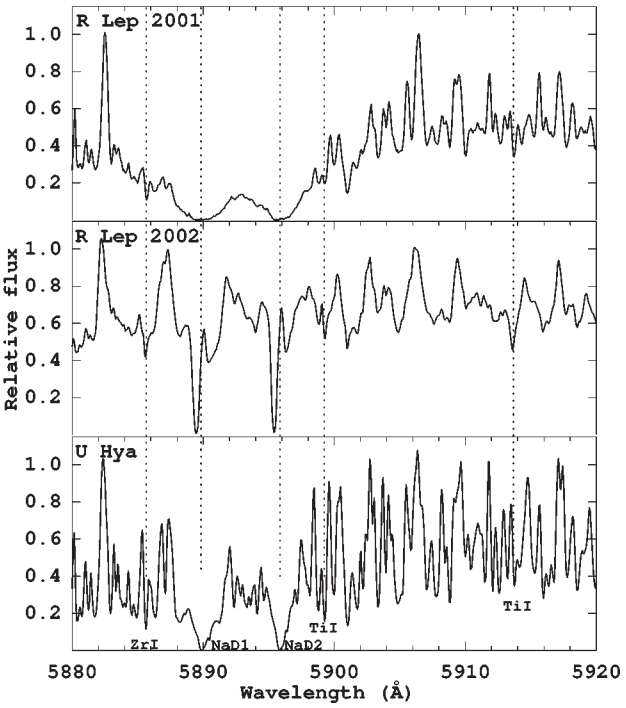


Figure 2: The observed spectra of R Lep around the Na I D12 lines for two different seasons, January 2001 (top panel) and November 2002 (middle panel), near the minima and maxima of light pulsations. Also shown is the spectrum for a comparison star U Hya. All spectra have been shifted in wavelengths to correct for the stellar radial velocities. Complicated profiles of sodium lines are visible in the spectrum of R Lep observed on November 2002.

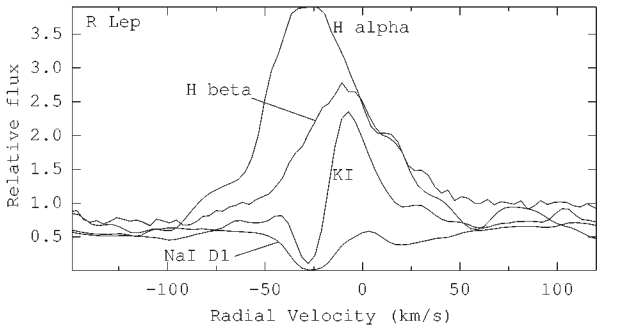


Figure 3: The emission features of Balmer $H_{\alpha}$ & $H_{\beta}$, K I at 7698 Å, and Na I D1 lines in the spectrum of R Lep observed on November 2002 in the radial velocity scale relative to the photospheric velocity of +38.4 km s$^{-1}$.

**References**

Mattei J.A., Foster G.: 2000, *in Wing R.F., ed., Proc. IAU Symp.177, The carbon Star Phenomenon*, Kluwer, Dordrecht, p. 155.

Raveendran A.V.: 2002, *MNRAS*, **336**, 992.

Whitelock P.A., Feast M.W., Marang F., Overbeek M.D.: 1997, *MNRAS*, **288**, 512.

*Наукове видання*

**Вісті Одеської астрономічної обсерваторії**
том 18 (2005)

***Англійською мовою***

Технічний редактор М. І. Кошкін

---

Підписано до друку 03.08.05. Формат 60x84/8.
Ум. друк. арк. 13.95. Друк офсетний. Папір офсетний. Тираж 300 прим. Зам. 452.

**Видавництво «АстроПринт»**
65026, м. Одеса, вул. Преображенська, 24.
Тел.: +38 (048) 726-96-82, 726-98-82, 37-14-25.